FEEDBACK CONTROL OF CYCLING IN SPINAL CORD INJURY USING FUNCTIONAL ELECTRICAL STIMULATION

A DISSERTATION

SUBMITTED TO THE DEPARTMENT OF MECHANICAL ENGINEERING

OF GLASGOW UNIVERSITY

FOR THE DEGREE OF

DOCTOR OF PHILOSOPHY

By

Thomas Schauer

October 2005

Abstract

The consequences of Spinal Cord Injury (SCI) can be severe. Depending on the level of the lesion, SCI causes a loss of motor and sensory function, and results in the immobilisation of the patient and possible lifelong dependency on a wheelchair. A complete loss of bladder, bowel and sexual function is also common. These primary effects of a spinal cord injury lead over time to a range of secondary medical complications, e.g. atrophy of the paralysed muscles and decreased cardiovascular fitness.

In SCI patients with upper motor neuron lesions, the signal path from the Central Nervous System (CNS) to the muscles is interrupted. However, the muscles themselves retain their ability to contract and produce force. Functional Electrical Stimulation (FES) applied to the lower motor neurons can replace the lacking signals from the CNS. This thesis is concerned with the realisation of leg cycling by means of FES in SCI individuals with complete paraplegia. FES lower-limb cycling can be safely performed by paraplegics on static ergometers or recumbent tricycles. Regular FES cycling represents an effective exercise intervention with reported therapeutic effects that help to reduce the severity of the secondary medical complications arising from SCI.

In this work, different FES cycling systems were developed for clinical and home use. Two design approaches have been followed. The first is based on the adaptation of commercially available recumbent tricycles. This results in devices which can be used as static trainers or for mobile cycling. The second design approach utilises a commercially available motorised ergometer which can be operated while sitting in a wheelchair. The developed FES cycling systems can be operated in isotonic (constant cycling resistance) or isokinetic mode (constant cadence) when used as static trainers. This represents a novelty compared to existing FES cycling systems. In order to realise isokinetic cycling, an electric motor is needed to assist or resist the cycling movement to maintain a constant cadence. Repetitive control technology is applied to the motor in this context to virtually eliminate disturbances caused by the FES activated musculature which are periodic with respect to the cadence. Furthermore, new methods for feedback control of the patient's work rate have been introduced.

A one year pilot study on FES cycling with paraplegic subjects has been carried out. Effective indoor cycling on a trainer setup could be achieved for long periods up to an hour, and mobile outdoor cycling was performed over useful distances. Power output of FES cycling was in the range of 15 to 20 W for two of the three subjects at the end of the pilot study. A muscle strengthening programme was carried out prior and concurrent to the FES cycling. Feedback control of FES assisted weight lifting exercises by quadriceps stimulation has been studied in this context.

In summary, this thesis describes new devices and feedback control methods for FES lower-limb cycling in paraplegia, and provides a preliminary assessment of these systems and methods.

Acknowledgements

I wish to acknowledge and thank those people who contributed to this thesis. First and foremost, I would like to thank my supervisor, Ken Hunt, who introduced me to the interesting field of functional electrical stimulation and has shown a large and consistent interest in my project during the times.
Moreover, I would like to thank the whole staff of the Department of Mechanical Engineering at the University of Glasgow as there are the secretarial staff, the computing staff, and the workshop people.
My thanks go also to my colleagues Nils-Otto Negård, Fabio Previdi, Markus Rothe and Robert Salbert for their collaboration and contribution to the development of this thesis. Thanks also to the subjects who have participated in the FES cycling study.
I would like to thank Simona Ferrante, Henrik Gollee, Einar Idsø and Andrew Pennycott for reviewing the thesis and for their critical and constructive comments.
Finally, I am forever indebted to my wife Kirsten for her understanding, endless patience and encouragement when it was most required. I would also like to thank my parents and friends for their support during all these years.

Contents

List of Tables

List of Figures

Nomenclature

Abbreviations

CFT	Constant Frequency Train
EKF	Extended Kalman Filter
FES	Functional Electrical Stimulation
FNS	Functional Neuromuscular Stimulation
MoI	Moment of Inertia
PRBS	Pseudo-Random Binary Sequence
PWM	Pulsewidth Modulation
SCI	Spinal Cord Injury
VFT	Variable Frequency Train

1 Introduction

This thesis is concerned with the development and control of new devices for Functional Electrical Stimulation (FES) assisted lower-limb cycling. FES cycling is a useful method for cardiovascular training of Spinal Cord Injured (SCI) individuals. Beside the exercise aspects, mobile FES cycling represents a locomotion method with a high recreational use. This chapter provides background information about spinal cord injury and FES and gives an overview of the thesis.

1.1 Spinal Cord Injury

Spinal cord injury results in an interruption of the neurological pathways from the brain to the muscles. Depending on the level of injury, this causes a loss of motor and sensory function and results in the immobilisation of the patient. Figure 1.1 shows the relationship between the spinal cord segments and the spinal nerves to the vertebral bodies. Each muscle in the body is supplied by a particular level or segment of the spinal cord and by its corresponding spinal nerve. The muscle and its nerve make up a myotome. The relationship between the skin and spinal nerves is described by dermatomes. A dermatome is an area of the skin supplied by nerve fibres originating from a single dorsal nerve root. The important dermatomes, myotomes, and reflex arcs are shown in Figure 1.2. These give an indication of the impairments caused by SCI.

Spinal cord damage caused either by injury or disease may result in tetraplegia or paraplegia depending upon the level at which the damage has occurred. Paraplegia is a complete paralysis of the lower half of the body including both legs. Tetraplegia is a paralysis of all four limbs. Paraplegia is slightly more common than tetraplegia. The lesion may be complete or incomplete. A complete lesion will give rise to

- bilateral upper motor neuron paralysis of the part of the body below the level of lesion,
- bilateral loss of all modalities of sensation below the level of lesion and
- complete loss of all bladder, bowel and sexual function.

Muscle spasm in paralysed muscles is also common and often exacerbates the disability.

In Britain, it is estimated that there are 40,000 people with SCI [3]. 80 % of the injuries are sustained at an age of 16-45. Spinal cord injury is not a notifiable disease, so figures for the annual incidence

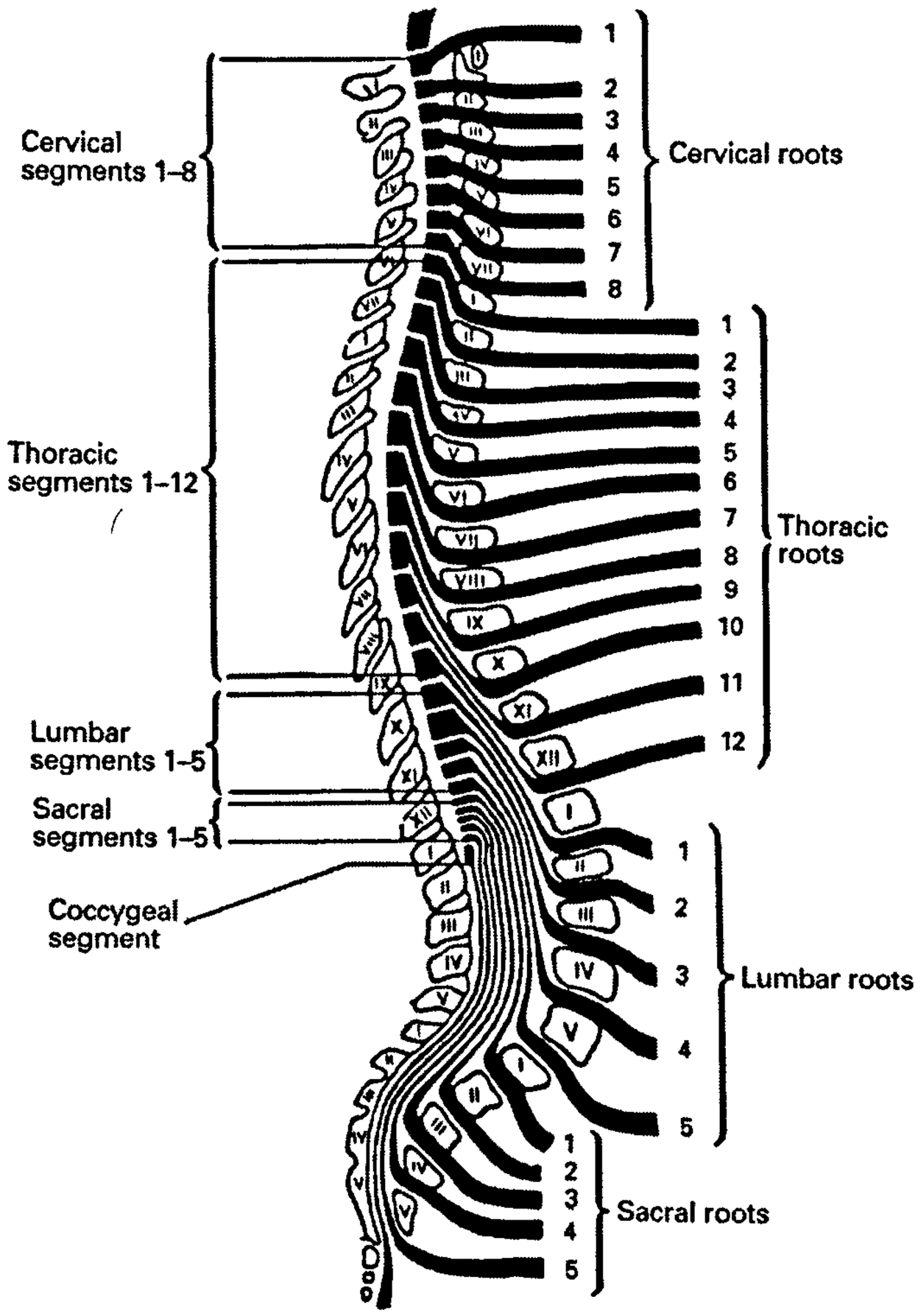

Figure 1.1: Relationship between the spinal cord segments and spinal nerves to the vertebral bodies. Cervical nerves (nerves in the neck) supply movement and feeling to the arms, neck and upper trunk. Thoracic nerves (nerves in the upper back) supply the trunk and abdomen. Lumbar and sacral nerves (from the lower back) supply the legs, the bladder, bowel and sexual organs. (from [8])

are inaccurate and may vary according to the source. In the UK, approximately 1000 new injuries are estimated to occur per year, excluding non-traumatic cases [17]. These numbers are augmented by the group of people with spinal cord damage caused by disease. Road traffic accidents involving motor cycles and cars are the commonest cause of traumatic SCI, followed by domestic falls, accidents at work and in sport. The order of frequency of injury in terms of neurological level is cervical, then thoracic and then lumbar [99].

In this work, the focus will be on paraplegia. A spinal cord damage in the sacral, lumbar or thoracic region results in paraplegia. As already mentioned, paraplegic persons are paralysed to some degree in the legs and abdomen. Movement in the trunk and chest will depend on the height of the lesion. This usually means that the person will use a wheelchair. Conventional wheelchairs have been widely

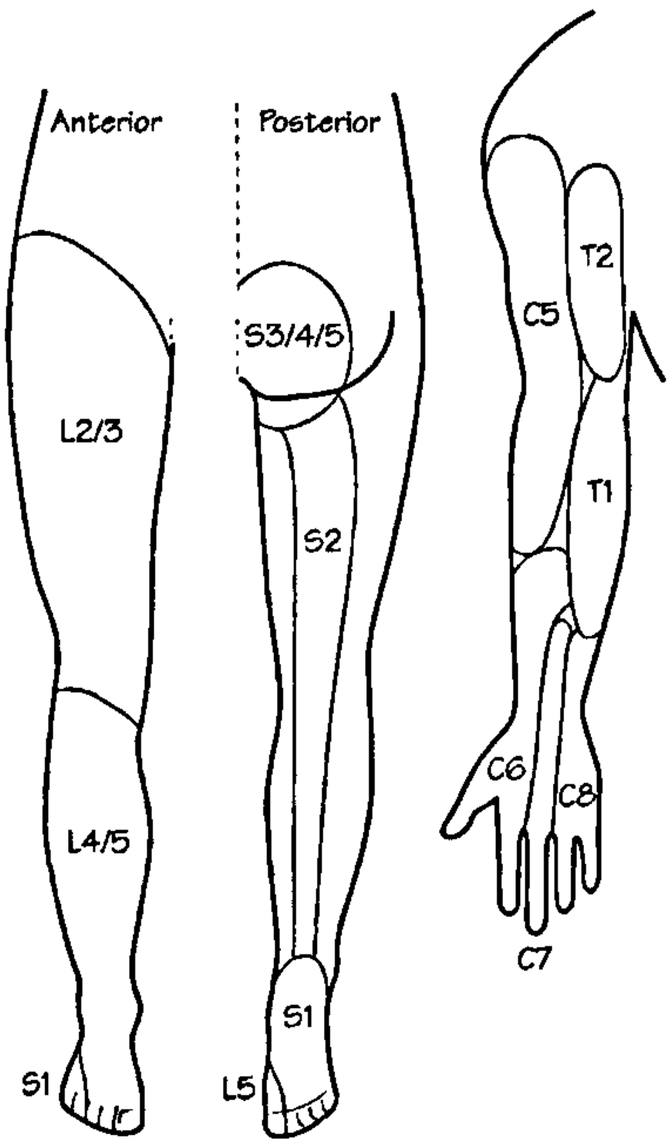

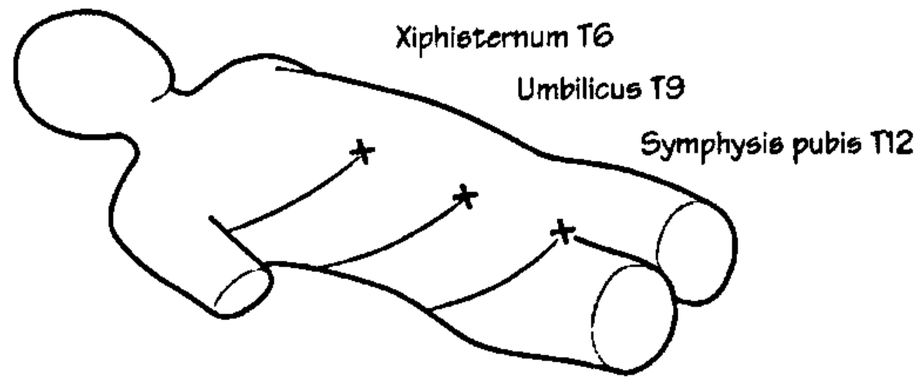

Shoulder abduction	C5		
Elbow flexion	C5/6	Biceps jerk	C5/6
Elbow extension	C7/8	Supinator jerk	C5/6
Finger extension	C7/8	Triceps jerk	C7/8
Finger flexion	C7/8		
Small hand muscles (e.g. finger abduction)	T1		
Hip flexion	L2/3		
Knee extension	L3/4	Knee jerk	L3/4
Foot/toe dorsiflexion	L4/5	Ankle jerk	S1/2
Foot/toe plantar flexion	S1/2		
Knee flexion	L5/S1		
Hip extension	L5/S1		

Figure 1.2: Important Dermatomes, myotomes and reflex arc segmental values (from [99]).

accepted by persons with motor disabilities and sufficient arm strength for propulsion. However, wheelchair life and resulting prolonged immobilisation cause several physiological problems:

- The disuse of the legs for persons who spend much of their time in a wheelchair leads to atrophy of leg muscles and osteoporosis of the long bones of the legs and an increased rate of bone breakage.
- The lack of whole body exercise leads to a decrease in cardio-respiratory fitness and an increased incidence of heart disease and Type 2 diabetes.
- Sitting in a chair all day with lack of sensation can lead to pressure sores and other skin problems that are difficult and costly to treat.
- Many, if not most, longterm wheelchair users, develop overuse injuries of their arms, as a result of the strenuous and somewhat unnatural movements that are needed to propel a wheelchair with the arms.

1.2 Functional Electrical Stimulation

In paraplegic patients with upper motor neuron lesions the signal path from the central nervous system to the muscles is interrupted. However, the muscles themselves retain their ability to contract and produce force. Functional Electrical Stimulation (FES) applied to the lower motor neurons can replace the missing signals from the central nervous system. A so-called neuroprosthesis may be used

to restore motor function in paraplegic patients on the basis of functional electrical stimulation. Apart from provoking contraction of skeletal muscle, FES is used in other neuroprosthetic devices, e.g. the cochlea implant, the phrenic pacemaker, and the sacral anterior root stimulator for bladder control (see [79] or [88] for an overview).

Applications of FES in paraplegia with the aim of motor function restoration include cycling (see Chapter 3), walking [e.g. 28], rowing [e.g. 16, 39], standing-up and sitting-down [e.g. 76, 77] and standing [e.g. 48].

Beyond the direct functional motor effects, some therapeutic effects of FES on the secondary medical complications that arise from SCI have been reported [e.g. 15, 50]. The benefits from FES may include for example improved muscle tone, bulk, and strength, reduced spasticity, improved limb blood flow, or a reduction in disuse osteoporosis. Additionally to these peripheral adaptations, central adaptations of the cardiovascular system can be achieved by FES induced exercises such as regular FES cycling [50]. Improvements in cardiopulmonary fitness are also helping to reduce the risk of the secondary medical conditions which commonly accompany the disability.

The underlying neurophysiological principle of FES is the generation of action potentials in the uninjured peripheral lower neurons by application of low levels of pulsed electrical current to the nerves. Muscle contractions can be artificially released by electrical stimulation of efferent (motor) nerves innervating the paralysed muscles or by electrical stimulation of afferent (sensory) nerves provoking reflexes via intact reflex arcs. An example for using reflexes is the stimulation of the peroneal nerve to elicit the withdrawal reflex. This is used for drop foot prevention in hemiplegic patients.

Stimulation electrodes can be implanted or attached to the motor nerves either centrally (in the spinal cord or on spinal-nerve roots) or peripherally. The electric pulses can also be applied percutaneously to peripheral nerves, using needle electrodes inserted through the skin. In the work reported here, transcutaneous stimulation was utilised where adhesive electrode are attached to the skin in location of the target muscle and its nerve supply (reflex stimulation was not performed). The applied pulses are charge balanced. Charge-balancing can be realised by means of a capacitor or using biphasic stimulation pulses. The stimulators used in this work are current controlled and deliver therefore constant current pulses. The current pulses have usually a duration between 5 and 800 μs and an amplitude between 0 and 125 mA (the exact ranges depend on the specific device).

The muscle force produced by FES depends on the number of recruited motor units and the activation rate. A motor unit is a single motor neuron and the group of muscle fibres (of the same type) innervated by it. When the pulse charge (pulsewidth$\times$ pulse amplitude) is sufficiently high and the neuron is close to the electrode, the motor neuron will be polarised above threshold and an electric action potential will be released. The muscle force increases with the number of recruited motor units (spatial summation), and therefore modulation of pulsewidth or pulse amplitude can be used to control this. The muscle force can also be controlled by modulation of the stimulation frequency (temporal summation). The traditional method for neuromuscular stimulation employs a train of brief rectangular stimulating current pulses, at a frequency of usually between 10 and 100 Hz. Low stimulation

frequencies (<15 Hz) produce unfused twitches rather than a smooth muscular contraction or tetanus. With increasing frequencies, the muscle is also subjected earlier to fatigue for prolonged stimulation. Regular stimulus pulse trains are conventional only because they are easy to generate. It has long been known that natural nerve impulse trains are not of constant frequency, but for example often contain a brief high-frequency burst, slowing to a lower sustained frequency. Such Variable Frequency Trains (VFT) take advantage of the catchlike property of the skeletal muscle and augment muscle performance compared with Constant Frequency Trains (CFT), especially in the fatigued state. A review of this topic by S. Binder-MacLeod and T. Kesar [80] was recently published.

Although FES can elicit strong and effective muscle contractions, there are significant limitations. Normally, muscles contain a mixed population of slow fatigue-resistant (type 1), fast fatigue-resistant (type 2A) and fast fatiguable (type 2B) motor unit types. The terms *fast* and *slow* refer to the contractile speed of the muscle fibres. Muscle atrophy by disuse of the muscle as a result of SCI tends to revert the fibre population to type 2B. Chronic electrical stimulation can be used to convert fast fatiguable muscles to fatigue-resistant type 1, but training for fatigue resistance takes several weeks [52]. Additionally, the fatigue resistant muscle possesses a lower work capacity than the fast fatiguable muscle with mainly type 2B motor units. The fast fatigue-resistant (type 2A) motor units would be most suitable for FES but there is as yet no muscle training schedule available which is generally agreed to result in a muscle populated entirely with type 2A fibres.

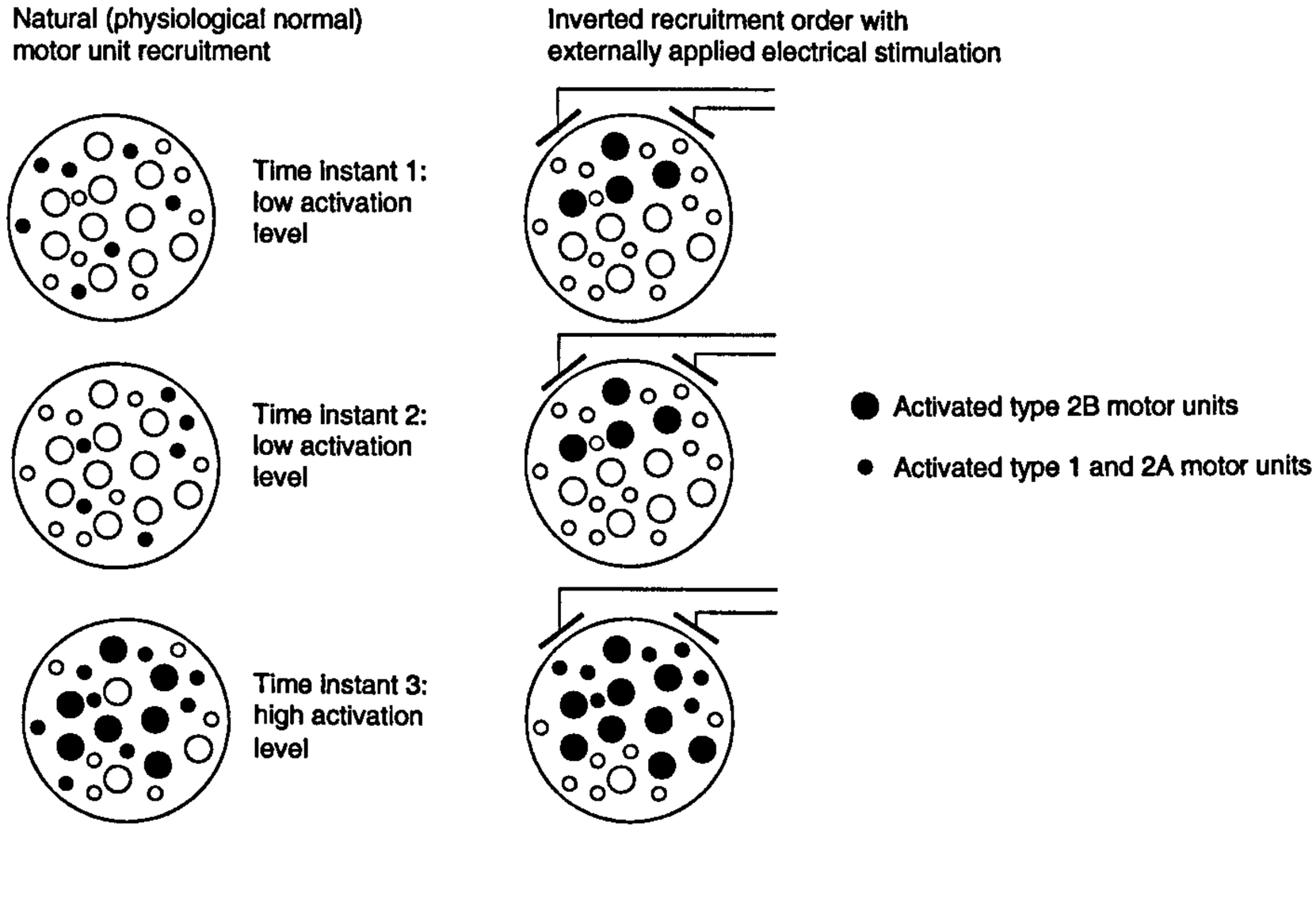

Figure 1.3: Natural versus artificial muscle activation by FES (adapted from J. Quintern)

Compared with the physiological recruitment order (the Hennemann *size principle* [38]), recruitment with FES is thought to be inverted [36]. When low muscle forces are desired, and thus low intensity electrical stimulation pulses are applied, mainly rapidly fatiguing large motor units which are close to the electrodes are activated. This is because the fast fatiguable fibres of type 2B motor unit are

associated with large-diameter nerve axons, which have a lower firing threshold to externally applied stimulation. With increasing intensity of the pulses, also small neurons (related to slow fatigue-resistant (type 1) and fast fatigue-resistant (type 2A) motor units) with higher firing threshold and neurons which are located further away from the electrodes are recruited. In addition to this, at a constant stimulation intensity and for the same electrode position, the same motor units are activated all the time. With FES, the action potentials of different motor units are triggered simultaneously. This is different from the CNS which activates motor units asynchronously.

Figure 1.3 illustrates the differences in motor unit recruitment for muscle contractions under FES and voluntary control. All the differences outlined above between artificial and natural nerve activation result in an early fatigue of FES induced muscle contractions.

Figure 1.4 shows a schematic illustration of the integration of FES within a musculoskeletal control system. The task is to control the angle of the knee joint using activation of the quadriceps muscle group. Artificial feedback control for an individual with lower-limb paralysis is shown in this figure; this can be contrasted with natural feedback control of movement. In both cases the problem requires the determination of knee-joint angle, control processing, and actuation (muscle contraction). In the natural case the joint angle is determined visually and through knee-joint receptors, while in the artificial case an external sensor such as a goniometer is required. Control processing is carried out in the brain in the natural case and is implemented in an external processor in the artificial case. Finally, the natural muscle contraction is achieved via motor control pathways under command of the brain while computer-controlled FES is used in the artificial system.

In summary, FES, together with appropriate sensor and control technology, can provide useful, controlled functional movement.

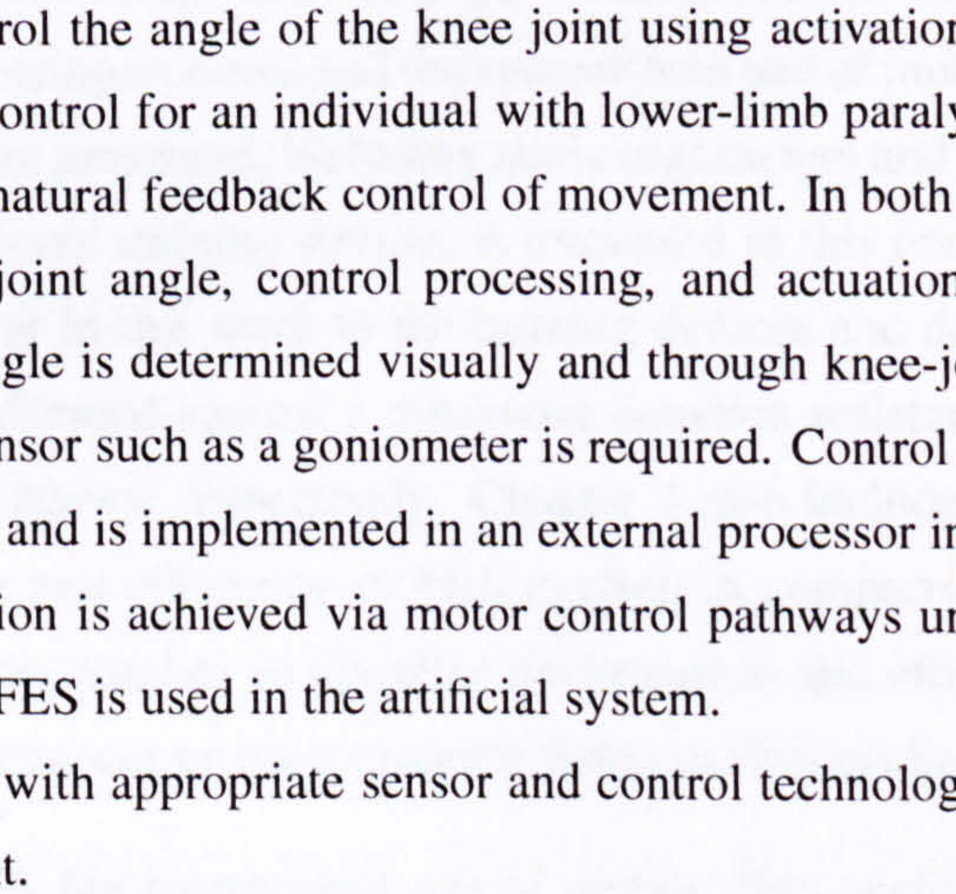

Figure 1.4: Musculoskeletal control system with FES.

1.3 Outline of the Thesis

The work presented in this thesis is concerned with the development and control of systems for FES lower-limb cycling in paraplegia.

- Chapter 2: A central scheme in much of the rehabilitation-engineering work presented in this thesis is the application of feedback control for control of FES-induced musculoskeletal motion or the control of an auxiliary electric drive used in some of the cycling systems. This chapter outlines the generic control approach used throughout the experimental work presented in this thesis.

- In Chapter 3, the state of the art in FES cycling is reviewed. The principles of this lower-limb FES application are described, and the major benefits are identified which are cardiovascular training by regular cycling exercise and the recreational use of mobile cycling. Existing apparatus for FES cycling are presented, including static ergometers and mobile systems. The concept of isokinetic and isotonic training devices is discussed in this context. The terms isotonic and isokinetic always refer in this work to the training devices and describe whether the muscular action by FES is performed against a piecewise constant resistance (load) or against a motor controlled constant cadence respectively. Chapter 3 also includes a discussion of reasons for the low performance and efficiency of FES cycling in comparison to cycling of able-bodied individuals. Recent approaches to optimise performance and efficiency are reviewed. Finally, a summary and the prospect of open research fields in FES cycling are given.

- Chapter 4 investigates the recreational use of mobile FES cycling. The results of a one year pilot study are described, in which regular periods of FES cycling (including mobile cycling) in paraplegic subjects were achieved. The design of FES cycling systems based on the adaptation of commercially available recumbent tricycles with optional motor assistance is presented. Realisation of isotonic and isokinetic training regimes for the developed cycling systems is discussed. Furthermore, it is shown how the stimulation patterns for cycling were obtained.

- In Chapter 5, a newly developed motorised FES ergometer system is described. The system can be used while sitting in a wheelchair. The overall design is based on a commercially available motorised ergometer, a newly designed stimulation device and an optional laptop computer. The operation and interaction of all components is discussed in detail. The focus of this chapter is on the motor control to realise both isotonic and isokinetic cycling regimes with the ergometer system. A repetitive control approach is introduced for the control of cadence during isokinetic cycling. Torque disturbances at the crank (e.g. by FES) which are periodic with respect to the cadence can be successfully eliminated by this repetitive controller.

- Chapter 6 is concerned with the control of the stimulation intensity during FES cycling in order to achieve a desired work rate (power output) of the cyclist. A well controlled work rate is

important to realise a prescribed training regime and for exercise testing. Work rate is defined as the product of cadence and active (muscularly produced) drive torque at the crank.
During isokinetic cycling, cadence is kept constant by the training device and the active drive torque has to be adjusted by electrical stimulation of the leg musculature to establish a desired work rate.
During isotonic training, a piecewise constant resistance (load) is realised by the device at the crank. The cadence is again kept constant, but by control of the electrically stimulated muscles. Due to this fact, work rate is adjusted by the selection of a suitable resistance.
Both cases (isotonic and isokinetic) are treated in this chapter and experimental results are presented.

Conclusions and recommendations for future work are given in the final chapter 7.

1.4 Contributions of the Thesis

Contributions focus on two areas, FES cycling and control of lower limb movement.

1.4.1 FES Lower-Limb Cycling

Development of FES Cycling Systems. New FES cycling systems have been developed. Two design approaches were realised. The first design approach is based on the adaptation of commercially available recumbent tricycles. This results in devices which can be used as static trainers (when mounted on a standard cycle trainer) or mobile devices. The tricycles offer a wide wheelbase option and a low centre of gravity for increased stability. Optionally, an auxiliary electric motor can be used to assist the cycling. The second design approach is based on a commercially available motorised ergometer, which was integrated with a newly developed stimulation device and laptop computer (optional). Use of the FES cycling ergometer is possible while sitting in a wheelchair which reduces the size of the system.
Both approaches (recumbent tricycles and ergometer) yield inexpensive systems which are useful for clinical and home use. Mobile FES cycling can be carried out with the recumbent tricycles for recreational use. The developed FES cycling systems can be operated in isotonic or isokinetic mode when used as static trainers. This represents a novelty compared to existing FES cycling systems. During isokinetic training, muscular action is performed at a constant pedalling cadence which is maintained by an electric motor. Constant resistance (load) is realised by the devices during isotonic cycling. The accurate control of the cadence and resistance as well as the provided measurements (angle, torque and cadence at the crank) make the systems suitable for research purposes.

Repetitive Control of Cadence during Isokinetic Training. Isokinetic FES cycle training is characterised by constant cycling cadence. Typically, a controlled electric motor assists or resists the

cycling movement to achieve this aim. The crank torque induced by the FES activated leg musculature represents a periodically changing disturbance with frequency components which are an integer of the cadence. Rejection of this disturbance is often inadequate and only feasible on average, as the available motor controllers (included in the motor electronics) has a limited bandwidth. To solve this problem, a repetitive controller design is introduced in this work which compensates any disturbance which is periodic with respect to the cadence. The repetitive controller can be plugged into an already existing feedback control loop.

Work Rate Control in FES Cycling. New methods for work rate control in isotonic and isokinetic FES cycling have been developed. These control design methods are based on polynomial methods. In the case of isokinetic training, the averaged active (muscularly produced) crank torque over one cycle is controlled by a self-tuning controller which adjusts the stimulation intensity. The reference torque is calculated from the desired power (work rate) and the given constant cadence. Controller parameters are calculated online on the basis of a recursively estimated model describing the relationship between muscle stimulation and torque.
In isotonic cycling ergometers, a desired work rate is established by setting a suitable piecewise constant resistance while a FES control algorithm attempts to maintain a constant cadence. A controller design based on a linear model of the stimulation intensity–cadence dynamics, which was identified off-line, is proposed for cadence control.
The feasibility of the new feedback control methods has shown in experiments.

Pilot Study on the Recreational Use of FES Cycling. The use of the developed FES tricycles has been investigated in a one year pilot study on FES cycling with three paraplegic subjects. This study also looked at the feasibility of mobile FES cycling and a possible recreational use. The results of this study are reported.

1.4.2 Modelling and Control of FES Induced Single Limb Movement

As part of the development of training regimes for paraplegic cycling, dynamic modelling and feedback control design approaches for the electrically-stimulated quadriceps muscle group under non-isometric conditions were investigated.
Before carrying out a functional task like FES cycling paraplegics usually undergo an exercise regime to strengthen and rebuild their paralysed muscles. This is often performed under non-isometric conditions while generating periodic movements (weight lifting exercise with the shank). Since optimal stimulation patterns are difficult to determine and dependent on subject and day, fixed patterns such as ramps are applied in clinical use and implemented open loop in available stimulation hardware. Such patterns have the drawback that changing muscle conditions due to fatigue and disturbances cannot be taken into account. Manual readjustment of the stimulation is therefore often necessary to avoid dangerous situations such as hyper-extension of the knee or an excessively rapid decline of the shank

from knee extension phases (which can cause muscle spasms), and to compensate for muscle fatigue. As already illustrated in Figure 1.4, FES, together with appropriate sensor and control technology, can provide useful, controlled movements. A weight lifting training with controlled FES of the quadriceps was therefore developed. The stimulation pattern is automatically adjusted by robust closed-loop control in order to generate a desired movement pattern. During a training session, the angle profile can be easily re-programmed while the desired movement can have an arbitrary shape over time. The linear polynomial controller design used is based on estimated linear models of the knee-joint dynamics [81]. Experimental system identification is carried out at the start of each training session. This procedure takes the day-to-day variation of the neuro-musculoskeletal system into account. Tests with paraplegic subjects show that robustness against changing muscle properties due to fatigue and external/internal disturbances is achieved while stability is guaranteed [83]. The achievable tracking performance of the controller is sufficient for the application (weight lifting exercise).

In order to shorten the time for controller design, a direct data-driven controller design has been investigated [73]. This controller design approach is directly based on open loop measured input-output data and fits the controller in such a way that the closed-loop meets a model reference objective. The use of this strategy, avoiding the system modelling step, significantly reduces the time required for controller design.

The author established further a method for the non-invasive in vivo identification of parametric models of the electrically stimulated quadriceps muscle group in paralysed individuals under non-isometric conditions [85]. This technique can be used to determine muscle parameter models for biomechanical computer simulations, model-based controller design and for real-time adaptive control and monitoring of muscle response variations such as fatigue.

In order to identify the muscle dynamics (relationship between stimulation pulsewidth and active knee moment) from discrete-time angle measurements only, a hybrid model structure is postulated for the shank-quadriceps dynamics. The model consists of a relatively well known time-invariant passive component and an uncertain time-variant active component. Rigid body dynamics, described by the Equation of Motion (EoM), and passive joint properties form the time-invariant part. The actuator, i.e. the electrically stimulated muscle group, represents the uncertain time-varying section. A recursive algorithm is outlined for identifying the stimulated quadriceps muscle group online. The algorithm requires EoM and passive joint characteristics to be known a priori. The muscle dynamics represent the product of a continuous-time nonlinear activation dynamics and a nonlinear static contraction function described by a Normalised Radial Basis Function (NRBF) network which has knee-joint angle and angular velocity as input arguments (modified Hill-type model). An Extended Kalman Filter (EKF) approach is chosen to estimate muscle dynamics parameters and to obtain full state estimates of the shank-quadriceps dynamics simultaneously. The latter is important for implementing real-time adaptive controllers in state-space form.

The results of this work on modelling and control of FES induced single limb movement have been published in peer reviewed journal and conference papers (included in full within this thesis).

The author's contribution to these publications consist of the controller design (complete for the linear control, partly for the direct data-driven control) and in the development of the identification method for the quadriceps muscle group. Furthermore, the author has been responsible for the development and implementation of the experimental software, the planning and execution of experiments, and the analysis and interpretation of the results.

1.5 Publications

The results presented in this thesis have previously been published, in part, as follows:

1. K.J. Hunt, M. Rothe, T. Schauer, A. Ronchi, and N.-O. Negård. Automatic speed control in FES cycling. In *Proc. of the 6th Annual Conference of the International Functional Electrical Stimulation Society (IFESS 2001)*, pages 300–302, Cleveland (Ohio), USA, June 2001.

2. K.J. Hunt, T. Schauer, N.-O. Negård, M.H. Fraser, and W. Stewart. A pilot study of lower-limb FES cycling in paraplegia. In *Proc. of the 7th Annual Conference of the International Functional Electrical Stimulation Society (IFESS 2002)*, pages 350–352, Ljubljana, Slovenia, June 2002.

3. K.J. Hunt, B. Stone, N.-O. Negård, T. Schauer, M.H. Fraser, A.J. Cathcart, C. Ferrario, S. Grant, and S.A. Ward. Control strategies for integration of electrical motor assist and functional electrical stimulation in paraplegic cycling: Utility for exercise testing and mobile cycling. *IEEE Trans. Neural Syst. Rehabil. Eng.*, 12(1):89–101, 2004.

4. T. Schauer, K.J. Hunt, N.-O. Negård, M.H. Fraser, and W. Stewart. Cadence control for recumbent cycling of paraplegics (in German). *at - Automatisierungstechnik*, 50(6):271–278, 2002.

5. T. Schauer, R. Salbert, N.-O. Negård, K. Hunt, and J. Raisch. Power control of electrical stimulation induced cycle ergometry (in German). *at - Automatisierungstechnik*, 53(12):607–614, 2005.

Original papers included in full within this thesis:

1. F. Previdi, T. Schauer, S.M. Savaresi, and K.J. Hunt. Data-driven control design for neuroprotheses: A virtual reference feedback tuning (VRFT) approach. *IEEE Transactions on Control System Technology*, 12(1):176–182, 2004. **This thesis: pp. 139–145.**

2. T. Schauer and K. Hunt. Linear modelling and controller design for the single limb movement of paraplegics using FES. In E. Carson and E. Salzsieder, editors, *Modelling and Control Biomedical Systems 2000 (Including Biological Systems): A Proceedings Volume from the 4th IFAC Symposium*, pages 7–12, Karlsburg/Greifswald, Germany, March-April 2000. Elsevier Science Ltd. **This thesis: pp. 146–151.**

3. T. Schauer, K.J. Hunt, A. Ronchi, M.H. Fraser, and W. Stewart. Robust control of knee-joint motion. In *Proc. of the 6th Annual Conference of the International Functional Electrical Stimulation Society (IFESS 2001)*, pages 232–234, Cleveland (Ohio), USA, June 2001. **This thesis: pp. 152–154.**

4. T. Schauer, N.-O. Negård, F. Previdi, K. J. Hunt, M.H. Fraser, E. Ferchland, and J. Raisch. Online identification and nonlinear control of the electrically stimulated quadriceps muscle. *Control Engineering Practice*, 13(9):1207–1219, 2005. **This thesis: pp. 155–167.**

2 Generic Controller Design

2.1 Summary

The purpose of this chapter is to introduce terminology, concepts and algorithms of the controller design which is used throughout the experimental work presented in this thesis. The design method used is based on the estimation of dynamic models of the system's input-output response. Experimental system identification [58] is applied to obtain linear discrete-time transfer function models from sampled input-output data. As the sampling frequency is typically limited by the stimulation frequency, a direct digital control design method is chosen. Physically- and physiologically-based modelling would represent an alternative to the experimental system identification used here. However, this would be difficult to perform for a specific individual as physiological parameters would need to be identified in vivo. The models obtained by this method would also be more complex and are often not suitable for direct controller design. Further model reduction steps might then be necessary.
The underlying control problems investigated in this thesis are

- cadence control of an ergometer, using either the stimulation intensity of the electrically stimulated muscles or the PWM duty cycle of the auxiliary electric motor as control signal, and
- torque/resistance control of an ergometer, again using either the stimulation intensity of the electrically stimulated muscles or the PWM duty cycle of the auxiliary electric motor as control signal.

Work rate control is also investigated in this thesis and leads to simultaneous control of cadence and torque on a ergometer. In this case, decoupling of the control loops can be achieved by using different time scales (frequency ranges) for both control loops.

The structure of this chapter is as follows. Section 2.2 describes the employed linear transfer function models. The design of the general two degree of freedom feedback controller and the analysis of the closed-loop behaviour are outlined in Section 2.3. In Section 2.4, repetitive control as a tool to cancel periodic disturbances is investigated. Periodic disturbances are particularly relevant in FES cycling in the form of periodic moment variations at the crank. Section 2.5 looks at the controller implementation with respect to the problem of controller output saturation. A summary and conclusions are given in Section 2.6.

2.2 Model Description

Dynamic processes which are investigated in Chapters 5 and 6 can be sufficiently well described as linear dynamic systems. In this section, a general linear discrete-time model structure is introduced from which all linear models used can be derived by simplifications. The system output $y(k)$ is the superposition of a deterministic model response $x(k)$ and an arbitrary noise signal $d(k)$ which represents the net effect of all disturbances as well as measurement noise. The argument k is the index of the sample.

By filtering the system input $u(k)$ through a linear pulse transfer function $H_p(q^{-1})$ the deterministic output component can be computed as follows

$$x(k) = H_p(q^{-1})u(k) = \frac{q^{-n_k}\mathsf{B}(q^{-1})}{\mathsf{A}(q^{-1})}u(k). \tag{2.1}$$

Here, $\mathsf{B}(q^{-1})$ and $\mathsf{A}(q^{-1})$ are polynomials in the delay operator q^{-1} ($q^{-1}f(k) = f(k-1)$):

$$\mathsf{B}(q^{-1}) = b_0 + b_1 q^{-1} + \cdots + b_{n_b} q^{-n_b} \tag{2.2}$$

$$\mathsf{A}(q^{-1}) = 1 + a_1 q^{-1} + \cdots + a_{n_a} q^{-n_a}. \tag{2.3}$$

The integer $n_k \geq 1$ describes an input-output time delay.

Filtering white noise $e(k)$ through a linear transfer function gives the signal $d(k)$:

$$d(k) = H_d(q^{-1})e(k) = \frac{\mathsf{C}(q^{-1})}{\mathsf{A}(q^{-1})\mathsf{D}(q^{-1})}e(k) \tag{2.4}$$

with $\mathsf{C}(q^{-1})$ and $\mathsf{D}(q^{-1})$ defined as

$$\mathsf{C}(q^{-1}) = c_0 + c_1 q^{-1} + \cdots + c_{n_c} q^{-n_c} \tag{2.5}$$

$$\mathsf{D}(q^{-1}) = 1 + d_1 q^{-1} + \cdots + d_{n_d} q^{-n_d}. \tag{2.6}$$

Thus, the system output is given as

$$y(k) = H_p(q^{-1})u(k) + H_d(q^{-1})e(k). \tag{2.7}$$

Figure 2.1 shows the resulting model. The transfer functions $H_p(q^{-1})$ and $H_d(q^{-1})$ are called the input transfer function and noise transfer function respectively.

By making special assumptions on the polynomials the model structures listed in Table 2.1 are obtained [58]. Some of these special model structures have been used.

Modelling Deterministic Disturbances

Deterministic disturbances can be characterised through the polynomial $\mathsf{D}(q^{-1})$. Table 2.2 shows typical classes of disturbances and the corresponding polynomial $\mathsf{D}(q^{-1})$. Often, the integrating term $(1 - q^{-1})$ is included in the plant's disturbance path to model the effect of stepwise-changing

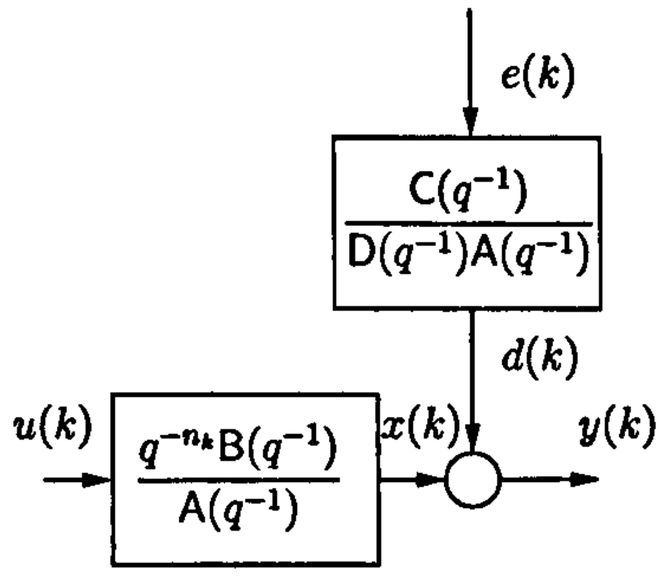

Figure 2.1: General model structure.

Table 2.1: Model structures used throughout the experimental work of this thesis.

Model structures	Model equations
ARX	$y(k) = q^{-n_k}\mathsf{B}(q^{-1})/\mathsf{A}(q^{-1})u(k) + 1/\mathsf{A}(q^{-1})e(k)$
ARARX	$y(k) = q^{-n_k}\mathsf{B}(q^{-1})/\mathsf{A}(q^{-1})u(k) + 1/(\mathsf{D}(q^{-1})\mathsf{A}(q^{-1}))e(k)$
ARMAX	$y(k) = q^{-n_k}\mathsf{B}(q^{-1})/\mathsf{A}(q^{-1})u(k) + \mathsf{C}(q^{-1})/\mathsf{A}(q^{-1})e(k)$
ARARMAX	$y(k) = q^{-n_k}\mathsf{B}(q^{-1})/\mathsf{A}(q^{-1})u(k) + \mathsf{C}(q^{-1})/(\mathsf{D}(q^{-1})\mathsf{A}(q^{-1}))e(k)$

(piecewise-constant) disturbances and offsets. The idealised assumption of piecewise constant disturbances approximates the true situation where some of the disturbances and system parameters are slowly time-varying.

Such nonstationary disturbances can be represented in the stochastic framework by considering $e(k)$ to be a compound or generalised Poisson process, i.e. a sequence consisting of random pulses of variable magnitude occuring at random times. See [41] for details.

Table 2.2: Signals $d(k)$ with corresponding polynomial $\mathsf{D}(q^{-1})$. Note that parameters a, b and c are arbitrary.

$d(k)$	$\mathsf{D}(q^{-1})$
a	$1 - q^{-1}$
$a + bk$	$(1 - q^{-1})^2$
$a + bk + ck^2$	$(1 - q^{-1})^3$
$a\sin(\omega k + b)$	$1 - 2\cos\omega q^{-1} + q^{-2}$
$d(k) = d(k - N)$	$1 - q^{-N}$

Notice that the normalised frequency $\omega := \omega \cdot t_s$ is used where t_s is the sampling time.

2.3 Two Degree of Freedom Controller

2.3.1 Controller Structure

A controller structure with two degrees of freedom has been chosen. This allows an individual adjustment of disturbance and command signal responses. Figure 2.2 depicts the control system structure. The controller equations are given by

$$\begin{aligned} y_v(k) &= \mathsf{S}_d(q^{-1})\, y(k) \\ u(k) &= \frac{1}{\mathsf{R}_d(q^{-1})} u_v(k) \\ u_v(k) &= \frac{1}{\overline{\mathsf{R}}(q^{-1})} \left(\frac{\mathsf{B}_t(q^{-1})}{\mathsf{A}_t(q^{-1})} r(k) - \overline{\mathsf{S}}(q^{-1}) y_v(k) \right) \end{aligned} \tag{2.8}$$

with the controller polynomials S_d, R_d, $\overline{\mathsf{S}}$, $\overline{\mathsf{R}}$, A_t and B_t in the delay operator q^{-1} and the reference $r(k)$. The signals $u_v(k)$ and $y_v(k)$ represent a new virtual system input and output respectively derived from the weighted original system input u and output y. By choosing appropriate weighting filters $\mathsf{S}_d(q^{-1})$ and $\mathsf{R}_d(q^{-1})$ the closed-loop behaviour with respect to disturbances and parameter changes can be influenced. Further, well damped stable system zeros and poles may be cancelled by including pre-defined factors in $\mathsf{R}_d(q^{-1})$ and $\mathsf{S}_d(q^{-1})$. Guidelines for choosing the polynomials $\mathsf{R}_d(q^{-1})$ and $\mathsf{S}_d(q^{-1})$ are given in the Sections 2.3.3 and 2.3.4. When designing the controller, first the filters S_d and R_d are fixed. In the next step, the polynomials $\overline{\mathsf{R}}$ and $\overline{\mathsf{S}}$ are calculated in order to guarantee a desired closed-loop behaviour, whereas stability is of course the least requirement. Having two degrees of freedom, one will choose initially $\overline{\mathsf{R}}$ and $\overline{\mathsf{S}}$ to fulfil the requirements on the disturbance signal response. After having finished this design step, the desired command signal response from the reference signal $r(k)$ to the output $y(k)$ is matched by determining the pre-filter $\mathsf{B}_t(q^{-1})/\mathsf{A}_t(q^{-1})$ for

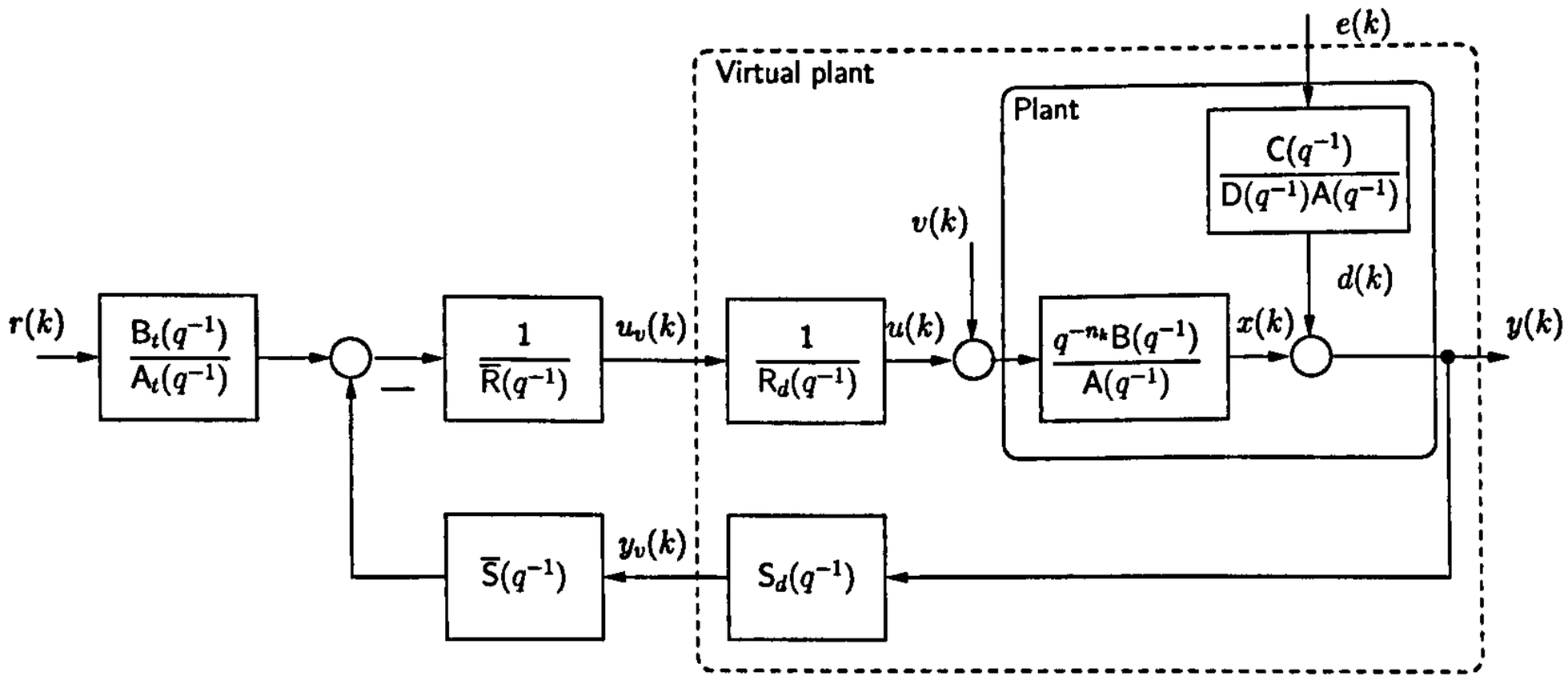

Figure 2.2: General controller structure.

a given reference model. Sections 2.3.5 and 2.3.6 outline the pole-placement method and the Linear Quadric Gaussian (LQG) controller design as two possible approaches for calculating the controller polynomials $\overline{\mathsf{R}}$ and $\overline{\mathsf{S}}$. In Section 2.3.7, the problem of reference model matching will be treated.

2.3.2 Closed-Loop Transfer Functions

The closed-loop equations for the system shown in Figure 2.2 are given by

$$y(k) = \underbrace{\frac{\overline{\mathsf{R}}\mathsf{R}_d\mathsf{A}}{\mathsf{A}_{cl}}}_{S(q^{-1})} d(k) + \underbrace{\frac{q^{-n_k}\mathsf{B}_t\mathsf{B}}{\mathsf{A}_t\mathsf{A}_{cl}}}_{T_r(q^{-1})} r(k) + \underbrace{\frac{q^{-n_k}\mathsf{B}\overline{\mathsf{R}}\mathsf{R}_d}{\mathsf{A}_{cl}}}_{S_v(q^{-1})} v(k) \tag{2.9}$$

$$u(k) = \underbrace{\frac{\overline{\mathsf{S}}\mathsf{S}_d\mathsf{A}}{\mathsf{A}_{cl}}}_{W(q^{-1})} d(k) + \frac{\mathsf{B}_t\mathsf{A}}{\mathsf{A}_t\mathsf{A}_{cl}} r(k) + \underbrace{\frac{\mathsf{A}\overline{\mathsf{R}}\mathsf{R}_d}{\mathsf{A}_{cl}}}_{W_v(q^{-1})} v(k) \tag{2.10}$$

$$x(k) = \underbrace{\frac{q^{-n_k}\overline{\mathsf{S}}\mathsf{S}_d\mathsf{B}}{\mathsf{A}_{cl}}}_{T(q^{-1})} d(k) + \frac{q^{-n_k}\mathsf{B}_t\mathsf{B}}{\mathsf{A}_t\mathsf{A}_{cl}} r(k) + \underbrace{\frac{q^{-n_k}\mathsf{B}\overline{\mathsf{R}}\mathsf{R}_d}{\mathsf{A}_{cl}}}_{S_v(q^{-1})} v(k). \tag{2.11}$$

The arguments indicating the delay operator in the polynomials have been dropped to simplify the presentation. All closed-loop transfer-functions share the characteristic polynomial A_{cl} given by

$$\mathsf{A}_{cl}(q^{-1}) = \overline{\mathsf{R}}(q^{-1})\mathsf{R}_d(q^{-1})\mathsf{A}(q^{-1}) + q^{-n_k}\overline{\mathsf{S}}(q^{-1})\mathsf{S}_d(q^{-1})\mathsf{B}(q^{-1}). \tag{2.12}$$

In the equations above, $S(q^{-1})$ and $T(q^{-1})$ are the output sensitivity function and the complementary output sensitivity function respectively. The former describes the effect of a net output disturbance $d(k)$ on the measurable system output $y(k)$ while the latter determines the effect of the output disturbance $d(k)$ on the output signal $x(k)$ which is not directly affected by disturbances and measurement noise. Noise sensitivity of the feedback system is analysed via the complementary sensitivity function $T(q^{-1})$ while the capability of rejecting deterministic output disturbances by the closed-loop system is studied via the sensitivity function $S(q^{-1})$. Furthermore, the transfer functions $W(q^{-1})$ and $T_r(q^{-1})$ describe the response of the control signal u on disturbances and the command signal response respectively. A feedback controller design focusing on output disturbances may not be optimal for input disturbances $v(k)$ entering the closed-loop before the plant. The closed-loop behaviour with respect to such input disturbances is determined by the input sensitivity function $S_v(q^{-1})$ and the transfer function $W_v(q^{-1})$.

It is assumed that disturbances are mainly acting at the output and the focus is therefore on analysing the output sensitivity function $S(q^{-1})$ and complementary output sensitivity function $T(q^{-1})$. Notice, that from the definition of $S(q^{-1})$ and $T(q^{-1})$ these functions are related by

$$T(q^{-1}) + S(q^{-1}) = 1. \tag{2.13}$$

This reveals the fundamental tradeoff between disturbance rejection and measurement noise effects. To reject disturbances $S(q^{-1})$ should be "small", and to make the output insensitive to measurement noise $T(q^{-1})$ should be also "small". This is cleary not possible due to the constraint (2.13). Making $S(q^{-1})$ small in frequency ranges where disturbances occur (usually low frequencies) while letting $S(q^{-1})$ grow in frequency ranges where measurement noise is known to predominate (usually high frequencies) is one possible solution to this problem in practice.

Stability of the closed-loop system is guaranteed if $\mathsf{A}_{cl}(q^{-1})$ has all its zeros inside the unit circle, i.e. $|\lambda_i| < 1$ where $\mathsf{A}(\lambda^{-1}) = 0$. The zeros of $\mathsf{A}_{cl}(q^{-1})$ are poles of the closed-loop system. Traditionally, poles and zeros of a discrete-time transfer function are defined for the forward shift operator representation. For this reason there may be further stable poles at the origin which are not showing up when looking only at $\mathsf{A}_{cl}(q^{-1})$. Consider the sensitivity function $S(q^{-1})$ for example. Converting it to the forward shift operator q format yields

$$\begin{aligned} S^*(q) &= \frac{\mathsf{N}^*_{s_y}(q)}{\mathsf{A}^*_{cl}(q)} = S(q^{-1})\frac{q^{\max(\deg \overline{\mathsf{R}}\mathsf{R}_d\mathsf{A},\deg \mathsf{A}_{cl})}}{q^{\max(\deg \overline{\mathsf{R}}\mathsf{R}_d\mathsf{A},\deg \mathsf{A}_{cl})}} \\ &= \frac{\overline{\mathsf{R}}(q^{-1})\mathsf{R}_d(q^{-1})\mathsf{A}(q^{-1})}{\mathsf{A}_{cl}(q^{-1})}\frac{q^{\max(\deg \overline{\mathsf{R}}\mathsf{R}_d\mathsf{A},\deg \mathsf{A}_{cl})}}{q^{\max(\deg \overline{\mathsf{R}}\mathsf{R}_d\mathsf{A},\deg \mathsf{A}_{cl})}}. \end{aligned} \tag{2.14}$$

There are then $(\max(\deg \overline{\mathsf{R}}\mathsf{R}_d\mathsf{A}, \deg \mathsf{A}_{cl}) - \deg(\mathsf{A}_{cl}))$ zeros of $\mathsf{A}^*_{cl}(q))$, i.e. poles of $S^*(q)$, located at the origin.

Stability is the most important property and the primary requirement on a control system. In practice it is often not enough that the system is stable. There must be some stability margins. Analogously to continuous-time systems, amplitude and phase margin can be defined. Both margins are inspired by Nyquist's stability criterion, which is based on the plot of the loop transfer function $L(q^{-1})$ given by

$$L(q^{-1}) = \frac{q^{-n_k}\overline{\mathsf{S}}(q^{-1})\mathsf{S}_d(q^{-1})\mathsf{B}(q^{-1})}{\overline{\mathsf{R}}(q^{-1})\mathsf{R}_d(q^{-1})\mathsf{A}(q^{-1})}. \tag{2.15}$$

An increase in open loop gain expands the Nyquist plot radially while an increase in open loop phase leads to a clockwise twist of the Nyquist plot. Figure 2.3 shows a Nyquist plot where ω_{180} is the smallest frequency where the phase lag of the open loop transfer function is 180 degree. The amplitude margin is then defined as

$$g_m = \frac{1}{|L(\mathrm{e}^{-j\omega_{180}})|}. \tag{2.16}$$

Further let the gain crossover frequency ω_{gc} be the smallest frequency such that

$$|L(\mathrm{e}^{-j\omega_{gc}})| = 1. \tag{2.17}$$

The phase margin is then defined as

$$\varphi_m = \pi + \arg(L(\mathrm{e}^{-j\omega_{gc}})). \tag{2.18}$$

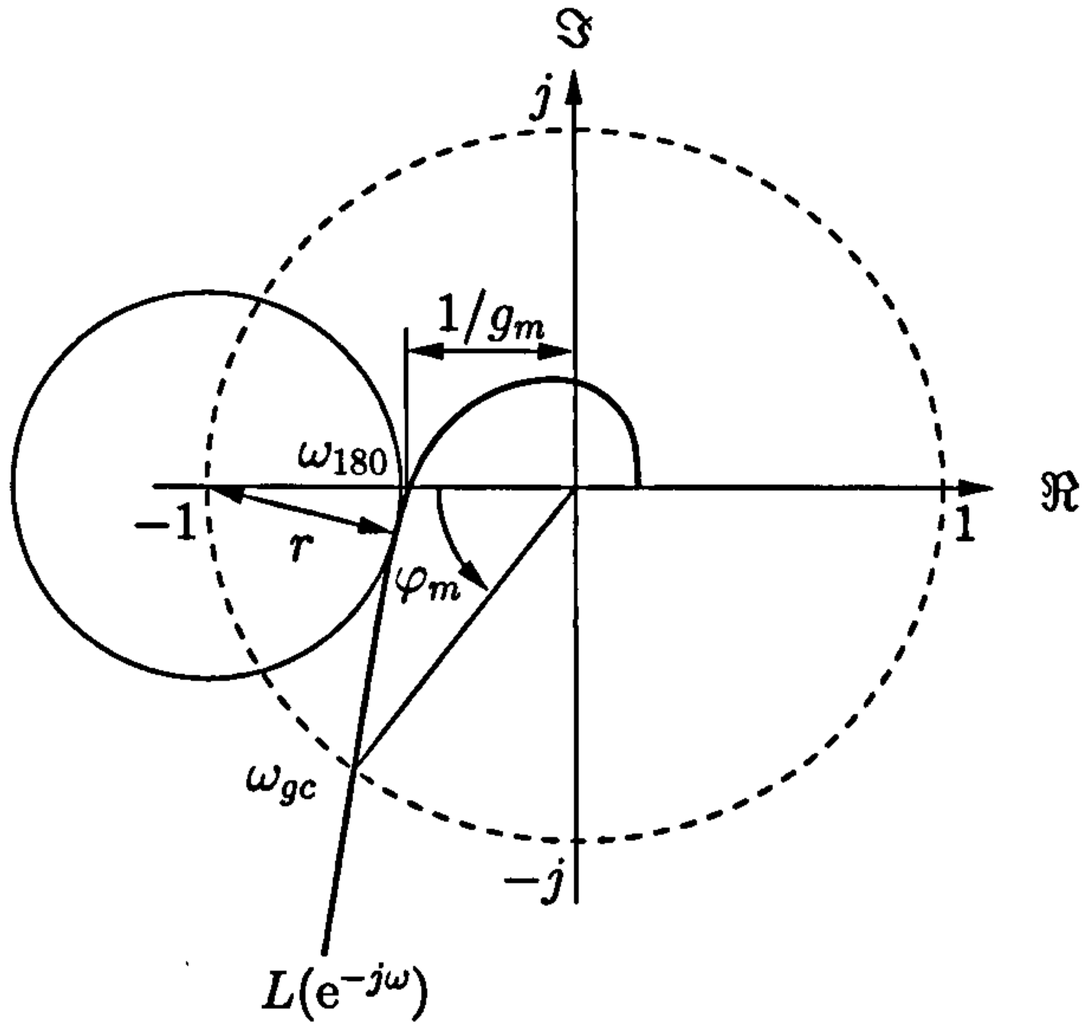

Figure 2.3: Nyquist plot of the open loop transfer function with stability margin $s_m = 1/r$, phase margin φ_m and amplitude margin g_m.

In words, the amplitude margin specifies the factor by which the open loop gain can be increased before the closed-loop system becomes unstable. The phase margin is a measure of how much extra phase lag is allowed before the closed-loop system becomes unstable. Phase loss is related to time delay. The phase margin can therefore be translated to a delay margin $d_m = \varphi_m/\omega_{ph}$.

A drawback with gain and phase margins is that it is necessary to give both of them in order to guarantee that the Nyquist curve is not close to the critical point. One way to express margins by a single number is the stability margin s_m, which is defined as the reciprocal of the smallest distance r from the Nyquist curve to the critical point. To obtain s_m the sensitivity function is rewritten as

$$S(q^{-1}) = \frac{1}{1 + \dfrac{q^{-n_k}\bar{\mathsf{S}}(q^{-1})\mathsf{S}_d(q^{-1})\mathsf{B}(q^{-1})}{\bar{\mathsf{R}}(q^{-1})\mathsf{R}_d(q^{-1})\mathsf{A}(q^{-1})}} = \frac{1}{1 + L(q^{-1})}. \tag{2.19}$$

Note that the complex number $1 + L(e^{-j\omega})$ can be represented as the vector from the point -1 to the point $L(e^{-j\omega})$ on the Nyquist curve. Consider the largest disc centred at -1 with a radius r such that the disc touches the Nyquist curve (cf. Fig. 2.3). Thus, the stability margin can be defined as

$$s_m = \max |S(\mathrm{e}^{-j\omega})| = \max \frac{1}{|1 + L(\mathrm{e}^{-j\omega})|} = \frac{1}{r}. \tag{2.20}$$

Guaranteed bounds on the margins g_m and φ_m are additionally given

$$g_m \geq 1/(1-r), \tag{2.21}$$

$$\varphi_m \geq 2\arcsin(r/2). \tag{2.22}$$

By requiring $s_m = \max|S(e^{-j\omega})| < 2$, the system will have at least the robustness margins $g_m \geq 2$ and $\varphi_m \geq 29°$. This represents a controller design objective applied throughout the thesis.

2.3.3 Cancellation of Plant Zeros and Poles

It is further assumed that the controller can cancel some of the plant poles and zeros. Assume that the polynomials $A(q^{-1})$ and $B(q^{-1})$ are factorised as $A(q^{-1}) = A^+(q^{-1})A^-(q^{-1})$ and $B(q^{-1}) = B^+(q^{-1})B^-(q^{-1})$ where $A^+(q^{-1})$ and $B^+(q^{-1})$ are the stable factors that will be cancelled. Because a process pole that is cancelled must be a controller zero and vice versa, the polynomials $R_d(q^{-1})$ and $S_d(q^{-1})$ must have the following structure

$$R_d(q^{-1}) = \bar{R}_d(q^{-1})B^+(q^{-1}), \tag{2.23}$$

$$S_d(q^{-1}) = \bar{S}_d(q^{-1})A^+(q^{-1}). \tag{2.24}$$

The characteristic polynomical is then

$$A_{cl}(q^{-1}) = B^+(q^{-1})A^+(q^{-1})\bar{A}_{cl}(q^{-1}) \tag{2.25}$$

$$\bar{A}_{cl}(q^{-1}) = \bar{R}(q^{-1})\bar{R}_d(q^{-1})A^-(q^{-1}) + q^{-n_k}\bar{S}(q^{-1})\bar{S}_d(q^{-1})B^-(q^{-1}) \tag{2.26}$$

where the polynomials $A^+(q^{-1})$ and $B^+(q^{-1})$ are thus factors of the closed-loop polynomial $A_{cl}(q^{-1})$. The cancelled factors must therefore correspond to stable modes. If this is not the case the system will have unstable modes that are unreachable or unobservable.

In practice, only well damped poles and zeros should be cancelled. Note that the cancellation of a badly damped pole-pair takes place in the output sensitivity function $S(q^{-1})$ but will not appear in the input sensitivity function $S_v(q^{-1})$ (see (2.9)-(2.11)). Hence, the input sensitivity function will show a nasty peak, revealing that an undamped response can be expected if a disturbance enters at the process input.

2.3.4 Disturbance Attenuation

The response to disturbances can be controlled by choosing the right factors $\bar{R}_d(q^{-1})$ and $\bar{S}_d(q^{-1})$ of the controller polynomials $R_d(q^{-1})$ and $S_d(q^{-1})$. In order to asymptotically eliminate the effect of disturbances on a closed-loop signal the transfer function from the disturbances to the closed-loop signal of interest must be stable and further must include a factor in the numerator polynomial which absorbs the disturbance. Including the right absorption polynomials into the controller is called the *internal model principle* [27]. Table 2.2 shows the absorption polynomials for some disturbance classes.

First, assume that a constant output disturbance $d(k) = a$ with an arbitrary constant a has to be eliminated from the output y. The transfer function from $d(k)$ to $y(k)$ is $(q^{-n_k}B\bar{R}\bar{R}_dA^+)/(A_{cl})$. Selecting $\bar{R}_d(q^{-1}) = 1 - q^{-1}$ will ensure that the constant disturbance is eliminated since

$$\bar{R}_d d(k) = (1 - q^{-1})d(k) = d(k) - d(k-1) = a - a = 0. \tag{2.27}$$

Thus, integral action ($\overline{\mathsf{R}}_d = 1 - q^{-1}$) is required for rejection of constant output disturbances (if the factor $(1 - q^{-1})$ is not already in $\mathsf{A}(q^{-1})$).

Consider next the example of a sinusoidal output disturbance $a\sin(\omega_s k + b)$ of frequency ω_s which is above the closed-loop bandwidth. The constants a and b are arbitrary. The design objective may be to reduce the effect of this disturbance on the control signal $u(k)$ and let the disturbance pass to the output $y(k)$ unaltered. Thus, the transfer function from $d(k)$ to $u(k)$ given by $(\mathsf{A}\overline{\mathsf{S}}\,\overline{\mathsf{S}}_d\mathsf{B}^+)/(\mathsf{A}_{cl})$ is of interest. Selecting $\overline{\mathsf{S}}_d(q^{-1}) = 1 - 2\cos(\omega_s)q^{-1} + q^{-2}$ yields absorption of the disturbance. The disturbance $a\sin(\omega_s k + b)$ satisfies the equation

$$\overline{\mathsf{S}}_d(q^{-1})d(k) = d(k) - 2\cos(\omega_s)d(k-1) + d(k-2) = 0 \tag{2.28}$$

which can be verified by a direct calculation.

2.3.5 Pole-Placement Controller Design

By feedback, the closed-loop poles can be changed in order to render the closed-loop system stable and to adapt the system's bandwidth. The polynomials $\overline{\mathsf{S}}(q^{-1})$ and $\overline{\mathsf{R}}(q^{-1})$ have to be determined within this process. Taking into account the pre-defined controller polynomials $\mathsf{R}_d(q^{-1})$ and $\mathsf{S}_d(q^{-1})$, the still-adjustable factor $\overline{\mathsf{A}}_{cl}(q^{-1})$ of the characteristic polynomial becomes

$$\overline{\mathsf{A}}_{cl}(q^{-1}) = \overline{\mathsf{R}}(q^{-1})\underbrace{\overline{\mathsf{R}}_d(q^{-1})\mathsf{A}^-(q^{-1})}_{\overline{\mathsf{A}}(q^{-1})} + \overline{\mathsf{S}}(q^{-1})\underbrace{\overline{\mathsf{S}}_d(q^{-1})q^{\mp n_k}\mathsf{B}^-(q^{-1})}_{\overline{\mathsf{B}}(q^{-1})} \tag{2.29}$$

$$\overline{\mathsf{A}}_{cl}(q^{-1}) = \overline{\mathsf{R}}(q^{-1})\overline{\mathsf{A}}(q^{-1}) + \overline{\mathsf{S}}(q^{-1})\overline{\mathsf{B}}(q^{-1}). \tag{2.30}$$

One way of calculating the controller polynomials is *pole placement* where a desired stable polynomial $\overline{\mathsf{A}}_{cl}(q^{-1})$ is specified and then the resulting Diophantine equation (2.30) is solved for $\overline{\mathsf{S}}(q^{-1})$ and $\overline{\mathsf{R}}(q^{-1})$.

A solution exists if the polynomials $\overline{\mathsf{A}}(q^{-1}) = \overline{\mathsf{R}}_d(q^{-1})\mathsf{A}^-(q^{-1})$ and $\overline{\mathsf{B}}(q^{-1}) = \overline{\mathsf{S}}_d(q^{-1})q^{-n_k}\mathsf{B}^-(q^{-1})$ are coprime, i.e. they have no common factors [57].

Equation (2.30) can be written as a system of equations by identifying the coefficients of equal powers of q^{-1}:

$$\sum_{i=0}^{k}\overline{a}_{k-i}\overline{r}_i + \sum_{i=0}^{k}\overline{b}_{k-i}\overline{s}_i = \overline{a}_{c_k}, \quad k = 0, \ldots, n \tag{2.31}$$

where $n = \max \deg \left[\overline{\mathsf{A}}\,\overline{\mathsf{R}}, \overline{\mathsf{B}}\,\overline{\mathsf{S}}\right]$, or in matrix form

$$n+1 \left\{ \underbrace{\begin{pmatrix} \overline{a}_0 & 0 & \cdots & \overline{b}_0 & 0 & \cdots \\ \overline{a}_1 & \overline{a}_0 & \cdots & \overline{b}_1 & \overline{b}_0 & \cdots \\ \vdots & \vdots & \ddots & \vdots & \vdots & \ddots \end{pmatrix}}_{\deg \overline{\mathsf{R}}+1 \qquad \deg \overline{\mathsf{S}}+1} \right. \begin{pmatrix} \overline{r}_0 \\ \vdots \\ \overline{s}_0 \\ \vdots \end{pmatrix} = \begin{pmatrix} \overline{a}_{cl_0} \\ \overline{a}_{cl_1} \\ \vdots \\ \overline{a}_{cl_n} \end{pmatrix}. \tag{2.32}$$

The matrix is invertible if there are as many independent equations as unknowns, i.e. if

$$n+1 = \deg \overline{\mathsf{R}} + \deg \overline{\mathsf{S}} + 2. \tag{2.33}$$

Two possibilities arise since $n = \max \deg[\overline{\mathsf{A}}\,\overline{\mathsf{R}}, \overline{\mathsf{B}}\,\overline{\mathsf{S}}]$. For $n = \max \deg[\overline{\mathsf{A}}\,\overline{\mathsf{R}}, \overline{\mathsf{B}}\,\overline{\mathsf{S}}] = \deg \overline{\mathsf{A}}\,\overline{\mathsf{R}}$ it follows from (2.33) that

$$\deg \overline{\mathsf{S}} = \deg \overline{\mathsf{A}} - 1 \tag{2.34}$$

and consequently that

$$\deg \overline{\mathsf{A}}\,\overline{\mathsf{R}} = \deg(\overline{\mathsf{A}}_{cl} - \overline{\mathsf{B}}\,\overline{\mathsf{S}}) = \max \deg[\overline{\mathsf{A}}_{cl}, \overline{\mathsf{B}}\,\overline{\mathsf{S}}]. \tag{2.35}$$

Subtracting $\overline{\mathsf{A}}$ and using (2.34) gives

$$\begin{aligned} \deg \overline{\mathsf{R}} &= \max[\deg \overline{\mathsf{A}}_{cl} - \deg \overline{\mathsf{A}}, \deg(\overline{\mathsf{B}}\,\overline{\mathsf{S}}) - \deg \overline{\mathsf{A}}] \\ &= \max[\deg \mathsf{A}_{cl} - \deg \mathsf{A}, \deg(\mathsf{B}\,\mathsf{A}) - 1 - \deg \mathsf{A}] \\ &= \max[\deg \overline{\mathsf{A}}_{cl} - \deg \overline{\mathsf{A}}, \deg \overline{\mathsf{B}} - 1] \end{aligned} \tag{2.36}$$

Analogously, we obtain for $n = \max \deg[\overline{\mathsf{A}}\,\overline{\mathsf{R}}, \overline{\mathsf{B}}\,\overline{\mathsf{S}}] = \deg \overline{\mathsf{B}}\,\overline{\mathsf{S}}$:

$$\deg \overline{\mathsf{R}} = \deg \overline{\mathsf{B}} - 1 \tag{2.37}$$

$$\deg \overline{\mathsf{S}} = \max[\deg \overline{\mathsf{A}}_{cl} - \deg \overline{\mathsf{B}}, \deg \overline{\mathsf{A}} - 1] \tag{2.38}$$

The two solutions coincide if $\deg \overline{\mathsf{A}}_{cl} \leq \deg \overline{\mathsf{A}} + \deg \overline{\mathsf{B}} - 1$ whereas the polynomial $\overline{\mathsf{A}}_{cl}$ is a design choice. Hence, a standard choice is

$$\deg \overline{\mathsf{A}}_{cl} \leq \deg \overline{\mathsf{A}} + \deg \overline{\mathsf{B}} - 1 \tag{2.39}$$

$$\deg \overline{\mathsf{R}} = \deg \overline{\mathsf{B}} - 1 \tag{2.40}$$

$$\deg \overline{\mathsf{S}} = \deg \overline{\mathsf{A}} - 1 \tag{2.41}$$

Note, in this case the closed-loop system has $(\deg \overline{\mathsf{A}} + \deg \overline{\mathsf{B}} - 1 + \deg \mathsf{A}^+ + \deg \mathsf{B}^+)$ poles. Choosing $\deg \overline{\mathsf{A}}_{cl} < \overline{\mathsf{A}} + \deg \overline{\mathsf{B}} - 1$ leads to $(\overline{\mathsf{A}} + \deg \overline{\mathsf{B}} - 1 - \deg \overline{\mathsf{A}}_{cl})$ stable poles placed at the origin. The simple choice $\deg \overline{\mathsf{A}}_{cl} = 1$ results in $\deg \overline{\mathsf{A}} + \deg \overline{\mathsf{B}} - 1$ poles placed at the origin. Guidelines for specifying $\overline{\mathsf{A}}_{cl}$ are given in Section 2.3.8.

2.3.6 Linear Quadratic Gaussian Controller Design

Instead of specifying the closed-loop poles by hand the feedback controller and with it the closed-loop poles can be determined by minimising a cost function. The optimisation cost function J is chosen to allow a simple tradeoff between virtual output variance and virtual control effort. A suitable cost function to achieve this aim is

$$\begin{aligned} J &= \mathcal{E}\left\{y_v(k)^2 + \rho u_v(k)^2\right\} \\ &= \mathcal{E}\left\{\left(\mathsf{S}_d(q^{-1})y(k)\right)^2 + \rho\left(\mathsf{R}_d(q^{-1})u(k)\right)^2\right\} \end{aligned} \tag{2.42}$$

where is $\mathcal{E}$ the expectation operator and $\rho > 0$ is a tunable control weight.
The solution of the optimal control problem is summarised in the following theorem:

Theorem 2.3.1 *[41, 57] The optimal control problem (2.42) has a solution if and only if*

(C1) the polynomials $\mathsf{A}(q^{-1})\mathsf{R}_d(q^{-1})$ *and* $\mathsf{B}(q^{-1})\mathsf{S}_d(q^{-1})$ *have no unstable common factors and*

(C2) any unstable factors of $\mathsf{D}(q^{-1})$ *are also factors of* $\mathsf{R}_d(q^{-1})$ *or* $\mathsf{B}(q^{-1})\mathsf{S}_d(q^{-1})$.

The polynomials $\overline{\mathsf{R}}(q^{-1})$ *and* $\overline{\mathsf{S}}(q^{-1})$ *(along with* $\mathsf{X}(q^{-1})$*) are the solution having the property*

$$(\mathsf{D}_c(q)q^{-g})^{-1}\mathsf{X}(q^{-1}) \textit{strictly proper} \tag{2.43}$$

of the polynomial equations

$$q^{-g}\mathsf{D}_c(q)\overline{\mathsf{S}}(q^{-1}) + \mathsf{X}(q^{-1})\mathsf{A}(q^{-1})\mathsf{R}_d(q^{-1}) = q^{-g}q^{n_k}\mathsf{B}(q)\mathsf{S}_d(q)\mathsf{C}(q^{-1}) \tag{2.44}$$

$$q^{-g}\mathsf{D}_c(q)\overline{\mathsf{R}}(q^{-1}) - \mathsf{X}(q^{-1})q^{-n_k}\mathsf{B}(q^{-1})\mathsf{S}_d(q^{-1}) = \rho q^{-g}\mathsf{A}(q)\mathsf{R}_d(q)\mathsf{C}(q^{-1}), \tag{2.45}$$

where $g > 0$ *is the smallest integer which makes the equations polynomial in* q^{-1}. *The Hurwitz spectral factor* $\mathsf{D}_c(q^{-1})$ *is defined by the spectral factorisation*

$$\mathsf{D}_c(q^{-1})\mathsf{D}_c(q) = \mathsf{B}(q^{-1})\mathsf{S}_d(q^{-1})\mathsf{S}_d(q)\mathsf{B}(q) + \rho\mathsf{A}(q^{-1})\mathsf{R}_d(q^{-1})\mathsf{R}_d(q)\mathsf{A}(q). \tag{2.46}$$

Note that when the common polynomial $\mathsf{X}(q^{-1})$ is eliminated between (2.44) and (2.45), the implied linear equation arises

$$\mathsf{A}(q^{-1})\mathsf{R}_d(q^{-1})\overline{\mathsf{R}}(q^{-1}) + q^{-n_k}\mathsf{B}(q^{-1})\mathsf{S}_d(q^{-1})\overline{\mathsf{S}}(q^{-1}) = \mathsf{D}_c(q^{-1})\mathsf{C}(q^{-1}) = \mathsf{A}_{cl}(q^{-1}). \tag{2.47}$$

The conditions under which this single equation may be used to generate the unique optimal controller are summarised by the following theorem:

Theorem 2.3.2 *[42] The optimal controller polynomials* $\overline{\mathsf{R}}(q^{-1})$ *and* $\overline{\mathsf{S}}(q^{-1})$ *are uniquely determined by the implied equation (2.47) if and only if*

(C3) The system $\mathsf{C}(q^{-1})/\mathsf{A}(q^{-1})$ *is proper;*

(C4) $\mathsf{A}(q^{-1})\mathsf{R}_d(q^{-1})$ *and* $\mathsf{B}(q^{-1})\mathsf{S}_d(q^{-1})$ *are coprime.*

The unique solution has the property $(\mathsf{R}_d(q^{-1})\mathsf{A}(q^{-1}))^{-1}\overline{\mathsf{R}}(q^{-1})$ *strictly proper.*

Note that condition (C4) does not hold for pole-zero cancellations.

It is clear from (2.47) that the closed-loop poles are defined by both the polynomials $\mathsf{D}_c(q^{-1})$ and $\mathsf{C}(q^{-1})$. Sometimes it is hard to identify a meaningful polynomial $\mathsf{C}(q^{-1})$ from data. As an alternative, $\mathsf{C}(q^{-1})$ may be seen as a design choice in order to place some of the closed-loop poles. Poles related to $\mathsf{C}(q^{-1})$ correspond to observer poles in the state-space design. The degree of the polynomial $\mathsf{C}(q^{-1})$ should be chosen as follows

$$\deg \mathsf{C}(q^{-1}) \leq \deg\left(\mathsf{A}(q^{-1})\mathsf{R}_d(q^{-1})\right) + \deg\left(q^{-n_k}\mathsf{B}(q^{-1})\mathsf{S}_d(q^{-1})\right) - 1 - \deg\left(\mathsf{D}_c(q^{-1})\right). \quad (2.48)$$

2.3.7 Reference Model Matching

A desired command signal response (tracking performance) can be specified by the introduction of a reference model:

$$y_r(k) = H_r(q^{-1})r(k) \quad (2.49)$$

where y_r is the desired output response. The output y of the closed-loop system is described by Equation (2.9). This yields the model matching problem

$$T_r(q^{-1}) \equiv H_r(q^{-1}). \quad (2.50)$$

Thus $y(k) = y_r(k), \forall k$ when (2.50) is fulfilled and $H_d(q^{-1})e(k) = 0$.

The following reference model is chosen

$$H_r(q^{-1}) = (\mathsf{A}_r(1)/\mathsf{B}^-(1))\frac{q^{-n_k}\mathsf{B}^-(q^{-1})}{\mathsf{A}_r(q^{-1})}, \quad (2.51)$$

where $\mathsf{A}_r(q^{-1})$ specifies the desired poles of $H_r(q^{-1})$ and the factor $(\mathsf{A}_r(1)/\mathsf{B}^-(1))$ ensures unity gain. $\mathsf{B}^-(q^{-1})$ contains the factors of the plant's numerator polynomial $\mathsf{B}(q^{-1})$ which have not been cancelled by the controller. The model matching requirement (2.50) then becomes

$$\frac{q^{-n_k}\mathsf{B}_t(q^{-1})\mathsf{B}(q^{-1})}{\mathsf{A}_t(q^{-1})\mathsf{A}_{cl}(q^{-1})} = \frac{q^{-n_k}\mathsf{B}_t(q^{-1})\mathsf{B}^-(q^{-1})}{\mathsf{A}_t(q^{-1})\overline{\mathsf{A}}_{cl}(q^{-1})\mathsf{A}^+(q^{-1})} \equiv (\mathsf{A}_r(1)/\mathsf{B}^-(1))\frac{\mathsf{q}^{-n_k}B^-(q^{-1})}{\mathsf{A}_r(q^{-1})} \quad (2.52)$$

which results in the following pre-filter

$$\frac{\mathsf{B}_t(q^{-1})}{\mathsf{A}_t(q^{-1})} = \frac{\overline{\mathsf{A}}_{cl}(q^{-1})\mathsf{A}^+(q^{-1})}{\mathsf{A}_r(q^{-1})}(\mathsf{A}_r(1)/\mathsf{B}^-(1)). \quad (2.53)$$

Notice that the closed-loop poles related to the polynomial $(\overline{\mathsf{A}}_{cl}(q^{-1})\mathsf{A}^+(q^{-1}))$ are cancelled in $T_r(q^{-1})$ but not in the output sensitivity function $S(q^{-1})$ and complementary output sensitivity function $T(q^{-1})$.

Therefore, a separation of the disturbance and command signal responses is possible.

A special case occurs if the polynomial $\mathsf{A}_r(q^{-1})$ is already a factor of the characteristic closed-loop polynomial A_{cl}. This can be achieved by choosing $\overline{\mathsf{A}}_{cl} = \mathsf{A}_r(q^{-1})\mathsf{A}_o(q^{-1})$ during the pole-placement design. Notice that under this condition the pre-filter renders to

$$\frac{\mathsf{B}_t(q^{-1})}{\mathsf{A}_t(q^{-1})} = \frac{\mathsf{A}_o(q^{-1})\mathsf{A}^+(q^{-1})(\mathsf{A}_r(1)/\mathsf{B}^-(1))}{1}. \tag{2.54}$$

where only the poles related to $\mathsf{A}_o(q^{-1})$ are cancelled by the pre-filter. However, the reference model poles are in this case also poles of the closed-loop transfer functions $S(q^{-1})$ and $T(q^{-1})$. Hence, there is no longer perfect separation of tracking and disturbance rejection.

2.3.8 Controller Performance Specification and General Design Steps

In the previous sections, polynomials had to be specified in order to place the poles of the closed-loop system and of the reference model. Adjustable closed-loop poles are related to $\overline{\mathsf{A}}_{cl}(q^{-1})$ in the pole-placement design and $\mathsf{C}(q^{-1})$ in the LQG design if necessary. The poles of the reference model are determined through the polynomial $\mathsf{A}_r(q^{-1})$.

The polynomials can be easily specified by first or second-order systems with given time-domain properties. For first order systems (polynomials of degree one) the rise time is used as a property yielding the corresponding polynomial

$$1 - \mathrm{e}^{-T_s/t_r}q^{-1} \tag{2.55}$$

in the operator q^{-1}. Again, the property rise time t_r and additionally damping are chosen to specify second-order systems, i.e. polynomials of degree two. Within this work, the desired damping factor is unity (critical damping) and only the rise time t_r must be specified. Having this constraint, the number of design parameters is kept small. A continuous-time second-order system $s^2 + 2\omega_0 s + \omega_0^2$ (represented using the Laplace operator s) with $\omega_0 = 3.2/t_r$ is then equivalent to the discrete-time representation

$$1 - 2\mathrm{e}^{-\omega_0 T_s}q^{-1} + \mathrm{e}^{-2\omega_0 T_s}q^{-2}. \tag{2.56}$$

Often, the maximal possible degree of $\overline{\mathsf{A}}_{cl}(q^{-1})$ or $\mathsf{C}(q^{-1})$ is not fully used by choosing first or second order polynomials. In this case, there will be additional stable closed-loop poles located at the origin. The entire dynamics is then dominated by the poles specified via the first or second order systems.

The controller design procedure can be summarised in the following steps

1. Identify a transfer function model by means of parameter identification methods from experimental data to obtain n_k, $\mathsf{B}(q^{-1})$ and $\mathsf{A}(q^{-1})$.

2. Decide if stable well damped poles and zeros shall be cancelled by the controller (cf. Section 2.3.4); if necessary, specify factors $\mathsf{A}^+(q^{-1})$ and $\mathsf{B}^+(q^{-1})$ in $\mathsf{S}_d(q^{-1})$ and $\mathsf{R}_d(q^{-1})$ respectively.

3. Discover the major disturbances and their frequency ranges in order to select suitable controller polynomials $\overline{\mathsf{R}}_d(q^{-1})$ and $\overline{\mathsf{S}}_d(q^{-1})$ for disturbance and noise rejection (cf. Section 2.3.4).

4. Decide for a preferred controller design method:

   a) **Pole-Placement**

      i. Check the maximal possible degree of $\overline{\mathsf{A}}_{cl}(q^{-1})$ using (2.39).

      ii. Choose between

         A. *Complete separation of command signal response and disturbance rejection response:* Select a first or second order polynomial $\overline{\mathsf{A}}_{cl}(q^{-1})$ depending on the possible degree by means of the rise time $t_r^{\overline{\mathsf{A}}_{cl}}$.

         B. *Incomplete separation of command signal response and disturbance and rejection response:* Select the polynomials $\mathsf{A}_r(q^{-1})$ and $\mathsf{A}_o(q^{-1})$ by rise times $t_r^{\mathsf{A}_r}$ and $t_r^{\mathsf{A}_o}$ respectively while ensuring that $\overline{\mathsf{A}}_{cl}(q^{-1}) = \mathsf{A}_r(q^{-1})\mathsf{A}_o(q^{-1})$ has suitable degree.

      iii. Solve the Diophantine equation (2.30) for the controller polynomials $\mathsf{R}(q^{-1})$ and $\mathsf{S}(q^{-1})$.

   b) **Linear Quadratic Gaussian (LQG) control**

      i. Choose the weight ρ and perform the spectral factorisation (2.46).

      ii. Specify the polynomial $\mathsf{C}(q^{-1})$ via the rise time t_r^{C} and check the maximal possible degree of $\mathsf{C}(q^{-1})$ using (2.48).

      iii. Solve the single linear implied equation (2.47) if the conditions of Theorem 2.3.2 are fulfilled, otherwise use Theorem 2.3.1 to determine the controller polynomials $\overline{\mathsf{R}}(q^{-1})$ and $\overline{\mathsf{S}}(q^{-1})$

5. Evaluate the output sensitivity function $S(q^{-1})$ and the complementary output sensitivity function $T(q^{-1})$ following the guidelines of Section 2.3.4. If necessary, choose new design parameters and return to Step 4. The Tables 2.3 to 2.5 show the influence of the tuning parameters for the different design methods.

6. Deal with the command signal response:

   a) Use the reference model (2.51) and specify (if not already done in Step 4) the polynomial $\mathsf{A}_r(q^{-1})$ by the rise time $t_r^{\mathsf{A}_r}$.

   b) Calculate the pre-filter $\mathsf{B}_t(q^{-1})/\mathsf{A}_t(q^{-1})$ by Equation (2.53) if $\mathsf{A}_r(q^{-1})$ is not a factor of $\overline{\mathsf{A}}_{cl}(q^{-1})$, otherwise use Equation (2.54).

Table 2.3: LQG controller design: Influence of the tuning parameters on the closed-loop behaviour ($\mathsf{A}_r(q^{-1})$ is not a factor of $\overline{\mathsf{A}}_{cl}(q^{-1})$; using (2.53) to design the pre-filter).

	Command response	Disturbance rejection	Noise sensitivity
$\rho \downarrow$	-	better	worse
$\rho \uparrow$	-	worse	better
$t_r^{\mathsf{C}} \downarrow$	-	better	worse
$t_r^{\mathsf{C}} \uparrow$	-	worse	better
$t_r^{\mathsf{A}_r} \downarrow$	faster	-	-
$t_r^{\mathsf{A}_r} \uparrow$	slower	-	-

Table 2.4: Pole-placement design: Influence of the tuning parameters on the closed-loop behaviour ($\mathsf{A}_r(q^{-1})$ is a factor of $\overline{\mathsf{A}}_{cl}(q^{-1})$; using (2.54) to design the pre-filter).

	Command response	Disturbance rejection	Noise sensitivity
$t_r^{\mathsf{A}_o} \downarrow$	-	better	worse
$t_r^{\mathsf{A}_o} \uparrow$	-	worse	better
$t_r^{\mathsf{A}_r} \downarrow$	faster	better	worse
$t_r^{\mathsf{A}_r} \uparrow$	slower	worse	better

Table 2.5: Pole-placement design: Influence of the tuning parameters on the closed-loop behaviour ($\mathsf{A}_r(q^{-1})$ is not a factor of $\overline{\mathsf{A}}_{cl}(q^{-1})$; using (2.53) to design the pre-filter).

	Command response	Disturbance rejection	Noise sensitivity
$t_r^{\overline{\mathsf{A}}_{cl}} \downarrow$	-	better	worse
$t_r^{\overline{\mathsf{A}}_{cl}} \uparrow$	-	worse	better
$t_r^{\mathsf{A}_r} \downarrow$	faster	-	-
$t_r^{\mathsf{A}_r} \uparrow$	slower	-	-

2.4 Plug-In Repetitive Controller

The term repetitive control is used to describe control algorithms designed to cancel errors which are periodic in time. Such disturbances occur in FES cycling, typically in cadence control problems. The weight of the legs as well as the cyclic stimulation of the leg musculature cause periodic moment variations at the crank. The internal model principle introduced in Section 2.3.4 can be used to handle disturbances with a period of N sample instants.

Including the polynomial $(1-q^{-N})$ in $\mathsf{R}_d(q^{-1})$ causes the rejection of the periodic disturbance at the system output $y(k)$ since

$$(1-q^{-N})d(k) = d(k) - d(k-N) = 0. \tag{2.57}$$

When N is large, it is difficult to determine a good feedback controller with the design procedure

outlined in Section 2.3. Tomizuka et al. [94] propose a strategy where first a feedback controller is designed without special consideration for the repetitive nature of the disturbance; instead the designer can concentrate his effort on other aspects like robustness and noise rejection, for example. Next, a plug-in controller $\mathsf{B}_{rc}(q^{-1})/\mathsf{A}_{rc}(q^{-1})$ as shown in Figure 2.4 is determined which asymptotically rejects periodic disturbances with known period N for the already-controlled servo system by observing the error $e_{rc}(k)$ and injecting the control signal $u_{rc}(k)$.

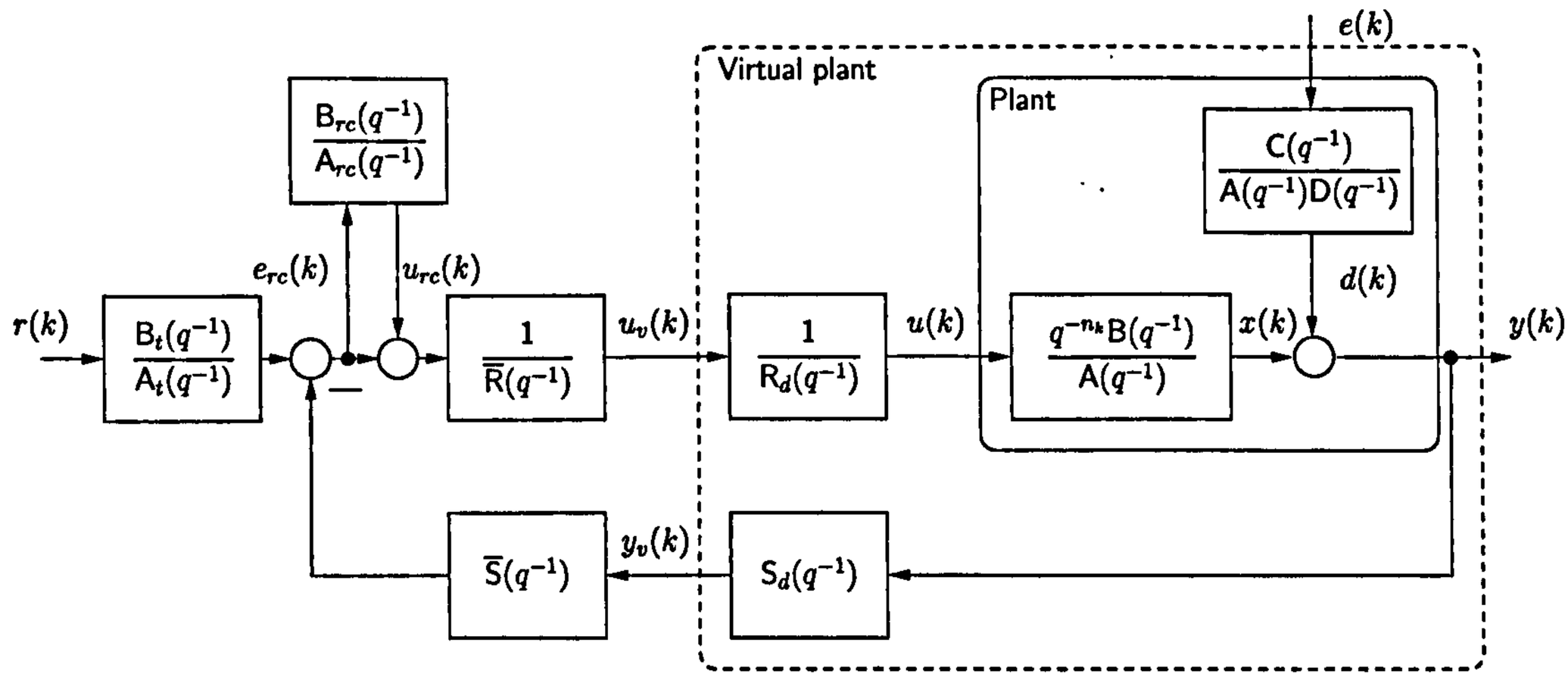

Figure 2.4: Plug-In repetitive control scheme.

The system seen by the repetitive controller is given by

$$\frac{e_{rc}(k)}{u_{rc}(k)} = \frac{q^{-n_k}\bar{\mathsf{S}}(q^{-1})\mathsf{S}_d(q^{-1})\mathsf{B}(q^{-1})}{\bar{\mathsf{R}}(q^{-1})\mathsf{R}_d(q^{-1})\mathsf{A}(q^{-1}) + q^{-n_k}\bar{\mathsf{S}}(q^{-1})\mathsf{S}_d(q^{-1})\mathsf{B}(q^{-1})} \tag{2.58}$$

$$= \frac{q^{-n_k}\mathsf{B}_p(q^{-1})}{\mathsf{A}_p(q^{-1})}. \tag{2.59}$$

Tomizuka et al. [94] proposed the following prototype repetitive controller

$$\frac{\mathsf{B}_{rc}(q^{-1})}{\mathsf{A}_{rc}(q^{-1})} = \frac{k_r q^{-N+n_k}\mathsf{A}_p(q^{-1})\mathsf{B}_p^-(q)}{(1-q^{-N})b\mathsf{B}_p^+(q^{-1})} \tag{2.60}$$

$$k_r \in (0,2) \tag{2.61}$$

$$b \leq \max|\mathsf{B}_p^-(\mathrm{e}^{-j\omega})|^2 \tag{2.62}$$

$$\omega \in [0,\pi]$$

where k_r is the repetive control gain, and $\mathsf{B}_p^+(q^{-1})$ and $\mathsf{B}_p^-(q^{-1})$ are cancellable and uncancellable parts of $\mathsf{B}_p(q^{-1})$. The term $\mathsf{B}^-(q)$ cancels the phase shift resulting from uncancellable zeros. The following choice of b will satisfy condition (2.62):

$$b = \left(|b_{p_0}| + |b_{p_1}| + \cdots + |b_{p_m}|\right)^2. \tag{2.63}$$

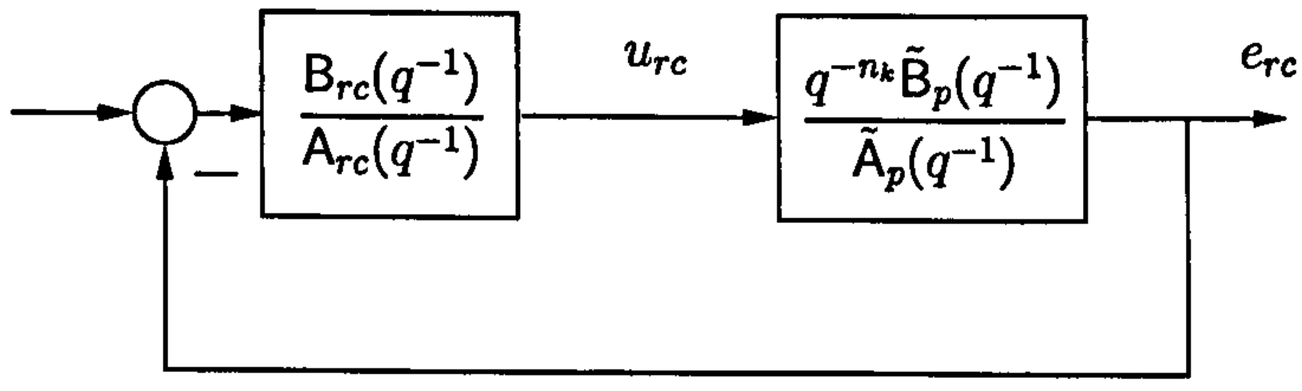

Figure 2.5: Repetitive control system.

The repetitive system with equations (2.59) and (2.60) is then asymptotically stable for $0 < k_r < 2$.

With the plug-in repetitive controller (2.60) the output sensitivity function becomes

$$\frac{y(k)}{d(k)} = S(q^{-1}) = \frac{A_{rc}R_d\bar{R}A}{R_d\bar{R}AA_{rc} + q^{-n_k}BS_d\bar{S}\,(A_{rc} + B_{rc})}. \tag{2.64}$$

The complementary output sensitivity function $T(q^{-1})$ is then given by

$$\frac{x(k)}{d(k)} = T(q^{-1}) = \frac{q^{-n_k}\,(A_{rc} + B_{rc})\,S_d\bar{S}B}{R_d\bar{R}AA_{rc} + q^{-n_k}BS_d\bar{S}\,(A_{rc} + B_{rc})}. \tag{2.65}$$

The transfer function $S(q^{-1})$ will be zero at the repetitive frequencies $\pm i2\pi/N$, $i = 0, 1, 2, \ldots N/2$ while $T(q^{-1})$ will be unity. Such a closed-loop system will be sensitive to modelling errors. Therefore, a modified repetitive controller with an asymptotically stable filter $Q(q^{-1})$ with $|Q(e^{-j\omega})| \leq 1$ was introduced by K.K. Chew and M. Tomizuka [55]:

$$\frac{B_{rc}(q^{-1})}{A_{rc}(q^{-1})} = \frac{k_r q^{-N+n_k} Q(q^{-1})A_p(q^{-1})B_p^-(q)}{(1 - Q(q^{-1})q^{-N})bB_p^+(q^{-1})} \tag{2.66}$$

In general, $Q(q^{-1})$ sacrifices high-frequency regulation for stability. The repetitive control system is shown in Figure 2.5. Notice that the system transfer function in Figure 2.5 differs from the one in Equation (2.60) to account for modelling errors. From the small-gain-theorem, the feedback system is stable if

$$\left| -\frac{B_{rc}(e^{-j\omega})}{A_{rc}(e^{-j\omega})} \cdot \frac{e^{-j\omega n_k}\tilde{B}_p(e^{-j\omega})}{\tilde{A}_p(e^{-j\omega})} \right| < 1,\ \omega \in [0, \pi]. \tag{2.67}$$

After some transformations and using (2.66) it follows that

$$\left| 1 - k_r \frac{A_p(e^{-j\omega})B_p^-(e^{j\omega})}{bB_p^+(e^{-j\omega})} \cdot \frac{\tilde{B}_p(e^{-j\omega})}{\tilde{A}_p(e^{-j\omega})} \right| < \left| \frac{1}{Q(e^{-j\omega})} \right|,\ \omega \in [0, \pi]. \tag{2.68}$$

Figure 2.6 shows the right hand side of Equation (2.68), i.e. the stability boundary, for two choices of $Q(q^{-1})$. Under conditions of no modelling error, the left hand side of (2.68) is smaller than unity for $0 < k_r < 2$ and the inequality holds for either choice of $Q(q^{-1})$. The stability region is extremely

large when $\mathsf{Q}_2(q^{-1}) = (q + 2 + q^{-1})/4$ is utilised with the price that high frequency regulation is worse. The choice of $\mathsf{Q}(q^{-1})$ depends on how precisely the system is modelled.

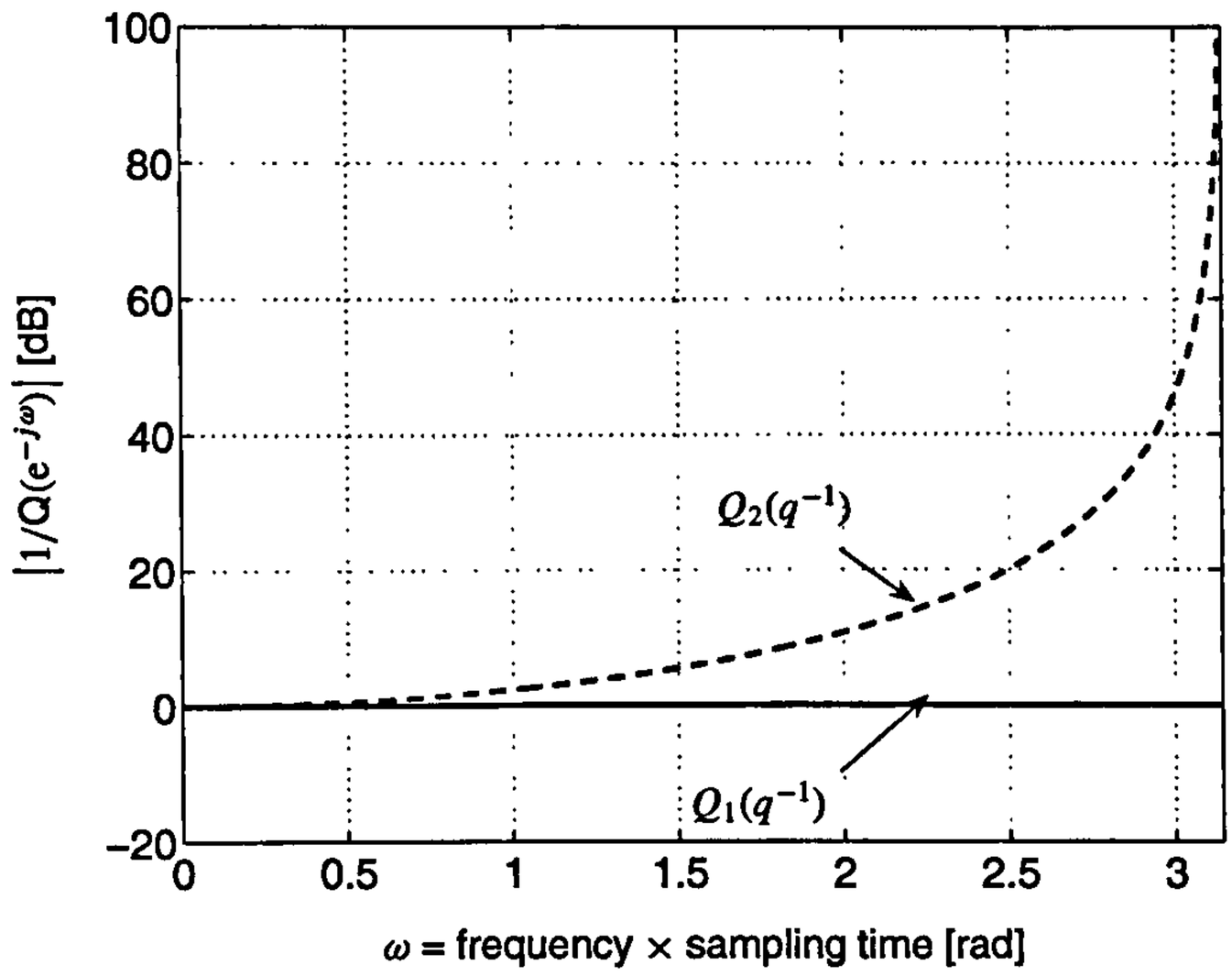

Figure 2.6: Stability bounds for modified repetitive control system ($\mathsf{Q}_1(q^{-1}) = 1, \mathsf{Q}_2(q^{-1}) = (q + 2 + q^{-1})/4$)

The design procedure for the plug-in repetitive controller can be summarized in the following steps:

1. Given data: n_k, $\mathsf{B}_p(q^{-1})$, $\mathsf{A}_p(q^{-1})$. Choose design parameter k_r and $\mathsf{Q}(q^{-1})$
2. Compute $\mathsf{B}_p^+(q^{-1})$, $\mathsf{B}_p^-(q)$ and b
3. Form the robust repetitive controller (2.66)
4. Evaluate the new closed-loop transfer functions $S(q^{-1})$ (2.64) and $T(q^{-1})$ (2.65); If necessary, choose new design parameters and return to Step 1.

An increase in the parameter k_r gives faster rejection of periodic disturbances while sensitivity to modelling errors and measurement noise worsens.

2.5 Implementation Issues

The controller presented in Section 2.3 as well as its extension with the plug-in repetitive controller of Section 2.4 can be brought into the compact form

$$u(k) = \frac{1}{\mathsf{R}(q^{-1})}\left(-\mathsf{S}(q^{-1}y(k) + \mathsf{T}(q^{-1})r(k)\right) \tag{2.69}$$

which is depicted in Figure 2.7. This controller configuration will be called an RST-controller in the sequel. The RST-controller polynomials for the controller without plug-in repetitive controller are given by

$$\mathsf{T} = \mathsf{B}_t/(\bar{\mathsf{R}}(0)\mathsf{R}_d(0)\mathsf{A}_t(0)) \tag{2.70}$$

$$\mathsf{S} = \bar{\mathsf{S}}\mathsf{S}_d\mathsf{A}_t/(\bar{\mathsf{R}}(0)\mathsf{R}_d(0)\mathsf{A}_t(0)) \tag{2.71}$$

$$\mathsf{R} = \bar{\mathsf{R}}\mathsf{R}_d\mathsf{A}_t/(\bar{\mathsf{R}}(0)\mathsf{R}_d(0)\mathsf{A}_t(0)). \tag{2.72}$$

With plug-in repetitive control the polynomials are

$$\mathsf{T} = \mathsf{B}_t(\mathsf{A}_{rc}+\mathsf{B}_{rc})/(\bar{\mathsf{R}}(0)\mathsf{R}_d(0)\mathsf{A}_t(0)\mathsf{A}_{rc}(0)) \tag{2.73}$$

$$\mathsf{S} = \bar{\mathsf{S}}\mathsf{S}_d\mathsf{A}_t(\mathsf{A}_{rc}+\mathsf{B}_{rc})/(\bar{\mathsf{R}}(0)\mathsf{R}_d(0)\mathsf{A}_t(0)\mathsf{A}_{rc}(0)) \tag{2.74}$$

$$\mathsf{R} = \bar{\mathsf{R}}\mathsf{R}_d\mathsf{A}_t\mathsf{A}_{rc}/(\bar{\mathsf{R}}(0)\mathsf{R}_d(0)\mathsf{A}_t(0)\mathsf{A}_{rc}(0)). \tag{2.75}$$

Notice that the polynomial $\mathsf{R}(q^{-1})$ is made monic, i.e. the leading coefficient r_0 is unity.

Avoiding Integrator Windup

Often, integral action will be part of the controller design strategy. This may be dangerous, when continuing integration of the control error takes place while the controller output saturates due to the limited output range of any real actuator. Degradation and even instability of the closed-loop system are possible consequences. A measure must be introduced to avoid windup of the integrator during controller output saturation. As proposed in [4], to avoid windup, the RST controller structure can be modified as follows

$$\begin{aligned} \mathsf{A}_{aw}(q^{-1})\bar{u} &= \mathsf{T}(q^{-1})r(k) - \mathsf{S}(q^{-1})y(k) + \left(\mathsf{A}_{aw}(q^{-1}) - \mathsf{R}(q^{-1})\right)u(k) \\ u(k) &= \mathrm{sat}(\bar{u}(k)) \end{aligned} \tag{2.76}$$

where the saturation function is defined as

$$u(k) = \mathrm{sat}\,\bar{u}(k) = \begin{cases} u_{low} & \bar{u}(k) \le u_{low} \\ \bar{u}(k) & u_{low} < \bar{u}(k) < u_{high} \\ u_{high} & \bar{u}(k) \ge u_{high} \end{cases} \tag{2.77}$$

with u_{low} and u_{high} being the allowed lower and upper bounds of the control signal, respectively. The polynomial $\mathsf{A}_{aw}(q^{-1})$ can be considered as the characteristic polynomial of the saturation observer. A block diagram of the modified RST-controller (2.76) is shown in Figure 2.8. Notice that the controllers (2.69) and (2.76) coincide for a non-saturated controller output.

The polynomial $\mathsf{A}_{aw}(q^{-1})$ can be specified again by first or second order systems with given time-domain properties. Taking the same rise-time as for the specification of the closed-loop poles is often a good choice. However, a simulation study of the RST-controller with anti-windup together with the actuator model and plant model should be performed before applying the controller to the real system.

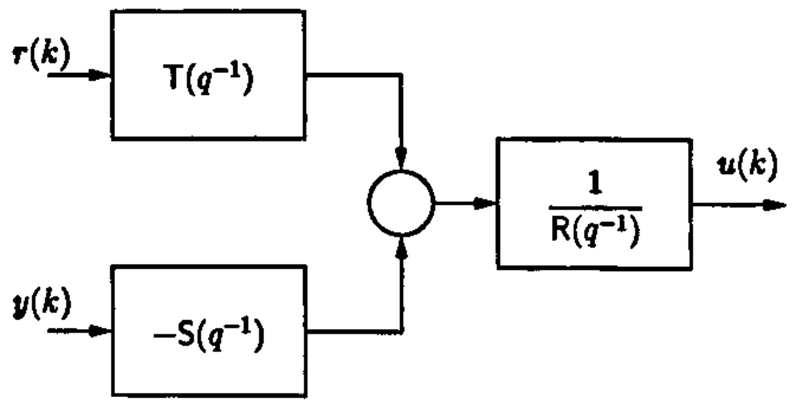

Figure 2.7: Block diagram of the RST-controller.

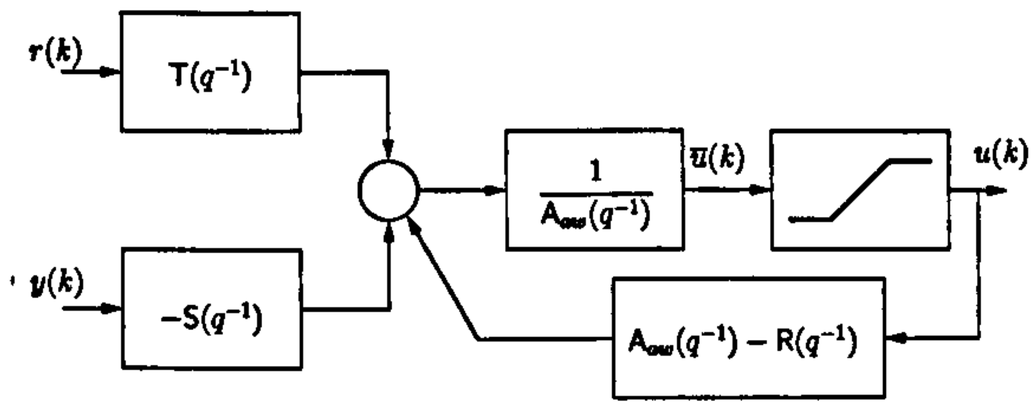

Figure 2.8: Controller structure with modification that avoids integrator windup.

Software

The controller design was carried out under MATLAB™[1] using the Polynomial Toolbox™ by PolyX. [2] The Identification Toolbox™ of MATLAB™ was employed for solving parameter estimation problems.

2.6 Summary and Conclusions

The controller design method used is an identification-based approach with two steps: (i) the open-loop response of the system output to variations in the system input is determined in an identification test. The parameters of a linear input-output model are determined from the measured data; (ii) the estimated model is used to analytically design a closed-loop controller.

Detailed guidelines for the general controller design have been given in this chapter taking into account the presence of disturbances, plant uncertainties and measurement noise. A step to step procedure has been presented for tuning of the controller. The last part of this chapter treated the practical implementation of the controller.

The controller design will be applied to the problem of power, cadence and torque control on an ergometer in Chapters 5 and 6.

[1] MATLAB is a registered trademark of The MathWorks, Inc., http://www.mathworks.com
[2] http://www.polyx.com

3 State of the Art in FES Cycling

3.1 Summary

This chapter gives an overview of Functional Electrical Stimulation (FES) induced lower-limb cycling in paraplegia and represents mainly a literature review with discussions. Section 3.2 outlines the advantages of FES cycling in comparison to other FES applications for the lower limbs. The principles of FES cycling and various technical realisations are presented in Section 3.3. This Section gives a survey of existing FES cycling systems covering static ergometers as well as mobile devices. The concept of isokinetic and isotonic training devices is explained. In Section 3.4, the efficacy and performance of FES cycling are analysed on the basis of published studies. Existing methods for designing and optimising stimulation patterns are presented in Section 3.5. The present knowledge of the influence of stimulation frequency, pulse train composition, and pedalling cadence is described in Section 3.5 as well. Finally, a summary and discussion of open research fields in FES cycling are given in Section 3.6.

3.2 Motivation

Neuro-prostheses based on functional electrical stimulation offer partial restoration of lost motor functions in paraplegia (cf. Chapter 1). In the following sections, FES supported lower-limb cycling is investigated as it provides a number of benefits which make it more attractive to a paraplegic individual than other FES activities. A major advantage is that cycling can be safely performed by individuals with SCI. Using a stationary exercise bicycle (ergometer) or a recumbent tricycle, with feet constrained by their attachment to the pedals, problems of balance can be avoided. Generally, patients are very motivated to perform FES cycling exercises. Perhaps the most attractive activity is recreational cycling outdoors. As such an exercise is fun and convenient, it makes it feasible for many patients. There is the real potential that mobile FES cycling systems can find a broad use outside of a clinical environment. Other neuro-prostheses, e.g. for walking, have not been transferred into the daily lives of paraplegics to a large extent, although applicable in a clinic. As a result, the success of introducing regular FES exercises to individuals with SCI so as to promote health has been disappointing until now. Unlike cycling, practical activities related with standing posture require upper body effort in maintaining balance (via crutches or walking frames). This disadvantage plus the

preparation time and the often poor appearance of the achieved gait outweigh the perceived benefits of use. FES cycling on the other hand does not require strenuous upper body support and may therefore be more acceptable.

Over the past twenty years a large number of studies have been carried out into the therapeutic and medical benefits of FES cycling. A review by Janssen et al. [50] summarises the key potential benefits: improved muscle size and strength, increased range of joint motion, and significant training effects giving improved cardiopulmonary fitness. These benefits may help to reduce the general and wide-ranging effects of the secondary complications which often accompany the disability (see Chapter 1) and may make the performance of activities of daily living relatively less stressful.

The main benefit from FES cycling lies in the cardiovascular conditioning that can be achieved by aerobic exercise. Aerobic cycling exercises, when conducted at an intensity that demands the cardiovascular system to operate near the anaerobic threshold, can cause significant training of the heart, the peripheral cardiovascular system in general and the lungs. Exercises like cycling which use the paralysed leg musculature are more efficient than arm exercises for the excitation of the cardiovascular system due to the significantly larger mass of the major leg muscles. In addition, the shoulders are ill adapting to load intensive arm exercises and so may be damaged.

Propelling a cycle by electrical stimulation of the large leg muscles is feasible and has been demonstrated for the first in the 1980s using surface electrodes [69, 70] and implanted electrodes [54]. Perkins et al. [64] realised FES lower-limb cycling in one SCI individual with an implanted lumbo-sacral anterior root stimulator.

Unfortunately, the intensity of FES lower-limb cycling exercises is rather low compared to normal cycling of able-bodied individuals, rarely exceeding an oxygen uptake of 1-1.5 litres per minute [60]. A detailed discussion about the performance of FES cycling is given in Section 3.4. The limited intensity constrains the physiological benefits to be obtained from FES ergometer cycling.

The intensity can be elevated by simultaneously performing an upper body exercise, such as arm cranking. Hybrid exercise provokes a significantly higher pulmonary oxygen uptake ($\dot{V}O_2$ 1.5-2.0 l/min) [60]. However, performing two cycling exercises simultaneously represents a rather unnatural movement. It is therefore questionable if this form of hybrid exercise will find a wide acceptance.

FES assisted rowing for persons with SCI is an alternative to FES lower-limb cycling [16, 39]. Pilot studies demonstrated that FES rowing is a safe and well-tolerated type of cardiovascular exercise for paraplegics. It gives reliably high $\dot{V}O_2$ values ($\geq$ 1.5 l/min) and involves the lower limb as well as the upper limbs and trunk musculature. Stress on the upper limbs is not increased as seen in wheelchair propulsion.

3.3 FES Cycling Systems

In this section, the state of the art in FES cycling technology is outlined. The focus will be on surface stimulation approaches. A summary of approaches from selected surface stimulation studies is given

in Table 3.1.

There are some common features which nearly all FES cycling devices share:

- The muscle stimulation is synchronised with the measured crank angle.
- The ankles are stabilised against plantar and dorsi flexion, internal/external rotation and inversion/eversion using orthoses. Additionally, varus/valgus of the legs is prevented by this bracing.
- The FES cycling systems can be simply operated by the paralysed cyclist. The paralysed person can transfer on and off the tricycle/ergometer independently. Some systems can be operated from the wheelchair without transfer.
- The distance between hip and pedals and the crank arm lengths are individually adjustable for each cyclist. This allows the range of motion for knees and hips to be limited as desired.

Independent pedalling by the paralysed individuals is mainly achieved by activating knee extensors via quadriceps stimulation, knee flexors via hamstrings stimulation and hip extensors via gluteus maximus stimulation. The quadriceps contributes most to the total power output in FES cycling, followed by the hamstrings and then the gluteus maximus [31].

In some studies, only a subset of these muscle groups has been employed. Such a strategy usually causes dead spots in the cycling motion which have to be overcome by injecting additional mechanical energy into the system which is not related to muscle stimulation.

Stimulation of other muscle groups such as iliacus, tibialis anterior and gastrocnemius (in addition to gluteus maximus, hamstrings and quadriceps) was also applied in experimental and simulation studies [2, 22, 24, 32, 35, 63, 72, 97].

The use of the withdrawal reflex in FES cycling by peroneal nerve stimulation was proposed by Angeli et al. [2] although the effects of this are little reported and analysed. A recent simulation study by Gföhler and Lugner [32] shows only a modest increase in power output by peroneal nerve stimulation.

In [24, 35], slightly higher magnitudes of metabolic and cardiopulmonary responses by the addition of shank muscles were reported while power output was nearly unaffected. In these studies, however, the ankle joint was kept fixed and, consequently, stimulation of the triceps surae only leads to a negligible moment contribution of the gastrocnemius at the knee. Van Soest et al. [97] used a forward dynamics modelling/simulation approach to assess the potential effect of releasing the ankle on the maximal mechanical power output. Triceps surae and tibialis anterior were additionally stimulated. Thus, releasing the ankle joint destroys the direct kinematical relationship between crank angle and joint angles. A new mechanical degree of freedom is introduced, the kinematics of the leg now depend on muscle forces, and thus muscle forces have to be coordinated in such a way that the resulting leg kinematics are appropriate. An inadequate muscle stimulation pattern may result in, for example, hyper extension of the knee. Releasing the ankle joint introduces injury hazards. The simulation study by Van Soest et al. [97] showed that releasing the ankle joint and stimulating the

triceps surae and tibialis anterior is expected to result in a modest increase in power output at best. The improvement in power output depends strongly on the location of the contact point between the foot and the pedal. A tuning of this position with respect to the relative strength of the ankle plantar flexors is necessary. For an inappropriate position, the power output may be smaller with a released ankle joint compared to the fixed ankle joint setup. The stimulation patterns applied in [97] are the result of a complex optimisation that maximises the power output. Muscle fatigue was not considered in the optimisation. A result of the optimisation is that the triceps surae has to be stimulated for most of the crank cycle. It should, however, be noted that a prolonged moment contribution by the plantar flexors using FES is not realistic since continuous electrical stimulation would cause muscle fatigue within a few minutes.

Table 3.1: Stimulated muscle groups or nerves using surface electrodes for FES cycling in selected studies / systems: Q - quadriceps, H - hamstrings, G - gluteus maximus, I - iliacus, TA - tibialis anterior, GAS - gastrocnemius, P - peroneal nerve.

Source / System	Q	H	G	I	TA	GAS	P	Motor	Flywheel	Type
Petrofsky et al. [70]	×			×					×	static
Eichhorn et al. [18]	×	×						×		static
Petrofsky et al. [69]	×		×							static
Ergys II[1]	×	×	×						×	static
Stimmaster Orion[2]	×	×	×						×	static
Pons et al. [72]	×		×			×		×		mobile
Petrofsky and Smith [67]	×	×	×							mobile
Jang et al. [49]	×	×							×	static
Glaser et al. [35]	×	×	×		×	×			×	static
Chen et al. [13]	×	×							×	static
Gföhler et al. [30]	×	×	×					×		mobile
Angeli et al. [2]	×	×	×				×	×		mobile
Perkins et al. [63]	×	×	×		×	×				mobile
Stein et al. [89]	×	×								mobile
Berkelmans et al. [7]	×	×	×							mobile
Chen et al. [14]	×	×	×						×	static
Szecsi et al. [91]	×	×	×							mobile
Takahashi et al. [92]	×	×	×					×		mobile
Fornusek et al. [26]	×	×	×					×		static

3.3.1 Static Isotonic Trainers

Based on a design study by Petrofsky et al. [70], a line of commercial FES cycling ergometers has been established by Therapeutic Alliances Inc., including the Regys I clinical rehabilitation system as well as the Ergys I and Ergys II home rehabilitation systems. Currently, these static ergometers

[1]Therapeutic Alliances Inc., United States, http://www.musclepower.com/

[2]Electrologic of America, Inc., United States, http://www.electrologic.com/

are mostly employed for clinical rehabilitation treatment. These ergometers are based on a standard Monarch bicycle ergometer used for non-paralysed individuals. Resistance levels have been reduced to adapt the devices to the limited power output ranges of paralysed cyclists. Glaser et al. [35] investigated possible modifications of the stimulation parameters and the additional recruitment of the shank muscles for the Ergys I ergometer system in order to improve the power output. However, success was limited.

Electrologic of America Inc. offers another commercial ergometer for FES cycling, named Stimmaster Orion. Notice that the commercial devices by Therapeutic Alliances Inc. and Electrologic of America Inc. are only certified for medical use in the United States and are used only within research projects in Europe.

Jang et al. [49] built a prototype FES cycling trainer with adjustable seat and load. The system was based on a commercially available exercise ergometer where the seat position is different from the commercially available high-chair type FES ergometers. Chen et al. [11] extended this FES cycling prototype system for multi-centre controlled studies. A tele-meeting system was built for online discussion and exchange of training protocols between clinical centres via the public Integrated Services of Digital Network (ISDN). The same research group also developed a hybrid exercise system which combines FES lower-limb cycling and arm cranking [14]. The patient can exercise on this static ergometer while sitting in the wheelchair.

Most static ergometers listed above are equipped with a large flywheel to maintain an initiated cycling motion in case of untrained and weak leg musculature and to overcome dead spots due to insufficient muscle stimulation. The cycling resistance (load) can be adjusted by applying resistance to the flywheel or using an hysteresis brake.

An isotonic training regime can be realised with such ergometers when a set constant amount of resistance is applied. This resistance is mainly viscous friction so that only for a constant speed the assumption of constant resistance and therefore perfect isotonic training can be achieved. To cycle at a given speed, the cyclist must produce a drive moment by stimulation which compensates for the externally applied viscous friction, the internal static and viscous friction and the passive crank moments caused by the legs due to gravity. Setting the resistance at the flywheel or brake to zero does not mean that the power output is truly zero. "Zero" power in isotonic ergometer systems is defined by the amount of power required to passively turn the legs and the unbraked flywheel at a given cadence. This offset can vary between subjects of disparate muscle tone and also depends on seating position.

3.3.2 Static Isokinetic Trainers

With isokinetic exercise devices muscular action is performed at a constant pedalling cadence. Therefore, an isokinetic FES lower-limb cycling system must use an active drive mechanism (e.g. an electric motor) to achieve the aim of constant cadence. The first FES cycling ergometer that used a motor

to assist or resist the pedalling has been described by Eichhorn et al. [18]. However, the motor control approach is not explicitly mentioned.

Fornusek et al. [26] developed a true isokinetic FES cycle ergometer. The design was based on a commercially available motorised ergometer which was integrated with a customised FES system, a laptop computer, and a specialised chair that restricted lateral leg movements.

Isokinetic training devices allow a larger proportion of SCI persons to undertake FES cycling, i.e. those unable to generate and maintain sufficient muscle force to rotate a large flywheel or those with low tolerance to FES due to residual sensation. The motor opposes FES-induced muscle forces exerted by the subject or assists pedalling during dead spots. Compared to isotonic ergometers, a wider range of pedalling cadences can be achieved (5-60 rpm). Cadences below 35 rpm are difficult to establish with isotonic trainers and have not been reported yet. Current findings on the effect of cadence in FES cycling are outlined in Section 3.5.3.

Accurate information on power output can be obtained from a power sensor at the crank or by calculation from cadence and applied motor torque which is reflected by the motor current [26]. The active crank torque produced by the electrically stimulated muscles can be easily determined by subtracting the passive motor torque (i.e., when the limbs are being moved solely by the motor) from the sensed motor torque during the FES cycling exercise. Notice that by using the active drive torque for power calculation the true active power output by stimulation is obtained. The passive torque is crank angle dependent and has to be obtained during periods of passive cycling. A readjustment has to be carried out in case of changes due to muscle tone or seating position.

Despite the large number of positive aspects in using isokinetic training devices, disadvantages also exist. The use of a motor driven system has the potential to injure the subject by forcing a limb movement in the presence of a strong muscle spasm. Special safety features that prevent muscle injury are required. Usually, only low power electrical drives (<200 W) are used. Muscle spasms are detected by crank moment measurements or estimates from motor current. The electric motor is powered off in the event of a spasm. Another problem is the fact, that the legs are always turning even without electrical stimulation and that the cyclist may lose the feeling of being able to cycle independently. This may diminish the motivation to perform such cardiovascular training.

3.3.3 Mobile Devices

Several locomotion devices by means of functional electrical stimulation have been developed. The majority of these mobile systems can be converted into a static ergometer and vice versa. Mostly three or four wheel constructions with a wide wheelbase are used to ensure stability especially in turns when carrying paraplegic cyclists. These vehicles are either built by modification of commercial devices [9, 63, 67, 69, 91] or specially constructed from scratch to better fit the demands of paralysed cyclists [30, 72, 91]. A travelling speed of 5-10 km/h can be achieved with these devices making them suitable for outdoor use. A problem is the limited manoeuvrability of a tricycle compared to a wheelchair, reducing the use indoors. Alternatively, cycling systems which work as a wheelchair

extension have been developed [2, 7, 92]. These systems offer better manoeuvrability that allows for indoor operation. The reported travelling speed however is below 2 km/h for some of the wheelchair cycling systems, making them less suitable for intensive outdoor use. An advantage of wheelchair cycling systems is their portability and small size. The system presented in [2] fits into a passenger car.

On all devices, the intensity of muscle stimulation can be manually adjusted by the cyclist often using a throttle (potentiometer) mounted to the handlebar.

FES cycling systems which are specially constructed for the purpose of paraplegic cycling are typically rather expensive. Locomotion devices with a similarity to a wheelchair in appearance may not be the favourite choice for paraplegic users if they can choose a "normal" tricycle with nearly the same functionality. These facts may lower the likelihood of specially constructed systems to be chosen by paralysed individuals for recreational use.

In contrast, the modification of commercially available standard recumbent tricycles by relatively simple means yields non-expensive, practical FES cycling systems. Riding such tricycles, one can barely distinguish between a paralysed cyclist and a neurologically intact cyclist. This may be a reason why such systems are already used outside a clinical environment [9, 63]. These mobile FES cycling devices have a low Centre of Gravity (CoG) for stability, while being suitable for transfer from a wheelchair.

An alternative approach for FES locomotion similar to cycling is presented in [33]. The authors modified a wheelchair so that it could be propelled by FES induced leg extension. The legs move sliding foot-plates which turn the back wheel via a ratchet transmission. Only the quadriceps muscles are stimulated as gravity is used to return the legs.

Stein et al. [89] also developed a leg-propelled wheelchair which has a number of different properties from Glaser's original design (e.g., rotary motion about the knee joint, rather than linear translation). The forces generated by flexion and extension about the knees are used to propel the wheelchair forward through a custom-built gear-box. The gear-box converts bi-directional rotations of the knee joint into unidirectional rotations that drive the rear wheel in a forward direction via a standard bicycle chain. The system can be also used as a static leg exercise trainer.

While training effects of regular static FES cycling exercises with static ergometers have been extensively studied, only limited results are reported on evaluating mobile devices with paraplegic subjects. Only three sources [9, 63, 91] provide data which prove the utility of mobile FES cycling devices for long-term usage outside laboratory conditions, including mobile cycling.

Assisted Mobile FES Cycling

A major problem of mobile FES cycling is the occurrence of rapid muscle fatigue due to the artificially induced muscle contractions (see Chapter 1). This fatigue diminishes the recreational benefits of cycling as only limited distances can be achieved. However the radius of action can be extended if an electric motor is integrated into the cycling system.

The auxiliary motor allows furthermore to initiate cycling by overcoming the initial inertia when the cycling device is started from rest. As explained subsequently in Section 3.4, the power output of FES lower-limb cycling is generally low compared with that of voluntary cycling of able-bodied individuals. While brief periods of cycling on flat ground are possible, longer periods of cycling as well as cycling on slopes and against strong winds may require an additional contribution from the motor to the leg power.

Several research teams have already designed mobile tricycles with an auxiliary motor [2, 30, 72, 92]. Notice that in the systems described in [30, 72] and [2], the motor and the electrically stimulated muscles are always controlled in a feedforward manner, e.g. manually by the cyclist. Gföhler et al. [30] fitted a hub motor in the front wheel of their tricycle. The total drive power (by motor and stimulation) is then adjusted by a throttle grip whereas the ratio of muscle and motor torque can be preselected.

Sophisticated feedback control of the electrical stimulation and the motor is not well developed at the moment. Recently, Takahashi et al. [92] proposed two control strategies and tested them experimentally. The aim of both strategies is to control the travelling velocity of the cycling system. A reference for the velocity is manually set by the cyclist. In the first control approach, a proportional-derivative (PD) controller determines the stimulation intensity of the electrical stimulation. The stimulation intensity is bounded, and the motor supports the movement only if the stimulation intensity reaches saturation. In this case, PD control is also applied to the motor. The second approach requires a complex model of the cycling device and the electrically stimulated muscles. A *Power Estimator* estimates the required power to make the system run at the desired speed and distributes the power to the motor and the muscles according to a pre-defined criterion.

Petrofsky and Smith [67] investigated another approach to resolve the "muscle fatigue" problem. The researchers designed a new "tricycle for two". This device allows a paralysed individual to cycle with a non-paralysed individual. A non-paralysed person can ride alongside the patient for safety, to provide additional pedalling force for example when the paralysed individual becomes fatigued through excessive functional electrical stimulation of their leg muscles.

The combination of FES lower-limb cycling and arm cranking to drive a vehicle has been presented in [7]. The FES systems described in [89] and [92] can also be additionally propelled by the arms.

Sitting Posture

The cyclist's position on the vehicle may be erect, as on a standard bicycle, or supine recumbent. The latter is preferable to ensure stability during cornering. Stability problems in the case of an erect sitting posture have been reported in [67]. In contrast to able-bodied individuals, paraplegic cyclists have often only limited control over their trunk muscles which makes it difficult to stabilise the trike by changing the centre of gravity of the upper body.

Gföhler et al. [30] designed a tricycle where the two rear wheels and the main tricycle frame can be inclined in parallel with adjustable hydraulic damping, in order to avoid stability problems when

cornering while using an erect sitting posture. Petrofsky and Smith [67] developed a tricycle where the basic design was a commercial tricycle made for two people with a side-by-side arrangement of the seats. This increases the stability of the system in bends.

3.4 Efficacy and Performance of FES Cycling

An important objective with FES cycling is to improve the cardiopulmonary fitness of the SCI subjects. This requires regular aerobic exercise for which the body uses oxygen to release energy for physical activity, in this case cycling. An aerobic metabolism occurs when the body breaks down fat and glucose by combining with oxygen. During intense aerobic exercises, the body uses more oxygen, and breathing and heart rate increase. An exercise period of 20-30 min with a heart rate of 60 to 80% of the maximum heart rate is considered necessary to stimulate aerobic (cardiopulmonary) adaptations. Therefore, a certain level of mechanical power output is necessary while cycling in order to start the aerobic metabolism.

Faghri et al. [20] have shown, that after 12 weeks of static FES cycling exercises (3 sessions per week) there were significant performance gains in which endurance increased from a few minutes to 30 minutes per session and power output capabilities increased from 5 to 18 W for 6 paraplegic subjects (5 of them complete SCI). The exercises were always limited to 30 min and started with minimal resistance (unbraked flywheel) during the first week. When fatigue occurred, up to three bouts were permitted to complete the session. When the subjects were able to exercise at a given power output for three consecutive sessions, the load was increased for the next session. These numbers plus cardiorespiratory variables recorded during these exercises indicate that aerobic exercises have been achieved, causing local (muscular) and central (cardiorespiratory) training effects.

Eser et al. [19] achieved average power outputs of up to 26 W, resulting from three weekly sessions of 30 min each. Petrofsky and Stacy [68] described more impressive results, with all of their eight subjects producing at least 55 W for 30 min after 24 weeks of training (however, the training frequency was not reported.)

Following a period of training, the magnitudes of cardiorespiratory responses in SCI patients caused by FES cycling may be similar to those of able-bodied individuals during walking and slow jogging [50]. However, one can state that even following intensive training, power output and maximal possible cycling time stay low compared to values obtained by normally trained able-bodied individuals. Hence cardiorespiratory responses will be different for SCI and able-bodied individuals during cycling exercises. Glaser et al. [34] showed in an experimental study, that efficiencies for FES cycling were significantly lower (by approximately 1/3 to 1/4) than those for voluntary cycling. More metabolic energy is utilised for producing the same mechanical power output. Reasons for this may be:

- **Non-physiological stimulation patterns:** The stimulation patterns to recruit muscles during

FES cycling are crude compared to those inherent in voluntary cycling exercises with able-bodied individuals. Using surface electrodes, there are typically also muscles unintentionally recruited and forces generated which do not contribute to the pedalling at all or in a highly inefficient way. The conversion of mechanical energy produced by the muscles to mechanical rotational energy at the crank may not be ideal for the chosen stimulation sequence.

Sinclair et al. [87] reported that paraplegic subjects apply significantly larger peak forces than able-bodied subjects cycling under voluntary muscle control because of the short duration of neuromuscular stimulation. Able-bodied subjects were able to achieve the same workload by applying smaller forces over a greater percentage of each crank revolution. While the work in healthy subjects is usually delegated to many muscles, in FES cycling only a few major muscles with consequently larger force outputs are propelling the crank. It was concluded that this fact contributes to the low efficiency of FES cycling.

- **Non-physiological cardiorespiratory responses in SCI individuals:** The sympathetic stimulation of the cardiorespiratory system may not occur to the same extent during FES cycling of SCI patients as for able-bodied individuals during voluntary exercise (especially for higher level injury (T5 and above)). This is caused by the interruption of some autonomic sympathetic outflows due to SCI. An insufficient delivery of blood and oxygen to the active muscles during FES cycling may be the result [20, 75, 93].

- **Limitations of electrically stimulated (paralysed) muscles:** The muscle fibre composition of the large paralysed leg muscles and metabolism within the muscles and the body are altered after SCI due to the disuse of muscles. This fact, plus the artificially induced muscle contractions may require more metabolic energy to produce forces than is necessary for voluntary contractions in healthy muscles. As explained in Chapter 1, electrically stimulated muscles also fatigue rapidly. Hence, SCI individuals are often not able to cycle for prolonged periods.

- **Poor mechanical setup:** Seat configuration and mechanical design also affect the efficiency of FES cycling. Muscle contraction properties which depend on joint angles and velocities as well as mechanical energy transfer from the muscles to the crank are influenced by the mechanical setup.

  The total mass of a mobile FES cycling system is another important factor which has an impact on cycling performance. A light device reduces the required muscle strengths to initiate mobile cycling. Some functionalities, like a hydraulic seat adjustment as described by Gföhler et al. [30], may make the operation of the devices easier, but increase the mass of the system unnecessarily.

To overcome these limitations, and to generally improve the performance of FES cycling several studies have been carried out. Most of them have focused on finding suitable stimulation sequences

and stimulation parameters. Section 3.5 contains a survey of such approaches.
Little effort has been spent on analysing the mechanical configuration. Schutte et al. [86] carried out an analysis of the efficacy of electrical stimulation induced leg cycle ergometry based on a dynamic musculoskeletal model. The performance of FES cycling was assessed in terms of 1) the probability that an SCI subject would be able to maintain a steady cadence, 2) the relative strength required by each muscle to pedal alone, and 3) the estimated rate of metabolic energy utilisation associated with steady state pedalling. The authors investigated the influence on the performance of different situations (for the Ergys I system):

(a) Change of seat configuration while applying a fixed stimulation pattern.
Main outcome: Very upright seat configurations with short hip to crank distances will increase the rate of metabolic energy utilisation but require slightly greater muscle strengths from the SCI subject compared to the standard configuration of the Ergys I system. This result and other conclusions drawn apply, however, only to the Ergys I system with the fixed standard stimulation pattern for all patients.

(b) Change of the seat configuration while applying a configuration-specific stimulation pattern which maximises the active drive torque produced by electrical stimulation (see also Section 3.5).
Results: Using configuration-specific stimulation patterns increase the probability to cycle and decrease the required muscle strengths for all investigated crank to hip distances. The probability to cycle as well as the required muscle strengths are less sensitive to the seat configuration. Metabolic energy utilisation was always increased compared to the set-up (a).

(c) Variation the output power (product of crank cadence and cycling resistance) while using standard seat configuration and stimulation sequences of the Ergys I system.
Main results: If the power is increased, which is demanded from the stimulated paralysed lower extremities, fewer individuals can pedal and in those who can, more metabolic energy is utilised.

Angeli et al. [1] constructed a special non-circular optimised pedal path which raises drive power output for FES cycling. The authors showed that spastic reactions can be decreased due to smaller angle ranges of the hip joint movement. The optimised pedal path has been realised in a mobile cycling system [2] and test bed [31]. Optimal stimulation patterns and further design optimisation for the non-circular pedal path are described in [32] and [74] respectively. Rasmussen et al. [74] argue that human legs are naturally built to provide their maximum force directed roughly in line with the hip and the ankle joint. It is therefore inevitable that each leg has one or several regions in a cyclic motion where it cannot provide much force tangential to the movement. In a conventional pedalling mechanism, the circular foot motion causes these dead centres for the two leg to coincide. For the special non-circular optimised pedal path the dead centre for one leg falls close to the point where the other leg has its maximum leverage [74].

3.5 Stimulation Sequences and FES Cycling Parameters

3.5.1 Pattern

The stimulation pattern (timing) is typically described by crank angle intervals during which certain leg muscle groups are activated by electrical stimulation. The demands on the stimulation pattern are different for isotonic and isokinetic cycling. The former requires a functional pattern that results in a smooth cycling movement generated by the leg musculature; typically, a certain number of muscles must be included into the pattern to achieve this goal. For isokinetic cycling, the task of the pattern is to generate a positive drive moment in order to obtain a positive power output. Functionality of the pattern is not important since smooth turning of the legs is ensured by the motor.

Imitating Voluntary Muscle Activation

Often, stimulation patterns have been derived from electromyographic (EMG) measurements during voluntary isotonic cycling of able-bodied subjects [21, 49, 65, 67, 72, 95]. However, in [72] a poor correlation was found between the EMG based stimulation sequence and the stimulation sequence finally chosen. Pons et al. [72] pointed out that the transposition of EMG patterns to FES may not result in the best motion.

Despite this, EMG measurements can give an indication of how to design realistic FES cycling patterns. EMG measurements show an increasing phase advance in muscle activity when the crank is rotating faster. This earlier muscle activation takes the presence of a time delay in muscle contraction and relaxation as well as the load dependent dynamical properties of the system into account. This latency behaviour of the muscles requires an earlier activation (stimulation) of the muscles in order to have the muscle forces generated at the correct crank angle ranges. Dependent on the muscle, the latency time varies and can be different for muscle contraction and relaxation. A stimulation pattern derived for a certain velocity consequently has to be modified when used at different pedal velocities. Speed dependent stimulation patterns where investigated by Petrofsky and Smith [67] first.

Wang et al. [98] observed from EMG recordings that voluntary muscle activation in healthy subjects varies for changing load conditions. Petrofsky [65] designed a stimulation pattern which depends on pedalling cadence and load. The pattern was derived from EMG measurements and significantly improved the power output of the paraplegic subject.

Fitting the Active Drive Torque to the Load Characteristics of the Crank Shaft

Smooth pedalling on an ergometer without a large flywheel and in mobile cycling is only possible if the active drive moment generated by the leg muscles at the crank corresponds to the load characteristic of the crank shaft.

In [13], an initial stimulation pattern has been designed by analysing the gravitational potential of

the lower limbs while cycling against a frictionless cycling ergometer. The stimulation is activated within crank angle intervals for which the gravitational potential is increasing. Further, the response delay of electrically stimulated muscles has been considered while cycling at higher velocities. The stimulation pattern finally applied was obtained by assessing experimentally the smoothness of the cycling for small variations of the previously derived pattern. Aspects of smoothness have often been neglected in other design approaches for stimulation patterns. However, cycling without jerks is desirable from a medical point of view to protect tendons and bones as well as to avoid spasms.

Szecsi et al. [90] used a crank angle dependent stimulation intensity profile to obtain a good fit of drive and load moment at the crank. This strategy was only evaluated in simulations where an improvement in the pedalling smoothness could be observed.

Minimising Muscular Fatigue/Stress, Maximising Metabolic Efficiency

Gföhler and Lugner [29] sought start and stop crank angles for the muscle stimulation intervals by numerical optimisation with the aim to obtain maximal average power output with minimal muscle force (load) at different pedalling velocities for a given constant stimulation intensity. A reduction in muscle fatigue is expected when applying such stimulation patterns. The intended use of the optimised pattern was for mobile FES cycling with the tricycle described in [30]. To carry out this optimisation task, a complex dynamical model of the rider-tricycle system including the electrically stimulated skeletal muscles was used. Gluteus maximus, rectus femoris, vasti and hamstrings were modelled as actuators. Additionally, passive forces generated by other muscles were considered as well. To simplify the problem, the timing for each muscle group has been individually optimised while setting the stimulation of other muscle groups to zero. In each optimisation step, the muscle force produced by the investigated muscle group and the resulting contribution to the power output were calculated for one crank rotation. Constant speed was assumed during this crank rotation.
The assumption of constant cadence is true for isokinetic cycling with good cadence control or for ergometers with a large moment of inertia provided by a flywheel. However, constant cadence cannot be guaranteed for mobile devices where a flywheel cannot be used and where the system mass is not large. The applied procedure neglects in this case any inherent mechanical feedback within the rider-tricycle system while carrying out the optimisation. It is highly questionable whether such a reduction complexity of the optimisation problem yields realistic results for a system with speed variation.
The optimal stimulation intervals are bounded to the specified fixed stimulation intensity. Optimality will be lost when a stimulation intensity different from the one chosen in the optimisation procedure is used. This represents a major drawback.

Idsø et al. [47] determined the optimal stimulation intensity and intervals for a desired constant pedalling cadence and work rate that minimise the total energy expenditure of the stimulated muscles. Not only is muscle stress considered as in the work of Gföhler and Lugner [29], but the full metabolic

cost of the muscles is taken into account. It is interesting that the lowest metabolic cost is achieved when the stimulation intensity is maximal and the stimulation interval length is at the shortest possible value for the specified work rate. This observation is in accordance with experimental results from paraplegics by Ferrario et al. [23] where metabolic efficiency was determined by oxygen cost measurements. A better understanding of this can be achieved when considering the fact that the transfer of muscle force to the crank is almost a sinusoidal function with the crank angle as the argument. Maximal transfer is achieved at the positive extreme of the curve, and the transfer function drops off more and more quickly as the distance from this point increases. It is evident that a shorter interval centred at the crank angle of maximal force transfer will ensure a higher average torque transfer from the joint to the crank. Idsø et al. [47] point out that the commonly applied technique to control the stimulation intensity while using a fixed stimulation interval is suboptimal. A better control technique may be to control the stimulation interval while maintaining a fixed stimulation intensity.

The stimulation pattern derived by Idsø et al. [47] optimises metabolic efficiency but is likely to cause some problems when applied to a paraplegic individual. The short intervals and maximal stimulation intensities can lead to jerky movements and possibly trigger muscle spasms. The impulsive crank moments generated with this pattern will put a high burden on the cadence control of isokinetic training devices. For isotonic cycling, there is no guarantee of smoothness in the cycling motion due to the neglected load characteristics at the crank shaft.

Maximising the active drive torque

In order to find the stimulation pattern which gives maximum active power output, Gföhler et al. [31] built a test bed with a non-circular pedal path for FES cycling with an auxiliary motor and a force measuring crank, which allows static and dynamic forces in three dimensions to be recorded. Only one leg is connected to the crank to make sure that the measurements are not influenced by spasms or forces of the other leg. Initially, a crude stimulation pattern is obtained from static force measurements indicating crank angle intervals for which the individual muscles generate positive drive torque. Baseline patterns for the online optimisation at different speeds are derived by applying a simple correction to the static pattern.

For optimisation, the motor drives the crank at constant velocity, while only one muscle group is stimulated. Forces over one crank rotation are recorded and the active drive power is calculated in real-time. Active muscle forces which are required to determine the active drive power are obtained by subtracting the passive forces which have been previously measured for a crank rotation without stimulation, from the measured forces.

During the optimisation procedure, start and stop angles of the stimulation are modified to find settings yielding the maximum active power output. Under isokinetic conditions, the resulting pattern yields maximal drive power.

However, the intention of Gföhler et al. [31] was to find a suitable pattern for the FES tricyle described in [2]. For the mobile system nearly isotonic conditions hold. In addition, the lightweight tricyle only

possesses a small moment of inertia with respect to the crank compared to a static ergometer with flywheel. Hence, crank velocity will be a function of stimulation and will have a direct influence on the muscle force generation via the force-length and the force-velocity relationships of the muscles. The active power achieved when stimulating all muscles during one crank rotation may be different in this case. Furthermore, the derived active crank torque profile will probably not fit well to the load characteristic of the crank shaft.

In summary, there are serious doubts whether the proposed strategy can give a realistic stimulation pattern for mobile FES cycling. An experimental validation of the pattern in "real" mobile FES cycling has still to be carried out.

The influence of various parameters on the pattern which maximises active drive torque has been investigated by Gföhler and Lugner [32] in a dynamic simulation of FES cycling. Equations for calculation of the optimal stimulation pattern as a function of the following parameters have been derived: ramp length at the beginning and at the end of the stimulation, body height, relation of thigh and shank lengths and seating geometry. It should be noted that the stimulation intensity does not influence the optimal pattern in this case.

Schutte et al. [86] also investigated the effects of a stimulation pattern which maximises the active drive torque for the Ergys system. The pattern was derived by optimisation methods (not specified) based on a complex dynamical musculoskeletal model for cycle ergometry. It was not clear for the authors how fatigue will be affected by the optimised pattern. Schutte et al. [86] showed furthermore in simulation that the metabolic energy utilisation will not be minimised by such a stimulation pattern.

Perkins et al. [63] and Trumbower and Faghri [96] took static pedal force readings for a set of crank angles, in order to determine favourable crank angles for stimulating each muscle group, yielding maximal positive drive torque. Only a single muscle group was stimulated at a time while analysing the static forces. Thigh and shank muscles were tested. The intervals derived were altered for different speeds in a simple manner [63].

Ferrante et al. [22] used dynamic crank moment measurements on an isokinetic training device to determine appropriate crank angle intervals at which muscle stimulation causes a positive drive torque. An electric motor kept the cadence at a chosen set point. One muscle at a time was stimulated for the entire cycle while the corresponding crank torque was measured.

In summary, maximising the active drive moment results in a good stimulation pattern for isokinetic cycling exercise if the power output has to be maximised. However, muscle fatigue will probably not be minimised when applying such a pattern. For isotonic ergometer training without a large flywheel or mobile cycling, the optimised pattern may lead to a non-smooth movement as the load

characteristic of the crank shaft has not been considered and the assumption of constant speed is possibly not fulfilled.

3.5.2 Stimulation Frequency and Pulse Train Composition

In most studies of FES cycling a fixed stimulation frequency in the range of 20 to 40 Hz has been used. Higher stimulation frequencies have not been applied as increased muscle fatigue was expected. However, with higher frequencies higher power output can be achieved (see Section 1).
The often used frequency range of 20 to 40 Hz has been found optimal in the sense of achieved muscle force, contraction smoothness and fatigue resistance for muscle strengthening programmes which consists of applying cyclic electrical stimulation to the knee extensor muscles, resulting in isotonic contractions, and for prolonged standing exercises with continuous quadriceps stimulation. For the first application, duty cycles (the relation of pulse train duration and pause) of 1/1 or 1/2 with pulse train durations in the range 4-8 s are typically used.
During FES cycling, the muscles are intermittently stimulated rather than continuously as for standing. In contrast to muscle strengthening programmes, duty cycles at crank velocities of 40 to 60 rpm are in the range of 1/3 to 1/6 with shorter pulse train durations of 200 to 600 ms.
It is well known that duty cycle and pulse train duration as well as stimulation frequency have a combined impact on fatigue resistance [56]. In this framework, a recent study by Matsunaga et al. [59] indicates, that higher stimulation frequencies up to 100 Hz can be applied in intermittent stimulation schemes with duty cycles above 1/15 (4 s stimulation burst repeated with a period more than 60 s), resulting in less fatigue and increase force compared to applying low frequencies such as 20 Hz. It is consequently questionable whether the range of 20 to 40 Hz is optimal for FES cycling exercise. In [19] first results are shown for FES cycling which indicate no significant increase in fatigue when using higher stimulation frequencies of 50 and 60 Hz while power output increased by up to 25 per cent.

The FES cycling devices by Petrofsky et al. [69] and Petrofsky and Smith [67] as well as all commercial cycling ergometers by Therapeutic Alliances Inc. offer a sequential muscle stimulation technique to obtain smoother muscle contractions and to increase muscle forces and power output. Three surface electrodes are used for each muscle instead of the conventional two electrodes used for standard electrical stimulation. The centre electrode is the reference electrode and the two outside electrodes are active electrodes. Stimulation is applied first to one active electrode and then, 180° out of phase, to the other electrode at a 30 Hz rate. By alternating across the head of the muscle, contraction of the muscle is obtained more powerfully and smoothly since the effective stimulation frequency at the single reference electrode amounts to 60 Hz. The inventors of this stimulation technique argue that fatigue of the muscle fibres will be mainly affected by the 30 Hz rate of stimulation and will be lower than when working directly with conventional stimulation at 60 Hz. Unfortunately, there are no comparable data available for FES cycling supporting this statement. In addition, the results obtained by Eser et al. [19] contradict this statement.

The ongoing development of stimulation technology and the better understanding of how healthy muscles work will lead to further improvements in FES cycling. For example possibilities for exploiting the "catch-like" effect [10] of muscles in FES cycling have received little attention. The catchlike property of skeletal muscle is the force augmentation as a result of the inclusion of an initial, brief, high-frequency burst of two to four pulses at the start of a subtetanic low frequency stimulation. Variable Frequency Trains (VFT) can take advantage of the catchlike property of the skeletal muscle and augment muscle performance compared with Constant Frequency Trains (CFT), especially during fatigue. A review of this topic by S. Binder-MacLeod and T. Kesar [80] was recently published. Only one study by Janssen et al. [51] describes the effect of VFT on FES cycling performance. The results of this study do not indicate that stimulation with catch-like inducing trains significantly improves the FES cycling performance. However, in the study, a large variability among the few subjects (five) was observed. Furthermore, each investigated pattern was only applied twice applied to each subject. The outcome measurement was the total work performed with each pattern while work rate was controlled. An individual resistance was chosen for each subject and cadence was controlled at 50 rpm. Experiments were performed on an ERGYS cycling ergometer (ie., an isotonic trainer). However, a changing offset in the power measurement due to changing seat position and muscle conditions (muscle tone) lead to problems with the work rate control and thus to varying testing conditions. This fact may help to explain the inconclusive results of this study. Further studies have to be carried out with better controlled testing conditions, preferably using isokinetic cycling ergometers.

The stimulation frequency has furthermore a direct influence on how exactly a muscle can be stimulated within a specified crank angle interval. This will be discussed in more detail in Chapter 4.

3.5.3 Pedalling Cadence

Fornusek and Davis [25] investigated the effect of pedalling cadence on muscle force and power output in FES cycling. SCI individuals performed 35 minute of isokinetic cycling exercise at constant stimulation intensity and pedalling cadences of 35 rpm and 50 rpm. Peak and average torques were significantly greater at the lower cadence. From 15 minutes onwards, power output was significantly higher at 50 rpm, compared with 15 rpm. A second test examined the effect of a low vs high pedal rate (20 and 50 rpm) upon isolated muscle fatigue over 5 minutes. Peak torque of the quadriceps decayed faster at the higher cadence, indicating a higher rate of fatigue. A main reason suggested for the larger forces at low cadences is the force-velocity relation [100] of a muscle. A significant difference in the muscle stimulation delivered at different cadences is the length of the contraction-relaxation period, which for FES cycling is inversely related to the pedalling cadence. High cadences therefore have short contraction-relaxation periods. For intermittent isometric contractions, shorter contraction-relaxation periods result in more rapid force decline [6, 40].

Fornusek and Davis [25] stated the hypothesis that low cadence training may be optimal for strength training while higher cadences may be best for power training. To confirm this, a prospective training study is required.

3.6 Summary and Conclusions

Over the last twenty years FES cycling has become an established approach for the cardiovascular training of SCI individuals. A wide range of FES cycling systems has been developed, including static ergometers and mobile devices. Some of these have been made commercially available. Recently, an isokinetic training device [26] has been developed as an alternative to the well established isotonic cycling ergometers that utilise a flywheel. Isokinetic training at a motor controlled constant cadence allows a larger proportion of SCI persons to undertake FES cycling. In addition, accurate power measurements can be obtained and training conditions can be controlled better. Thus, isokinetic training should be the preferred choice for exercise testing and studies of physiological effects of FES cycling. Furthermore, lower pedalling cadences can be achieved compared to an ergometer with flywheel. From the user's perspective, isokinetic training may not be the preferred choice since the motor induced movement does not give the feeling of "My legs are propelling the crank". None of the existing FES cycling devices offers both isokinetic and isotonic training. Two newly developed training systems are presented in Chapters 4 and 5 which can be used in both training modes. One design approach is based on the adaptation of a recumbent tricycle which can also be used as a mobile device. The other design approach is purely static and utilises a commercially available motorised ergometer.

The training effect of regular FES cycling exercise on static ergometers has been extensively studied. Major problems reported in all studies are the limited endurance, the low power output and the reduced metabolic efficiency of FES cycling compared to voluntary cycling of able-bodied individuals. Since we are unable to overcome most of the limitations inherent to FES cycling of SCI individuals, it is important to optimally tune the parameters which actually can be modified. The stimulation pattern is one such parameter. Several approaches for pattern optimisation are published but despite all efforts, endurance, power output and efficiency with optimised patterns are still below levels shown in able-bodied cyclists. It is further questionable whether model-based optimisation is the best tool for finding a patient specific pattern. It appears to be simply not practicable to adapt complex musculoskeletal models to an individual subject. Instead, the underlying physiological effects of FES cycling must be further studied. Therefore, comparable and better controlled testing methods have to be established. In Chapter 6, the control of work rate in isotonic and isokinetic FES cycling exercise will be investigated. A significant increase in power output may be achieved by eliciting catch-like effects in FES cycling, but further clinical studies are needed to test this hypothesis.

While the effects of regular static FES cycling exercise have been extensively studied, only limited

results are reported on evaluating mobile devices with paraplegics subjects. More evidence is required which demonstrates the usability of mobile FES cycling devices for long-term usage outside laboratory conditions. Chapter 4 presents the results of a pilot study which also included mobile FES cycling tests. Future research should be directed towards assisted mobile cycling systems; in particular, the use of feedback control in motor assisted devices represents a challenging task for which no satisfactory solutions exist at the moment. Another not entirely solved problem is to find optimal stimulation patterns for mobile cycling. An appropriate pattern must fit to the load characteristics of the crank shaft in order to give a smooth pedalling motion. An automatic tuning of the pattern based on angle, cadence and pedal force/torque information is desirable, but has not yet been fully developed.

4 Pilot Study of FES Cycling

4.1 Summary

Aim: The aim was to develop inexpensive FES cycling systems for home/recreational use and for investigational purposes (e.g. exercise testing). This work was further intended as a pilot study to achieve regular periods of FES cycling in paraplegic subjects over a period of one year to show feasibility of the recreational use of mobile FES cycling.

Methods: Recumbent tricycles have been adapted for paraplegic users, and instrumented for stimulation control. The cycling systems can be used as static trainers or mobile devices. An optional electrical motor is used to enable isokinetic training in addition to the standard isotonic training mode when the systems are operated as static ergometers. Three SCI subjects with a complete lesion participated in a one year pilot study. Training consisted of daily FES muscle strength exercises and weekly FES cycling sessions once the subjects were proficient in cycling. Stimulation patterns for the subjects were determined by a simple procedure where the rider-tricycle geometry and isometric force measurements caused by stimulation of isolated muscles are taken into account.

Results: Effective indoor cycling on the trainer could be achieved for long periods of up to an hour, and mobile cycling outdoors over useful distances. Power output of FES cycling was in the range of 15-20 W for two of the three subjects at the end of the pilot study.

Conclusion: Effective mobile cycling can be achieved with the developed FES cycling systems (non-motorised) and a low intensity cycling training regime combined with daily muscle strength training. The cycling systems are suitable for home/recreational use, and for investigational purposes (e.g. exercise testing).

Contribution: The author's contribution to this study consists of the development and realisation of the experimental software and hardware. Furthermore, the author was involved in the planning and execution of the experiments and in the analysis and interpretation of the results. Results of this work are published in [43, 44, 45, 46, 84].

4.2 Motivation

Mobile FES cycling for recreational use represents an interesting option for SCI individuals. It is fun and has therefore a greater potential than "static" ergometer training to introduce paraplegics to FES cycling. Performance of mobile FES cycling, including outdoor cycling, has only been described in three sources [9, 63, 91]. Two of them present results from a long-term usage outside laboratory conditions. It is remarkable that far more publications describe mobile FES cycling systems. Perkins et al. [63] reported on an SCI cyclist with incomplete lesion who is able to cycle with FES assistance for about 12 km at a time (both indoors and outside). A German paraplegic cyclist who uses an FES cycling system at home is able to cycle over distances of more than 10 km with slopes of up to 5 %. To achieve this performance, training over 1 1/2 years including 6 hours daily weight lifting (with FES) has been completed [9, 91]. These results are not representative for the majority of paraplegics. Szecsi et al. [91] investigated the cycling performance of 7 SCI individuals with complete paralysis of the lower limbs. All subjects were untrained with respect to FES cycling but performed other forms of FES muscle strength training for the lower limbs. A recent study by Petrofsky and Laymon [66] shows that previous weight training and concurrent weight training has a significant positive effect on the performance of FES cycling. This explains the surprising result that six out of the seven subjects in the study by Szecsi et al. [91] could cover distances in the range of 1300 to 1800 m during their first FES cycling trial.

The aim of the study presented here was to investigate the FES cycling performance of initially untrained SCI individuals with a complete lesion for a specified training protocol over one year.

4.3 Subjects

Three paraplegic subjects with a motor-complete spinal cord lesion at levels ranging from T7 to T10 were recruited for this study. Details of the subjects are given in Table 4.1. The results reported here

Table 4.1: Subjects of the pilot study.

Subject	Level of complete lesion	Age [years]	Time post-injury [years]
S1	T8/9	28	3
S2	T10	57	3
S3	T7/8	38	7

are taken from experiments carried out during the 12 months of the study. The data for age and post-injury time given in the table are with respect to the start of the subjects' participation. The subjects were recruited at the Queen Elizabeth National Spinal Injuries Unit at the Southern General Hospital in Glasgow. All procedures were approved by the Southern General Hospital Ethics Committee; the subjects provided informed consent prior to participation. None of the subjects had used FES for the

lower limbs before.

4.4 Apparatus and Methods

The mobile cycling devices used in this work are based on two commercially available standard recumbent tricycles which were specially instrumented and modified for FES lower-limb cycling. This design was initially proposed by Perkins et al. [63, 64], with appropriate adaptations, for FES induced paraplegic cycling. One tricycle[1] (cf. Figures 4.1 and 4.3), denoted as trike I, has a two front wheels - one rear (driven) wheel configuration. The other tricycle[2] (cf. Figure 4.2), denoted as trike II, has the opposite wheel arrangement. On this trike, only one of the two rear wheels is driven. Both trikes offer a wide wheelbase and a low centre of gravity for increased stability. Standard wheelchair cushions were fitted to the seats to reduce seat pressure. The handlebars of both tricycles can be turned aside to allow an obstacle-free patient transfer onto and from the tricycles.

The tricycles can be converted to static ergometers by mounting a commercially available resistance trainer[3] on the driven wheel. The cycle trainer employed for trike I comes with an electronically controlled and adjustable magnetic brake which allows the resistance to be altered in discrete steps. Additionally, online measurements of the power at the driving wheel are available via this cycle trainer.

Trike I was further equipped with an auxiliary electric motor to assist the cycling motion. Motor and rechargeable batteries are mounted behind the seat. The motor can be connected through gearing to the drive wheel of the tricycle (the rear wheel), and is also directly coupled to the cranks at the front of the tricycle. Thus, even when no power is supplied by the subject, the legs can be turned by the motor. If desired (e.g. for isotonic training), the motor can be completely decoupled from the system.

4.4.1 Mechanical Modifications

Customised ankle orthoses are fixed to the pedals. These stabilise the ankle and constrain the legs to movements in the sagittal plane. This was found to be an important factor to ensure smoothness of the generated cycling motion.

The distance between the seat and the pedals as well as the crank arm lengths can be individually adjusted to guarantee suitable knee and hip angle ranges for the paralysed cyclists. The adjustment of the seat-pedal distance was already possible with the unmodified commercial tricycles by simultaneously shortening or extending the boom and changing the chain length. To allow the adjustment of seat-pedal distance for frequently changing cyclists without time-consuming adaptation of the chain length, the following modifications were carried out:

[1] "Trice Classic", Inspired Cycle Engineering Ltd., UK, http://www.ice.hpv.co.uk
[2] "Hase Kett-Wiesel", Hase Spezialräder, Germany, http://www.hase-spezialraeder.de
[3] "Grand Excel" (trike I) and "Eco Tracks" (trike II), Tacx, The Netherlands, http://www.tacx.nl

- Trike I: An automatic chain tensioner (modified derailleur) was mounted on the tricycle. This allows the geometry to be changed while the subject is sitting on the trike.
- Trike II: The connection of seat and frame was redesigned to allow a forward and backward sliding of the seat with respect to the pedals. Constructional details are given in [62].

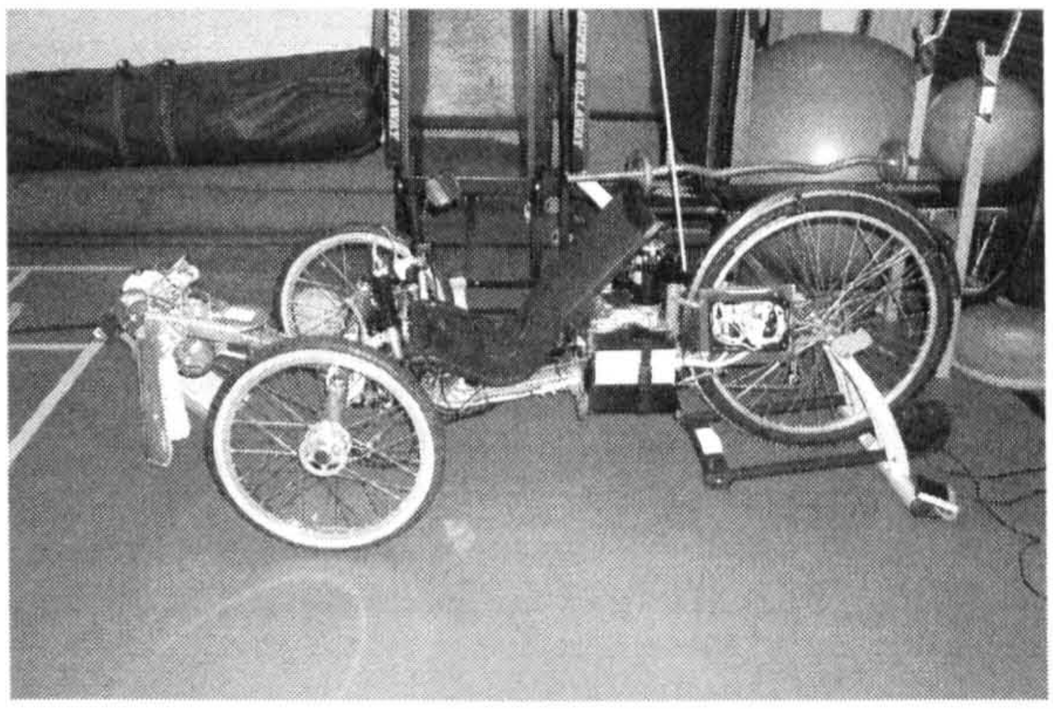

Figure 4.1: Recumbent tricycle (trike I): Setup for indoor cycling on the cycle trainer.

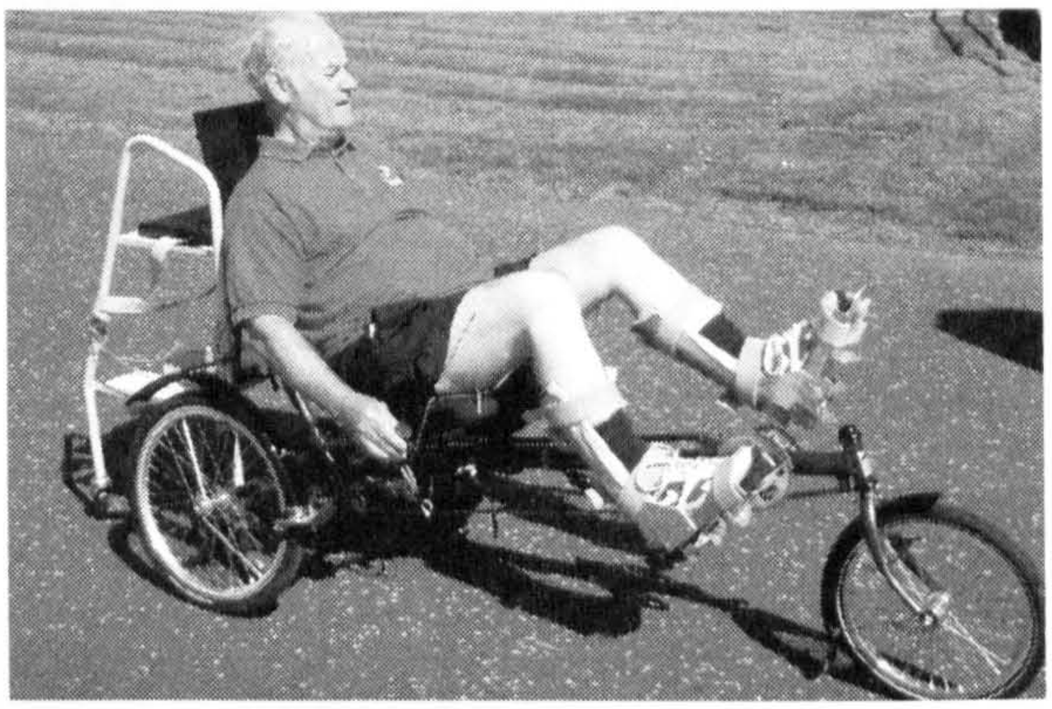

Figure 4.2: Recumbent tricycle (trike II): Paraplegic subject cycling outdoors.

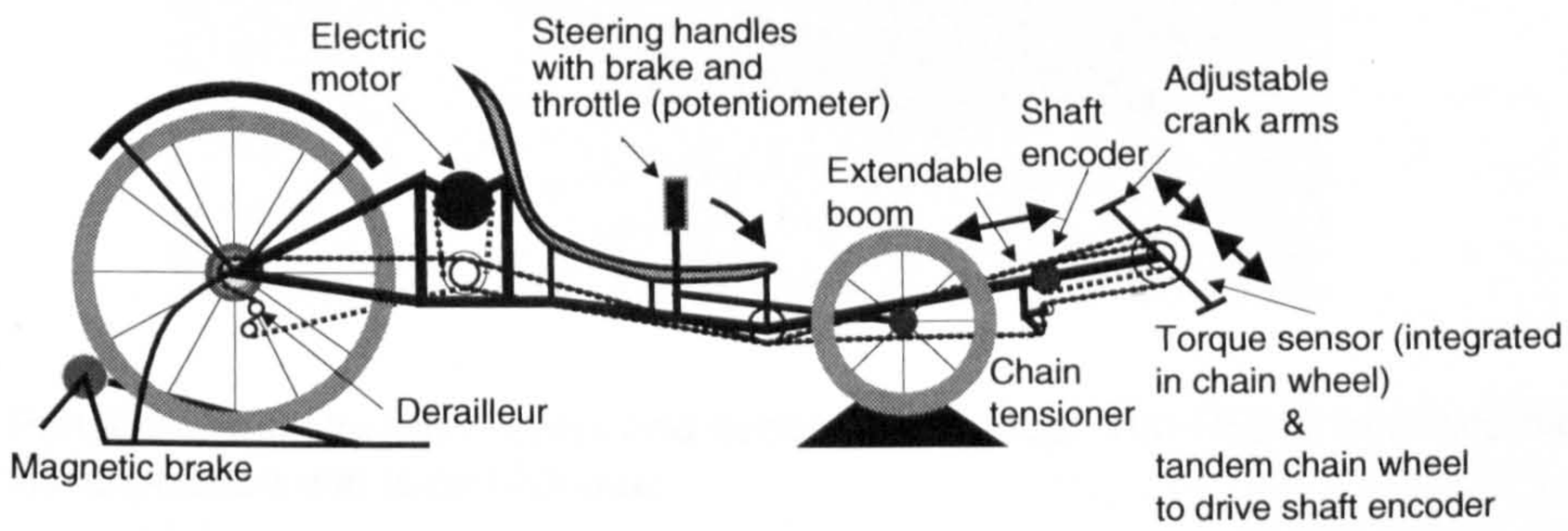

Figure 4.3: Schematic setup and instrumentation of the trike I (two wheels in the front and one driven wheel in the back).

4.4.2 Instrumentation and Device Operation

Both tricycles are equipped with an absolute optical shaft encoder [4] (10-bit resolution) which is driven by a short chain attached to the left crank (tandem version) (cf. Figure 4.4). Constructional details are given in [78]. This setup allows the measurement of the crank angle. The crank speed is obtained by differentiation (with low-pass filtering) of the sampled crank angle.

A throttle in the form of a potentiometer is integrated into the right hand grip. It is possible to set the stimulation intensity manually by using this throttle.

[4] Hengstler GmbH, Germany, http://www.hengstler.de

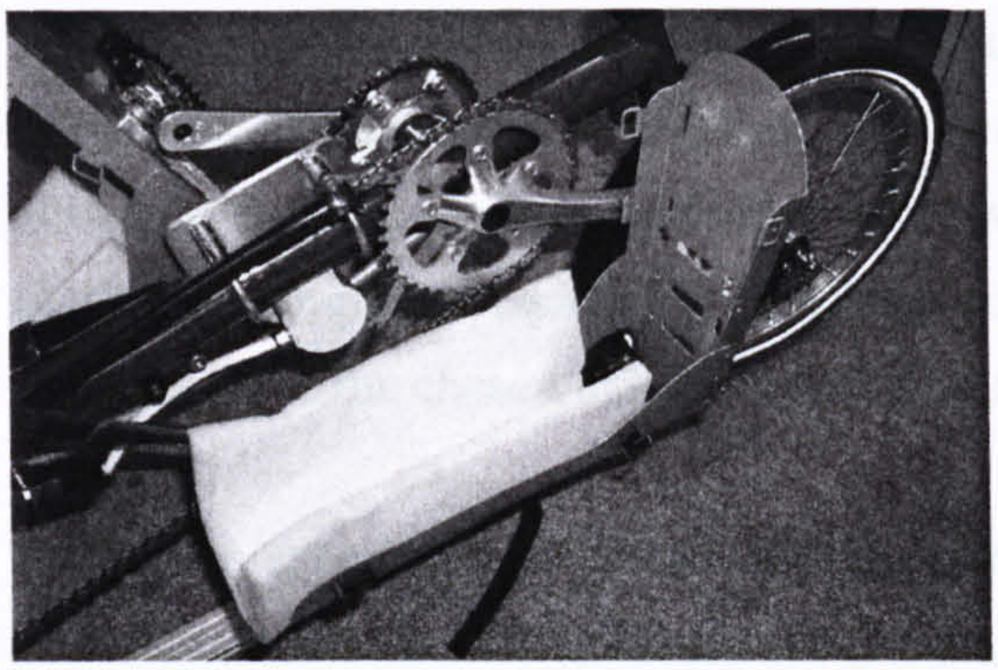

Figure 4.4: Shaft encoder and ankle orthosis arrangement on trike II.

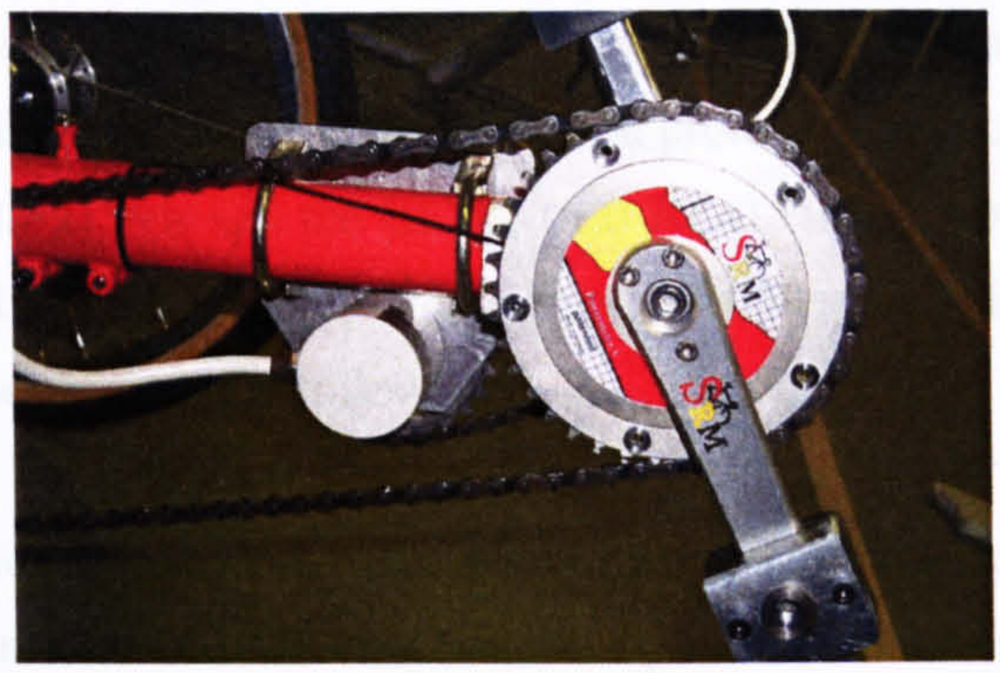

Figure 4.5: Torque measuring crank mounted on trike I.

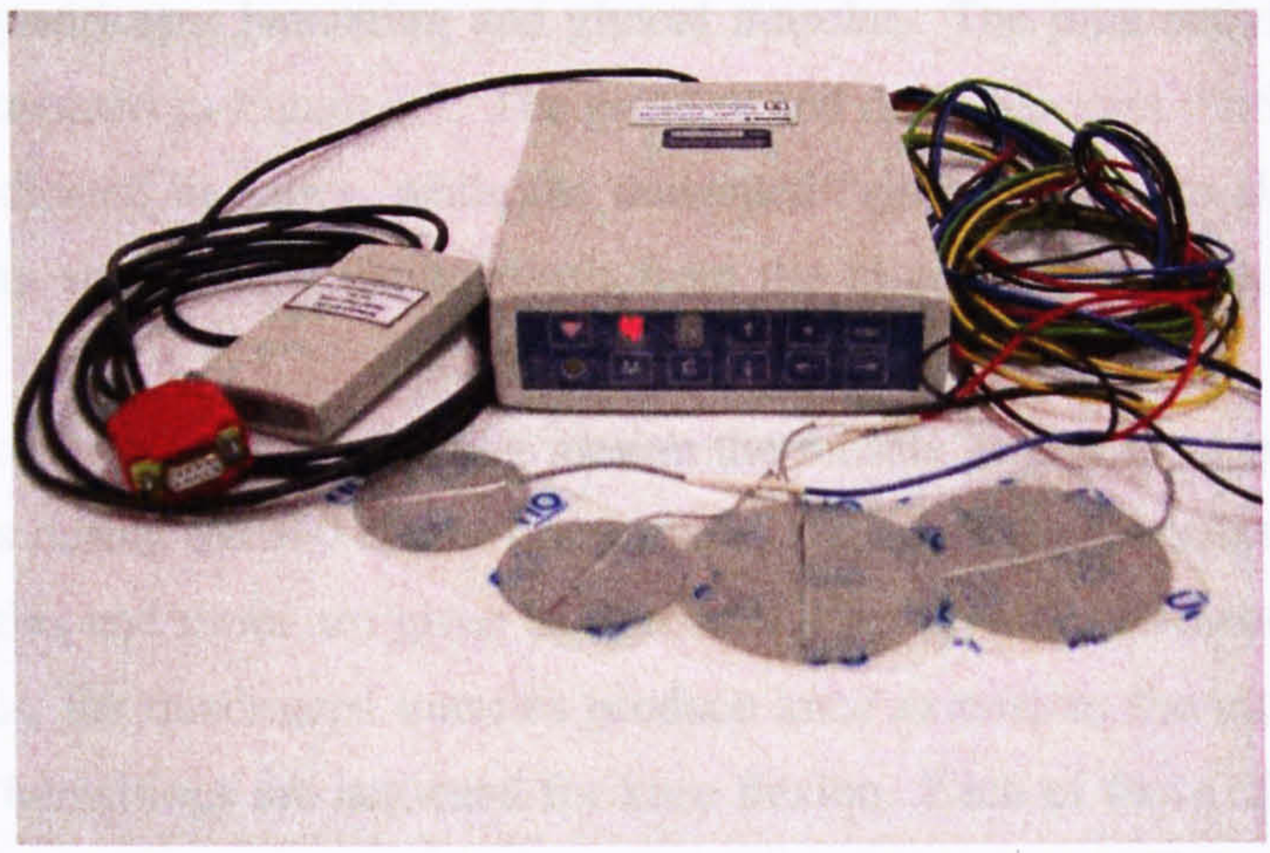

Figure 4.6: Portable stimulator with cables and surface electrodes. The RS232 interface has a galvanic isolation unit (small left box).

On trike I, a torque measuring crank[5] (resolution $\pm 2.5\%$) with four strain gauges was installed replacing the standard right crank (see Figure 4.5). The sensor also provides a measurement of cycling cadence. Thus, instantaneous power output at the crank can be computed as the product of instantaneous torque and angular speed.

Information arriving from the shaft encoder and potentiometer are processed either directly by the AD-converter and microcontroller of the portable 8-channel stimulator (cf. Figure 4.6) [71] or indirectly by a laptop-based data-acquisition system. The latter is preferable during test phases, where frequent changes of the program code are carried out. The signals from the torque/power sensor (trike I) are interfaced to analogue input channels of the data acquisition card installed in the laptop computer. The electric motor on trike I is speed controlled where the reference speed can be set by applying a voltage to the analog input port of motor electronics unit. This input is connected to an

[5]SRM - sensor kit, Schoberer Rad Messtechnik GmbH, Germany, http://www.srm.de

analogue output of the data acquisition card and serves as control signal for the motor.
While running the control software on the laptop, serial communication with the stimulator is established through an isolated RS232 link. Real-time data acquisition, communication protocols and control algorithms are implemented using MATLAB/SIMULINK and the EXTENDED REALTIME TOOLBOX[6]. The sampling frequency for feedback control was 20 Hz (i.e., sample interval of 50 ms), which corresponds to the chosen muscle stimulation frequency (see the following).

During the experiments reported here the stimulator operated at constant frequency (20 Hz), constant current for the individual muscle groups, adjustable in 10 mA increments up to a maximum of 120 mA, and the pulsewidth was varied on-line in the range $0 - 800\,\mu$s.

Stimulation Strategy: Pairs of surface electrodes are attached to each of the six muscle groups, i.e. the left and right quadriceps, hamstring and gluteal muscles. The joint activity generated by each muscle group is illustrated in Figure 4.7. The primary and desirable joint motion generated by each muscle group is indicated in italics, while the unwanted "side effects" are also shown. Unwanted muscle actions from surface stimulation result from the bi-articular nature of the quadriceps and hamstring muscles.
To achieve an effective and smooth cycling motion the muscle groups must be switched on and off at appropriate times during the 360 degree crank cycle. Details of the procedure for determination of the stimulation angles and times are given in Section 4.4.3. Typical stimulation patterns are shown in Figure 4.8. Thus, the quadriceps muscles produce knee extension, the gluteal muscles give hip extension, and the hamstrings are activated for knee flexion. Each of these effects is timed in order to produce significant positive crank moments. The stimulation pattern shown in Figure 4.8(a) indicates the positions where significant positive torque is generated by each muscle group under static conditions, i.e. for zero angular velocity. In order to compensate for dynamic muscle latency, i.e. the time following onset of stimulation before significant forces are produced, the stimulation patterns have to be shifted forward in time as cycle cadence increases. This is illustrated in Figure 4.8(b) for a cadence of 50 rpm. In general, the shift angle is directly proportional to cycling cadence.

The shaft encoder and throttle signals are interfaced to a stimulation program. Stimulation control ensures that the individual muscle groups are automatically switched on and off during cycling using a continuous measurement of the crank angle. To simplify the stimulation control, a common pulsewidth was applied to all muscles.

Mobile Cycling

The tricycles can be used for mobile cycling. In the work reported here only trike II was employed in experiments involving mobile cycling due to the reduced weight in comparison to the motorised trike

[6]Extended Real Time Toolbox, Humusoft, Czech Republic, http://www.humusoft.cz/rt/

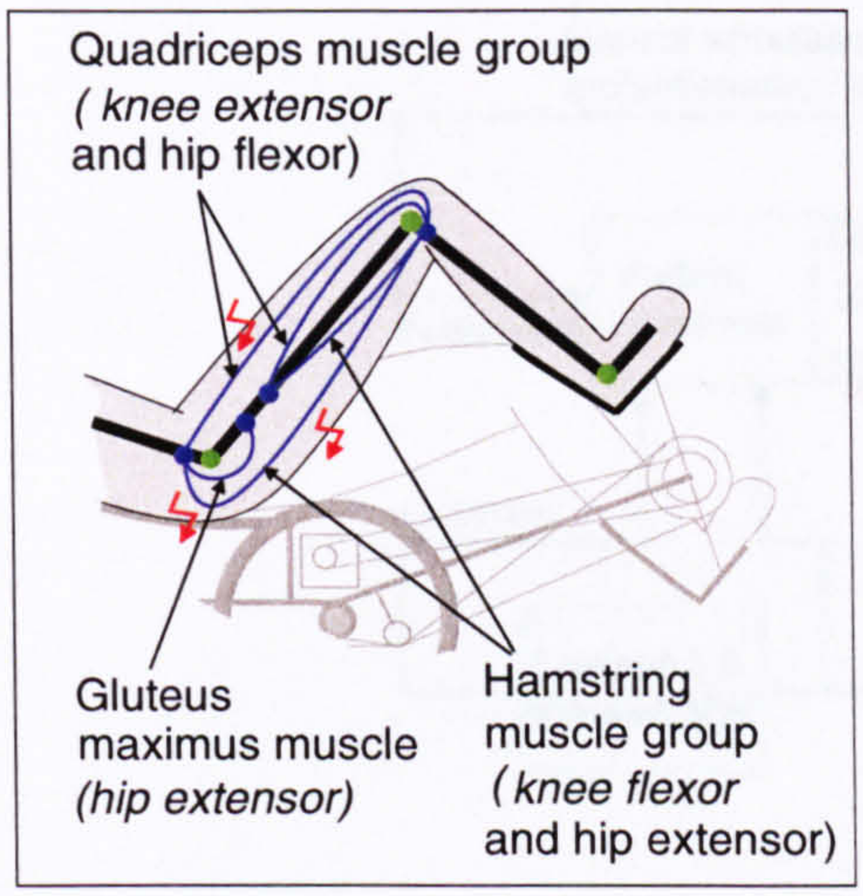

Figure 4.7: Stimulated muscle groups during FES cycling using surface electrodes. Desired muscle activities by the stimulation are shown in italics.

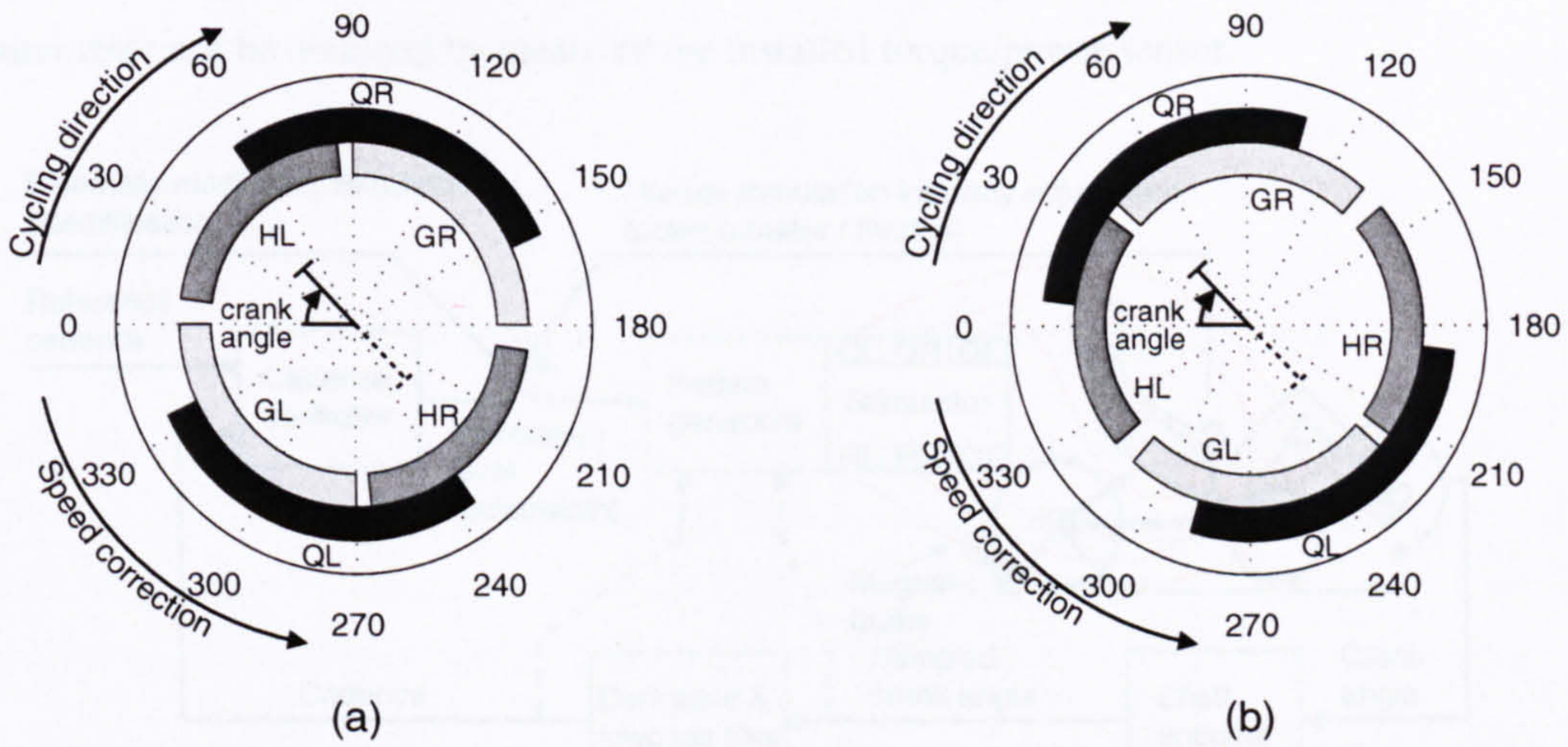

Figure 4.8: Stimulation patterns for one subject. (Q - Quadriceps, H - Hamstrings, G Gluteus, R/L - Right/Left) (a) "Static" pattern for zero cadence, (b) Shifted pattern at 50 rpm cycle cadence.

I. The stimulation intensity can be set by manual adjustment of the throttle so that the cycle's forward velocity can be controlled. This control structure is shown in Figure 4.9.

Isotonic Trainer Setup

When mounted on the cycle trainer, the tricycles can be operated as static isotonic ergometers. The resistance (load) can be adjusted on the cycle trainer. Stimulation intensity can be set manually by the cyclist, computer-controlled during identification periods, or set automatically under closed-loop cadence control dependent on the determined cadence as illustrated schematically in Figure 4.10. Feedback control of the cadence is described in detail in Chapter 6. With trike I, output power

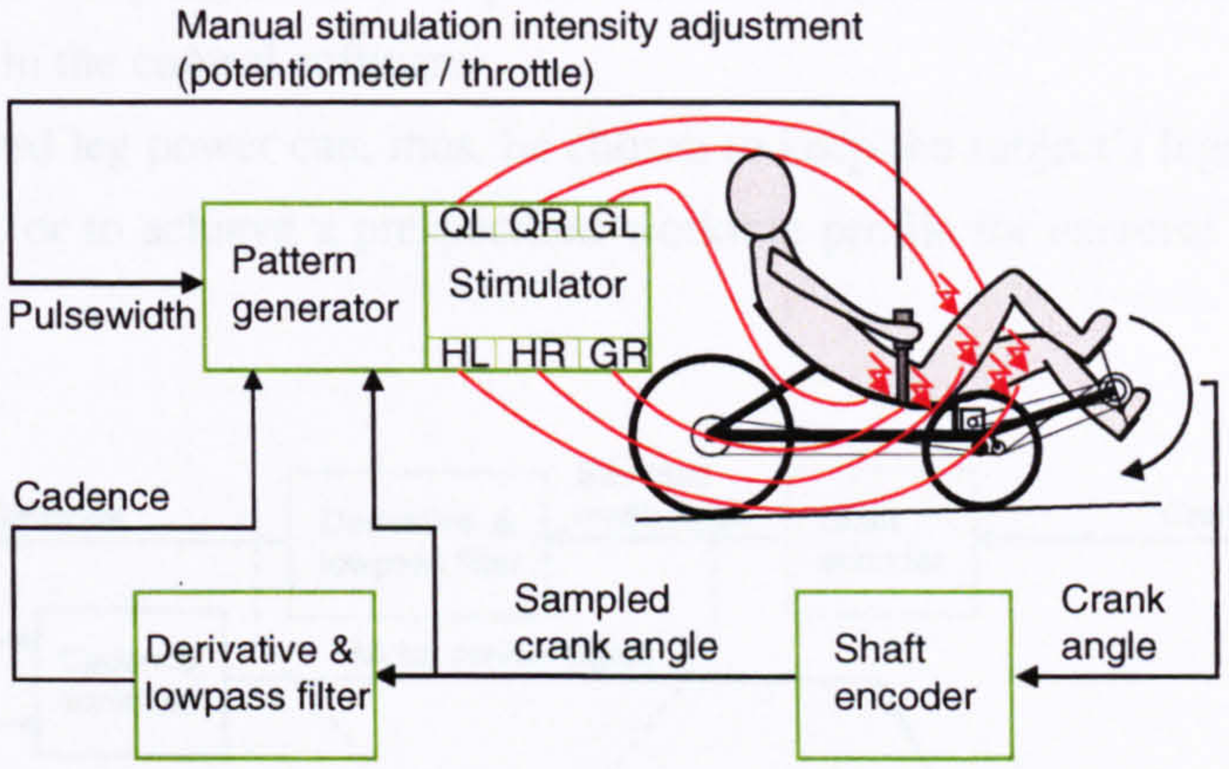

Figure 4.9: Control scheme for mobile FES cycling.

measurements can be obtained by means of the installed torque/power sensor.

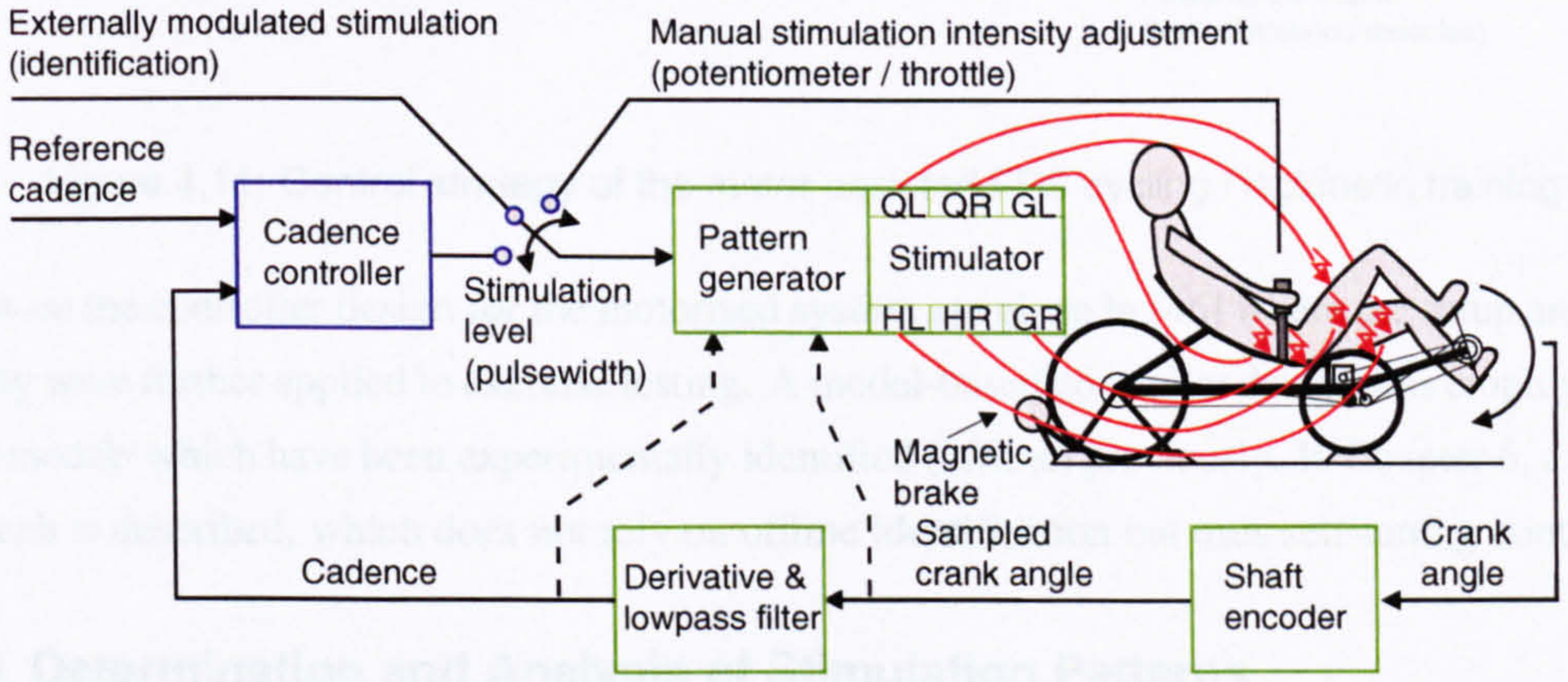

Figure 4.10: Control structure of the FES cycling system for isotonic training.

Isokinetic Trainer Setup – Motor Assisted Cycling

The motorised and instrumented trike I can be used for isokinetic training exercise where cycling cadence is maintained at a desired constant set point by the electric motor. The active power output of the cyclist by electrical muscle stimulation can be adjusted manually by using the throttle. Alternatively, simultaneous feedback control of cycling cadence and of leg power output can be applied. The control scheme with two independent feedback loops is shown in Figure 4.11. In the first loop, the electric motor input is automatically adjusted in such a way that the cycling cadence is controlled to a reference value by feedback. This feedback loop has a relatively high bandwidth. The second loop provides feedback control of leg power, as measured at the cranks. Stimulation intensity (here,

pulsewidth) is automatically adjusted to keep the measured power close to a reference value, which can be set arbitrarily in the control software.
The level of the desired leg power can, thus, be chosen to keep the subject's legs working at optimal operating conditions, or to achieve a prespecified workrate profile for exercise testing (e.g., step or incremental).

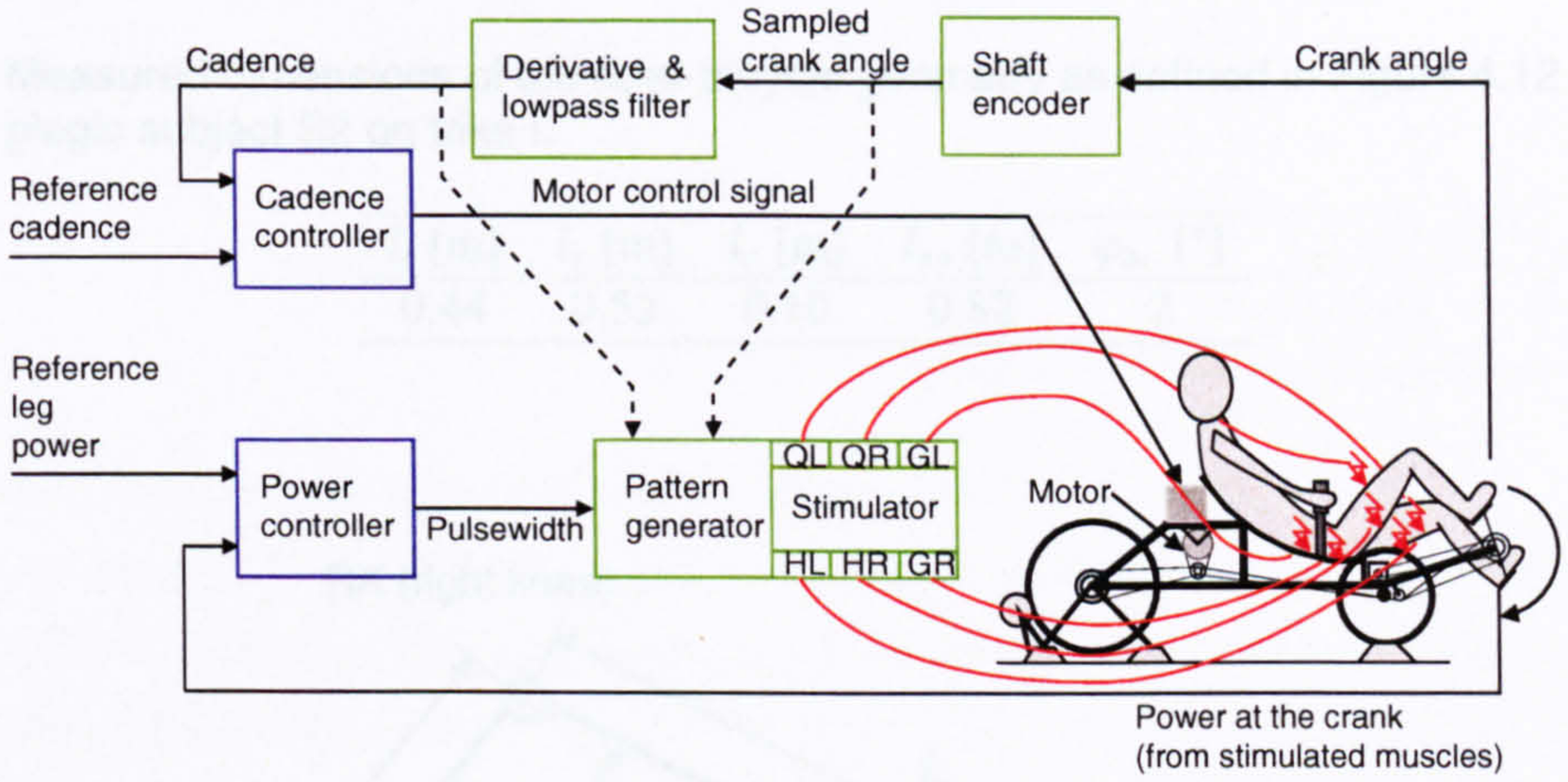

Figure 4.11: Control strategy of the motor assisted FES cycling / isokinetic training.

Details on the controller design for the motorised system are given in [46] where the setup and control stragety were further applied to exercise testing. A model-based controller design was employed using linear models which have been experimentally identified (offline) previously. In Chapter 6, a modified approach is described, which does not rely on offline identification but uses self-tuning control.

4.4.3 Determination and Analysis of Stimulation Patterns

Stimulation Intervals

An initial indication of suitable stimulation intervals can be gained by analysis of the rider-tricycle geometry. The aim is to parameterise the flexion and extension periods for the knee and hip joints in terms of the crank angle.

The mechanical structure of the rider-tricycle system can be described as a five-bar linkage, as depicted in Figure 4.12. The system is composed of the two lower legs consisting of shanks, feet and ankle orthoses, the two thighs and the link between left and right pedal axes formed by the left and right crank arm. All links are assumed to be rigid, and the ankle joints are fixed by the orthoses. Joints in the linkage are revolute joints with one degree of freedom, whereas the positions of hip joints and crank axis are fixed. The position where the crank arms are horizontally aligned and the right crank is close to the hip is defined as the zero crank angle. The entire system has one degree of freedom and

can be fully characterised by the crank angle. Note that freely movable ankle joints would increase the degrees of freedom by two.

The dimensions of the rider-tricycle system have been obtained by means of an ultrasound-based motion analysis systems[7]. Measurement markers were placed on one pedal axis, knee joint and hip joint. Table 4.2 gives the exact measurements for one subject which have served to generate the correctly-scaled linkage in Figure 4.12.

Table 4.2: Measured dimensions of the rider-tricycle geometry as defined in Figure 4.12 for the paraplegic subject S2 on trike I.

l_t [m]	l_s [m]	l_c [m]	l_{hc} [m]	φ_{hc} [°]
0.44	0.52	0.10	0.82	2

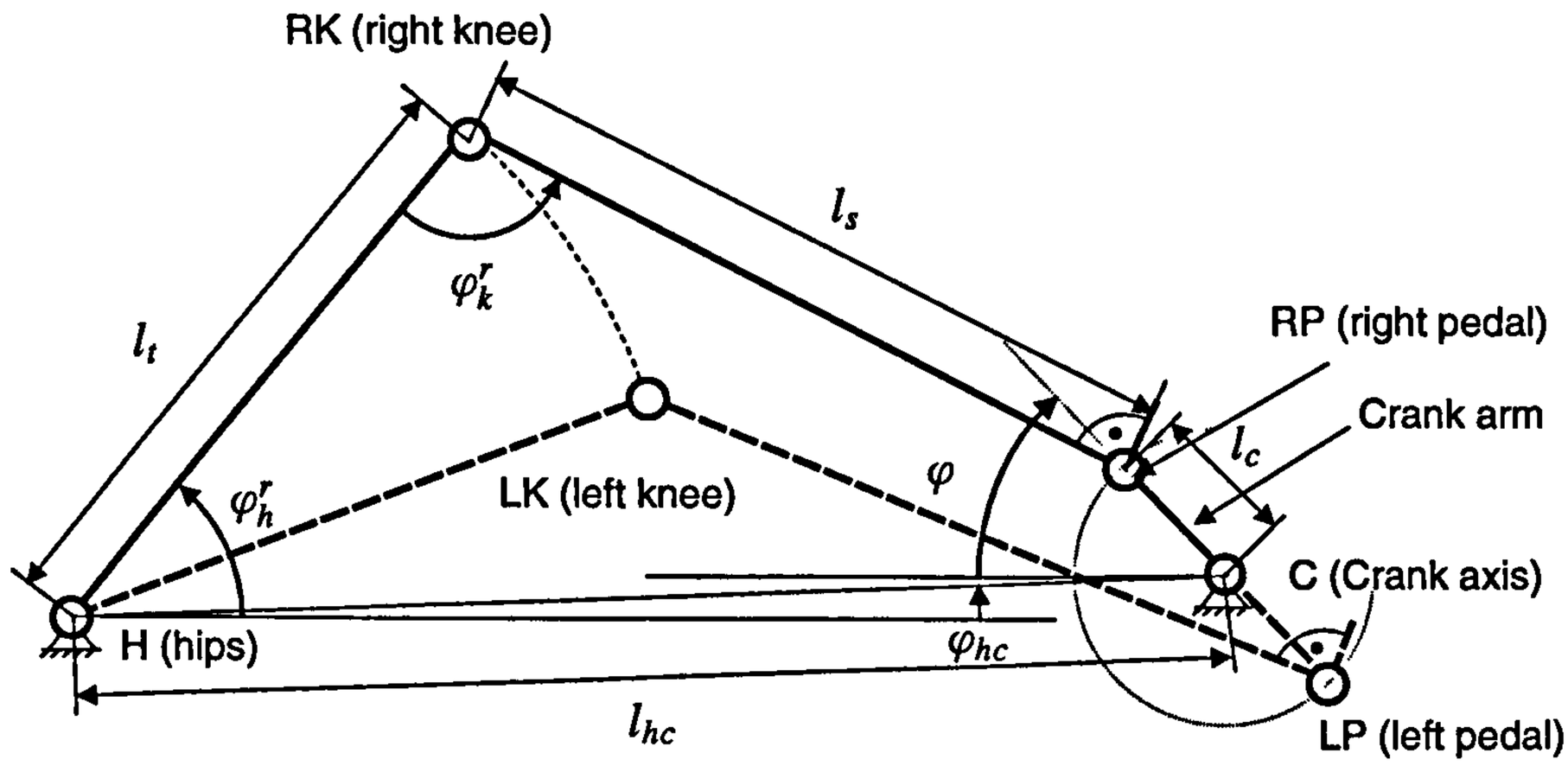

Figure 4.12: Rider-tricycle geometry. Five-bar linkage model for cycling including left and right lower and upper leg as well as the link formed by the two crank arms.

Due to symmetry, analysis of the linkage can be simplified by reducing the system to a four-bar linkage formed by only one leg and one crank arm. Thus, in the sequel, the right side only is analysed (the results are valid for the left leg with a phase shift of 180 degrees for the crank angle).

Using the triangles H(RP)C and H(RK)(RP) the right knee angle φ_k^r as defined in Figure 4.12 can be expressed in terms of the crank angle as follows

$$\varphi_k^r = \arccos\left(\frac{-l_{h,ra}^2 + l_s^2 + l_t^2}{2l_s l_t}\right) = \arccos\left(\frac{l_t^2 + l_s^2 - l_c^2 - l_{hc}^2}{2l_t l_s} + \frac{l_c l_{hc}}{l_t l_s}\cos(\varphi + \varphi_{hc})\right) \qquad (4.1)$$

where l_s, l_t and l_c are shank, thigh and crank arm lengths respectively, and φ is the crank angle. The

[7]Measurement system CMS-HS, zebris Medizintechnik GmbH, Germany, http://www.zebris.de

arrangement of the seat (hip) with respect to the crank axis C is described by its distance l_{hc} and the slope angle φ_{hc}. The distance $l_{h,ra}$ between the hip and the right ankle joint is then given by

$$l_{h,ra} = \sqrt{l_{hc}^2 + l_c^2 - 2 l_{hc} l_c \cos(\varphi + \varphi_{hc})}. \tag{4.2}$$

The relationship between the right hip angle and the crank angle becomes

$$\begin{aligned} \varphi_h^r &= \underbrace{\arccos\left(\frac{-l_s^2 + l_t^2 + l_{h,ra}^2(\varphi)}{2 l_t l_{h,ra}(\varphi)}\right)}_{\angle(RK)H(RP)} + \varphi_{hc} \\ &+ \operatorname{sign}(\pi - ((\varphi + \varphi_{hc}) \bmod (2\pi))) \underbrace{\arccos\left(\frac{-l_c^2 + l_{hc}^2 + l_{h,ra}^2(\varphi)}{2 l_{hc} l_{h,ra}(\varphi)}\right)}_{\angle(RP)HC}. \end{aligned} \tag{4.3}$$

Thus, the knee and hip angles are nonlinear functions of the crank angle.

Based on equations (4.1) and (4.3), the crank angle ranges for flexion and extension of knee and hips can be calculated. To do this, the crank angle arguments for the extreme values of hip and knee angles have to be determined. These are:

$$\begin{aligned} \varphi^{rk,min} &= \arg \min_{\varphi \in [0,2\pi)} \varphi_k^r(\varphi) = -\varphi_{hc} \\ \varphi^{lk,min} &= (\varphi^{rk,min} + \pi) \bmod (2\pi) \\ \varphi^{rk,max} &= \arg \max_{\varphi \in [0,2\pi)} \varphi_k^r(\varphi) = \pi - \varphi_{hc} \\ \varphi^{lk,max} &= (\varphi^{rk,max} + \pi) \bmod (2\pi) \\ \varphi^{rh,min} &= \arg \min_{\varphi \in [0,2\pi)} \varphi_h^r(\varphi) \\ \varphi^{lh,min} &= (\varphi^{rh,min} + \pi) \bmod (2\pi) \\ \varphi^{rh,max} &= \arg \max_{\varphi \in [0,2\pi)} \varphi_h^r(\varphi) \\ \varphi^{lh,max} &= (\varphi^{rh,max} + \pi) \bmod (2\pi). \end{aligned}$$

Thus, the crank angle argument $\varphi^{rk,min}$ is related to the minimum of the right knee angle φ_k^r etc. Figure 4.13 depicts the resulting flexion and extension ranges. Note that for the hips, the crank angle intervals related to flexion and extension differ in size.

To initiate and maintain a cycling movement, it is clear that the knee extensors (via quadriceps muscle group), knee flexors (via hamstring muscle group) and hip extensors (via gluteus maximus) must be activated by stimulation as the crank angle proceeds through the relevant flexion and extension intervals as summarised in Table 4.3 and Figure 4.13). The table also summarises the unwanted "side effects" of stimulation, i.e. activity at the hip which tends to act contrary to the primary desired cycling moments.

Having determined the crank angle intervals from the rider-tricycle geometry, the "static" (zero cadence) start and stop angles for stimulation are determined by the following strategy. Within an appropriate crank angle interval, relevant muscle groups are selectively stimulated at a range of discrete

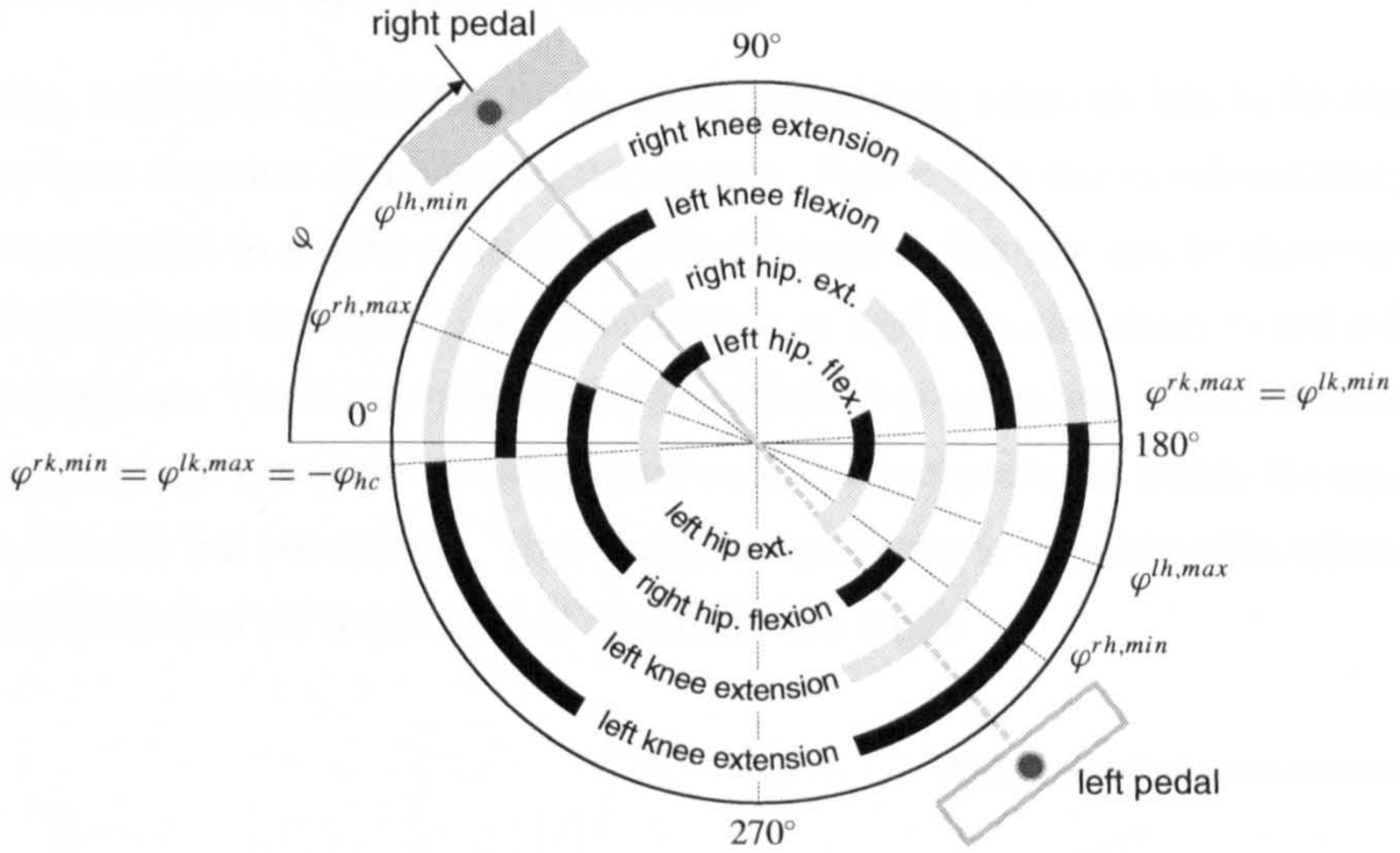

Figure 4.13: Ranges of joint flexion and extension derived from the rider-tricycle geometry.

Table 4.3: Muscle groups used for FES cycling and corresponding crank angle intervals.

Crank angle Interval	Required action	Stimulated muscle group	Unwanted side effect of the stimulation
$(\varphi^{rk,max}, \varphi^{rk,min})$	right knee flexion	right hamstring	right hip extension
$(\varphi^{lk,min}, \varphi^{lk,max})$	left knee extension	left quadriceps	left hip flexion
$(\varphi^{rk,min}, \varphi^{rk,max})$	right knee extension	right quadriceps	right hip flexion
$(\varphi^{lk,max}, \varphi^{lk,min})$	left knee flexion	left hamstring	left hip extension
$(\varphi^{rh,min}, \varphi^{rh,max})$	right hip flexion		
$(\varphi^{lh,min}, \varphi^{lh,max})$	left hip flexion		
$(\varphi^{rh,max}, \varphi^{lh,min})$	right hip extension	right gluteus maximus	
$(\varphi^{lh,max}, \varphi^{lh,min})$	left hip extension	left gluteus maximus	

crank angles while the pedal forces acting tangentially to crank rotation are assessed using a digital hand-held dynamometer.[8] The muscle activation (stimulation interval) was then limited to subintervals in which the stimulation intensity was justifiable with respect to the positive drive torque (to avoid injuries and rapid muscle fatigue), and where no strong co-activation of muscles was observed, working against the cycling motion. Avoiding ineffective muscle stimulation, with low force output, has the additional potential to reduce muscle fatigue as muscle recovery periods are extended. Static stimulation patterns obtained by this method are shown in Figure 4.8(a). The force measurements serve further to allow selection of the constant current amplitudes for the individual muscle groups. The aim is to even out differences in muscle strength for the muscle groups and body sides.

[8] "Portable Force Indicator", Mecmesin Ltd., UK, http://www.mecmesin.com

Dynamic correction of stimulation intervals

While cycling, a dynamic correction of the static stimulation intervals has to be carried out taking the dynamic force response of a muscle into account. Figure 4.14 shows schematically the isometric muscle force response to a train of stimuli. The dynamic behaviour can be characterised by a time delay t_1 and an increase time t_2 for muscle activation as well as a time delay t_3 and a decrease time t_4 for muscle relaxation. These parameters vary for different muscles and load conditions.

When cycling, the aim is to have the maximum muscle force available within the statically specified crank angle interval but not outside. Thus the stimulation has to be initiated in advance of the static start angle and switched off in advance of the static stop angle.

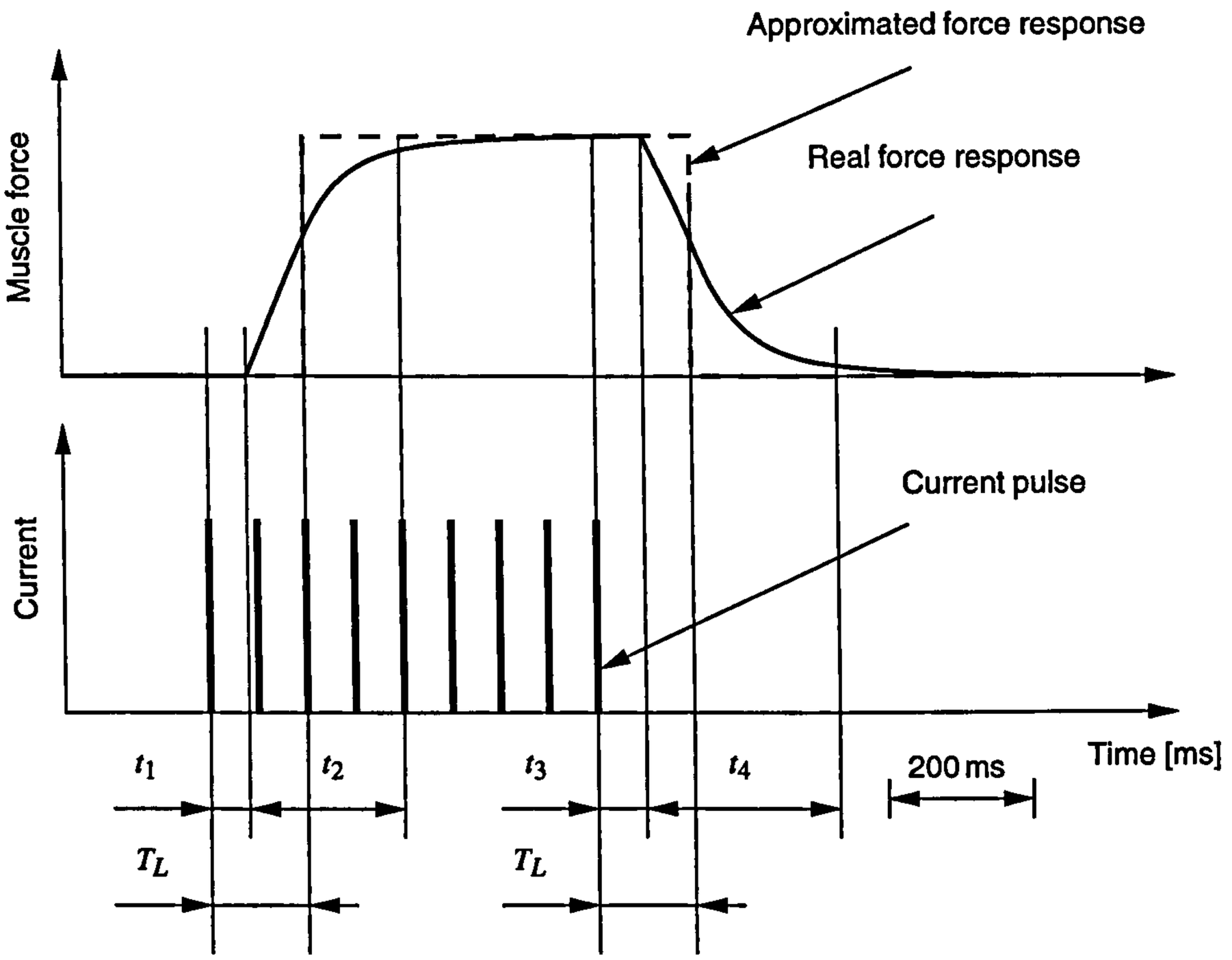

Figure 4.14: Isometric muscle force response to a train of stimuli.

For simplicity, we have assumed an approximated force response, as shown in Figure 4.14, with a unique latency time T_L for muscle contraction and relaxation. This latency time T_L corresponds to a pure time delay and is assumed to be the same for all muscles. Chen et al. [13] and Perkins et al. [63] also postulated an approximated force response in their work and reported a latency time T_L in the range of 100–250 ms.

Compensation of the latency time T_L is straightforward. The necessary time-advanced stimulation can be easily realised by rotating the entire static stimulation pattern opposite to the cycling direction and proportional to the speed. The start angle $\varphi^i_{start}(k)$ and stop angle $\varphi^i_{stop}(k)$ of the crank angle

interval for stimulating the i-th muscle group at the sampling time instant k are then given by

$$\varphi^i_{start}(k) = \varphi^i_{start,static} - T_L\omega(k) \qquad \text{and} \qquad \varphi^i_{stop}(k) = \varphi^i_{stop,static} - T_L\omega(k) \tag{4.4}$$

where $\varphi^i_{start,static}$ and $\varphi^i_{stop,static}$ are the statically-derived start and stop angles for the stimulation of the muscle group i, and ω is the angular velocity.

The latency time T_L is obtained using a simple trial and error strategy. While constant pulsewidth, stimulation frequency and current settings are applied, the proportionality factor T_L is altered in discrete steps. For each setting of T_L the resulting steady-state cycling movement is observed and subjectively assessed. A value of T_L which gives a high cycling speed with smooth motion (no jerks) over the crank rotations is then selected. A latency time of 130 ms was obtained for all subjects by the application of this strategy. Thus, the resulting stimulation pattern for a speed of 50 rpm based on the "static" pattern in Figure 4.8(a) is depicted in Figure 4.8(b).

Effect of Discrete-Time Stimulation and Crank Angle Sampling

Until now, muscle stimulation has been considered to be continuous in time when deriving the stimulation patterns. In reality, artificial muscle stimulation represents a discrete-time process. This fact has an impact on the smoothness of the FES cycling motion, especially if the stimulation frequency is low. As already mentioned, a frequency of 20 Hz has been applied during the experiments reported here. To keep the implementation simple and computational burden low, the decision on sending pulses is taken every 50 ms (corresponding to the stimulation frequency) based on the currently sampled crank angle. Assuming constant speed, the crank angle will change by $\Delta\varphi = \omega T_s$ (sampling time $T_s = 50$ ms), between two sampling instances where ω is the cycle cadence.

Crank angles at which electrical pulses can be sent will consequently differ from cycle to cycle. An ongoing variation of the stimulation pattern occurs. It is practically impossible that pulses are sent exactly at the begin and the end of the originally specified intervals. Hence, the actual stimulation always starts later and stops earlier than specified (see Figure 4.15). As a consequence, the indented stimulation range with respect to the crank angle will be reduced.

The effect of sampling the crank angle can be interpreted as an increase in muscle contraction delay and a reduction of the muscle relaxation delay. The magnitudes of these changes vary from cycle to cycle in the range 0-50 ms (for 20 Hz stimulation) and are different for muscle activation and muscle deactivation. Modifying the original stimulation pattern (basically extending the intervals to counteract the trimming) would only have an influence on the expectation value of the stimulation interval length but not on the variance. In this work, such a step is omitted as it would require the exact knowledge of latency times in muscle contraction and relaxation for the individual muscles which cannot be experimentally obtained using the current setup. It should be noted, that the previously determined latency time T_L reflects the net effect of muscle dynamics and discrete-time stimulation. Measurements of the crank angle at a higher rate than the stimulation frequency could be used to better detect at least the correct onset of stimulation better.

A higher stimulation frequency combined with fast crank angle sampling would definitively mitigate the negative effect of sampling on the stimulation accuracy.

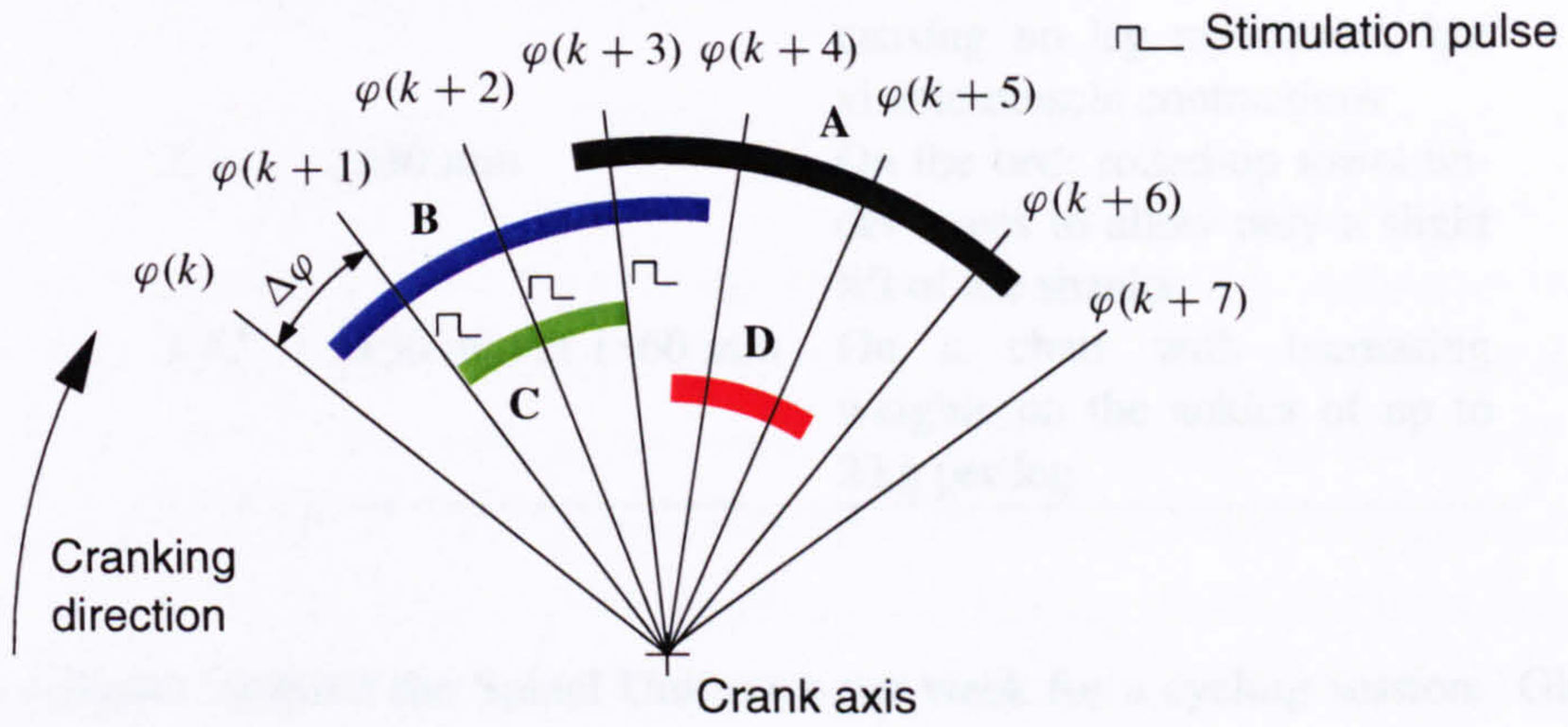

Figure 4.15: Effect of sampling on the stimulation: The statically determined crank angle interval **A** for stimulating one muscle group will be shifted anti-clockwise for higher speeds to compensate the latency effect in the force generation and degeneration. This rotation results in stimulation interval **B**. Assuming perfect continuous stimulation, effective muscle force will be built up over the desired interval **A**. However, the discrete time decision on sending electrical stimuli shortens the actual stimulation range to the interval **C** which results in an effective muscle force over the interval **D**. This interval is shorter than the interval **A**. The crank angles $\varphi(k+i), i = 0, 1, 2, \ldots$ are used to check if muscle stimulation has to be active or not. $\Delta\varphi$ is the speed dependent crank angle interval between two sampling instants.

4.5 Training Protocol

The subjects initially carried out a programme of muscle strengthening using a portable electronic stimulator[9] at home on a daily basis, which continued over the entire study period of one year. The training consisted of quadriceps and hamstrings stimulation. A stimulation frequency of 20 Hz was chosen. The knee extensors and flexors were stimulated one after the other in two separate phases. For each phase, stimulation was ramped up over two seconds, held for six seconds and ramped down over two seconds with a two second pause before the other phase was started. The exercise regime was gradually increased starting with low initial muscle action so that no damage was caused to the atrophied leg muscles. Table 4.4 shows the exercise regime which has been proven to be suitable. The flexion of the knee was always opposed by cushions or bedding.

During the initial training period of 6-8 weeks subjects attended the Spinal Unit at the Southern General Hospital one day per week, for progress monitoring and preparation for FES cycling. When the major cycling muscles (quadriceps and hamstrings) were judged to be sufficiently strong, subjects began a programme of "static" isotonic FES cycling with the tricycles mounted on cycle trainers. At

[9] Odstock 4 channel stimulator, England, http://www.salisburyfes.com/stimulat.htm

Table 4.4: Prescribed exercise regime for strengthening hamstrings and quadriceps.

Week	Daily duration	Comments
1	2x15 min	On the bed, limited stimulation causing no leg movements but visible muscle contractions
2,3	2x30 min	On the bed; rolled-up towel under knees to allow only a slight lift of the shanks
4-52	2x30 min or 1x60 min	On a chair with increasing weights on the ankles of up to 2 kg per leg

this stage subjects attended the Spinal Unit once per week for a cycling session. Gluteal muscles were trained only by the cycling exercises. When each subject became proficient in cycling on the trainer, they began sessions of mobile cycling outside. During the pilot study, outdoor cycling was investigated using only the trike II which weighs less than trike I due to the absence of an electric motor. Again, cycling sessions took place once per week. Motor assistance was not activated, neither for "static" nor for mobile cycling.

4.6 Results and Discussion

4.6.1 Cycling Performance

All subjects were able to start cycling after 6 to 8 weeks of home training. Subjects S1 and S2 improved progressively to the stage where they were able to cycle continuously and reliably on the trainer situated within the rehabilitation gymnasium for periods of 30-40 minutes, after approximately 3 months of participation in the programme. One year after starting the study, subjects S1 and S2 could cycle continuously for at least 1 hour on the trainer while sustaining a work rate of 15-20 W.
Progress with subject S3 was initially hindered by the appearance of spasms in the calf muscles (a clonus effect), which prevented him from cycling for more than a minute or two. However, persistence with the training regime and "tuning" of the mechanical arrangement of the apparatus improved results. Additionally, subject S3 carried out 15-20 minutes of standing in a standing frame prior to cycling, in order to stretch the calf muscles. This was found to significantly resists the onset of clonus. At the end of the study, subject S3 was able to cycle on the trainer for 30 minutes at a time.
Approximately 3-4 months after the subjects joined the programme they started to participate in mobile cycling sessions, on a tarmac track situated adjacent to the Spinal Unit. Subjects S1 and S2 have completed up to 3km in a single session with a speed of 4-7 km/h; and Subject S3 achieved a distance of 1.4km (with partial assistance). Each outdoor "session" lasted approximately 30-40 min and consisted of 10-minute bouts of cycling, each followed by a 5-minute rest period. As noted above,

Subject S3 became proficient in cycling later than S1 and S2. He was therefore significantly weaker and fatigued more rapidly.

4.6.2 Analysis of Cycling Motion Smoothness

The appearance of FES cycling was difficult to distinguish from the cycling of able-bodied individuals. Figure 4.16 shows an example of the time course of the cycle cadence (upper graph) during paraplegic cycling on the isotonic trainer setup while applying a constant stimulation intensity (lower graph). A plot of the averaged cadence over several crank rotations as a function of the crank angle is given in Figure 4.17. The ripple in the measured velocity is caused by the gravity of the legs in conjunction with the applied crude stimulation pattern, the differences in force generation of left and right leg as well as the asymmetries in the mechanical setup (e.g. slightly different crank arm lengths on left and right side). This intra-cycle speed variation consists mainly of two frequency components. Asymmetries in the mechanical setup and in left/right leg force generation are reflected by a frequency which is the same as the cadence, whereas the weight of the legs mainly causes velocity variations at a frequency which is twice the cadence. The calculated power spectrum (see Figure 4.18) of the cadence shows peaks close to the predicted frequency components of the ripple while the mean value of the cadence is 43.3 rpm which is equivalent to 4.53 rad/s.

The low frequency components in the power spectrum and the relatively large confidence interval of the speed parameterised by the crank angle in Figure 4.17 can be mainly explained by the varying stimulation pattern due to low sampling and low stimulation frequency. To visualise this effect for the experiment reported in Figure 4.16, the actual start and stop crank angles $\tilde{\varphi}^{QR}_{start}(j)$ and $\tilde{\varphi}^{QR}_{stop}(j)$ for right quadriceps stimulation of the cycle j have been used to calculate reversely the corresponding "virtual" static start and stop angle $\hat{\varphi}^{QR}_{start,static}(j)$ and $\hat{\varphi}^{QR}_{stop,static}(j)$ by

$$\hat{\varphi}^{QR}_{start,static}(j) = \tilde{\varphi}^{QR}_{start}(j) + T_L\hat{\omega}(j, \tilde{\varphi}^{QR}_{start}(j)) \quad \text{and} \quad \hat{\varphi}^{QR}_{stop,static}(j) = \tilde{\varphi}^{QR}_{stop}(j) + T_L\hat{\omega}(j, \tilde{\varphi}^{QR}_{stop}(j))$$

where $\hat{\omega}(j, \tilde{\varphi}^{QR}_{start}(j))$ and $\hat{\omega}(j, \tilde{\varphi}^{QR}_{start}(j))$ are the recorded angular velocities at the crank angles on which the first and last pulse for the j-th cycle have been generated. Sufficient force by the right quadriceps is then approximately generated within the crank angle interval $(\hat{\varphi}^{QR}_{start,static}(j), \hat{\varphi}^{QR}_{stop,static}(j))$ for the cycle j. In the upper part of Figure 4.19, the "virtual" static start and stop angles are plotted together with the originally specified static start and stop angle. The resulting interval length for right quadriceps stimulation is depicted in the lower graph. The ongoing variation and shortening of the interval are clearly recognisable.

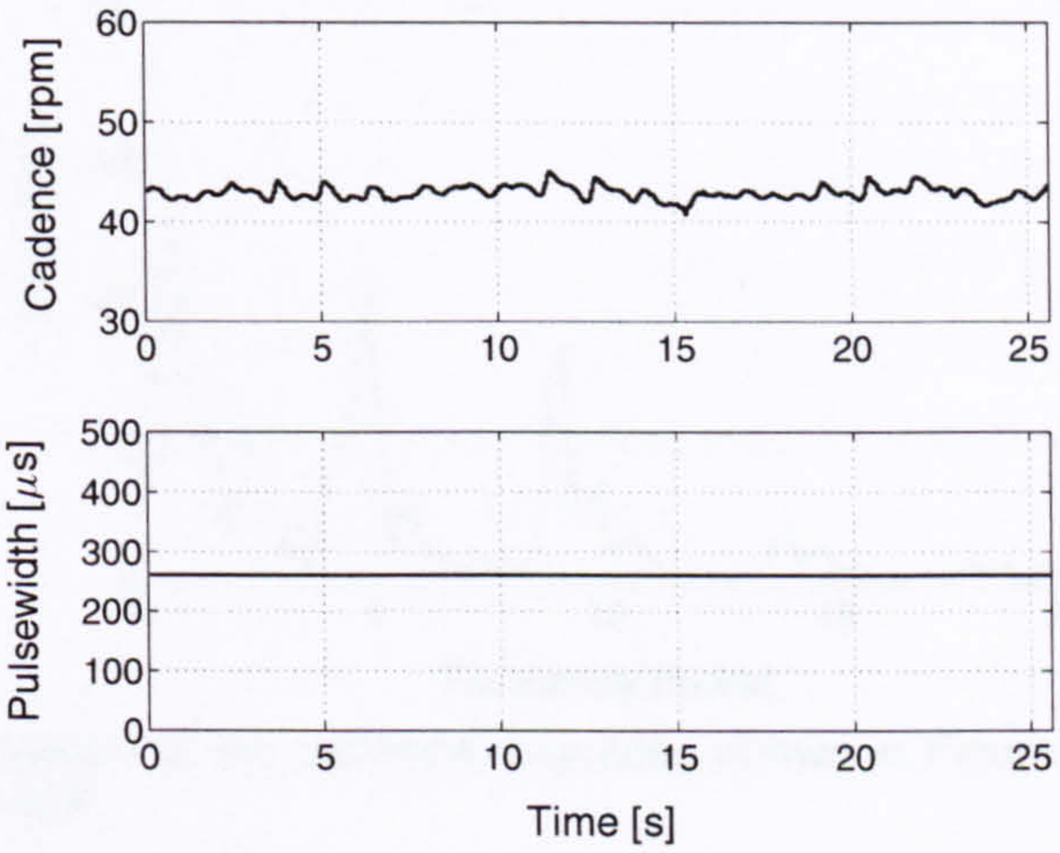

Figure 4.16: Measured steady-state cadence for constant stimulation intensity.

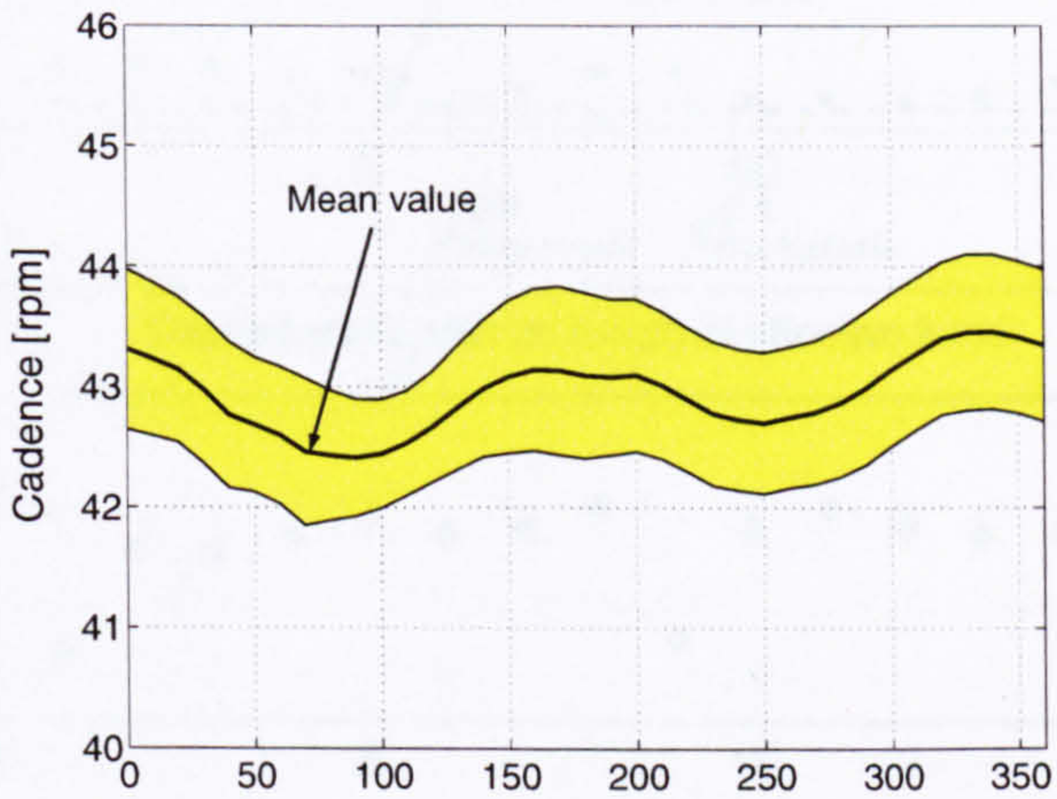

Figure 4.17: Cadence versus crank angle for steady-state cycling. Cadence mean value and standard deviation (shown as 68% confidence interval) have been estimated from the cadence shown in Figure 4.16, covering 16 full crank rotations.

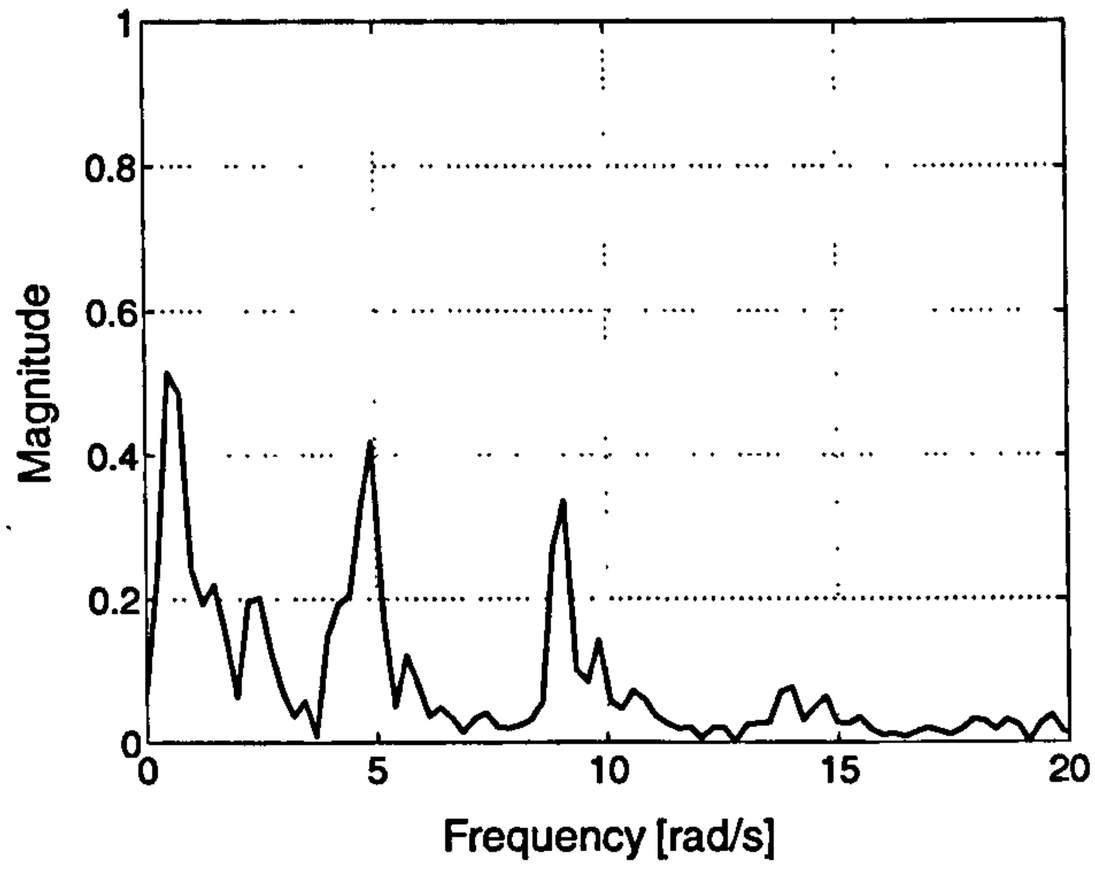

Figure 4.18: Power spectrum of the cadence sequence shown in Figure 4.16 after removing mean value and drift.

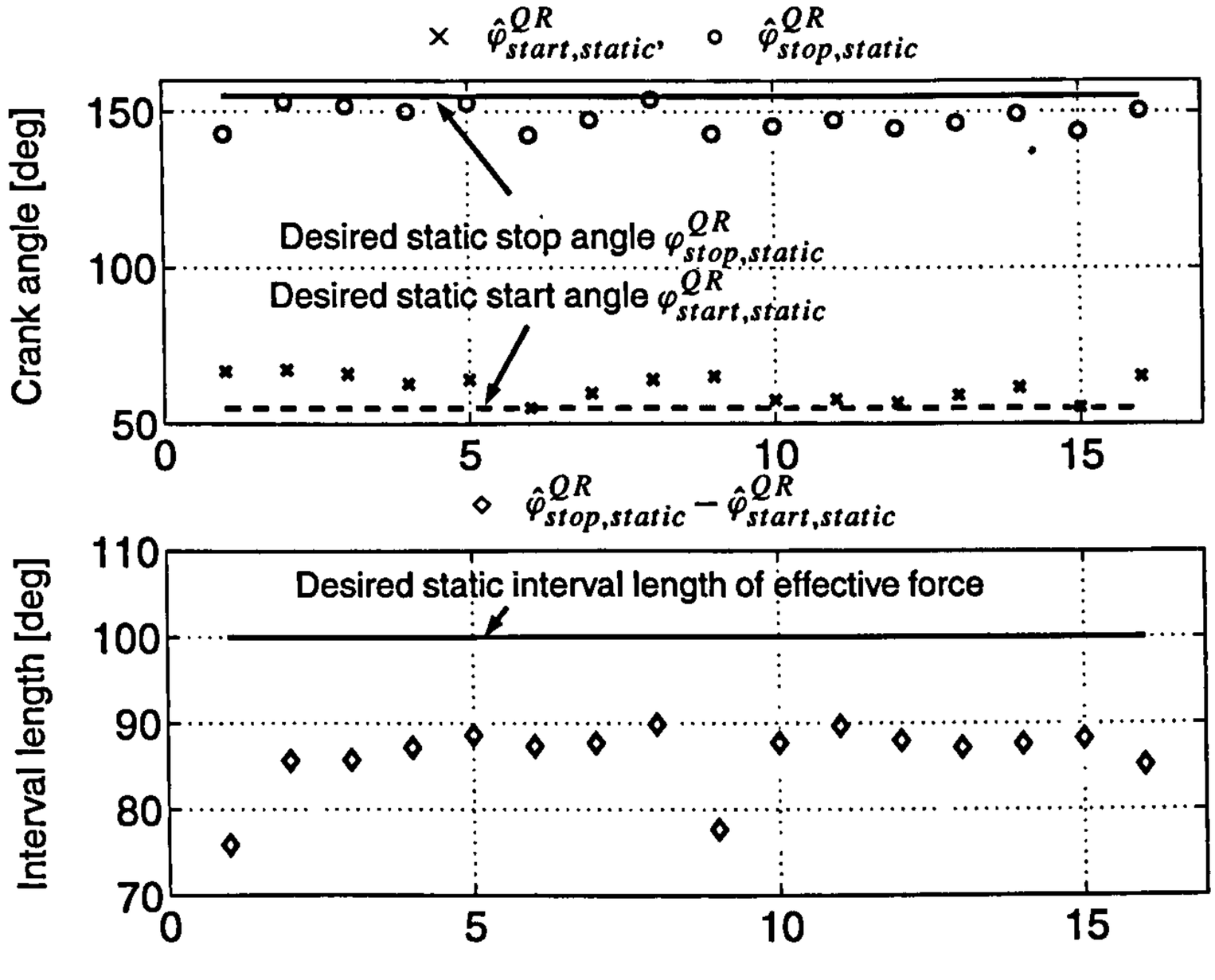

Figure 4.19: "Virtual" static stimulation intervals of the right quadriceps for the experiment reported in Figure 4.18. The estimated intervals are given by ($\hat{\varphi}^{QR}_{start,static}$, $\hat{\varphi}^{QR}_{start,static}$). The resulting interval length $\hat{\varphi}^{QR}_{stop,static} - \hat{\varphi}^{QR}_{start,static}$ is smaller than the length of the originally specified static interval which is given by $\varphi^{QR}_{stop,static} - \varphi^{QR}_{start,static}$. The cycle to cycle variation of the stimulation interval due to sampling is clearly visible.

4.7 Summary and Conclusions

Mobile FES cycling systems have been developed based on the adaptation of commercially available recumbent tricycles. The systems can be either used as a static ergometer for training exercises or as a mobile device for recreational use. One system has been further equipped with an electric motor to assist the FES cycling. This enables isokinetic training and exercise testing. Stimulation patterns have been derived by a simple strategy where the rider-tricycle geometry and static (isometric) pedal force measurements are taken into account. The resulting patterns are subject specific. The long term usage of the developed systems with paraplegic individuals has been reported proving the effectiveness and usability of the devices. Regular periods of FES cycling have been achieved, including outdoor cycling over significant distances on a tarmac track. It can be concluded that mobile FES cycling over useful distances is a realistic option for the paraplegic population.

In the future, a higher stimulation frequency could be applied to increase the power output as proposed by Eser et al. [19]. This would also improve the accurancy of stimulation. The objective is to stimulate as well as possible within the specified angle intervals while having minimal variation of the pulse positions with respect to the crank angle between rotations.

Variable frequency trains would be another measure to increase power output. However, the stimulator used in the experiments with the tricycles did not allow the straightforward implementation of variable frequency trains. In Chapter 6, a new static motorised FES ergometer system is presented. In co-operation with a company, a new stimulator device has been developed. Bottlenecks of the old stimulator have been removed in the new stimulator design. The new stimulator can be also used for the recumbent tricycle based cycling systems. Experimental validation of the systems with the new stimulator device must be conducted in future.

Isotonic cycling exercise on the trainer setup has been carried out by the subjects during the pilot study mainly because of the motivation aspect. Furthermore, the technical solution for isokinetic cycling was not available from the beginning of the study. Isokinetic cycling exercise at lower cadences for muscle strength training of the atrophied muscles would have been an alternative to the muscle strength training at home. This option should be considered for new paraplegic subjects who are introduced to FES cycling.

The motorised tricycle (trike I) was not used for mobile cycling within this pilot study. Further research has to focus on mobile cycling with motor assistance. Initially a simple open-loop strategy to balance the energy input from the motor and from the stimulated muscles can be tested. The integrated control strategy used for the isokinetic cycling on the trainer can also be applied for mobile cycling. The net effect of this control scheme is that smooth cycling motion at constant cadence (or, equivalently, depending on the gear engaged the cycle's forward speed) can always be achieved by the motor control loop, even if the leg power contribution varies or becomes low as a result of fatigue, or if the total load changes. Effectively, the total mechanical power output of the rider-tricycle system, which is comprised of the sum of motor power and leg power, is automatically varied

in order to maintain the instantaneous value of desired cadence. Independently, the muscle stimulation loop could attempt to keep the muscles working at an arbitrarily specified work rate, and, thus, it is the motor power which automatically varies in order to meet the overall total instantaneous power requirements.

5 Motorised Static Ergometer System for FES Cycling

5.1 Summary

Aim: The work presented in this chapter aimed to develop a compact and inexpensive motorised FES ergometer system which can be used while sitting in a wheelchair. An isotonic and an isokinetic training mode were realised by controlling the electric motor in appropriate ways.

Methods: A commercially available motorised ergometer system has been integrated with a newly developed stimulation device. Stimulator and ergometer are connected to a laptop computer which runs the control software. Crank angle, cadence and motor torque are estimated from the ergometer signals provided through a serial communications link. Sensor fusion by an extended Kalman filter was applied and signal calibration methods were developed and implemented to obtain the data. The ergometer was further instrumented with an absolute shaft encoder to gain an accurate angle measurement as reference to validate the angle estimate obtained by the extended Kalman filter.
The crank angle is checked every 5 ms to detect whether muscles have to be stimulated or not. In addition, variable frequency trains can be generated by the stimulation device in a simple manner.
The standard motor control of the ergometer was used to realise isotonic and isokinetic training modes for FES cycling. Furthermore, a customised cadence controller for the isokinetic training mode has been designed as an alternative to the built-in cadence controller of the ergometer to allow a better rejection of disturbances which are periodic with respect to the cadence. The control scheme includes a plug-in repetitive controller as described in Chapter 2. The duty cycle of the motor pulsewidth modulation (PWM) is used as the control signal for the customised cadence controller.
The developed ergometer system for FES cycling has been experimentally tested by one of the investigators.

Results: The commercially available ergometer used is suitable for realising isotonic and isokinetic training in FES cycling. No modifications to the ergometer have to be carried out. Pedalling cadence during isokinetic training and resistance (load) during isotonic training can be well controlled when using the standard built-in motor controller. Cadence varies only slightly during the isokinetic training with a variation below 10 rpm for typical crank moments caused by the electrical stimulation.

By using the customised cadence controller, the amplitude of the cadence variation can be significantly reduced to below 1 rpm. However, an angle sensor has to be mounted on the ergometer for the technical realisation of this controller.
Accurate information about the active crank moment and power output caused by the electrical stimulation of the muscles can be obtained with this system.

Conclusions: The developed motorised FES cycling system represents the first static ergometer which offers both isotonic and isokinetic training mode. It is compact and relatively inexpensive (about GBP 4000). The system can be used for research purposes due to its accuracy, provided measurements and FES parameter flexibility, while its size and cost also make it appropriate for home use. The solution with customised cadence control is interesting for research where accurate control of cadence is required. Standard cadence control is sufficient for clinical and home use.

Contribution: The author's contribution to this study consists of the development of the concept for the motorised FES cycling ergometer system. Control algorithms have been developed and implemented in software on the laptop and microcontroller of the stimulator device. Furthermore, the author has planned and conducted the experimental tests and analysed and interpreted the results.

5.2 Motivation

FES cycling systems based on recumbent tricycles can be used for mobile cycling and stationary training (cf. Chapter 4). In conjunction with an auxiliary motor, cyclists with a weak or fatigued musculature can also perform cycling exercises. However, there are some drawbacks to this solution. Firstly, the system requires quite a lot of space and is therefore not perfectly suitable for in-house use. Second, converting the mobile system into a trainer and vice versa cannot be carried out by the paraplegic cyclist alone; assistance is required. And third, a transfer of the paralysed cyclist between tricycle and wheelchair is always necessary. Transfers may require further assistance and carry the risk of falls. Space and assistance are usually no problem in a clinical or research environment but may be limitations in using such an FES cycling system at home.
These considerations have led to the idea of using commercially available ergometers with motor assistance for FES cycling which can be operated while the cyclist sits in a wheelchair. The motor can be utilised to enable both isokinetic and isotonic training. Fornusek et al. [26] followed independently of this work the same idea and developed an FES cycling ergometer for isokinetic training.
Within this chapter a newly developed FES cycling system based on a commercial ergometer is presented which allows both isokinetic and isotonic cycling exercise. The structure of this Chapter is as follows. In Section 5.3, the experimental setup will be outlined, with the focus on the ergometer used. Cadence, torque and crank angle are signals needed for the algorithms in FES cycling. Estimation and calibration of these signals from available measurements at the ergometer side as well as

the PC control of the ergometer are explained throughout Section 5.4. After this, in Section 5.5, the stimulator device and pattern generator will be described. Subsequently, the control of the DC motor in order to realise isokinetic and isotonic cycling exercises is discussed in the Sections 5.6 and 5.7. Finally, a summary is given in Section 5.8.

5.3 Experimental Setup

The commercially available ergometers THERA-vital™ and THERA-live™ by the German company medica Medizintechnik GmbH[1] have been chosen for the purpose of FES cycling. Both trainers are motor driven and controlled by a microcontroller. The main difference between the devices is in the provided control unit. The user interface of the THERA-vital provides more information such as biofeedback to the cyclist. The construction of the THERA-live is slightly more robust compared to the THERA-vital. According to manufacturer, a new generation of THERA-vital devices will be available by the end of 2005 having the same base construction and thus stability as the THERA-live. In the sequel, the words trainer and ergometer refer to THERA-vital and THERA-live equally. Experiments within this thesis are based on a THERA-vital trainer.

The ergometer is a certified medical device which is suitable for use at home, in clinics, homes for the elderly or hospitals. It is meant for mobilisation of persons that are disabled in their movement after accidents, surgeries, or after general illnesses which concern the apparatus of movement. The trainer can be used as a leg trainer and as an upper torso trainer. Within this work, only the leg trainer is of interest. It is appropriate for active and passive exercise. Indications are neurological disabilities such as stroke, paraplegia, hemiplegia/hemiparesis, Parkinson's disease and multiple sclerosis. The medical use of the trainer for spinal cord injured persons was recently investigated [53]. In paraplegia, benefits of passive, motor supported cycling exercises are a reduction of spasticity, the prevention of joint contractures and the improvement of range of motion. During the training the patient is seated on a chair or in a wheel-chair in front of the ergometer (cf. Figure 5.1). The feet are fixed to foot rests and the legs are stabilised by ankle joint orthoses. Depending on the chosen accessories crank arm lengths in the range 50–110 mm can be realised. These settings are similar to those of Chapter 4.
By applying electrical stimulation to the paralysed muscles during the cycling, the exercise can be rendered from passive to active for the paraplegic subject. Typically, stimulated muscles are the quadriceps, hamstrings, gluteus maximus and gastrocnemius.
The experimental setup for the lower-limb FES cycling ergometry is shown in the Figures 5.2 and 5.3. Two approaches can be distinguished. For clinical research the stimulation control is PC-based as shown in Figure 5.2. The stimulator's functionality reduces in this case to the generation of stimulation pulses that are requested by the PC software. The stimulation intensity can be controlled

[1] http://www.theravital.de/

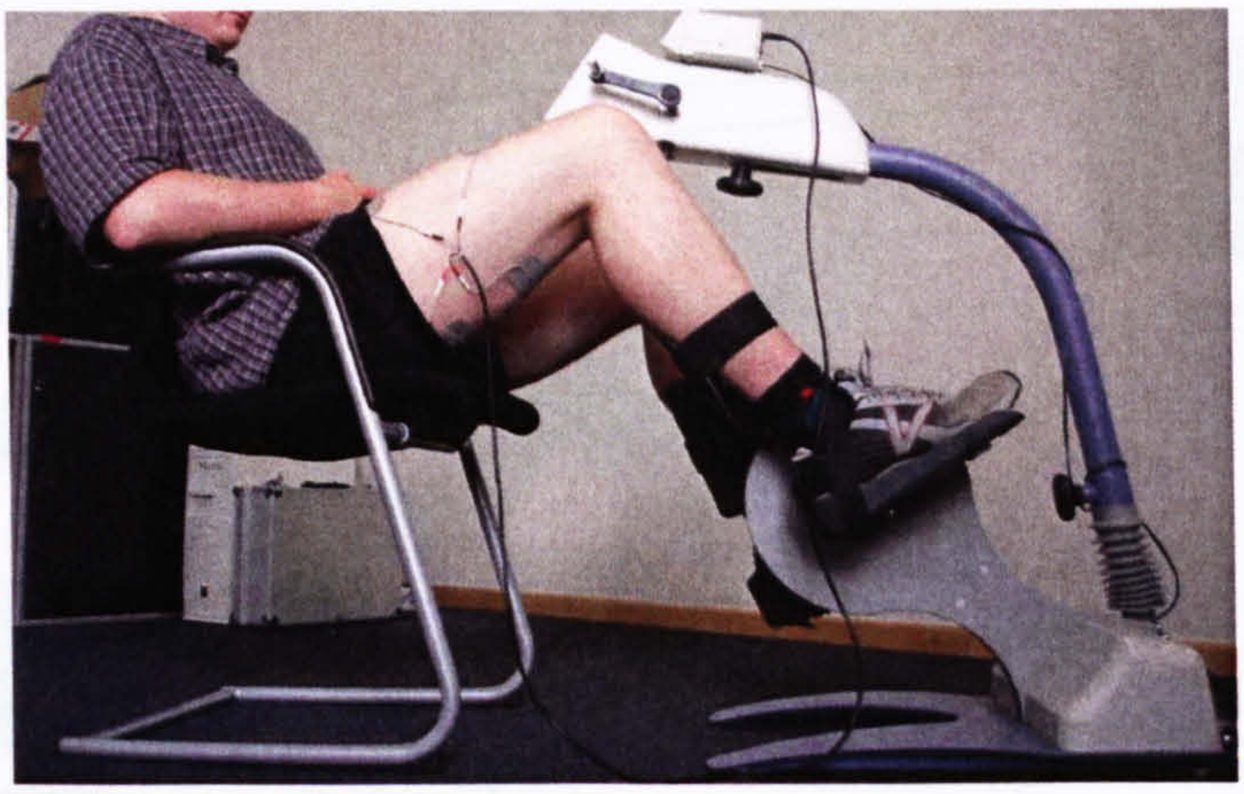

Figure 5.1: Motorised ergometer used for FES cycling (physical apparatus).

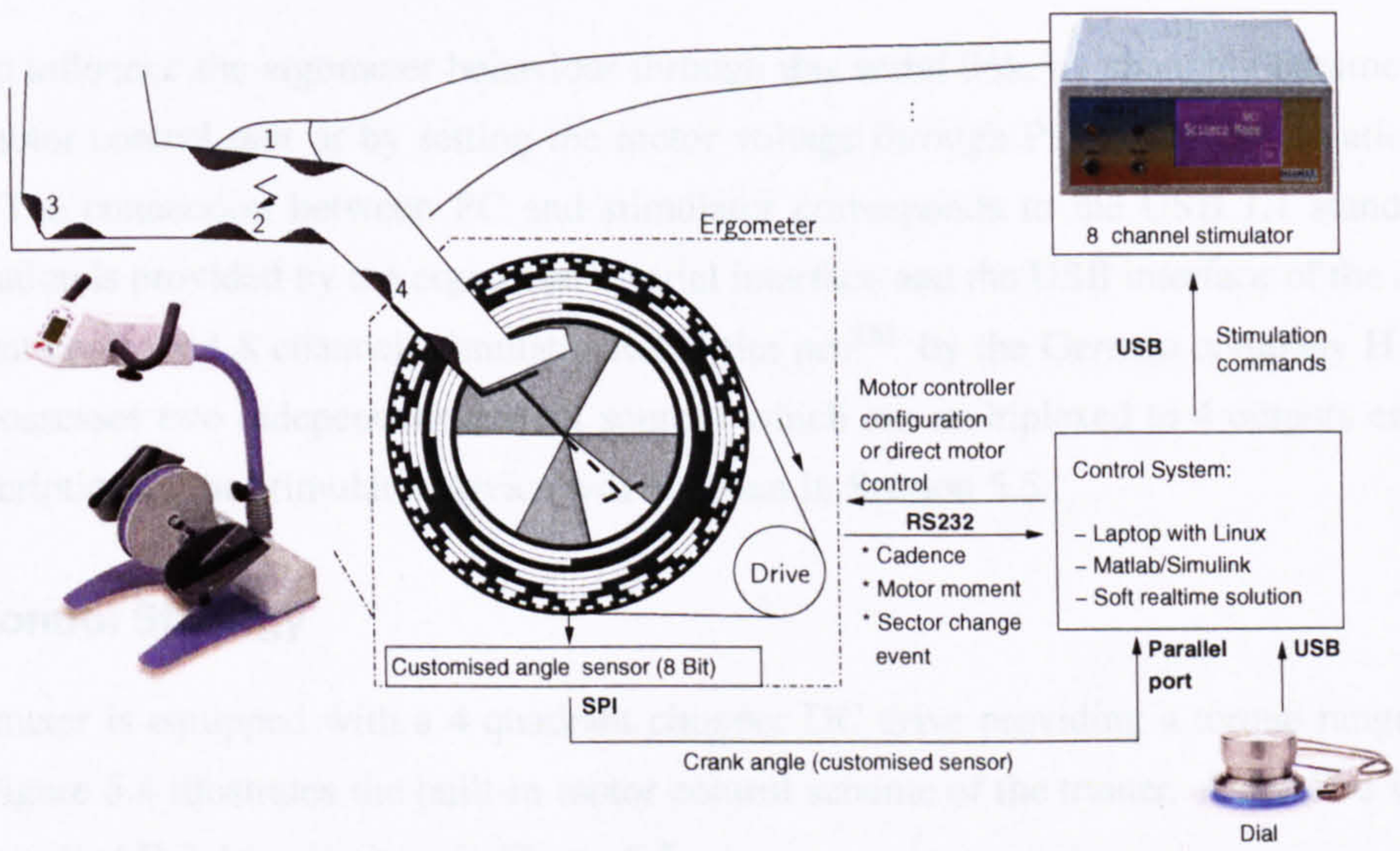

Figure 5.2: Ergometer system for lower-limb FES cycling with PC-control.

automatically (see Chapter 6) or is adjusted manually by means of an electronic dial/switch[2] which is connected to the laptop's USB port. The FES cycling algorithms and ergometer/stimulator interface have been implemented in Matlab/Simulink under Linux. A customised soft real-time solution has been employed.

For daily clinical or home use, the stimulation is directly controlled by the stimulator's built-in microcontroller bypassing the PC as shown in Figure 5.3. Data logging and complexity of control algorithms are reduced in this configuration. The ergometer offers a serial interface (RS232) to enable the periodic transfer of ergometer signals to an external device (PC or stimulator). It is further

[2]http://www.griffintechnology.com/products/powermate/

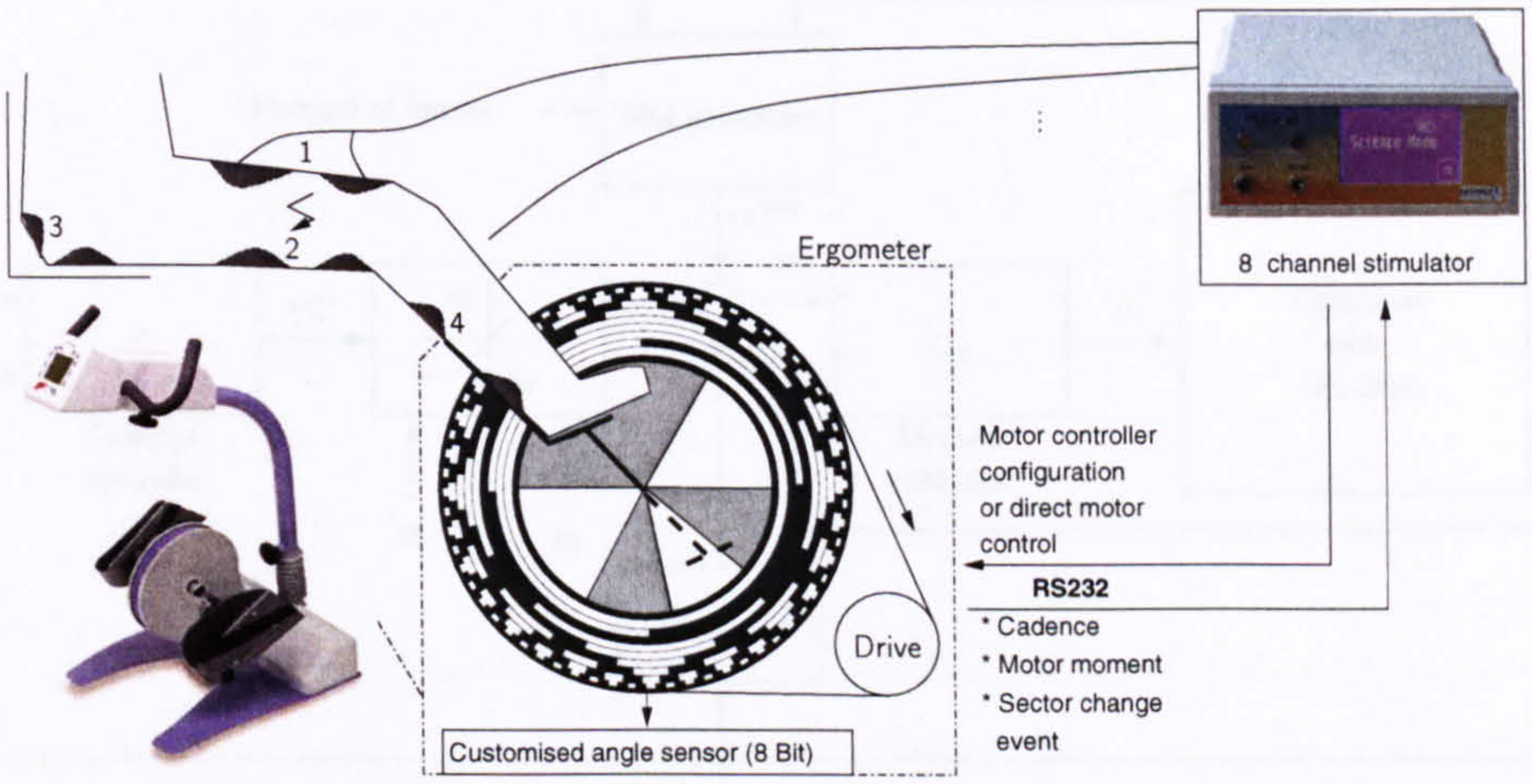

Figure 5.3: Stand-alone ergometer system for lower-limb FES cycling without PC-control.

possible to influence the ergometer behaviour through this serial link, by changing parameters of the internal motor control unit or by setting the motor voltage through Pulsewidth Modulation (PWM) directly. The connection between PC and stimulator corresponds to the USB 1.1 standard. Galvanic isolation is provided by the ergometer's serial interface and the USB interface of the stimulator. The current-controlled 8 channel stimulator RehaStim pro™ by the German company HASOMED GmbH[3] possesses two independent current sources which are multiplexed to 4 outputs each. A detailed description of the stimulator device will be given in Section 5.5.

Motor Control Strategy

The ergometer is equipped with a 4 quadrant chopper DC drive providing a torque range of -15 to 15 Nm. Figure 5.4 illustrates the built-in motor control scheme of the trainer. A detailed view of the PWM controlled DC drive is given in Figure 5.5.

A cascade controller structure is employed. The inner loop controller, C_m, controls the motor moment and has the duty cycle γ of the pulsewidth modulator as controller output. The sensed motor moment

$$m_M^{\mathrm{T}} = \hat{k}_m i \tag{5.1}$$

is proportional to the measured motor current i where $\hat{k}_m$ is an estimate of the true motor torque constant k_m. The sensed crank cadence ω^{T} is controlled by the outer loop controller, C_c, which has the moment m_r^C as controller output. This moment contributes to the reference moment of the inner loop together with the moments m_r^{MoI} and m_r^{FC}. The moment m_r^{MoI} is negatively proportional to the crank acceleration and emulates the effect of a flywheel or to be precise a large moment of inertia (MoI) at the crank; this smooths the cycling movement. The estimated static friction of the system ($\hat{M}_s \operatorname{sign} \omega^{\mathrm{T}}$)

[3] http://www.hasomed.de

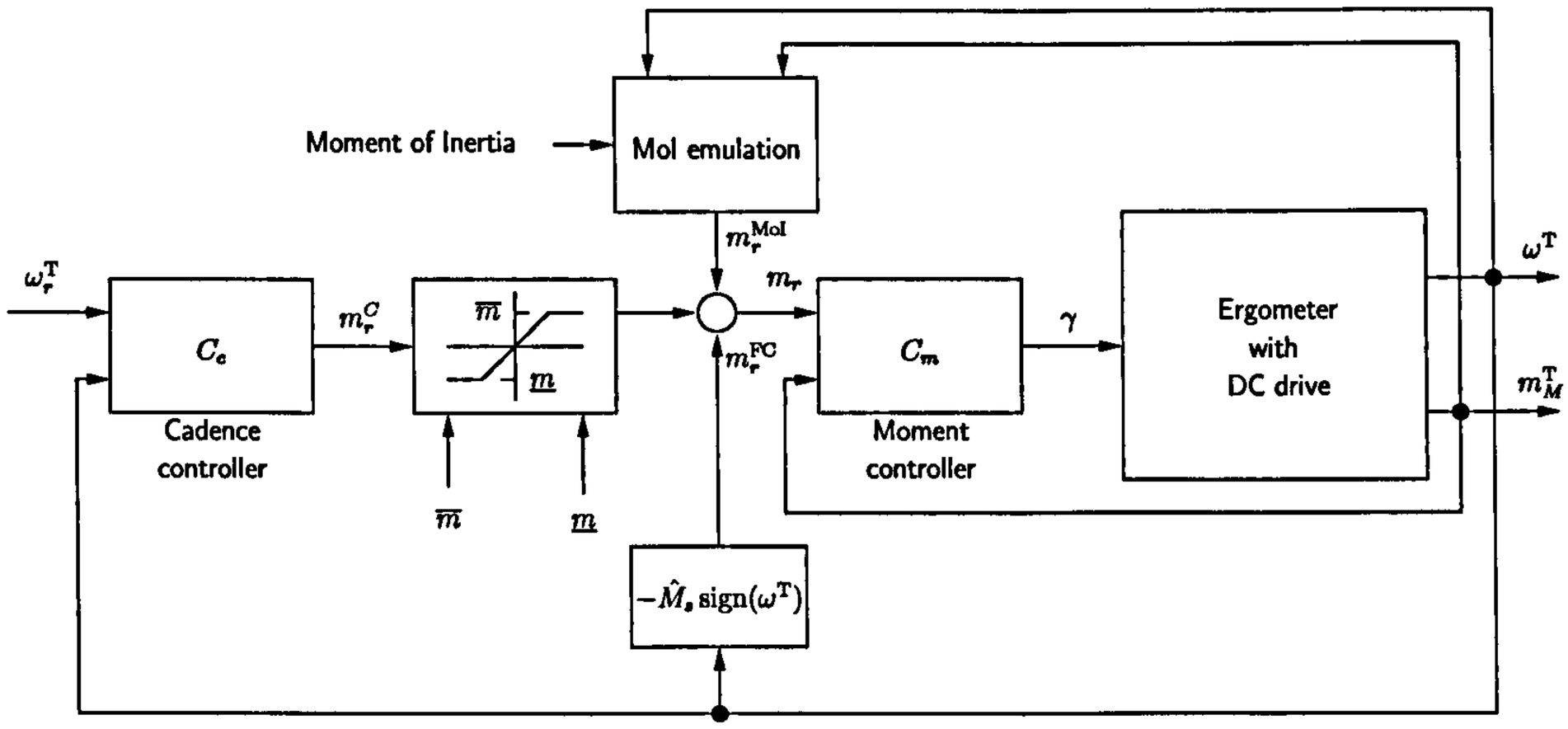

Figure 5.4: Motor control scheme of the ergometer.

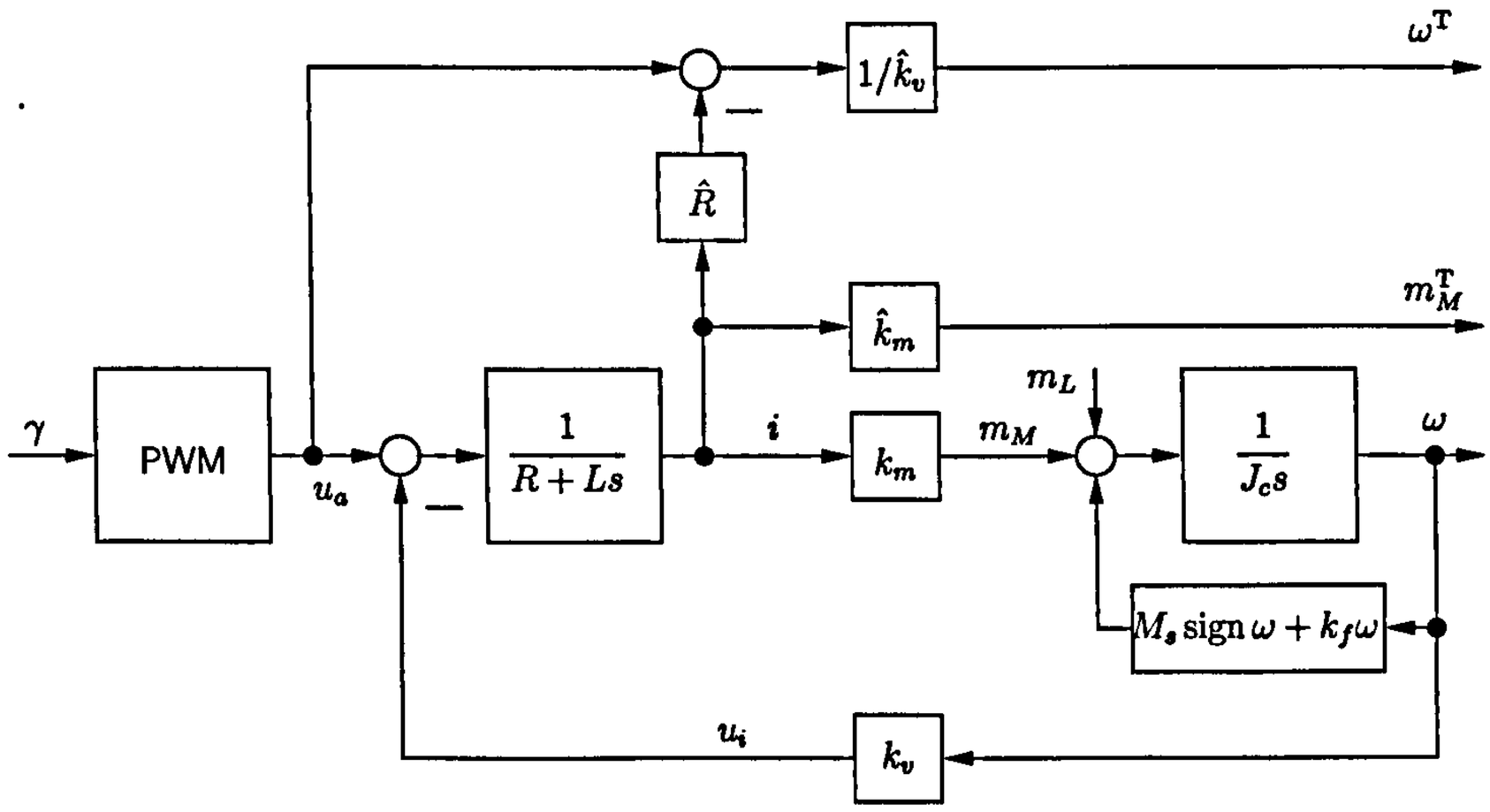

Figure 5.5: Detailed model of the PWM controlled DC drive.

will be compensated by the reference moment contribution m_r^{FC} which reduces the amount of muscle force required to initiate a cycling movement. The reference moment m_r^c contributed by the speed controller C_c can by limited be a lower bound $\underline{m}$ and an upper bound $\overline{m}$.

Assume a given positive reference cadence ω_r^{T}. The value $\underline{m} + \hat{M}_s$ specifies how much the motor is resisting a voluntary cycling which tries to exceed the reference cadence ω_r^{T}. On the other hand, the value $\overline{m} + \hat{M}_s$ specifies how much the motor shall support the cycling movement in order to achieve ω_r^{T} when the cyclist is passive or actively resists the movement.

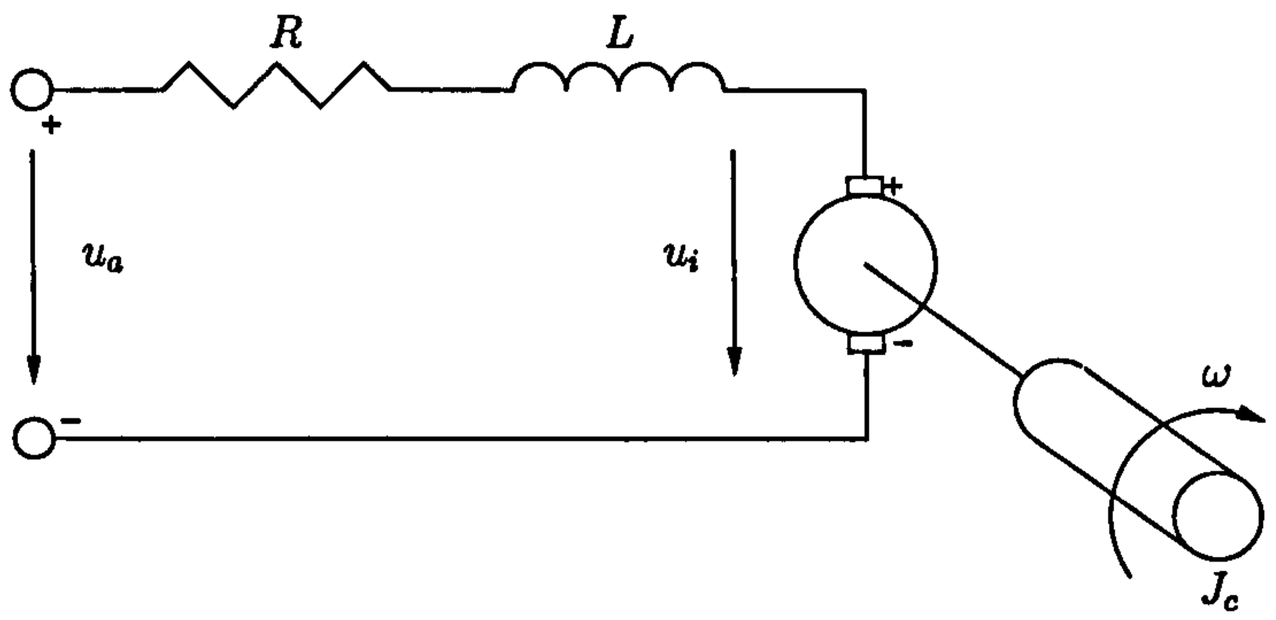

Figure 5.6: Electrical circuit of the DC motor.

IR compensation is applied for the PI-type speed controller, C_c. The sensed cadence ω^{T} is determined from motor voltage u_a and motor current i. Let us consider the model of the PWM controlled motor shown in Figure 5.5. The equivalent electrical circuit is illustrated in Figure 5.6. It can be represented by a voltage source u_a across the coil of the armature. The electrical equivalent of the armature coil can be described by an inductance L in series with a resistance R in series with an induced voltage u_i which opposes the voltage source. The induced voltage is generated by the rotation of the electrical coil through the fixed flux lines of the permanent magnets. Kirchoff's voltage law states that the sum of all voltages around a loop must equal zero

$$u_a(t) - i(t)R - L\frac{\mathrm{d}\,i(t)}{\mathrm{d}\,t} - u_i(t) = 0. \tag{5.2}$$

The induced voltage u_i is proportional to the real crank cadence ω

$$u_i = k_v\omega \tag{5.3}$$

where k_v is the velocity constant. Thus, a simple approach to determine a "measurement" of the cadence is to insert (5.3) into (5.2) and solve it for ω. In practice, the current i is assumed to be slowly varying (derivative almost zero), so that the sensed cadence ω^{T} is then given by

$$\omega^{\mathrm{T}} = \frac{u_a - i(t)\hat{R}}{\hat{k}_v} \tag{5.4}$$

where $\hat{R}$ and $\hat{k}_v$ are estimates of the resistance R and the velocity constant k_v. Of course, the quality of this "measurement" depends on the agreement of $\hat{R}$ and $\hat{k}_v$ with their true values. Notice that the cadence ω^{T} is load dependent because of i. The accuracy of a speed controller with IR compensation is usually low and stationary errors due to a biased cadence measurement occur also with integral action. However, since IR compensation is cheap and no speed sensor is required, it is used in the ergometer.

Measurements and Communication Protocol

The ergometer manufacturer provides a complex communication protocol for reading out data from the ergometer and/or controlling the ergometer. The serial communication runs with 9600 Bauds.
The signals of interest for FES cycling are the crank angle, cadence and motor torque. The internal ergometer signals, sensed cadence ω^{T} and sensed motor torque m_M^{T}, are provided by the trainer. These measurements are sent automatically by the ergometer's microcontroller without request to an external device with a rate of approx. 50 Hz.
Acquiring an accurate angle measurement is more difficult. The trainer comes without an accurate angle sensor. The device possesses only a simple mechanism to determine a fixed number of crank positions at which the crank can be positioned by the motor for facilitating the placement of the legs into the foot-rests (get-in support). For this, a disk with six white and black sectors of different size is mounted on the crank shaft and rotates while cycling. An optical sensor, fixed to the device frame, senses the sector colour. For nearly constant speed, the sectors can be identified because of their different size and colour. Knowing the current sector and cycling direction, the event of entering a new sector can be related to a known angle. The sector transitions can be matched to six fixed angles which yields a discrete-event angle measurement. The optical sensor output is polled by the trainer's microcontroller every 10 ms. In the event of a changing colour, a command will be send out to the PC or stimulator giving the colour of the current sector. The angle detection based on this signal is described in Section 5.4.2. Accurate angle estimates can be obtained by sensor fusion. An extended Kalman filter combines cadence and angle measurements in order to provide angle estimates between the angle measurements. For details see Section 5.4.3.
The ergometer used in this work was instrumented with a customised 8 Bit absolute angle sensor. In addition to the standard disk with six sectors, a disk with Gray code was mounted on the crank shaft. A fixed optical sensor reads the actual absolute position from the Gray code and provides this reading through a Serial Peripheral Interface (SPI). The parallel port at the PC side was used to control the SPI. This angle measurement was employed as a reference to validate the angle estimate obtained by the extended Kalman filter.
Table 5.1 summarises the available measurements at the ergometer. The signal resolution is only 8 bit, so that a considerable amount of quantisation noise is present in the data. In the sequel, noisy measurements are indicated by the superscript $*$.
Table 5.2 summarises ergometer variables which can be altered through the serial link. With the provided communication protocol, the cadence reference ω_r^{T} and the constraints $\underline{m}$ and $\overline{m}$ can be set online. Commands pointing to the ergometer can be sent with 20 Hz when the motor control is active. The update of $\underline{m}$ and $\overline{m}$ represents one command, the update of ω_r^{T} another. Assuming the same priority for changing ω_r^{T}, $\underline{m}$ and $\overline{m}$, results in an individual update rate of 10 Hz. The desired Moment of Inertia (MoI) and the static compensation moment $\hat{M}_s$ can be set as well. During cycling these parameters are usually not altered.
An interesting option is to switch the built-in motor control off entirely and to control the duty cycle

of the PWM directly. The duty cycle can be updated in this mode every 20 ms. Due to a firmware bug sector colour changes are no longer sent by the ergometer in this mode. The customised angle sensor is therefore used to obtain an angle measurement.

Depending on the motor control mode, two measurement configurations may be distinguished as indicated in Table 5.3. Section 5.4 describes how sufficiently accurate estimates of cadence, torque and crank angle can be obtained by the use of an extended Kalman filter for the two configurations.

Table 5.1: Available measurements at the trainer side.

Variable	Computer representation by	Factory calibration	Interface	Frequency
Cadence ω^{T*}	signed char `cadence`	0.5·`cadence` [rpm]	RS232	50 Hz
Motor torque m_M^{T*}	signed char `torque`	unkown	RS232	50 Hz
Angle φ^*	signed char `angle`	1.4·`angle` [°][4]	Parallel port	200 Hz[5]
Sector change event	boolean `sce`[6]	-	RS232	100 Hz

Table 5.2: Ergometer variables which can be changed through the serial link.

Variable	Computer representation and range	Factory calibration	Frequency
Cadence reference ω_r^T [rpm]	signed char `cad_r`, $-80\ldots80$	$\omega_r^T = 0.75$`cad_r`	10 Hz
Resisting torque limit $\underline{m}$ [Nm]	unsigned char `lb_m`, 0...150	$\underline{m}$=-0.14`lb_m`+1	10 Hz
Supporting torque limit $\overline{m}$ [Nm]	unsigned char `ub_m`, 0...150	$\overline{m}$=0.15`ub_m`	10 Hz
Duty cycle of PWM γ [%]	signed char `gamma`, $-100\cdots100$	`gamma`	50 Hz
Moment of Inertia[7]	unsigned char `moi`, 1 (max.)...250 (min.)	unknown	set once
Static compensation moment $\hat{M}_s$	unsigned char `scm`, 0...150	unknown	set once

[4]Customised absolute angle sensor

[5]Other frequencies are possible but 200 Hz has been used throughout this work.

[6]0 - black sector, 1 - white sector

[7]The setting `moi`=50 was used throughout the experimental work presented in this thesis.

Table 5.3: Measurement configurations of the trainer for FES cycling. Measurement configuration 1 is the used when the built-in motor control is activated. Measurement configuration 2 is used when the duty cycle of the PWM is directly controlled by the laptop.

Measurements	Configuration	
	1st: Standard mode	2nd: PWM control mode with customised angle sensor
Cadence ω^{T*}	×	×
Motor torque m_m^{T*}	×	×
Angle φ^*		×
Field change event e_{fc}	×	

5.4 Signal Processing

5.4.1 Signal Calibration

The default factory calibrations for the values shown in Tables 5.1 and 5.2 are not exact enough for scientific purposes so that a re-calibration procedure is required. Results of this procedure are newly calibrated measurements ω^{C*} and m_M^{C*} for cadence and motor moment, respectively.
In order to assign the correct moment limits and to achieve zero steady state error for the cadence controller, new calculation rules for `lb_m`, `ub_m`, `scm` and `cad_r` have to be determined (for factory calibration cf. Table 5.2).

Cadence Calibration

The cadence ω^{T*} sent by the ergometer is determined by Equation (5.4) and subsequent A-D conversion. Accuracy is low because of uncertainties in the parameters $\hat{R}$ and $\hat{k}_v$. Thus, a time-varying calibration

$$\omega^{C*} = k_\omega(t)\omega^{T*} \tag{5.5}$$

is applied where the factor $k_\omega(t)$ varies slowly under different load conditions. The proportionality factor $k_\omega(t)$ is estimated online by means of an extended Kalman filter (see Section 5.4.3) based on angle measurements.

Moment Calibration

The motor moment measurement has to be calibrated for each ergometer. For the unitless value $m_M^{T*} = \texttt{moment}$ a calibration of the form

$$m_M^{C*} = k_{m_a} m_M^{T*} + k_{m_b} \tag{5.6}$$

is introduced with the constants k_{m_a} and k_{m_b}. This leads to the calibrated motor moment measurement m_M^{C*} with the unit Nm. The constant k_{m_b} is employed to take a possible offset (due to the A-D conversion) into account.

Motor Moment Calibration Procedure: The equation of motion is given by

$$M_s \operatorname{sign}(\omega(t)) + k_f \omega(t) + m_L(t) + m_M(t) = J_c \frac{\mathrm{d}\,\omega(t)}{\mathrm{d}\,t} \tag{5.7}$$

where m_M is the real motor moment, M_s is the amount of static friction, k_f is the damping constant related to the crank shaft, m_L is load moment acting at the crank shaft and J_c is the total moment of inertia at the crank shaft. The term $J_c\,\mathrm{d}\,\omega/\mathrm{d}\,t$ will be zero for constant speed. Assuming zero acceleration and inserting Equation (5.6) into (5.7) yields

$$M_s \operatorname{sign}(\omega) + k_f \omega + m_L(t) + k_{m_a}(m_M^{T*}(t) + k_{m_a}) = 0. \tag{5.8}$$

The constants M_s, k_f, k_{m_a} and k_{m_b} can be experimentally identified using a least squares procedure under the following conditions:

1. The load moment $m_L(t)$ is varying and known.

2. Data have been acquired at different positive and negative constant speeds ω.

The first condition has been fulfilled by attaching a 4 kg weight on one crank arm only, leaving the other crank arm unloaded. The load moment can then be calculated by

$$m_L(t) = -4\,\mathrm{kg} \cdot 9.81\mathrm{m/s^2} \cdot l_c \cdot \cos(\varphi(t)) \tag{5.9}$$

with the crank angle φ defined as shown in Figure 5.7 and the crank arm length $l_c = 0.11$ cm. In order to achieve constant cadence and fulfilment of condition two, a customised cadence controller (see Section 5.7) was designed and applied during the tests. The controller gives zero tracking error, i.e. perfect constant speed, due to repetitive control techniques but requires an accurate angle sensor. The built-in motor control of the ergometer may be used if no accurate angle sensor is mounted. However, speed variations will occur in this case because of the limited bandwidth, so that the assumption of constant speed is not entirely true.

Table 5.4 lists the identified parameters for the ergometer used in this work. Data have been acquired for -50, -30, 30 and 50 rpm with the built-in and customised speed controller. Figure 5.8 shows the calibrated motor moment m_M^{C*} (solid line) together with the moment $-(M_s \operatorname{sign}(\omega^{C*}) + k_f \omega^{C*} + m_L(t))$ (dashed line) for the built-in speed controller. Figure 5.9 illustrates the result for the customised speed controller. Data for different cadence trials have been plotted together. A good fit of the curves indicates good moment calibration. While the estimates obtained with the two speed controllers differ as expected, the calibration with perfect constant speed is better. However, the results are relatively close, so that the simpler approach with built-in motor control is preferred in practice.

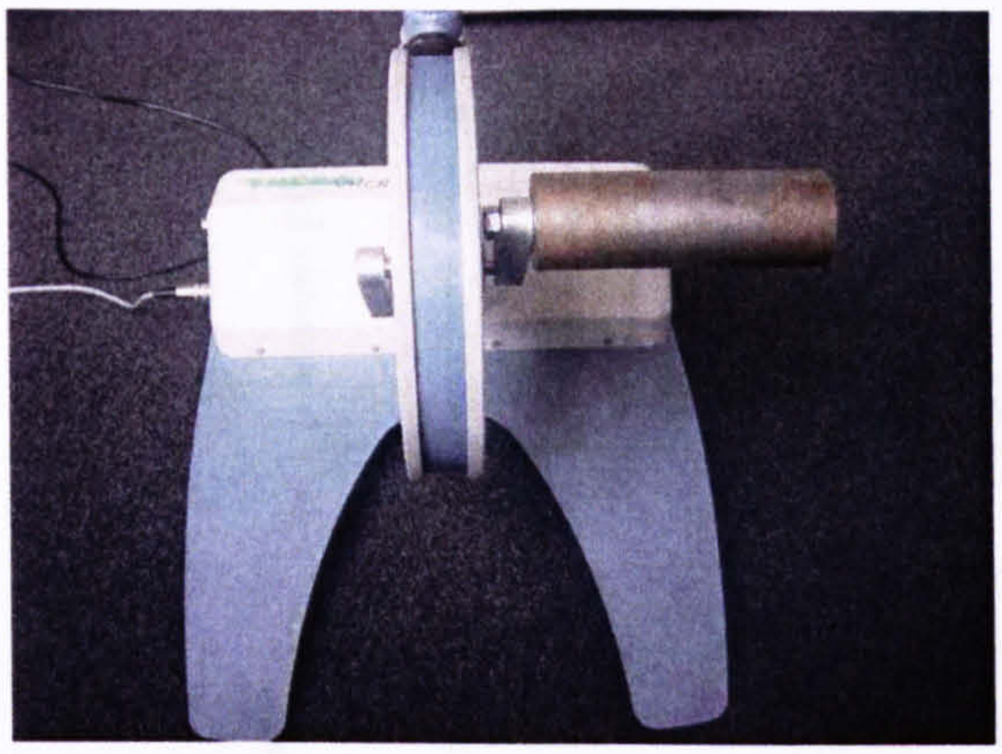

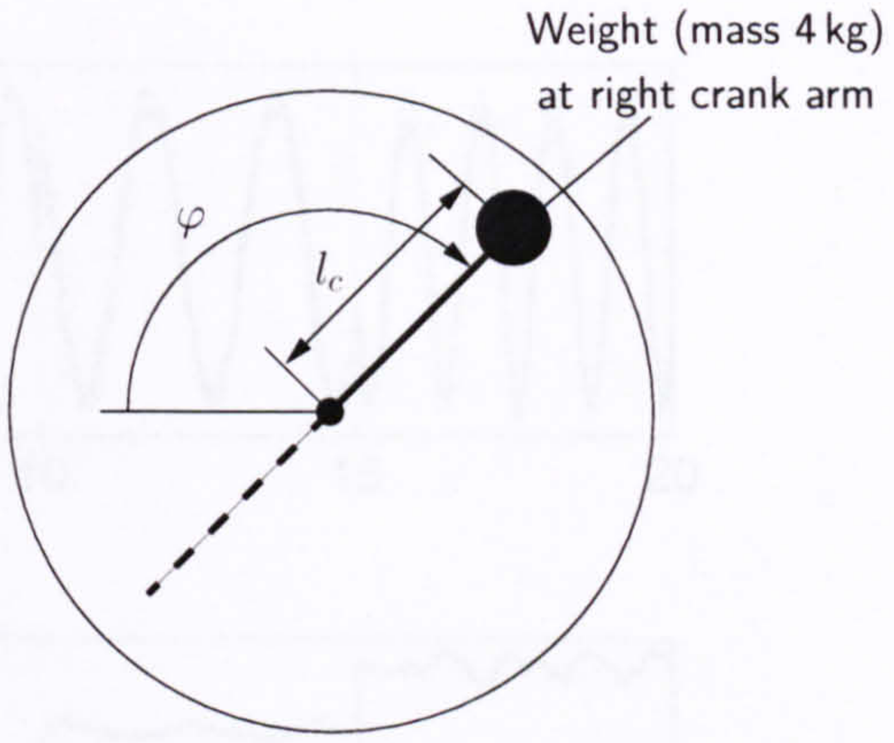

Figure 5.7: Moment calibration. A 4 kg weight is mounted at one crank arm in order to produce a known load moment at the crank shaft.

Table 5.4: Results of the moment calibration.

Parameter	Value (customised controller)	Value (built-in motor controller)
k_{m_a}	0.3389 Nm	0.3226 Nm
k_{m_b}	-0.135 Nm	-0.0591 Nm
M_s	-3.97 Nm	-3.38 Nm
k_f	-0.0001 Nm·s	-0.0101 Nm·s
error (standard deviation)	0.505 Nm	0.607 Nm
error (mean value)	0.000 Nm	0.000 Nm

Setting up the Static Compensation Moment

For the static compensation moment $\hat{M}_s$ (see figure 5.4) the same calibration as for the motor torque measurement can be applied

$$\hat{M}_s = k_{m_a}\,\mathtt{scm} + k_{m_b}. \tag{5.10}$$

For a specified moment $\hat{M}_s$ the setting sent to the ergometer is then given by

$$\mathtt{scm} \;=\; \mathrm{floor}((\hat{M}_s - k_{m_b})/k_{m_a}). \tag{5.11}$$

The function *floor* rounds its argument down to the nearest integer.

Setting up Moment Limits

The upper limit of the moment $\overline{m}$ is re-calibrated by

$$\overline{m} = k_{\overline{m}_a}\,\mathtt{ub\_m} \tag{5.12}$$

where $k_{\overline{m}_a}$ is a positive constant. For the lower limit the following relation

$$\underline{m} = k_{\underline{m}_a}\,\mathtt{lb\_m} + k_{\underline{m}_b} \tag{5.13}$$

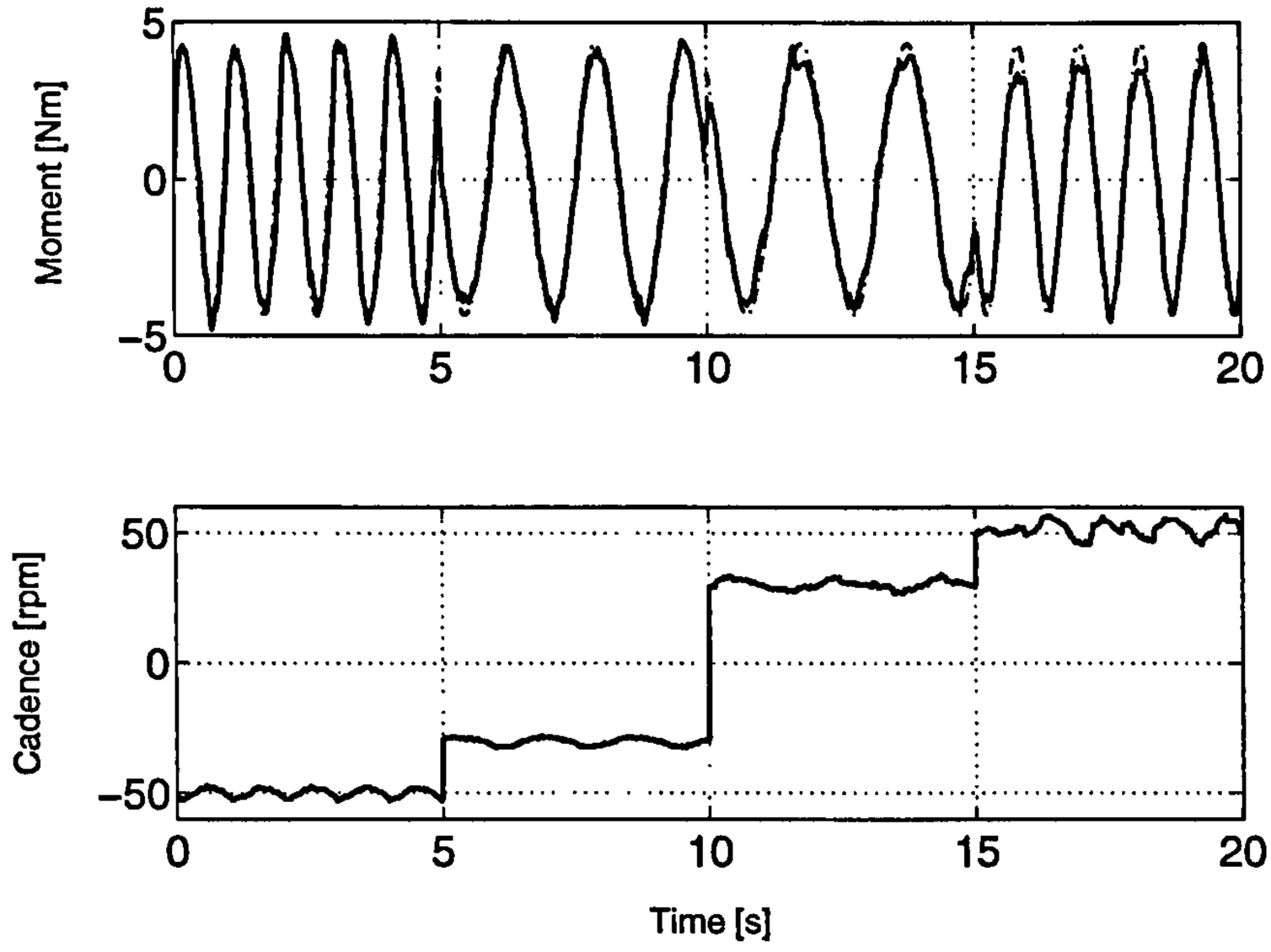

Figure 5.8: Motor moment calibration results with built-in motor control. The upper graph shows the calibrated motor moment m_M^{C*} (solid line) and calculated reference moment $-(M_s \operatorname{sign}(\omega^{C*}) + k_f \omega^{C*} + m_L(t))$ (dashed line).

with the constants $k_{\underline{m}_a}$ and $k_{\underline{m}_b}$ holds.

Having completed the calibration of the motor moment measurement, the constants in the Equations (5.12) and (5.13) can be experimentally identified as follows:

1. Voluntary cycling at a specified constant cadence with cadence reference and supportive moment limitation set to zero (`cad_r`=0 and `ub_m`=0) while applying staircase-like changes to `lb_m`; The averaged calibrated motor torque measurement minus the compensation moment $\hat{M}_s$ corresponds in this case to $\underline{m}$ and the coefficients $k_{\underline{m}_a}$ and $k_{\underline{m}_b}$ can be determined using the least squares method.

2. Voluntary cycling at a specified constant cadence with cadence reference set to the highest possible value exceeding the actual cycling cadence and the resisting moment limitation set to zero (`cad_r`=80 and `lb_m`=0) while applying staircase-like changes to `ub_m`; The averaged calibrated motor torque measurement minus the compensation moment $\hat{M}_s$ corresponds in this case to $\overline{m}$ and the coefficient $k_{\overline{m}_a}$ can be determined using the least squares method.

Figure 5.10 shows an example of an experiment to calibrate the moment limit $\underline{m}$. The calibrated motor moment measurement m_M^{C*} subtracted by $\hat{M}_s$ is plotted as a light solid line; the calibrated limit $\underline{m}$ (dashed line) is also shown in the upper graph. The obtained calibration parameters for the lower

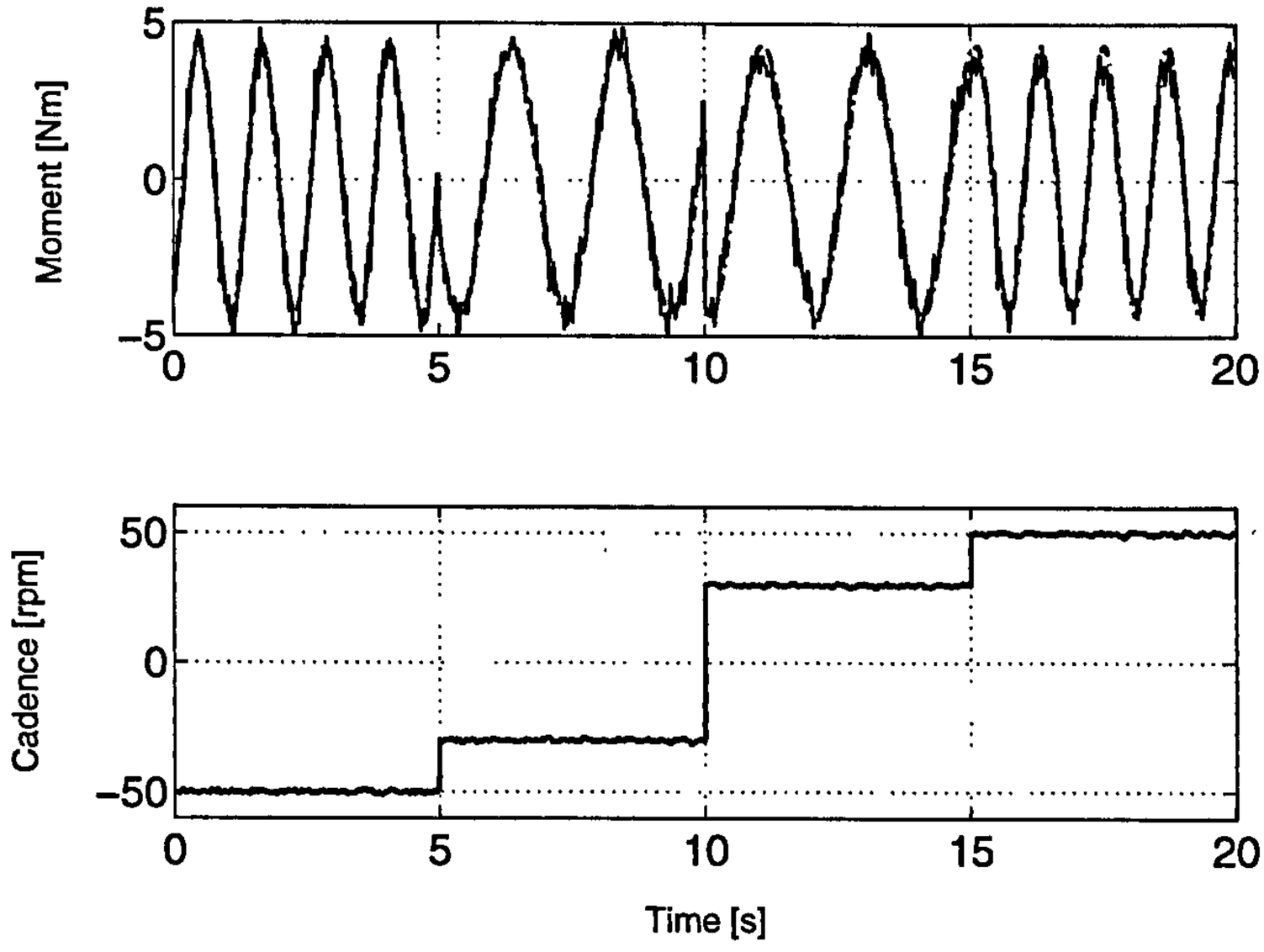

Figure 5.9: Motor moment calibration results with customised motor control. The upper graph shows the calibrated motor moment m_M^{C*} (solid line) and calculated reference moment $-(M_s \operatorname{sign}(\omega^{C*}) + k_f \omega^{C*} + m_L(t))$ (dashed line).

moment limit $\underline{m}$ are

$$k_{\underline{m}_a} = -0.12\,\text{Nm} \text{ and } k_{\underline{m}_b} = -1.37\,\text{Nm}.$$

The calibration of $\overline{m}$ did in fact correspond to the factory calibration given in Table 5.2.
Finally, after calibration, the controller moment limits which have to be sent to the ergometer can be calculated by

$$\texttt{lb\_m} = \text{floor}((\underline{m} - k_{\underline{m}_b})/k_{\underline{m}_a}) \tag{5.14}$$

$$\texttt{ub\_m} = \text{floor}(\overline{m}/k_{\overline{m}_a}) \tag{5.15}$$

where $\underline{m}$ and $\overline{m}$ are the desired physical limits.

Setting up the Cadence Reference

The reference cadence ω_r^T should be calibrated by

$$\omega_r^T = \omega_r / k_\omega(t). \tag{5.16}$$

with 0.75 as the factory calibration factor (cf. Table 5.2). The factor k_ω will be determined on-line using the extended Kalman filter described in Section 5.4.3. Notice that ω_r^T represents the reference

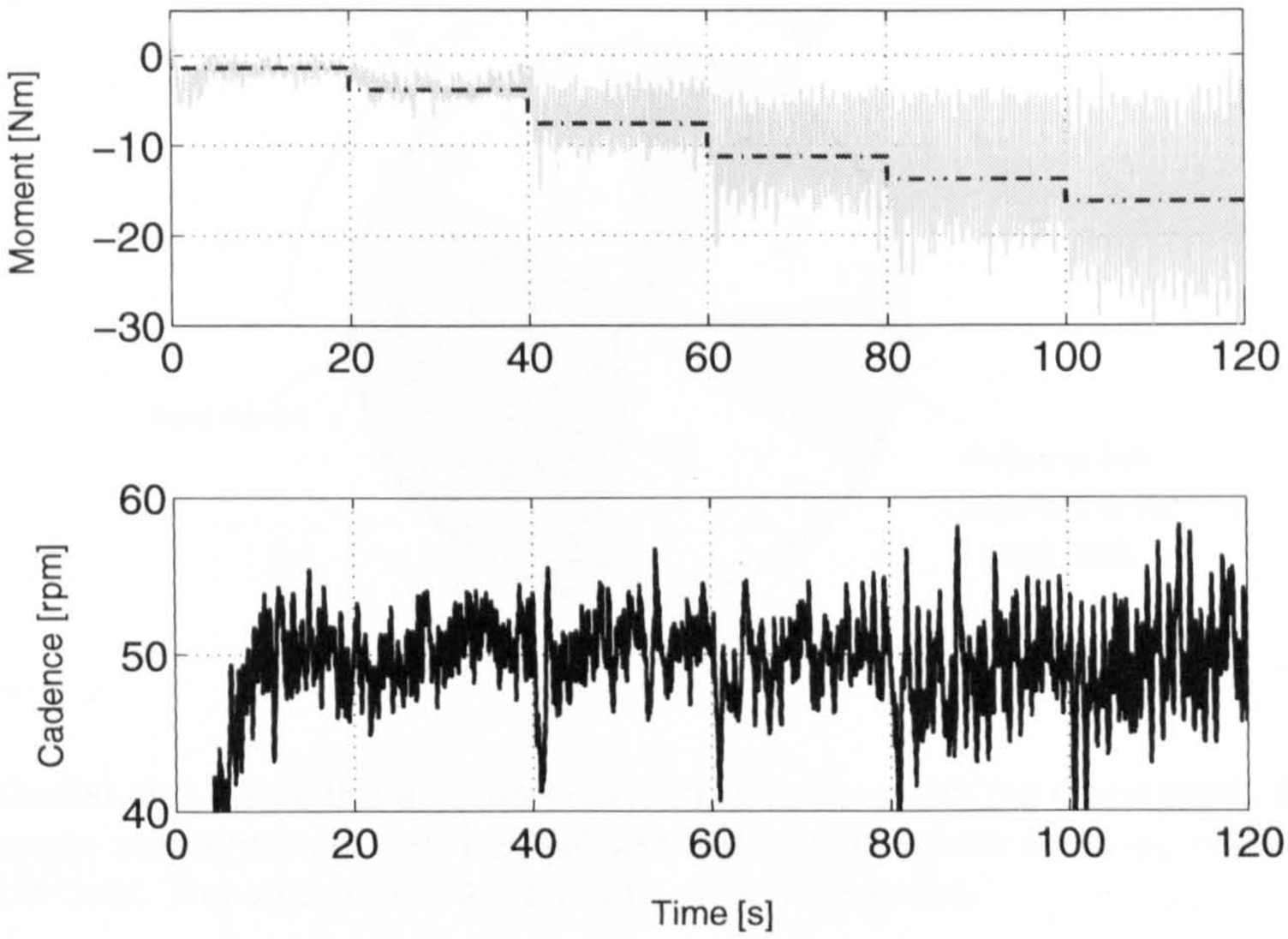

Figure 5.10: Result of lower moment limit calibration; The upper graph shows the calibrated limit $\underline{m}$ (dash-dotted line) together with the calibrated motor moment m_M^{C*} which is lowered by the amount of the compensation moment $\hat{M}_s$.

for the sensed cadence ω^T within the ergometer while ω_r represents the reference for the real physical cadence ω. Thus, the actual reference `cad_r` which is sent to the ergometer can be calculated by

$$\texttt{cad\_r} \;=\; \text{floor}(\omega_r / k_\omega(t) / 0.75). \tag{5.17}$$

5.4.2 Crank Angle Detection

The standard ergometer does not have an accurate angle sensor. Discrete-event angle measurements can be obtained by analysing the timing of the *Sector Change Event* commands which are sent automatically towards the PC or stimulator and inform about the colour of the entered sector. Length of stay in a sector is measured as a counterpart to sector size for almost constant speed. Through the lengths of stay, the individual sectors are identified and their borders related to known angle measurements. As shown in Figure 5.11, six angle measurements can be obtained in this way. The assumption of constant speed for detecting the angle can be dropped as soon as the sectors have been identified and an absolute position has been obtained. After this, the disk serves as a standard incremental angle sensor with different large angle increments.

5.4.3 Extended Kalman Filter

The Figure 5.12 illustrates the signal processing for the use of the ergometer's built-in motor control (measurement configuration 1). Figure 5.13 shows the signal processing when the duty cycle of the

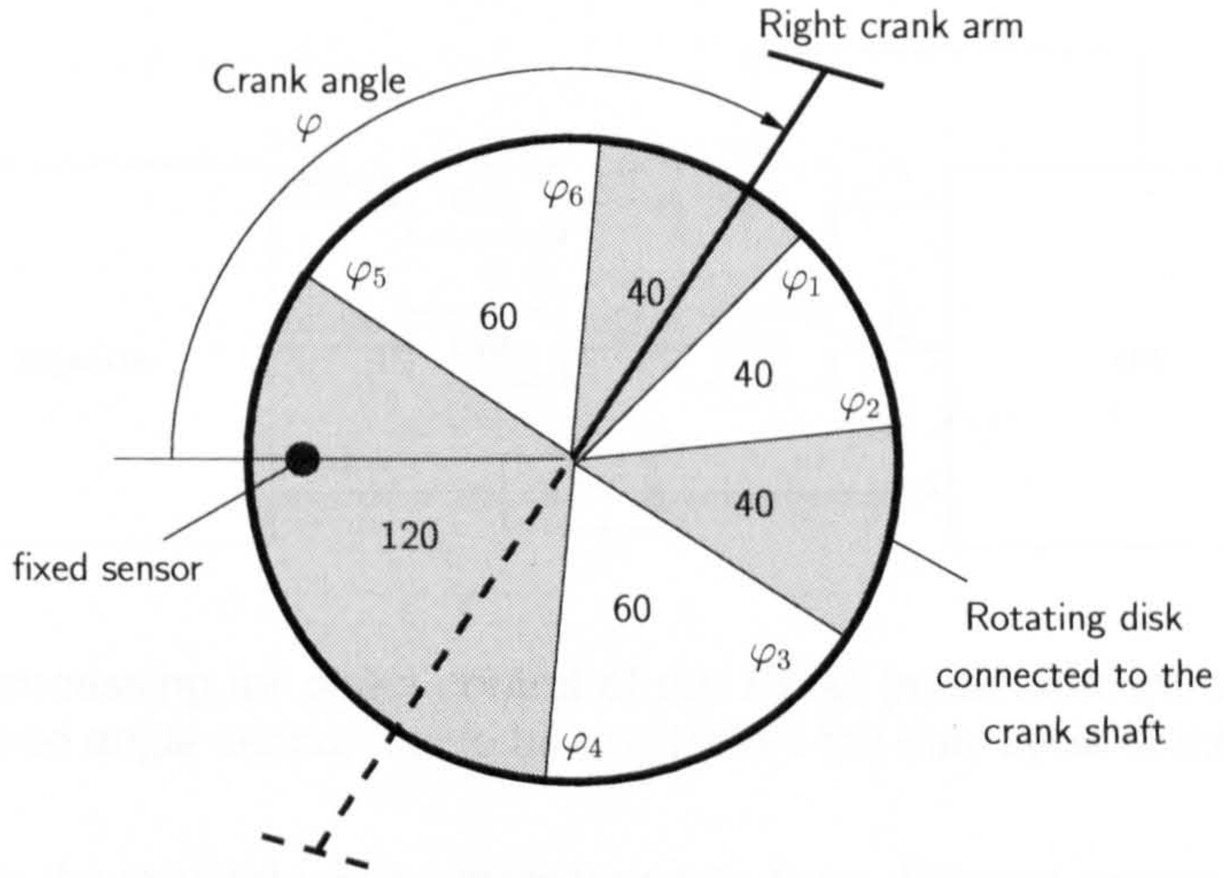

Figure 5.11: Coded disk inside the ergometer; The disk rotates with the crank shaft. A discrete-event angle measurement can be realised with angle values φ_1 to φ_6 related to the sector borders. The sizes of the sectors are given in degrees.

PWM is directly controlled (measurement configuration 2). In both cases, an Extended Kalman Filter (EKF) is applied for sensor fusion and signal estimation.

Kalman filters are optimal state observers for linear systems that take into account statistical properties of the system like measurement and system noise. Extended Kalman filters are a modification of Kalman filters for nonlinear systems. They are usually utilised when it is important that the state estimate produced by the observer is as accurate as possible and where the statistical properties of the noise in the measurements can be determined. Extended Kalman filters are suboptimal state estimators for nonlinear systems based on local linearisations of the nonlinearities. The popularity of extended Kalman filters is due to their relatively simple implementation.

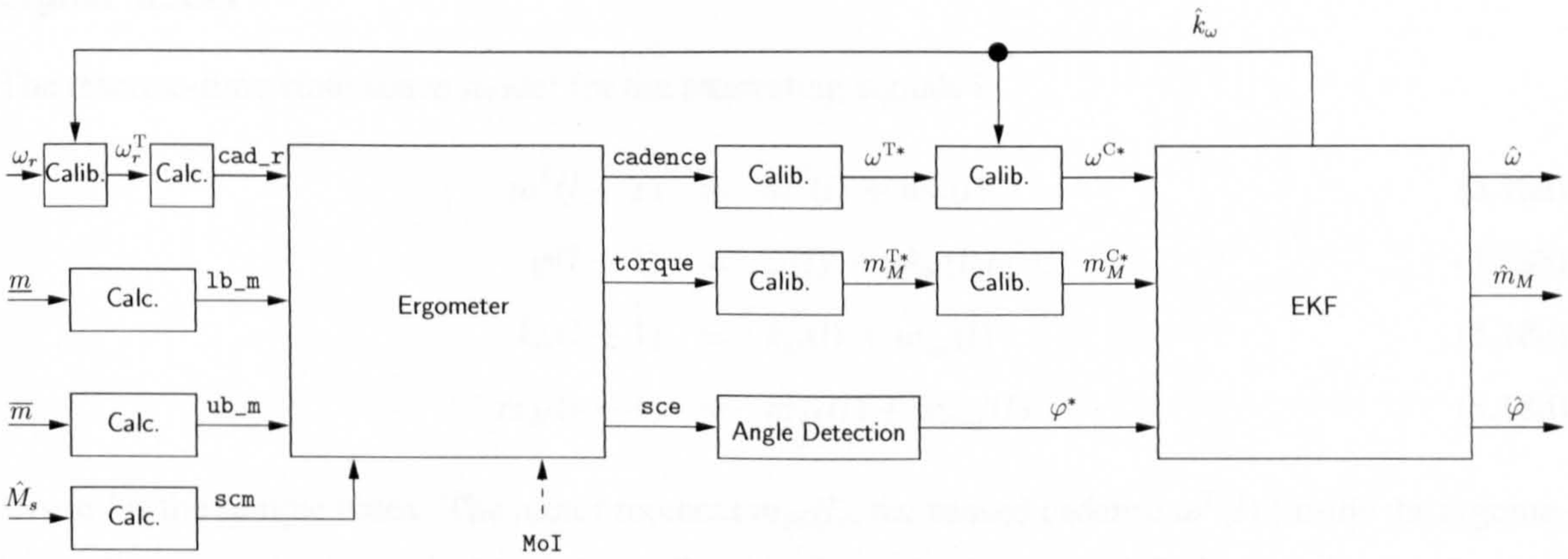

Figure 5.12: Signal processing for the standard measurement configurations 1. Cadence, motor torque and angle measurements are available from the ergometer. The angle measurement is derived from sector change events.

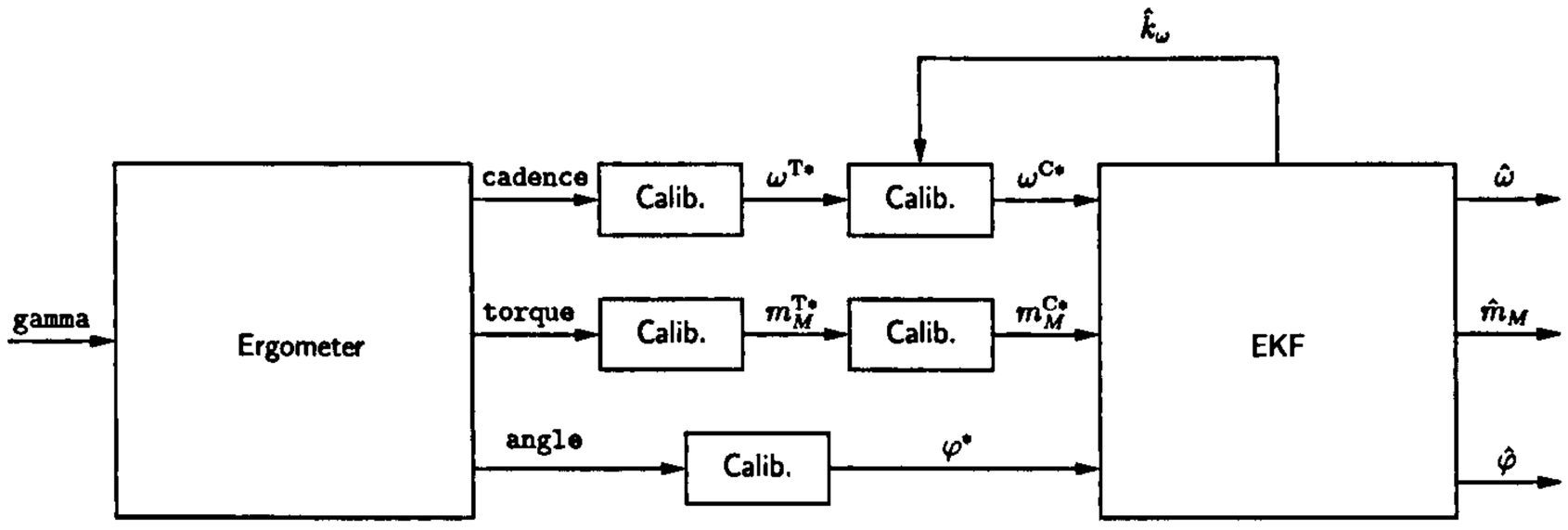

Figure 5.13: Signal processing for direct control of the PWM (measurement configuration 2). The customised angle sensor has to be used when the duty cycle of the PWM is set directly.

The filter is driven by the available noisy measurements from different sensors arriving at different sample rates. The discrete-time filter delivers estimates of

- crank cadence $\hat{\omega}$,
- motor moment $\hat{m}_M$,
- crank angle $\hat{\varphi}$, and
- cadence calibration factor $\hat{k}_\omega$

at a constant sampling-time t_k which may be smaller than the sampling-times of the measurements. Estimates between measurements are based on the integration of an assumed dynamic model. In order to obtain good estimates, the noise characteristic of each measurement has to be taken into account. The sampling-time t_k of the filter has been chosen as 5 ms. This allows fast reaction to incoming measurements.

Signal Model

The discrete-time state-space model for the interesting signals is

$$\omega^{\mathrm{T}}(l+1) = \omega^{\mathrm{T}}(l) + w_\omega(l) \tag{5.18a}$$

$$\varphi(l+1) = \varphi(l) + t_k k_\omega(l)\omega^{\mathrm{T}}(l) \tag{5.18b}$$

$$k_\omega(l+1) = k_\omega(l) + w_{k_\omega}(l) \tag{5.18c}$$

$$m_M(l+1) = m_M(l) + w_{m_M}(l) \tag{5.18d}$$

where l is the sample index. The motor moment $m_M(l)$, the sensed cadence $\omega^{\mathrm{T}}(l)$ (inside the ergometer without quantisation noise) and the calibration factor $k_\omega(l)$ are modelled as random walks with the uncorrelated white noise signals $w_{m_M}(l)$, $w_\omega(l)$ and $w_{k_\omega}(l)$ respectively. Introduction of the state noise guarantees the convergence of the state estimate even for a long running time of the Kalman

filter. For changing load conditions, alterations of k_ω will be detected. The system equation (5.18b) of the crank angle describes just the discrete-time integration of the calibrated cadence $\omega(l) = k_\omega(t)\omega^{\mathrm{T}}$. The states of (5.18) can be combined in the state vector $\boldsymbol{x}$ as follows:

$$\boldsymbol{x}(l) = \left[\omega^{\mathrm{T}}(l) \quad \varphi(l) \quad k_\omega(l) \quad m_M(l)\right]^T. \tag{5.19}$$

Some state measurements are available but corrupted by measurement noise mainly caused by quantisation. The relation between measurements and states is given by

$$\boldsymbol{y}(l) = \begin{bmatrix} \omega^{\mathrm{T}*}(l) \\ \varphi^*(l) \\ m_M^{\mathrm{C}*}(l) \end{bmatrix} = \underbrace{\begin{bmatrix} \delta_1(l) & 0 & 0 & 0 \\ 0 & \delta_2(l) & 0 & 0 \\ 0 & 0 & 0 & \delta_1(l) \end{bmatrix}}_{\boldsymbol{H}(l)} \boldsymbol{x}(l) + \underbrace{\begin{bmatrix} \delta_1(l) & 0 & 0 \\ 0 & \delta_2(l) & 0 \\ 0 & 0 & \delta_1(l) \end{bmatrix}}_{\boldsymbol{L}(l)} \underbrace{\begin{bmatrix} v_\omega(l) \\ v_\varphi(l) \\ v_{m_M}(l) \end{bmatrix}}_{\boldsymbol{v}(l)}$$

where $v_\omega(l)$, $v_{m_M}(l)$ and $v_\varphi(l)$ are the measurement noise signals related to the uncalibrated cadence, the calibrated motor moment and the crank angle. Dependent on the availability of measurements, the signals $\delta_1(l)$ and $\delta_2(l)$ are assigned to one or zero. In the case of a torque and cadence measurement arriving on the serial link, $\delta_1(l)$ will be one, or else zero. The signal $\delta_2(l)$ is one if a new angle measurement is available, or else zero.

The time-discrete model can be written in a compact form as

$$\boldsymbol{x}(l+1) = \boldsymbol{f}(\boldsymbol{x}(l)) + \boldsymbol{w}(l) \tag{5.20}$$

$$\boldsymbol{y}(l) = \boldsymbol{H}(l)\boldsymbol{x}(l) + \boldsymbol{L}(l)\boldsymbol{v}(l) \tag{5.21}$$

with

$$\boldsymbol{f}(\boldsymbol{x}(l)) = \begin{bmatrix} x_1(l) \\ x_2(l) + T_k x_3(l) x_1(l) \\ x_3(l) \\ x_4(l) \end{bmatrix}, \quad \boldsymbol{w}(l) = \begin{bmatrix} w_\omega(l) \\ 0 \\ w_{k_\omega}(l) \\ w_{m_M}(l) \end{bmatrix}. \tag{5.22}$$

Extended Kalman Filter (EKF) Equations

The state-space model (5.18) is nonlinear so that an Extended Kalman Filter (EKF) algorithm is required [37]. Recursive execution of the following steps is necessary:

1. Correction of the covariance matrix $\tilde{\boldsymbol{P}}(l)$ of the estimation error after new measurements:

$$\hat{\boldsymbol{P}}(l) = \tilde{\boldsymbol{P}}(l) - \tilde{\boldsymbol{P}}(l)\boldsymbol{H}(l)^T \left(\boldsymbol{H}(l)\tilde{\boldsymbol{P}}(l)\boldsymbol{H}(l)^T + \boldsymbol{R}_v\right)^{-1} \boldsymbol{H}(l)\tilde{\boldsymbol{P}}(l) \tag{5.23}$$

2. Correction of the state estimates after new measurements:

$$\hat{\boldsymbol{x}}(l) = \tilde{\boldsymbol{x}}(l) + \hat{\boldsymbol{P}}(l)\boldsymbol{H}(l)^T \boldsymbol{R}_v^{-1} \left(\boldsymbol{y}(l) - \boldsymbol{H}(l)\tilde{\boldsymbol{x}}(l)\right) \tag{5.24}$$

3. Propagation of the system state:

$$\tilde{\boldsymbol{x}}(l+1) = \boldsymbol{f}(\hat{\boldsymbol{x}}(l)) \tag{5.25}$$

4. Propagating the covariance matrix of the estimation error:

$$\tilde{\boldsymbol{P}}(l+1) = \boldsymbol{\Phi}(l)\hat{\boldsymbol{P}}(l)\boldsymbol{\Phi}^{T}(l) + \boldsymbol{R}_{w} \tag{5.26}$$

with

$$\boldsymbol{\Phi}(l) = \left.\frac{\partial \boldsymbol{f}(\boldsymbol{x}(l))}{\partial \boldsymbol{x}(l)}\right|_{\boldsymbol{x}(l)=\hat{\boldsymbol{x}}(l)}.$$

Within the EKF equations, the notation $\{\tilde{\cdot}\}$ stands for *a priori* values (before a measurement) and $\{\hat{\cdot}\}$ stands for *posterior* values (after a measurement). The matrices $\boldsymbol{R}_w$ are $\boldsymbol{R}_v$ are the covariance matrices of the noise vectors $\boldsymbol{w}$ and $\boldsymbol{v}$. The system representation is based on equations (5.20) and (5.21).

Filter Parameters

Parameters of the extended Kalman filter are the initial error covariance matrix $\tilde{\boldsymbol{P}}(0)$, the initial *a priori* state vector $\tilde{\boldsymbol{x}}(0)$, as well as the covariance matrices of the noise signal vectors $\boldsymbol{w}$ and $\boldsymbol{v}$.

The initial error covariance matrix $\tilde{\boldsymbol{P}}(0)$ is chosen to be a diagonal matrix. Larger values indicate that there is a larger discrepancy between initial state estimates and real values.

For increasing measurement noise variances, the EKF will trust the internal model predictions more than the measurements. Smaller corrections of the *a priori* state estimate are generated by discrepancies between the measurement and the predicted output. The noise covariance matrix $\boldsymbol{R}_v$ is set according to the specification of the measurement system, i.e. depending on the measurement configuration used.

The state noise variances are the most critical tuning parameters of the EKF. The EKF can be seen as a low pass filter for the measurements $\omega^{\mathrm{T}*}$ and $m_M^{\mathrm{C}*}$. Smaller noise variances for states result in smoother state estimates with respect to the measurements but more phase shift.

EKF parameter sets which are suitable for the different measurement configurations are given below.

Settings for measurement configuration 1:

$$\boldsymbol{R}_v = \begin{bmatrix} 1\,\mathrm{rpm}^2 & 0 & 0 \\ 0 & 10\,\mathrm{deg}^2 & 0 \\ 0 & 0 & 1\,\mathrm{Nm}^2 \end{bmatrix}, \boldsymbol{R}_w = \begin{bmatrix} 0.1\,\mathrm{rpm}^2 & 0 & 0 & 0 \\ 0 & 0.001 & 0 & 0 \\ 0 & 0 & 0 & 0 \\ 0 & 0 & 0 & 0.05\,\mathrm{Nm}^2 \end{bmatrix}$$

$$\tilde{P}(0) = \begin{bmatrix} 10^3\,\mathrm{rpm}^2 & 0 & 0 & 0 \\ 0 & 1 & 0 & 0 \\ 0 & 0 & 10^6\,\mathrm{deg}^2 & 0 \\ 0 & 0 & 0 & 10^2\,\mathrm{Nm}^2 \end{bmatrix}, \tilde{x}(0) = \begin{bmatrix} 0 \\ 1 \\ 0 \\ 0 \end{bmatrix}$$

Settings for measurement configuration 2:

$$R_v = \begin{bmatrix} 1\,\mathrm{rpm}^2 & 0 & 0 \\ 0 & 1.6^2\,\mathrm{deg}^2 & 0 \\ 0 & 0 & 1\,\mathrm{Nm}^2 \end{bmatrix}, R_w = \begin{bmatrix} 0.1\,\mathrm{rpm}^2 & 0 & 0 & 0 \\ 0 & 0.001 & 0 & 0 \\ 0 & 0 & 0 & 0 \\ 0 & 0 & 0 & 0.05\,\mathrm{Nm}^2 \end{bmatrix}$$

$$\tilde{P}(0) = \begin{bmatrix} 10^3\,\mathrm{rpm}^2 & 0 & 0 & 0 \\ 0 & 1 & 0 & 0 \\ 0 & 0 & 10^6\,\mathrm{deg}^2 & 0 \\ 0 & 0 & 0 & 10^2\,\mathrm{Nm}^2 \end{bmatrix}, \tilde{x}(0) = \begin{bmatrix} 0 \\ 1 \\ 0 \\ 0 \end{bmatrix}$$

Evaluation of the EKF for Measurement Configuration 1

The accuracy of the filter was investigated for the most challenging case, measurement configuration 1. The angle measurement from the installed customised sensor was used as reference φ_{ref} to validate the angle estimate obtained by the EKF. Two tests were carried out. In the first test (Test A), the ergometer motor maintains the cadence at 40 rpm and the cyclist tries to cycle actively, working against the motor. In the second test (Test B), the motor is only resisting the movement slightly ($\underline{m} = -1\,\mathrm{Nm}, \overline{m} = 0\,\mathrm{Nm}, \omega_r = 0\,\mathrm{rpm}, \hat{M}_s = 3\,\mathrm{Nm}$), and the cyclist is instructed to cycle at different constant speeds.

Figures 5.14 and 5.15 show the result of Test A. The estimated cadence $\hat{\omega}(l) = \hat{k}_\omega(l)\hat{\omega}^T(l)$ (solid line) is depicted together with the uncalibrated cadence measurement ω^{T*} (dotted line) in Figure 5.14. The middle graph shows the cadence calibration factor k_ω which increases during the active cycling phase (15 to 32 seconds). The estimated motor torque $\hat{m}_M(l)$ is plotted in the lower graph. The angle estimation results are presented in Figure 5.15. After 8 s, the EKF estimates the angle accurately. Estimate (solid line), reference angle (dashed line) and discrete-event angle measurements (circles) are plotted in the upper graph of Figure 5.15. The estimation error, shown in the lower graph, is smaller than 5 degrees after the initial filter convergence.

The result of Test B is depicted in Figures 5.16 and 5.17. The representation of the data corresponds to that in Figures 5.14 and 5.15. The results show that also for varying cadence, a good estimate of the crank angle can be achieved with measurement configuration 1.

The not instrumented ergometer can therefore be directly used for FES cycling with respect to the required measurements. However, measurement configuration 1 also has a drawback. Accurate estimates are not available before the disk sectors have been identified and angle measurements are fed

into the EKF. This requires an initial turning of the crank at almost constant speed. Fulfilment of this prerequisite with paraplegics is straightforward by initially using motor assistance.

5.4.4 Active Crank Torque Estimation

Estimation of the muscularly produced crank torque is possible for isokinetic cycling where the motor maintains constant speed. In this situation, the moment balance at the crank can be written as

$$m_A(t) + m_P(t) + m_M(t) = 0. \tag{5.27}$$

The motor moment m_M counterbalances the passive moment (friction, gravitation of the legs) and the active (muscularly produced) moment of the legs. In order to allow an assessment of the active moment, the passive moment has to be identified first from a passive cycling trial with motor support only. Without active cycling or stimulation, the passive moment is determined easily by the measured motor moment. The passive moment can be expressed as a function of the crank angle in the form of a Look-Up-Table (LUT) [61]:

$$m_P(\varphi) = -m_M(\varphi) = \mathrm{LUT}(\varphi), \quad m_A(t) = 0. \tag{5.28}$$

Consequently, the estimate of the active moment is then given by

$$\hat{m}_A(l) = -\hat{m}_M(l) - \mathrm{LUT}(\hat{\varphi}(l)). \tag{5.29}$$

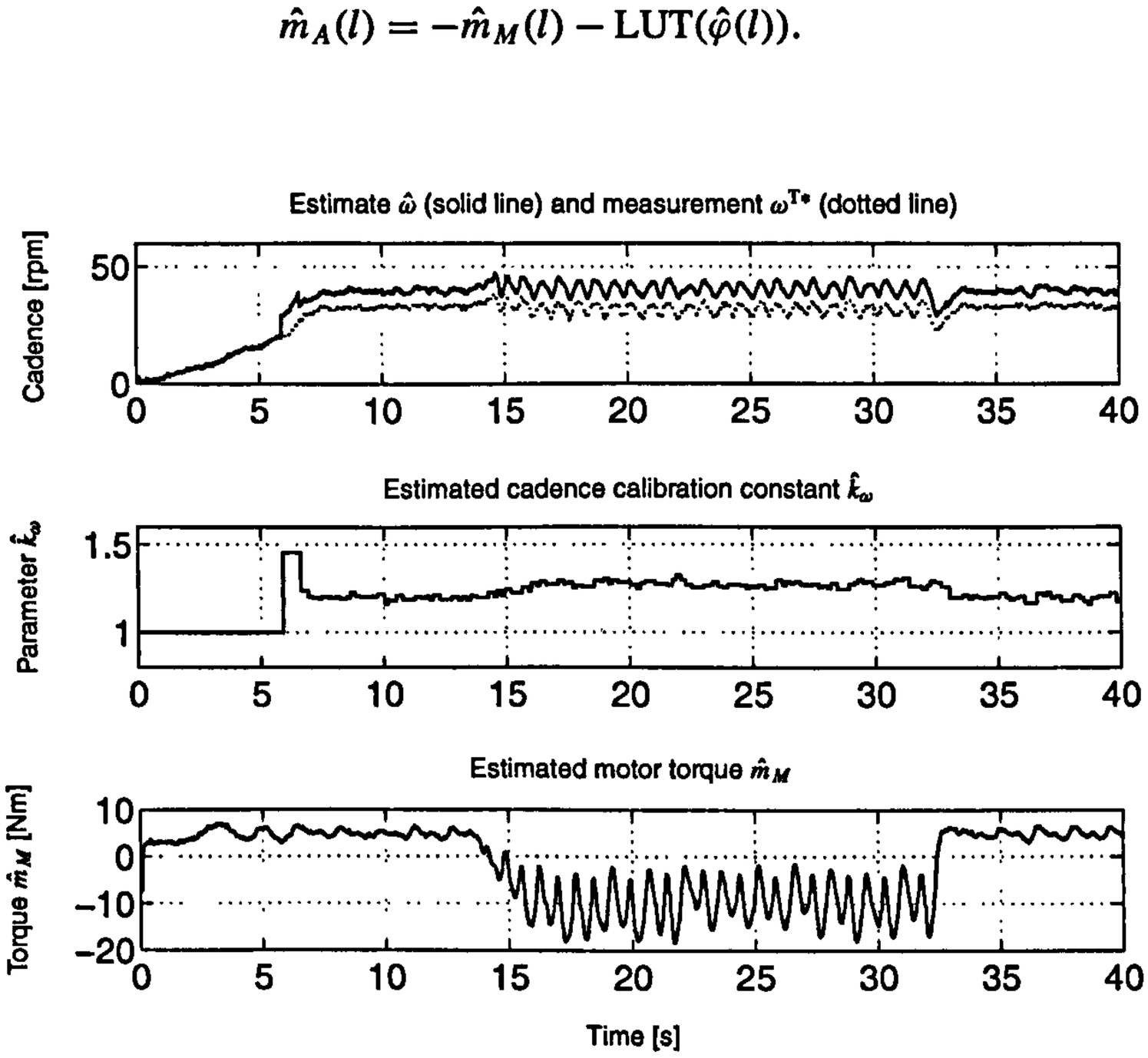

Figure 5.14: Cadence and torque estimates of the EKF during an isokinetic trial.

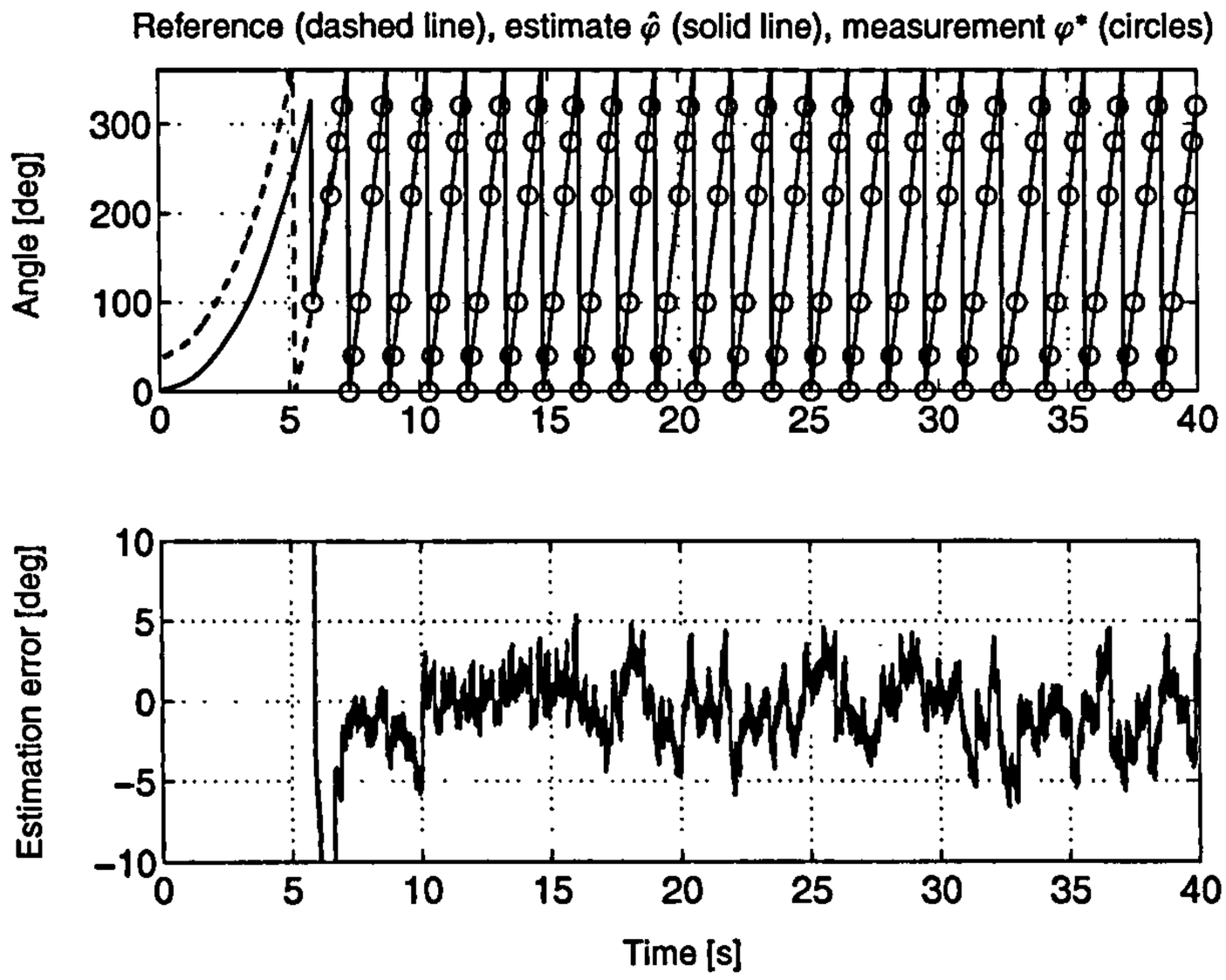

Figure 5.15: Angle estimate of the EKF during an isokinetic trial.

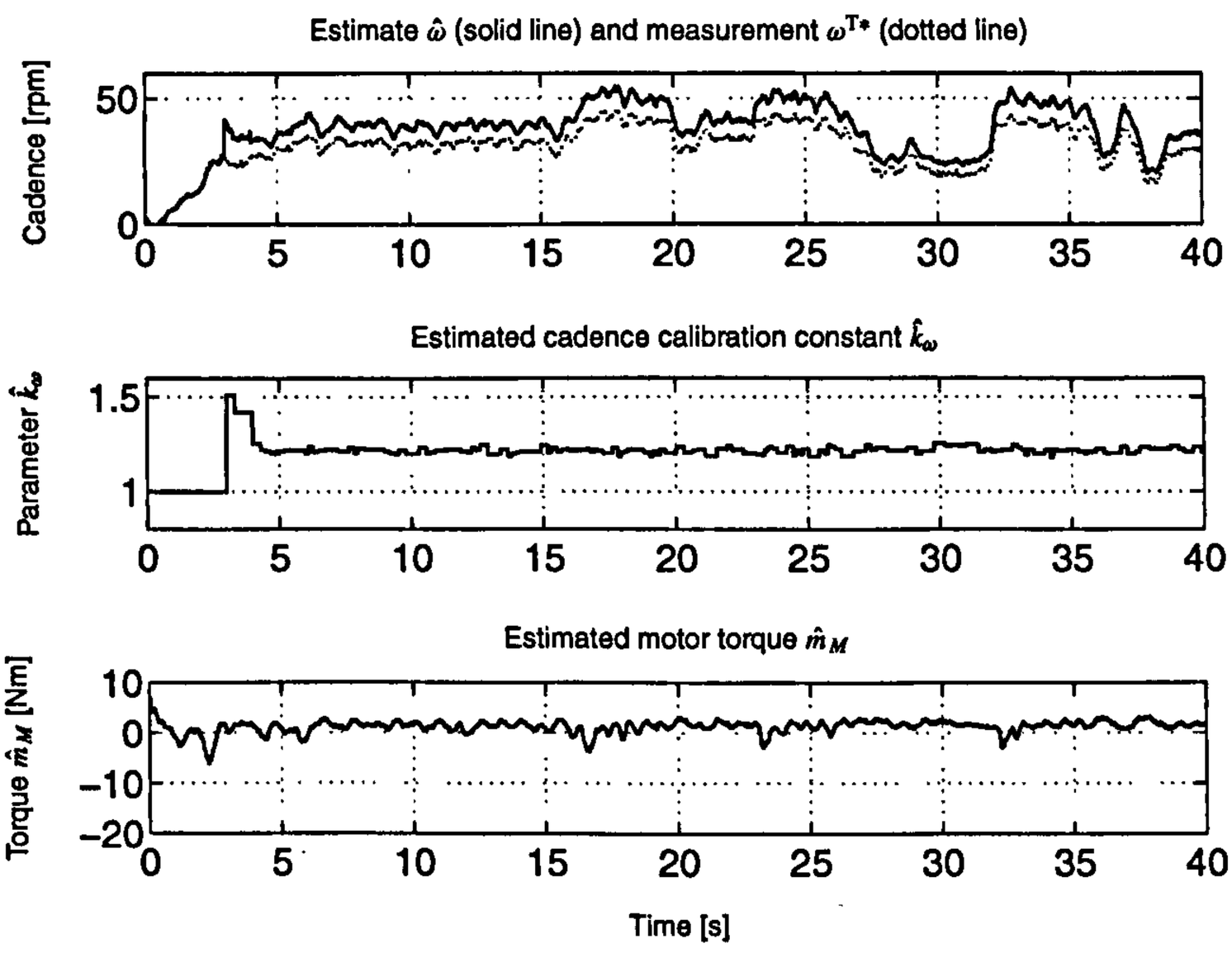

Figure 5.16: Cadence and torque estimates of the EKF during an isotonic trial.

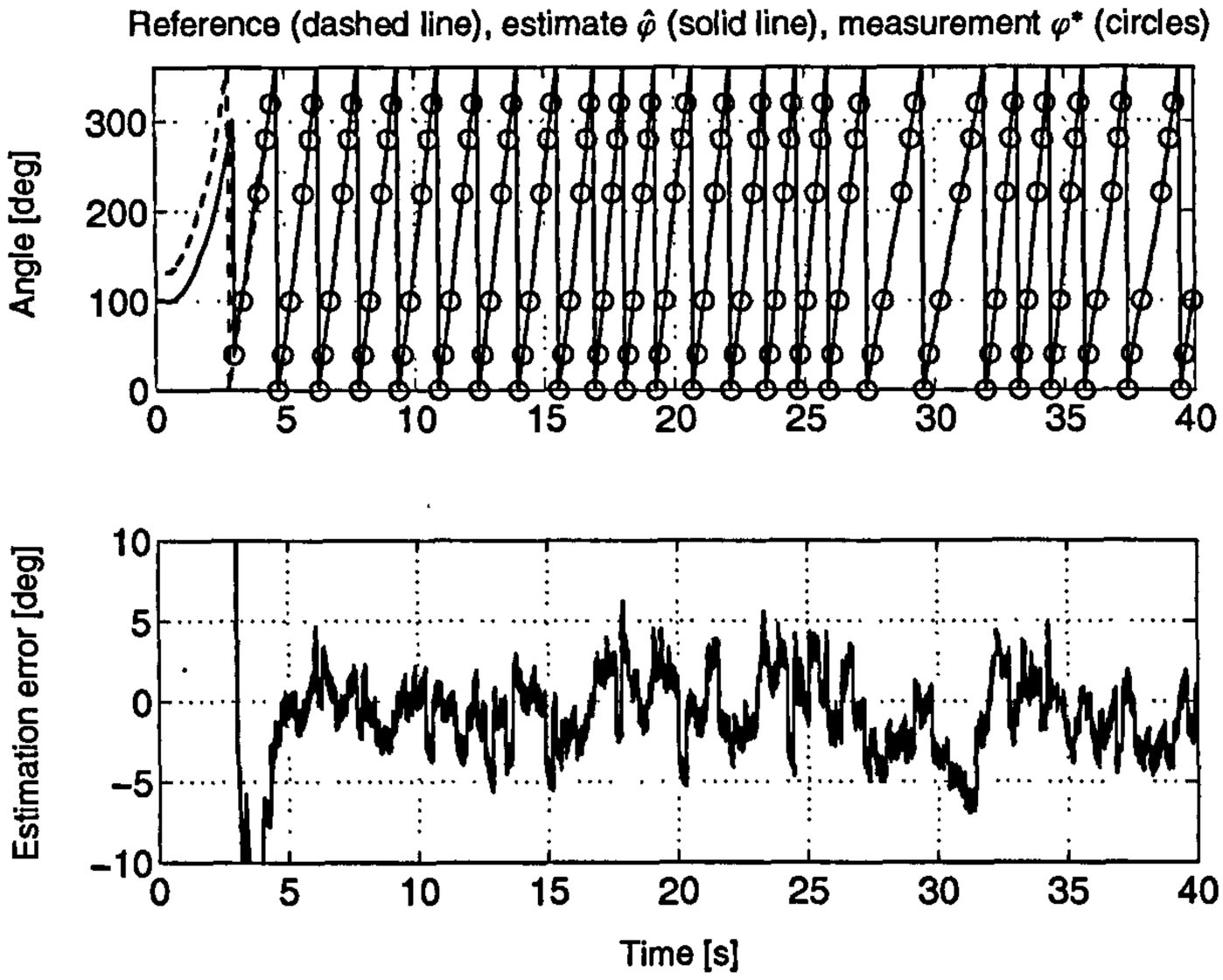

Figure 5.17: Angle estimate of the EKF during an isotonic trial.

5.5 Stimulation Device and Pattern Generator

The portable stimulation device employed has been developed in cooperation with the German company HASOMED GmbH. The author's contribution was to put forward the specifications for the stimulation parameters and timing, the interfaces and the communications protocol. Furthermore, the FES cycling algorithms inside the stimulator have been designed and implemented.

The current-controlled 8 channel stimulator RehaStim pro™ is a certified medical product and possesses two independent current sources which are multiplexed to 4 outputs each. The main processor of the stimulator is an ultra-low-power 16-bit RISC mixed-signal processor from Texas Instruments (MSP430F169). There are two independent stimulation modules hosting each one of the current sources. Each stimulation module owns another microprocessor (MSP430F149) which is responsible for the pulse generation timing. The stimulation module A has the stimulation channels 1 to 4, stimulation module B has the stimulation channels 5 to 8. Since both modules function independently simultaneous pulse generation on module A and B is possible.

Figure 5.18 shows the stimulator device. The device is operated by a touch panel with illumination. The technical specifications are listed in the Table 5.5. Notice that the RS232 and USB interfaces share the same UART interface of the MSP430 so that multiplexing must be applied when using both interfaces at the same time. This is the case for the stand-alone operation of ergometer and stimulator which are connected by RS232 and where the USB port of the stimulator can be optionally used for data logging. In the PC-controlled configuration the USB interface is employed for communication with the PC and the RS232 is free. The stimulator possesses additional inputs and outputs which are not used here. Galvanic isolation between high voltage generation/electrodes and the rest of the stimulator electronics has been realised for safety reasons.

Figure 5.18: Portable 8 channel stimulator of the FES cycling system.

Table 5.5: Technical details of the stimulation device.

Current	0 . . . 126 mA in 2 mA steps
Pulsewidth	0, 20 . . . 500 μs in 1 μs steps
Frequency	see Section 5.5.1
Pulse form	biphasic
Channels	8 (2 times 4 on two modules)
Serial ports	RS232 and USB with galvanic isolation
Digital and analogue I/O	8 pins which can be assigned individually as 12-bit analogue inputs (8 available), 12-bit analogue outputs (2 available) or digital inputs/outputs (8 available)
Sensor supply	5 V / 100 mA

Figure 5.19 shows the form of a delivered bi-phasic pulse on an ideal resistive load. Current amplitude and pulsewidth are defined in the figure. Notice that there is a fixed pause of 100 μs between the two phases of the pulse. At the end of the pulse the remaining charge on the electrodes and skin is removed by an active shortcut (change of electrode polarity for 1 μs).

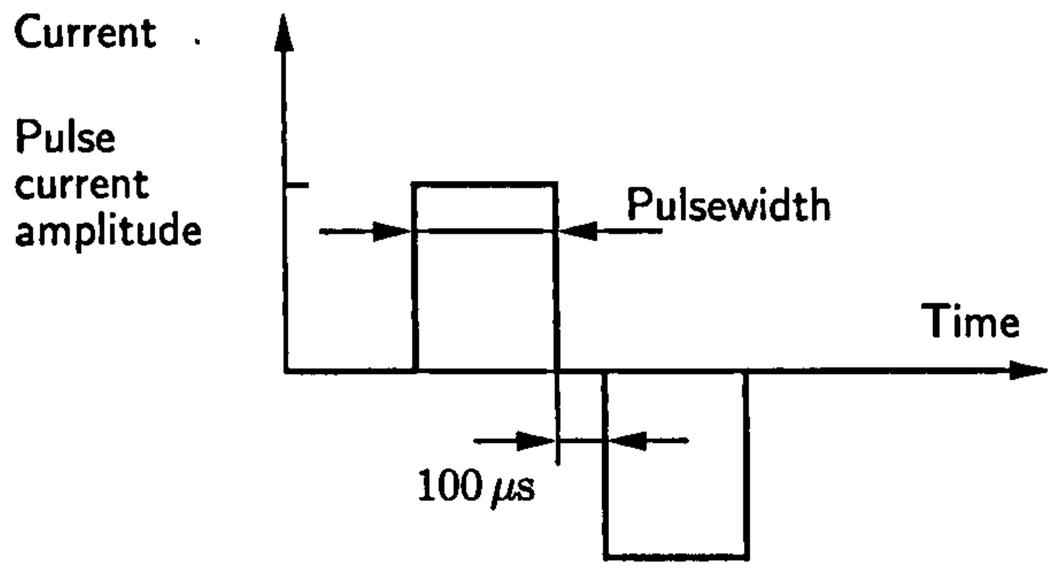

Figure 5.19: Definition of pulsewidth and current amplitude for a biphasic pulse.

5.5.1 Pulse Generation Modes

The stimulator offers different modes of stimulation pulse generation. An Application Programming Interface (API) is provided which enables the development of customised stimulator applications using the different modes of pulse generation. Moreover, a serial communication protocol is available so that the pulse generation can also be controlled by sending commands with 115200 Bauds from an external device, preferably a PC.

The following modes of pulse generation are available:

- **Single Pulse Mode:** On an external command or an API function call the stimulator generates

a single pulse on a specified channel with desired current amplitude and pulsewidth. The stimulator will generate the pulse immediately after processing the command. Complex stimulation patterns may be generated by sending more than one command. The application program inside the stimulator or the external device (PC) are responsible for controlling the stimulation timing, i.e. the stimulation pulse interval. Therefore, the API of the stimulator provides a 16-bit timer with a resolution of 1 ms.

- **Continuous Channel List (CCL) Mode:** Using this mode, the generation of complex patterns is greatly simplified. The main processor and the processors of the stimulation modules control the pulse generation by means of timer-interrupts. A list of stimulation channels has to be specified, on which pulses or even pulse groups (doublets or triplets) will repeatedly be generated. Figure 5.20 defines the main stimulation period t_1 and the inter-pulse time t_2 of doublets and triplets with the help of an example. The channel list is repeatedly processed with time period t_1. Pulse generation takes place on the selected channels, ordered by the channel numbers. For each selected channel a time slot of 1.5 ms is reserved, even if current or/and pulsewidth are zero for the channel or if the pulsewidth is smaller than 1.5 ms. At least 1.5 ms pass between the stimulation of different channels of one module. The stimulation modules A and B process the channel list in parallel with a time offset of 0.6 ms. Module A generates pulses on the channels 1 to 4 if applicable, and module B generates pulses on the channels 5 to 8 if applicable. The inter-pulse time t_2 of doublets and triplets is fixed for all channels and is set during an initialisation step. When doublets or triplets have to be generated the channel list will be processed two or three times more with period t_2. Stimulation takes place only on the channels on which doublets or triplets have to be generated.

  The main stimulation frequency is specified by the period t_1. Some channels of the channel list can be assigned to a lower frequency which has the period nt_1 where n is a positive integer.

  The CCL mode must be initialised by an API function call or a command (external control). Used channels, main time t_1, inter-pulse time t_2 and the maximal size of pulse groups must be chosen at this stage. The minimal possible inter-pulse time t_2 depends on the maximal number of channels assigned to the individual stimulation modules as follows

$$t_2 \geq 1.5\,\text{ms} \cdot \max(n_{ch_A}, n_{ch_B}) \tag{5.30}$$

  where n_{ch_A} and n_{ch_B} are the number of selected channels of stimulation modules A and B respectively. The minimal possible period t_1 depends on t_2 and the maximal size n_{pg} of pulse groups used ($n_{pg} = 1$ for single pulses, $n_{pg} = 2$ for doublets, $n_{pg} = 3$ for triplets). The constraint for t_1 is then

$$t_1 \geq n_{pg} \cdot t_2 + 1.5\,\text{ms} \tag{5.31}$$

  where the 1.5 ms above results from a communication between the main processor and the stimulation modules as indicated in Figure 5.20. The period t_1 can be changed in the range

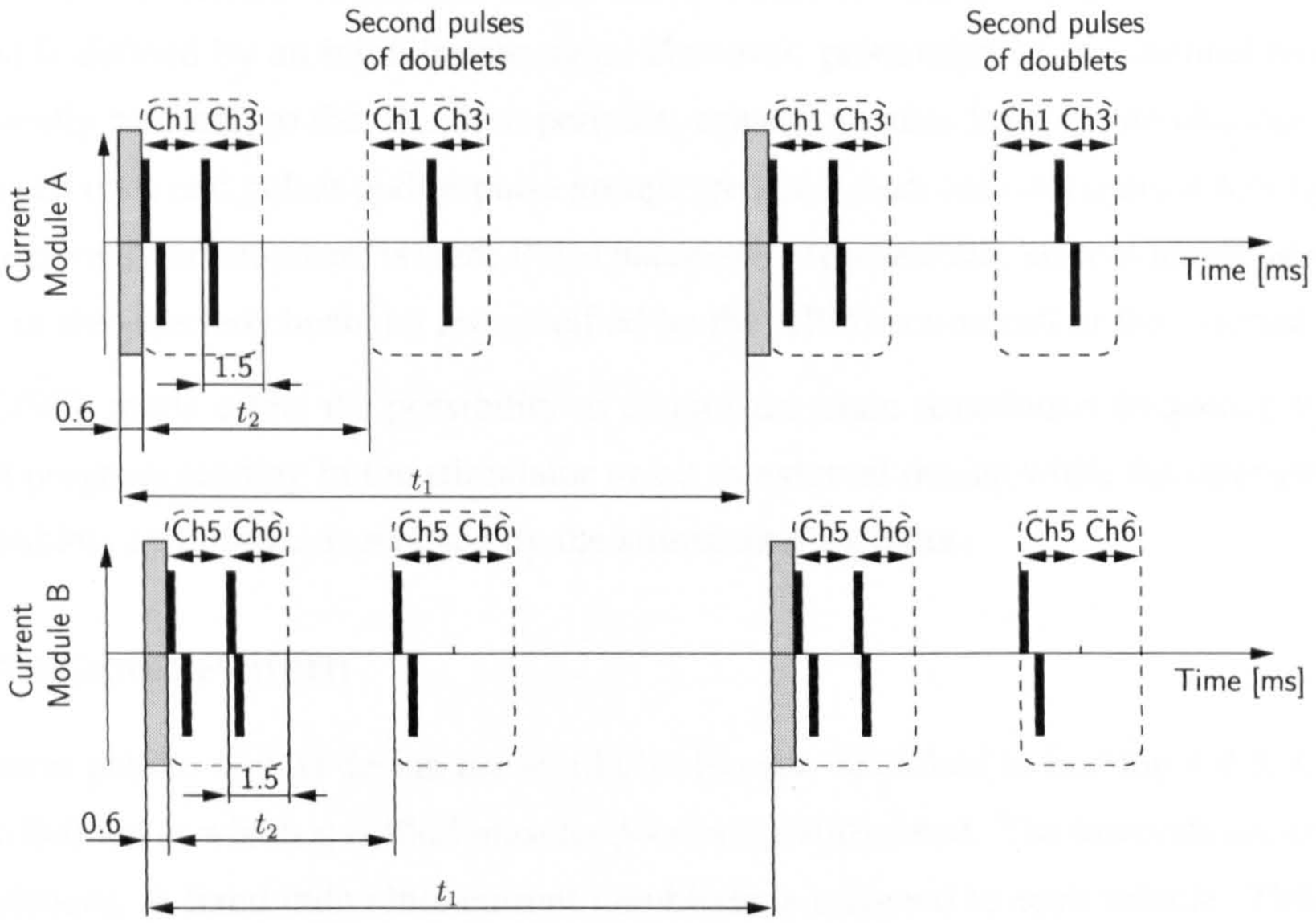

Figure 5.20: Example for the Continuous Channel List Mode of the stimulator. The channel list encloses the channels 1, 3, 5 and 6. The main stimulation frequency is $1/t_1$. Doublets are generated on the channels 3 and 5 with a frequency $1/t_2$. The grey bars indicate some communication periods in which the actual stimulation settings are transfered from the main controller to the stimulation modules. Stimulation pulses are represented by black bars where the same width and amplitude have been assumed for simplicity.

3 . . . 1023.5 ms in 0.5 ms steps subject to the constraint (5.31), and t_2 can be altered in the range 3 . . . 16 ms in 0.5 ms steps subject to the constraint (5.30). Using all 8 channels, a minimal group time t_2 of 6 ms can be achieved, i.e. a doublet or triplet frequency of 180 Hz. When only doublets and single pulses with a frequency of 180 Hz are applied ($n_{pg} = 2$), a minimal value of 13.5 ms for period t_1 is obtained, i.e. a maximal possible main frequency of 74.1 Hz.

Another API function call or external command deactivates the CCL mode. When the CCL mode is active, the pulse parameters (pulsewidth, current amplitude and group mode (single pulse, doublet or triplet) of the selected channels can be altered by a corresponding API function call or an external command. The new parameters will be used from the next processing of the channel list onwards.

The main processor controls the frequency $1/t_1$ by which the channel list is processed. Each time the stimulation cycle repeats, the main processor sends the actual stimulation settings to the two stimulation modules which then generates the individual pulses on the selected channels. The processors on the stimulation modules guarantee that specified pulsewidths and interpulse times of the doubles and triples are realised.

- **One Shot Channel List (OSCL) Mode:** Just as in the Continuous Channel List Mode a channel list is defined by an initialisation step. However, processing of the channel list is not automatically repeated so that the time period t_1 ceases to exist. Instead, the channel list will be processed once and pulses and/or pulse groups are generated, only if a special API function call or an external command are issued. Pulse parameters (pulsewidth, current amplitude and group mode of the selected channels) are specified by the API function call or the external command.

  The OSCL mode offers the possibility to control the main stimulation frequency by an application program running in the stimulator or by an external device while the inter-pulse time of the doublets and triplets is realised by the stimulation modules.

5.5.2 Stimulation Pattern

The stimulation pattern and its design are similar to the one described in Section 4.4.3. Crank angle intervals are defined in which specified muscles groups are stimulated. The intervals are corrected for different cadences. A fixed individual current amplitude is assigned to each muscle. This amplitude is kept constant while the pulsewidth is varied during the cycling to control the stimulation intensity. In order to simplify the system the same pulsewidth is applied to all muscle groups.
Differences in the stimulation pattern and design compared to Section 4.4.3 are:

- A gradual onset of stimulation is possible defined by a ramp over some stimulation pulses. This option is useful for low cadences where stimulation phases of the muscles are longer. A slowly rising pulsewidth may avoid unwanted triggering of spastic reflexes.

- The stimulation pattern can be assessed now on the basis of the estimated active drive moment during isokinetic cycling. This allows determination of stimulation ranges where only positive drive torque is generated. Ferrante et al. [22] recently proposed a strategy to automate this process.

5.5.3 PC-Controlled Stimulator Operation

Stimulator and PC are connected by USB. Galvanic isolation is provided by the stimulator. The One Shot Channel List Mode is used in this setup. This means that the main stimulation frequency is controlled by the PC software. The stimulation conditions are checked every 5 ms synchronised to the extended Kalman filter updates. This is 10 times faster than with the implementation for the tricycle. Stimulation of a channel is activated as soon as the crank angle enters the corresponding angle interval. Any stimulation period can be defined which is an integer of the 5 ms base sampling-time.
The test of the stimulation conditions and the generation of the stimulation pulses are in this case synchronised. A more accurate fit of the stimulation to the specified angle intervals (at least starting angles) is thus achieved. However, noisy angle estimates of jerky movements may represent a problem

with this approach since a stimulation interval could be entered and left several times very quickly in succession. If pulses were generated each time the interval is entered then an unwanted high frequency stimulation pulse train would arise. To avoid this effect, activation of stimulation for a channel will be inhibited for the stimulation period after the stimulation interval was left.
Variable frequency trains can be easily generated as explained above with the new stimulator.

5.5.4 Stand-Alone Stimulator Operation

For stand-alone operation of ergometer and stimulator, the Continuous Channel List Mode is employed. The extended Kalman filter is implemented in fixed-point arithmetic running at only 20 Hz. The stimulation conditions are tested at this frequency and an API function is called for stimulation parameter update when stimulation settings change. Notice that no synchronisation of pulse generation and stimulation condition check takes place. This implementation is comparable to the one in Section 4.4.3.

5.6 Use and Limitations of the Built-In Motor Controller

The built-in controller setup has been described in Section 5.3. It can be used for FES cycling but has some limitations. The two cases, isokinetic and isotonic training, are studied separately to discuss the usefulness of the built-in controller.

5.6.1 Isokinetic Training

In the case of an isokinetic cycling exercise, the motor is controlled to maintain a desired cadence while the cyclist tries to work against the motor aiming to accelerate to crank. If integral action is included in the controller and if the bandwidth of the closed-loop system is sufficiently high, then the motor will maintain the true cadence on average close to the reference. Limited bandwidth will result in cadence variations around the reference. The variations may be larger when the active drive moment produced by the cyclist does not act uniformly at the crank. This is very likely for paraplegic cyclists where the electrical stimulation usually does not result in a uniform moment generation. In order to realise isokinetic training with the ergometer's motor control, the moment limit $\overline{m}$ has to be set to the maximum and the moment limit $\underline{m}$ to the largest possible negative value. In summary, the ergometer can be directly used to realise FES cycling under isokinetic conditions.

Experimental Test

The feasibility of isokinetic FES cycling has been experimentally tested by one investigator (neurologically intact, male, age of 26, body weight of 90 kg). The quadriceps and hamstrings on both legs were stimulated. Table 5.6 summarises the stimulation parameters. The results of the isokinetic cycling test are shown in Figure 5.21. In the upper graph, the desired cadence $\omega_r = 40$ rpm

(dashed line) is plotted together with the estimated cadence $\hat{\omega}$ (solid line). Stimulation intensity has been adjusted manually by the experimenter using the dial. The middle graph indicates the applied pulsewidth which was the same for all stimulated muscles. Finally, the active drive moment by FES is depicted in the bottom graph. The first 35 s were passive cycling without stimulation in order to estimate the passive moments at the crank.

Table 5.6: Stimulation settings during the isokinetic and isotonic FES cycling tests. A stimulation frequency of 20 Hz has been chosen for all muscles.

Muscle	Stimulation interval [degree]	Current [mA]	Muscle activation and relaxation delay [ms]
Right quadriceps	60-185	40	150
Left quadriceps	240-5	40	150
Right hamstring	210-360	35	150
Left hamstring	30-180	35	150

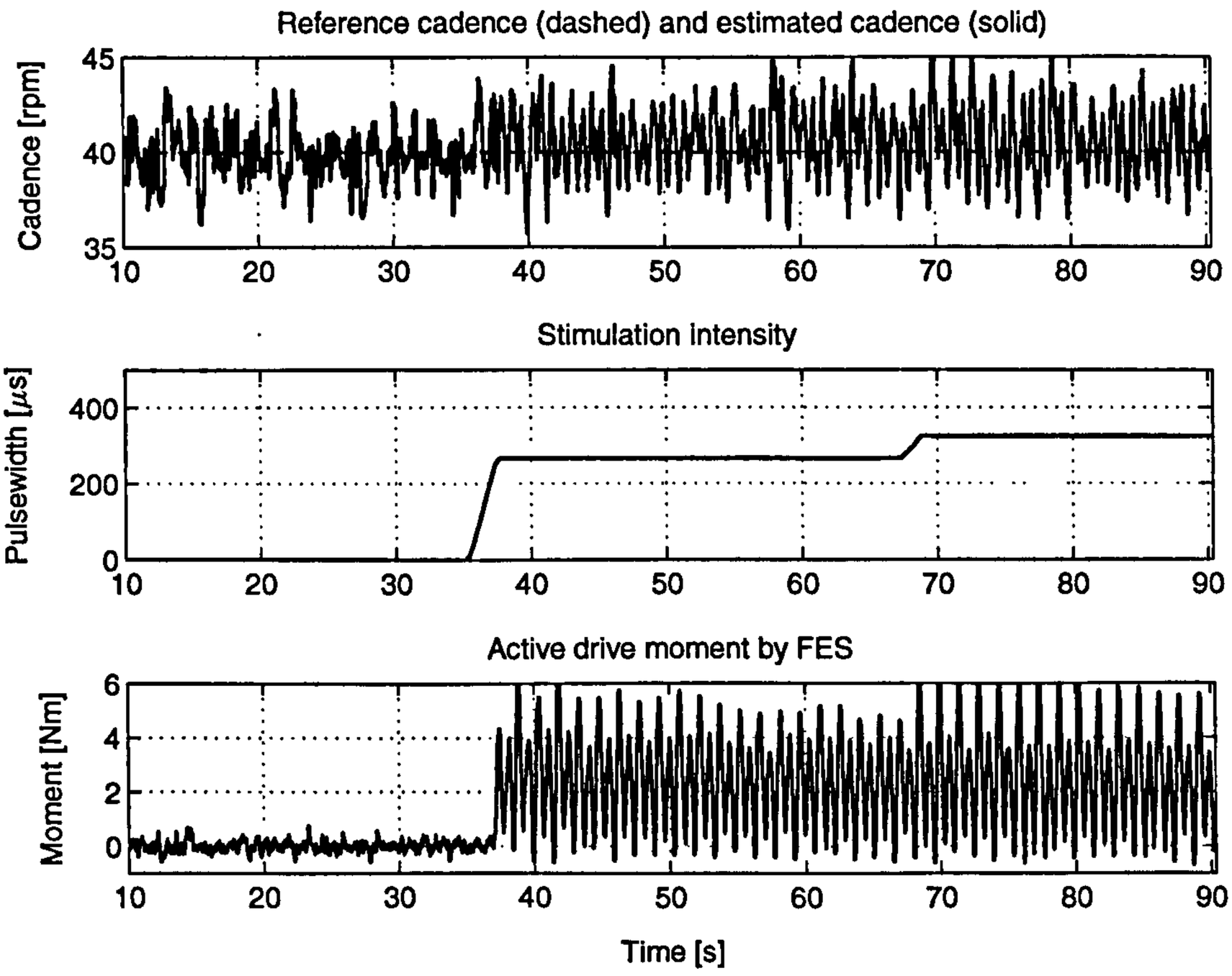

Figure 5.21: Isokinetic FES cycling test.

5.6.2 Isotonic Training

A resisting moment at the crank is realised under isotonic training conditions by the DC drive. Compared to purely mechanical trainers, the motor can provide not only a resisting moment but can also

support the cycling. A strategy is to set-up a low base cadence first. This may be a cadence of 10 to 20 rpm which initiates the cycling movement, and most important, helps to get the angle detection with measurement configuration 1 running. In order to achieve the base cadence ω_b, the upper moment limit $\overline{m}$ is set to its maximum and the reference cadence ω_r is chosen as ω_b.
As soon as the electrical stimulation is active, the required motor torque for maintaining ω_b is reduced by the amount of active (muscular) moment at the crank. For stronger increasing active moment, the motor starts to work against the cyclist up to a resistive moment specified by

$$m_R = \underline{m} + \hat{M}_s \tag{5.32}$$

where $\hat{M}_s$ is the positive static friction compensation moment of the built-in controller which can be set to a desired value. This offers the possibility to choose the resisting moment by setting $\underline{m}$ and $\hat{M}_s$. For any cadence larger than the base cadence, the motor moment m_R is realised at the crank shaft on average.
The moment $\hat{M}_s$ should be chosen once to compensate for the true static friction moment as well as possible. An estimate of the friction M_s is obtained by the moment calibration procedure. This value will of course increase slightly for the ergometer system with cyclist. Recall that, motor moment calibration was performed only with a reference weight.
During cycling the resistance is controlled by adjusting $\underline{m}$. Using $\hat{M}_s = 3\,\text{Nm}$ for example, the lowest resistance (with the calibration given in Section 5.4) is $m_R = -1.37\,\text{Nm} + 3\,\text{Nm} = 1.7\,\text{Nm}$. Notice that this is in fact still a supporting torque. The paraplegic has to produce at least the difference between the real static friction moment M_s and the positive minimal resistance m_R by electrical stimulation of the musculature in order to achieve any cadence larger than ω_b. The largest possible resisting moment is $m_R = -19.85\,\text{Nm} + 3\,\text{Nm} = -16.85\,\text{Nm}$. Hence, the resisting moment m_R can be varied from a small supporting torque to a rather large braking torque.
The cycling cadence may be controlled by the electrical stimulation and so maintained at a constant level, while the resisting moment can be varied to set different cycling powers. Control of cadence by muscle stimulation is described in detail in Section 6.3.
In summary, the ergometer can be used directly for FES cycling under isotonic conditions. Exact control of resistance is possible. Further, the moment of inertia control of the ergometer guarantees smooth cycling movements. Hence, there is no need for changing the controller with respect to this application.

Experimental Test

Figure 5.22 shows a feasibility test for isotonic cycling. The same stimulation parameters are used as in the isokinetic trial. In the upper graph, the set base cadence $\omega_b = 20\,\text{rpm}$ (dashed line) is plotted together with the estimated cadence $\hat{\omega}$. Stimulation intensity has been adjusted manually by the experimenter using the dial in order to achieve a steady state cadence of 40 rpm for the initial chosen resistance. The middle graph indicates the applied pulsewidth which was the same for all stimulated

muscles. Finally, the motor moment is depicted in the bottom graph. The resisting motor moment m_R was 1.7 Nm for the first 40 s and was changed then to 1 Nm. Notice that the m_R is actually positive, i.e. the motor still supports the movement and partly compensates for the passive moments of the system. The cadence drops to the lower value of m_R to 30 rpm due to less motor support. A higher stimulation intensity would be required to keep a cadence of 40 rpm.

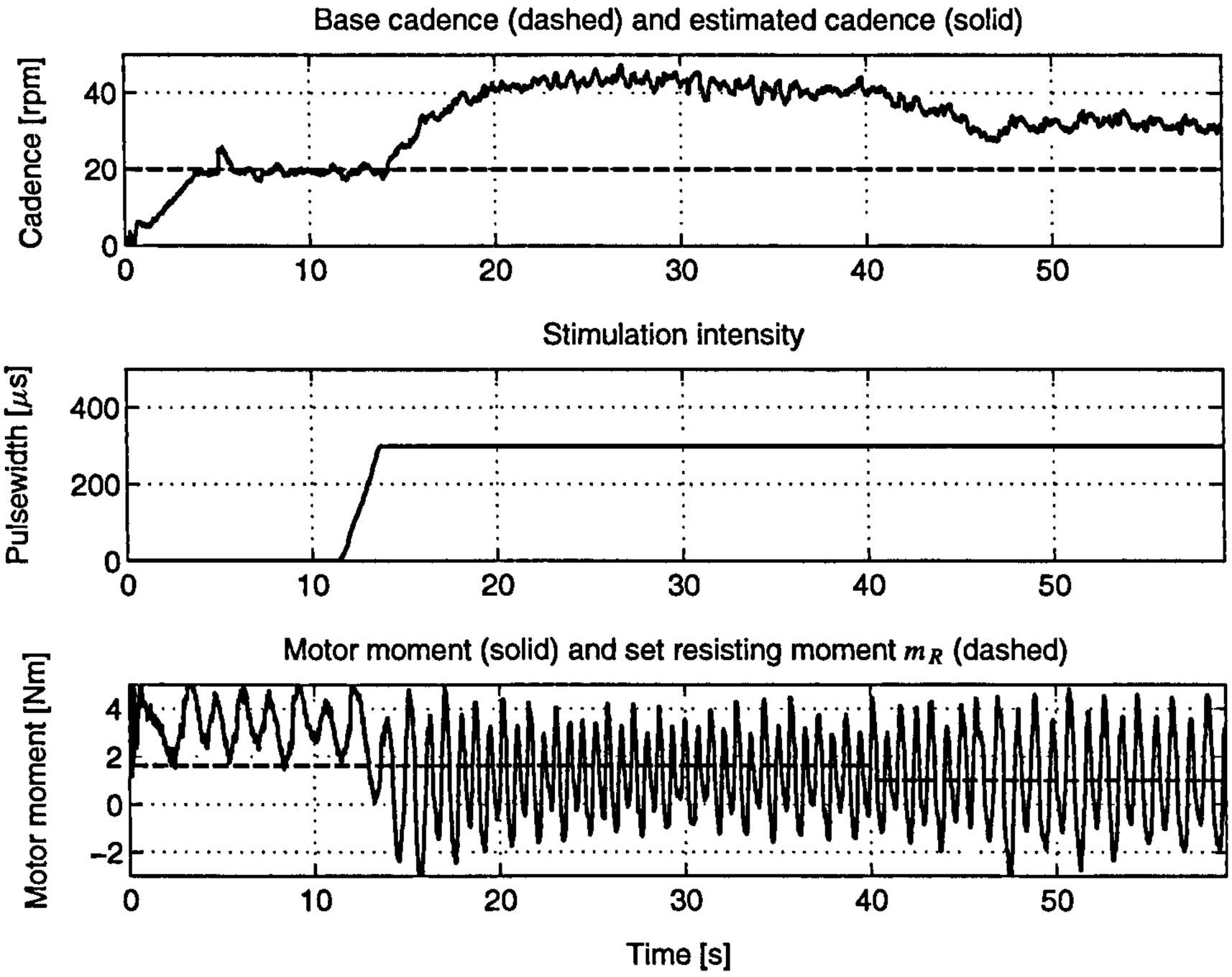

Figure 5.22: Isotonic FES cycling test.

5.7 Customised Cadence Controller

The built-in motor controller has integral action, but comes with a limited bandwidth. The isokinetic FES cycling test with an intact subject, shown in Figure 5.21, reveals cadence variations with an amplitude of 8 rpm during active stimulation. Certainly, one can live with such a controller performance in clinical practice. There are however situations, where "perfect" constant cadence is required, e.g. studies on stimulation pattern optimisation. Accurate cadence control also improved the moment calibration of the ergometer. An accurate estimation of the active drive moment depends as well on the assumption of constant speed. This provided the motivation to investigate the design of a customised cadence controller.

5.7.1 Experimental Setup

In order to realise a customised cadence controller for isokinetic training the ergometer motor must be controlled directly. The duty cycle of the PWM signal is therefore adjusted by a cadence controller C_c as illustrated in Figure 5.23. The reference cadence $\omega_r(k)$ is specified by the experimenter, where k is the index of the sampling instances. The sensed cadence $\hat{\omega}(k)$ is the output of the EKF where measurement configuration 2 must be used together with the PWM control mode. An update of the duty cycle $\gamma(k)$ can be performed every 20 ms. Thus, the cadence estimate of the EKF is downsampled to the same sampling rate.

A dynamic model is identified between the duty cycle $\gamma(k)$ and the cadence $\hat{\omega}(k)$ without active electrical stimulation but with person in the ergometer. The duty cycle is altered by a Pseudo Random Binary Sequence (PRBS) and the corresponding $\hat{\omega}(k)$ is recorded. An ARMAX-type model (see Section 2.2) is estimated from the input/output data using the prediction error method. The identification procedure provides for controller design the input transfer function $H_p(q^{-1})$ defined by the integer n_k and the polynomials $\mathsf{A}(q^{-1})$ and $\mathsf{B}(q^{-1})$. Typically, the dynamics are stable and of first order with no zeros and a three step input/output delay which is mainly caused by the serial communication.
The generic design procedure of Section 2.3 and Section 2.4 was applied to the identified model subject to the following definitions:

- The controlled output $y(k)$ is the cadence $\hat{\omega}(k)$.
- The control signal $u(k)$ is the duty cycle $\gamma(k)$.
- The reference signal $r(k)$ is the desired cadence $\omega_r(k)$.

The pole-placement method is used to design the controller. Integral action is included into the controller, i.e. $\overline{\mathsf{R}}_d = 1 - q^{-1}$. To make sure that measurement noise does not generate large signals, $\overline{\mathsf{S}}_d = 1 + q^{-1}$ was assigned. By this means, measurement signals at the Nyquist frequency do not give any error at the output variable $y(k)$. No poles and zeros are cancelled by the controller. Taking this controller configuration, the degree estimate for the characteristic polynomial factor $\overline{\mathsf{A}}_{cl}$ is obtained

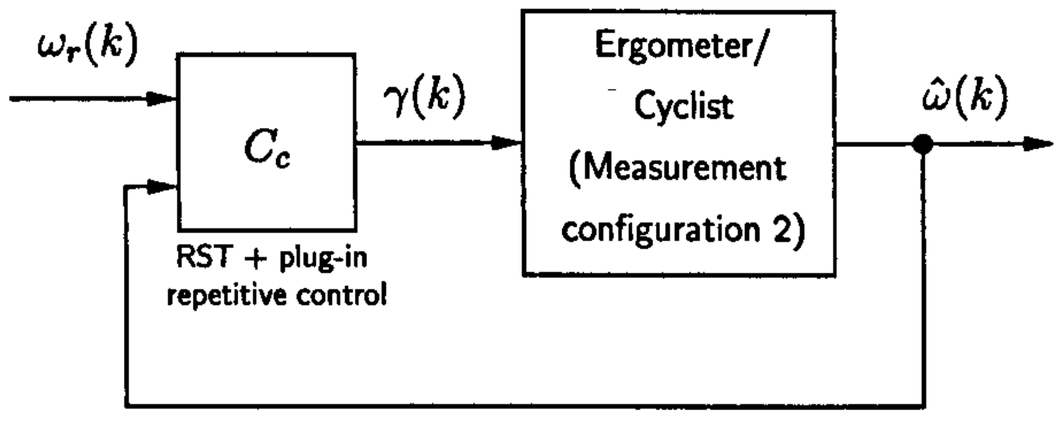

Figure 5.23: Closed-loop structure for the customised motor control.

by Equation (2.39) as

$$\deg \overline{\mathsf{A}}_{cl} \leq 5.$$

Incomplete separation of command and disturbance response is selected in the controller design process, and two second order polynomials $\mathsf{A}_o(q^{-1})$ and $\mathsf{A}_r(q^{-1})$ are chosen, specified by the rise times $t_r^{\mathsf{A}_r}$ and $t_r^{\mathsf{A}_o}$. The characteristic polynomial of the windup observer is equated with the polynomial $\mathsf{A}_o(q^{-1})$.

The main aim of designing a new cadence controller is to obtain better rejection of periodic disturbances and as a consequence less cadence variation during the isokinetic training. The input/output delay of the model as well as the relatively large sampling time for the motor control limit the achievable bandwidth under the standard controller design methodology. The bandwidth required to reject the periodic disturbances cannot be achieved without intolerable noise sensitivity. Alternatively, a plug-in repetitive controller is designed as described in Section 2.4. Tuning parameters of the plug-in controller are the gain k_r and the period N of the disturbance. For a given desired cadence ω_r the period is determined by

$$N = \text{floor}\left(\frac{1}{\omega_r t_s}\right). \tag{5.33}$$

where t_s is the sampling-time of the controller. Notice that a redesign of the repetitive controller must be carried out when the desired cadence changes.

5.7.2 Experimental Procedure

The following experimental procedure has to be carried out to design and validate the customised cadence controller:

1. **Identification.** A PRBS is designed off-line. The signal has to excite the major dynamics of the system. The PRBS used has a period of 2000 samples and is constant for at least 50 samples after each transition. The mean value and amplitude of the signal are 40% and 10% respectively.

The PRBS of the duty cycle is applied to the ergometer with cyclist in an open-loop test, labelled **Test PRBS**. No electrical stimulation is active. The obtained set of input/output data is employed for model identification. This step also involves model validation.

2. **Controller Design.** Based on the experimentally identified model the feedback control system is designed following the guidelines given in the Sections 2.3 and 2.4. Design parameters are the rise times $t_r^{A_r}$ and $t_r^{A_o}$, the gain k_r as well as the disturbance period N. The latter is defined by the desired constant cadence ω_r.

3. **Experimental controller test (Test C).** The closed-loop system performance is experimentally validated. For a given constant cadence ω_r, the resulting cadence variations caused by electrical stimulation of just the quadriceps on both legs are assessed. Stimulation intensities for the quadriceps are chosen so that torque disturbances of a magnitude of at least 4 Nm are generated. Following the analysis of the control system, the design parameters are sometimes changed and Test C is repeated.

5.7.3 Experimental Results

The control approach has been experimentally tested by one investigator (neurologically intact, male, age of 26, body weight of 90 kg). All results are from the same experimental session.

Results of Test PRBS and the Model Identification

Results of Test PRBS are shown in Figure 5.24. In the upper plot, the input signal (duty cycle) is depicted. The measured cadence (solid line) is plotted in the lower graph together with simulated output (dashed line) of the estimated model. The first second is cut off for the identification process. The estimated input transfer function of the ARMAX model is

$$H_d(q^{-1}) = \frac{0.3217q^{-3}}{1-0.4576q^{-1}} \tag{5.34}$$

possessing a DC gain of 1.16 rpm/(%duty cycle). The model (5.34) describes only the deterministic system behaviour. Notice in Figure 5.24 that cadence disturbances caused by the gravity of the legs are of course not captured by the identified input transfer function.

Results of the Controller Design

The results of the controller design are illustrated in the form of the closed-loop frequency responses in Figure 5.25. The responses of the output sensitivity function S (solid line), the complementary output sensitivity function T (dashed line) and the reference model H_r (dash-dotted line) are shown for the design with plug-in repetitive controller (thin lines) and without plug-in repetitive controller (bold line). A period of $N = 75$ was used for the repetitive controller, corresponding to a desired cadence of $\omega_s = 40$ rpm. In addition, the rise times $t_r^{A_r} = 0.10$ s and $t_r^{A_o} = 0.08$ s as well as the gain

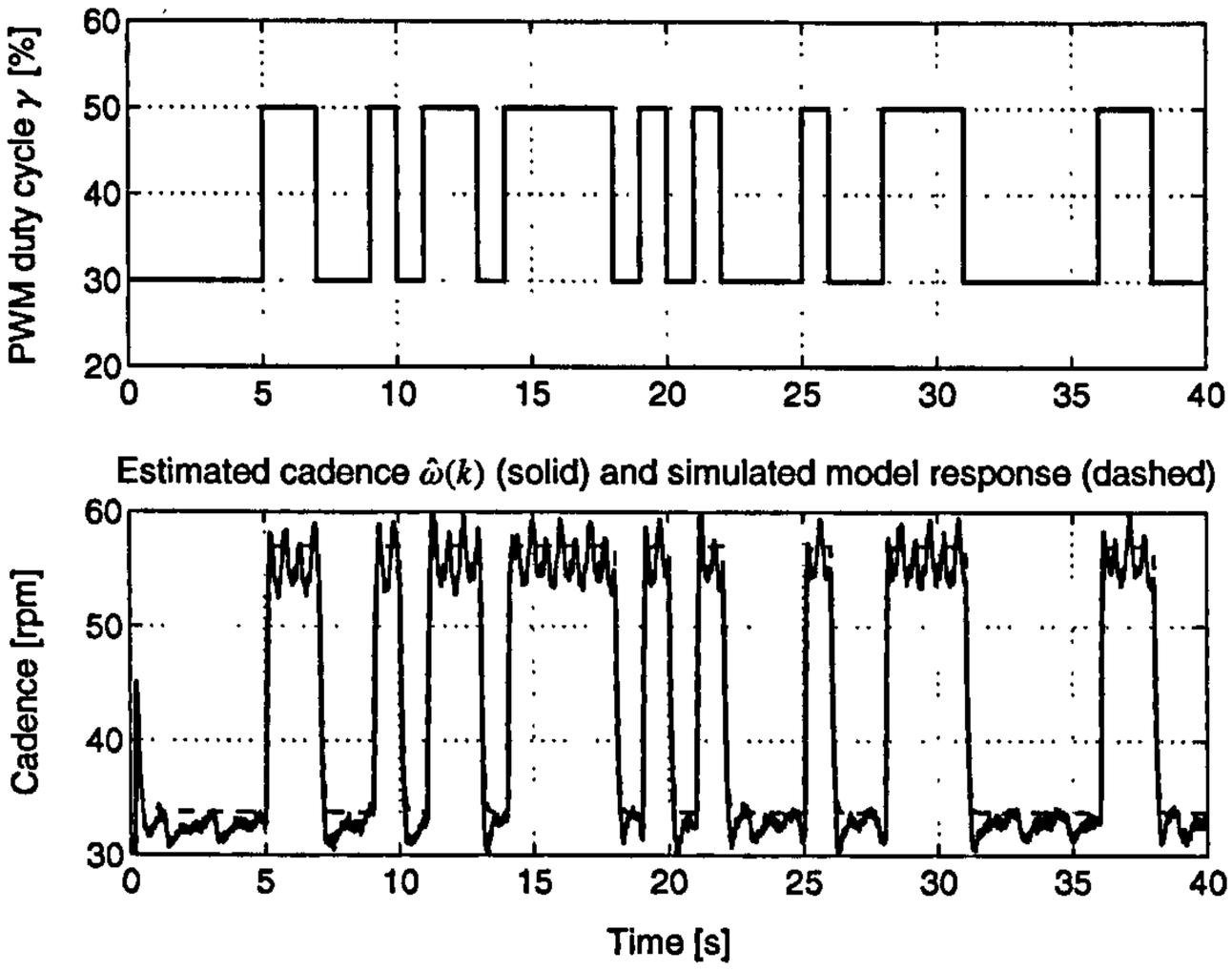

Figure 5.24: Motor identification data.

$k_r = 0.2$ were used. These design parameters give a good tradeoff between sufficient disturbance rejection and noise sensitivity. The main frequencies of the periodic disturbance for a cadence of 40 rpm are 4.18 rad/s (cadence) and 8.36 rad/s (twice the cadence). Disturbances at these frequencies are sufficiently attenuated by using the plug-in repetitive controller.

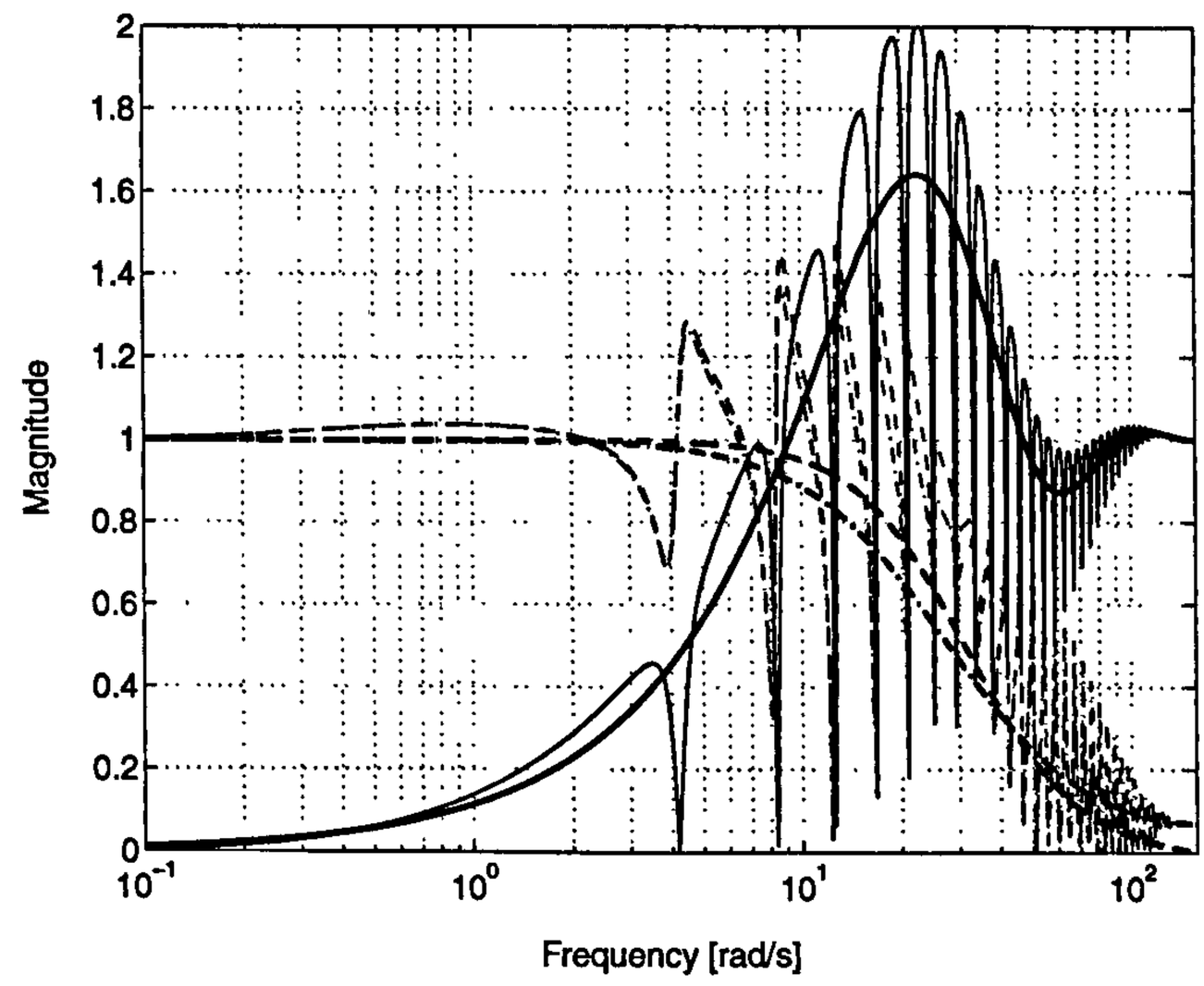

Figure 5.25: Frequency responses of the output sensitivity function S (solid), complementary output sensitivity function T (dashed) and reference model H_r (dash-dotted) for the customised cadence control. Thin lines indicate the controller design with plug-in repetitive controller, and bold lines represent the design without plug-in repetitive controller.

Results of Test C

The results of Test C are presented in Figure 5.26. The upper graph shows the cadence estimate (solid line) and reference (dashed line). The time instant when the repetitive controller is switched on is indicated by a dash-dotted vertical line. Initially, the plug-in repetitive controller is deactivated. The second subplot shows the control signal u. The active drive torque and the applied pulsewidth are shown in the lower two subplots. There was an increase in pulsewidth after 70 s to investigate the behaviour of the plug-in repetitive control with respect to a change in the periodic disturbance. Stimulation parameters are equivalent to the settings given in Table 5.6, but with zero current amplitudes, i.e. no stimulation, for the hamstrings.

5.7.4 Conclusions

The experimental results with the intact subject show that the proposed control approach performs reliably, and according to the design formulations. Rejection of periodic moment disturbances can be achieved by means of the plug-in repetitive controller. When switching the plug-in repetitive controller on, absorption of the disturbances takes place within 6 cycles. After a change in the disturbance, due to an altered stimulation intensity the repetitive controller needs a very short time to adapt to the new situation. The designed controller possesses a sufficiently large stability margin ($s_m = 2$), and is robust enough to function for different cyclists. A redesign for a new cyclist is not absolutely necessary.

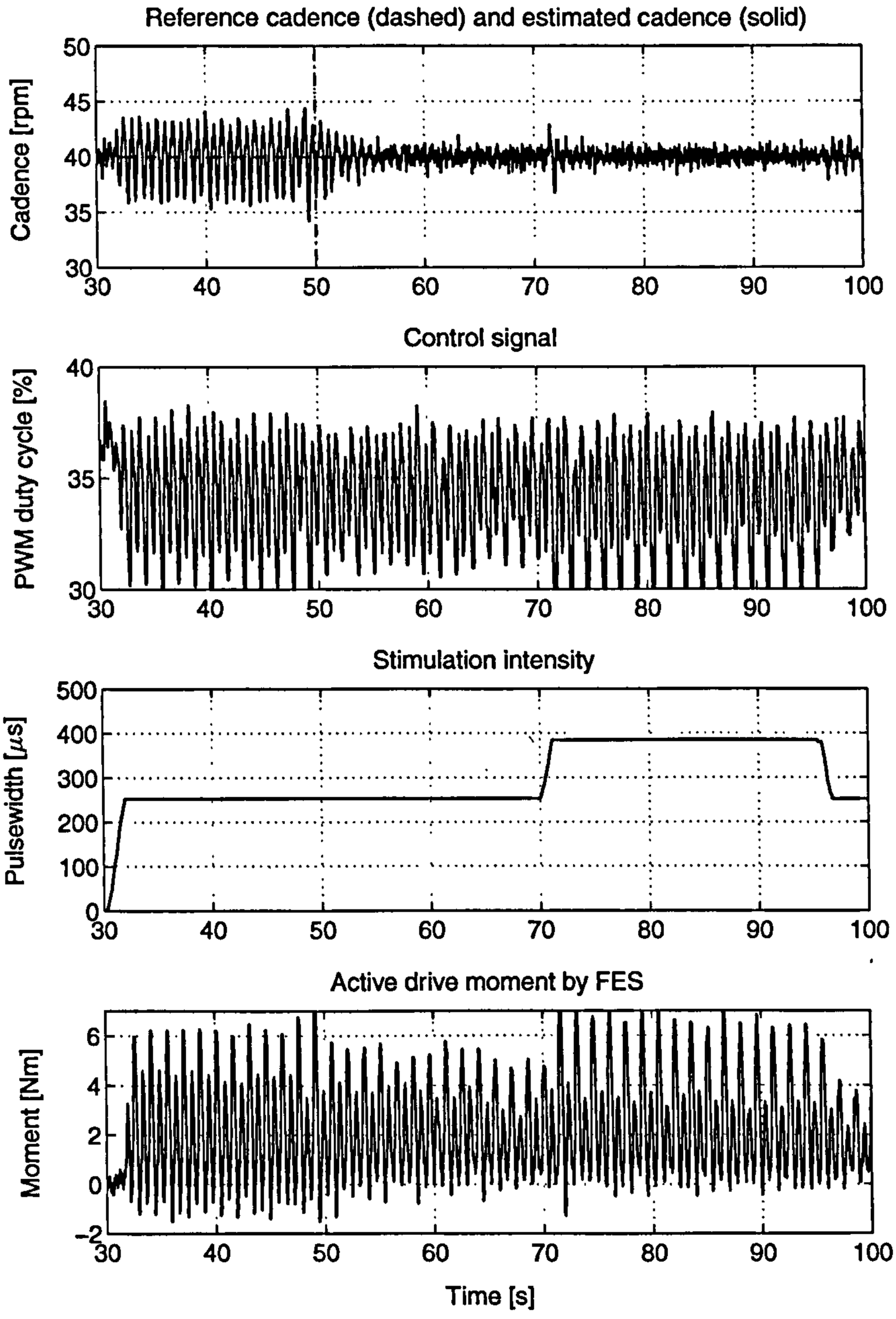

Figure 5.26: Test of the customised cadence control (Test C). The plug-in repetitive controller is initially deactivated. The dash-dotted vertical line indicates the time instant when the plug-in controller is switched on.

5.8 Summary and Conclusions

FES cycling can be established in conjunction with a commercially available ergometer. No modifications are necessary to use the ergometer. Required signals for the FES cycling algorithms can be estimated by an extended Kalman filter which is driven by the internal ergometer signals provided by serial communication. A detailed calibration procedure is given for the motor moment and several ergometer settings. Isokinetic and isotonic cycling exercises can be realised with help of the DC motor inside the ergometer. The cadence control can be improved by a customised cadence controller. However, in this case the ergometer has to be instrumented with an additional, more accurate angle sensor. The 8 channel stimulator employed was newly developed in cooperation with a biomedical company. The stimulation timing was improved allowing a faster reaction to the crank angle measurement (estimate) and easy use/generation of variable frequency trains. This opens the road to further research on the use of variable frequency trains in FES cycling. The feasibility of the developed system for FES cycling has been proven in experiments. Future work will involve tests with paraplegics. The simpler setup consisting of stimulator and ergometer only is basically ready for everyday clinical use where exact calibration and stimulation timing are not so critical.

6 Work Rate Control in FES Lower-Limb Cycle Ergometry

6.1 Summary

Aim: The aim was to investigate closed-loop control of the cyclist's work rate in FES cycling. A well controlled work rate is important to realise a prescribed training regime and for exercise testing.

Methods: Work rate (power) is defined as the product of cadence and active drive torque produced by the cyclist at the crank.
When using isotonic cycling ergometers, the cadence is controlled at a constant level by adjusting the stimulation intensity of the FES activated musculature. A desired work rate is then realised by applying an appropriate resistance (load) at the crank. Under steady state conditions the active drive torque at the crank counterbalances the resistive load at the crank. For the cadence control problem, an analytical controller design based on a linear model of the stimulation intensity–cadence dynamics which are identified off-line, is proposed in this chapter.
During isokinetic cycling, cadence is kept constant by the training device (motor controlled), and the active drive torque has to be controlled by adjusting the electrical stimulation of the leg musculature in order to achieve a desired work rate. The averaged active crank torque over one cycle is controlled by a self-tuning controller which adjusts the stimulation intensity. The reference torque is calculated from the desired power and the given constant cadence. Controller parameters are determined online on the basis of a recursively estimated model which describes the relationship between the stimulation and torque.

Results: The feasibility of the new feedback control methods has been proven in experiments. Accurate work rate control can be achieved by application of the developed feedback control methods. For the isotonic case, the smallest achievable work rate by the cyclist is technically determined by the crank torque required to passively turn the legs at the smallest adjustable cycling resistance (unbraked system). For many SCI subjects, the magnitude of this work rate will be a substantial fraction of their maximal exercise capacity. In contrast to this, work rate control in isokinetic cycling devices extends the lower range of realisable work rates towards 0 W.

Conclusions: Work rate control with isokinetic cycling ergometers shows several advantages compared to work rate control with isotonic cycling ergometers. Firstly, the full work rate range starting from 0 W can be realised. Furthermore, self-tuning control of the active drive moment for isokinetic cycling ergometers yields a subject specific controller without the need of a labour-intensive off-line system identification as required for the cadence control in the isotonic case.

Contribution: The author developed the methods, and implemented the experimental software. Furthermore, the author planned and ran the experiments. Parts of this work are published in [43, 82, 84].

6.2 Introduction

The control of work rate is essential in studies focusing on the effect of FES cycling exercise on cardiopulmonary fitness. To achieve a desired work rate, it is crucial that both cadence and active crank torque are well controlled. Failure to do so would represent a serious methodological weakness in FES exercise testing studies.

Isotonic exercise devices. Most previous studies have utilised stationary FES cycling ergometers with a large flywheel where only an isotonic cycling exercise can be performed. With such devices, the resistance at the flywheel is set to specify the desired work rate while a control algorithm attempts to maintain a target cadence of 50 rpm. The desired power can be established until fatigue develops and the stimulation level reaches its maximal value. In this case, the cadence is allowed to drop as low as 35 rpm before the resistive load is reduced in an attempt to increase cadence. The use of simple integral control for feedback regulation of cadence is possible, as the stimulation intensity–cadence dynamics is relatively slow because of the large moment of inertia introduced by the flywheel.

The cadence control problem becomes more challenging if the moment of inertia at the crank is small. The open loop system bandwidth increases and disturbances influence the cycling cadence consequently faster. A controller has to react quicker but must be still insensitive to measurement noise. Only one other research group [12, 13] has previously developed closed-loop controllers for control of cycling cadence in an isotonic FES cycling system without a flywheel. In [12] a fixed parameter PID controller is developed which is based upon a system designed for feedback control of knee angle in response to quadriceps stimulation. A nonlinear fuzzy-logic controller is presented in [13]. Both of these approaches lead to fixed non-model-based controllers which are difficult to adapt to take account of inter-subject variability.

A serious problem in isotonic cycling is that the cyclist has to produce a drive torque which entirely counterbalances the resistance (load) at the crank at a constant cadence in order to pedal. The smallest possible work rate is therefore determined by the smallest realisable resistance at the crank (usually unbraked flywheel) and the established cadence (usually 50 rpm). The minimal resistance depends on

the internal system friction and on the subject. An increased muscle tone and passive joint moments contribute to this resistance as well. A realistic range for the smallest possible work rate is 5 to 10 W. Power output for isotonic training devices is often incorrectly defined as increase of work rate above the minimal possible work rate. "Zero" power in isotonic ergometer systems is then defined by the amount of power required to passively turn the legs and the unbraked flywheel at a given cadence.

Isokinetic exercise devices provide a number of benefits with respect to work rate control. The motor assists the cycling so that cycling at true zero work rate is possible for the subject. At zero work rate, the legs are solely turned by the motor. Before active cycling by means of FES starts, the passive crank torques can be measured and approximately described as a function of the crank angle. Subtraction of the passive torque from the measured crank torque gives the active drive torque during the FES cycling. The work rate is then obtained as the product of active drive torque and angular velocity at the crank. Since the cadence is constant, the other variable, active drive torque, must be controlled by adjusting the stimulation intensity in order to obtain a desired work rate. The feasibility of this strategy has been experimentally proven in [26] and [46]. Hunt et al. [46] used an approach based on system identification and analytical feedback design. To obtain a controller which is optimally tuned for a specific subject, the system identification and control design procedures have to be carried out at the start of each experimental session.

Figure 6.1 illustrates the work rate control strategies for isotonic and isokinetic training devices. During operation of isotonic training devices, cadence is normally kept constant by a control algorithm that adjusts the stimulation intensity. The reference resistance (load) is determined from the reference work rate and the selected constant cadence. As the desired work rate is usually piecewise constant, the same is true for the resistance. The resistance is adjusted open-loop on the flywheel or through an electromagnetic brake. Closed-loop control of resistance is applied when an electric motor is used to brake the pedalling.

In the case of isokinetic cycling, a control algorithm attempts to keep the cadence constant by means of an electric motor. The desired work rate is defined via the active (muscularly produced) crank torque when the cadence is constant. The active crank torque is closed-loop controlled with the stimulation intensity as control signal.

A new feedback control method for the cadence control in isotonic training devices is introduced in Section 6.3. It is assumed that the resistance (load) at the crank is well controlled. Self-tuning control of the FES induced crank torque for isokinetic cycling is studied in Section 6.4 under the assumption that cadence is well controlled by the motor. The stimulation intensity is in both cases modulated by the pulsewidth which is the same for all stimulated muscles.

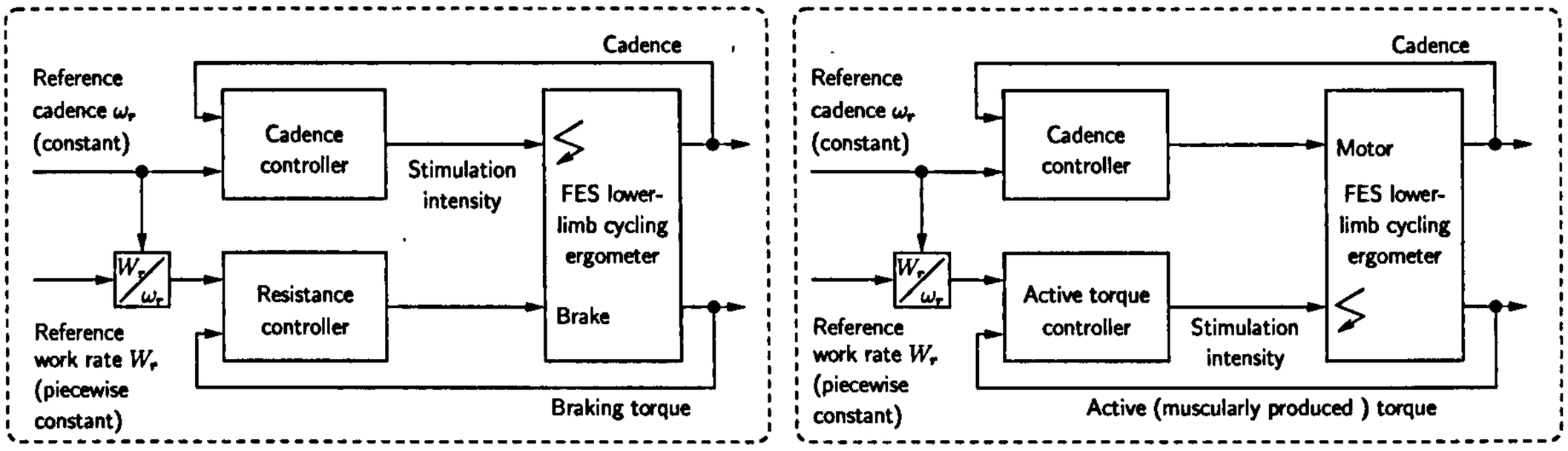

Figure 6.1: Work rate control for isokinetic and isotonic cycling ergometers.

6.3 Isotonic Training: Cadence Control via FES

In this section, a new method for the control of cadence on an isotonic cycling ergometer is introduced. This control problem represents an important sub control problem of the work rate control for isotonic cycling ergometers.

6.3.1 Methods

For the cadence control, an analytical controller design is proposed based on a linear model. The model is identified from experimental data and describes the relationship between the stimulation intensity (pulsewidth) and the cadence for a specified constant resistance at the crank. In the identification experiment, the leg muscles are stimulated by a pulsewidth signal in the form of a Pseudo-Random Binary Sequence (PRBS), and the corresponding cadence is measured. An ARMAX-type model (see Section 2.2) is estimated from the recorded input/output data using prediction error methods. The identification procedure provides the polynomials $\mathsf{A}(q^{-1})$, $\mathsf{B}(q^{-1})$ and $\mathsf{C}(q^{-1})$ as well as the input/output delay n_k. Typically the dynamics obtained are first order and stable. Using a sampling time of T_s=50 ms, an input/output delay n_k of 3 sampling steps is observable.
The generic controller design of Section 2.3 is then applied to the cadence model, subject to the following conditions:

- The controlled output $y(k)$ is the cadence $\omega(k)$.
- The control signal $u(k)$ is the stimulation intensity (pulsewidth).
- The reference signal $r(k)$ is the desired cadence.

Linear Quadric Gaussian (LQG) controller design is used to determine the controller parameters while the identified polynomial $\mathsf{C}(q^{-1})$ (part of the noise transfer function) is not used for the controller design. Instead, a new polynomial $\mathsf{C}(q^{-1})$ is chosen in order to place the observer poles as outlined

in Section 2.3.6. No poles and zeros are cancelled by the controller. Integral action is included in the controller, i.e. $\overline{\mathsf{R}}_d = 1 - q^{-1}$. In Section 4.6.2 it was shown that the resulting cadence in FES cycling has intra-cycle variations. These variations consist mainly of two frequency components which correspond to the cadence and two times the cadence. The plant gain is low at these frequencies so that a large control effort would be required to eliminate these variations by a cadence controller. The closed-loop sensitivity to measurement noise would also increase when increasing the bandwidth to eliminate these intra-cycle variations. For these reasons, cancellation of these variations was not considered in the controller design. Instead of this, the controller is determined in such a way, that the intra-cycle speed variations do not unnecessarily excite the control signal (pulsewidth). This can be approximately achieved, for a constant reference cadence ω_r, by choosing the controller polynomial $\overline{\mathsf{S}}_d$ as follows

$$\overline{\mathsf{S}}_d = 1 - 2\cos(\omega_r T_s)q^{-1} + q^{-2}. \tag{6.1}$$

The intra-cycle variations are here treated approximately as a sinusoidal disturbance with a frequency equivalent to the cadence.

Taking this controller configuration, the degree estimate for the characteristic polynomial factor C by using Equation (2.48) is

$$\deg \mathsf{C} \leq 2.$$

Complete separation of command and disturbance response is selected in the controller design process. One tuning parameter of the controller is the weight ρ. In addition, two second order polynomials $\mathsf{C}(q^{-1})$ and $\mathsf{A}_r(q^{-1})$ have to be chosen, specified by the rise times t_r^{C} and $t_r^{\mathsf{A}_r}$. The characteristic polynomial of the windup observer is equated with the Hurwitz spectral factor $\mathsf{D}_c(q^{-1})$ which is defined by the spectral factorisation within the LQG design process.

6.3.2 Subjects

The new approach was experimentally tested with two paraplegic subjects. Both subjects participated in the pilot study on FES cycling which is described in Chapter 4. Details of the two subjects (S1 and S2) are given in Table 4.1.

6.3.3 Experimental Procedure

The cadence control approach was tested with the FES tricycle I which was mounted on a cycle trainer. The device and setup is described in detail in Section 4.4. The experimental procedure for identification and control design consists of the following steps:

- **Open-loop Pseudo-Random Binary Sequence (PRBS) test:** A stimulation intensity signal of PRBS form is applied in open loop for a specified constant resistance (load). The PRBS has

a specified mean level (usually close to the midrange of the input signal) and amplitude. The resulting cadence is measured.

- **Model identification:** A linear dynamic (transfer function) model (ARMAX) is fitted to the input–output (pulsewidth–cadence) data using prediction error methods. A range of model orders can be tested and models compared and validated.

- **Control design:** The validated model is used to design the feedback controller for cadence. LQG design is used, with specified control weight ρ and rise times t_r^C and $t_r^{A_r}$.

In order to test the efficacy of the cadence strategy, two separate feedback-control tests are defined.

1. **Test CT:** Cadence tracking control. This is a closed-loop test of cycle cadence tracking. During this test, the resistance at the crank is kept constant, but the reference cadence is subject to step changes.

2. **Test DR:** Disturbance rejection. During this test, the reference value for cycle cadence is kept constant. The resistance acting at the drive wheel is then varied to investigate the effect of resistances changes on the cadence control.

The subjects sit normally on the tricycle with legs attached to the pedal orthoses during all the tests.

6.3.4 Experimental Results

Exemplary, experimental results with the paraplegic subject S1 are represented. All results are from the same experimental session. The stimulation parameters used for subject S1 are summarised in Table 6.1.

Table 6.1: Stimulation settings for the subject S1 during for the cadence control (stimulation frequency of 20 Hz).

Muscle	Stimulation interval [degrees]	Current [mA]	Muscle activation and relaxation delay [ms]
Right quadriceps	55–155	90	150
Left quadriceps	235–335	80	150
Right hamstring	190–265	80	150
Left hamstring	10–85	90	150
Right gluteus	90–180	70	150
Left gluteus	270–0	80	150

Results of Test PRBS and the Model Identification

Results of Test PRBS are shown in Figure 6.2. On the lower axis, the input signal (stimulation intensity) is shown. The measured cadence (solid line) is plotted in the upper graph together with

Table 6.2: Identified pulsewidth-cadence models for subject S1 and S2 (sample time T_s=50 ms).

	Subject S1	Subject S2
$H_d(q^{-1})$	$\frac{0.0035q^{-3}}{1-0.985q^{-1}}$	$\frac{0.0039q^{-3}}{1-0.968q^{-1}}$
Rise time	7.29 s	4.38 s
DC gain	0.23 $\frac{\text{rpm}}{\mu\text{s}}$	0.12 $\frac{\text{rpm}}{\mu\text{s}}$

simulated output (dashed line) of the estimated model. The simulated model response describes only the deterministic system behaviour. A high-frequency ripple is clearly visible in the measured output. These cadence variations are caused by the gravity of the legs are are therefore not captured by the identified input transfer function model. Furthermore, some muscle fatigue is observable in the PRBS Test which results in a slow but steady decline of the measured cadence. This trend in the cadence has been removed before identification of the ARMAX model.

Table 6.2 gives information about the identified pulsewidth–cadence models for both subjects. The model for subject S2 is included for comparison. Rise time and DC gain vary significantly between the subjects.

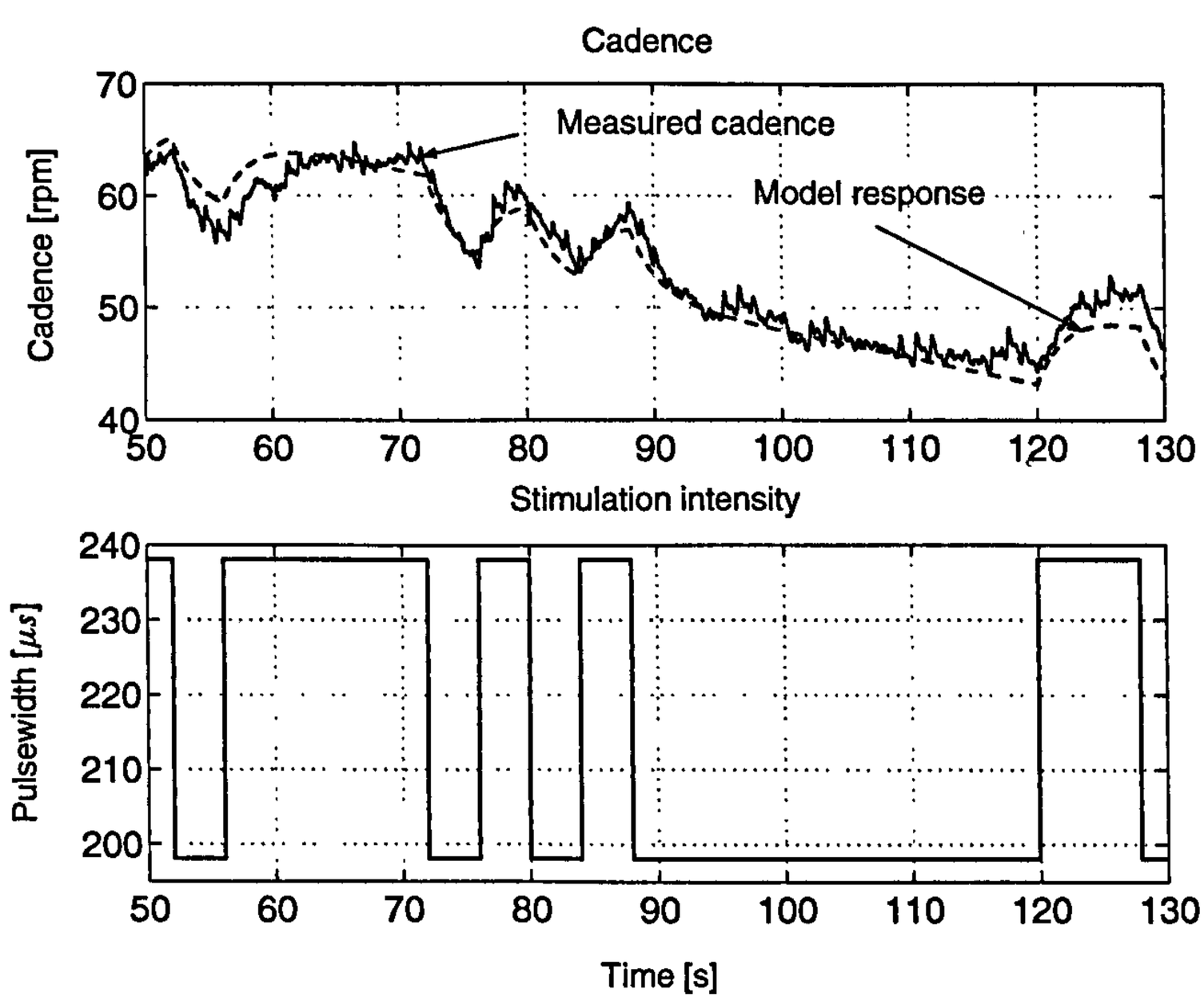

Figure 6.2: Cadence identification data (result of Test PRBS).

Results of the Controller Design

The identified model was used to compute a feedback controller for cycle cadence. The result of the controller design for subject S1 is illustrated in form of the closed-loop frequency responses in Figure 6.3. The responses of the output sensitivity function S (dotted line), the complementary output sensitivity function T (solid line), and the reference model H_r (dash-dotted line) are shown. Additionally to this, the frequency response of the transfer function from an output disturbance to the control signal is plotted as a dashed line (normalised by the factor 7). The rise times $t_r^{\mathsf{C}} = 1\,\mathrm{s}$ and $t_r^{\mathsf{A}_r} = 2\,\mathrm{s}$ as well as the weight $\rho = 0.1$ were used. These design parameters give a good tradeoff between sufficient disturbance rejection and noise sensitivity. The main frequency of the intra-cycle cadence variations for a cadence of 50 rpm is 5.27 rad/s. Figure 6.3 shows that disturbances at this frequency pass unaltered to the output and do not unnecessarily excite the control signal.

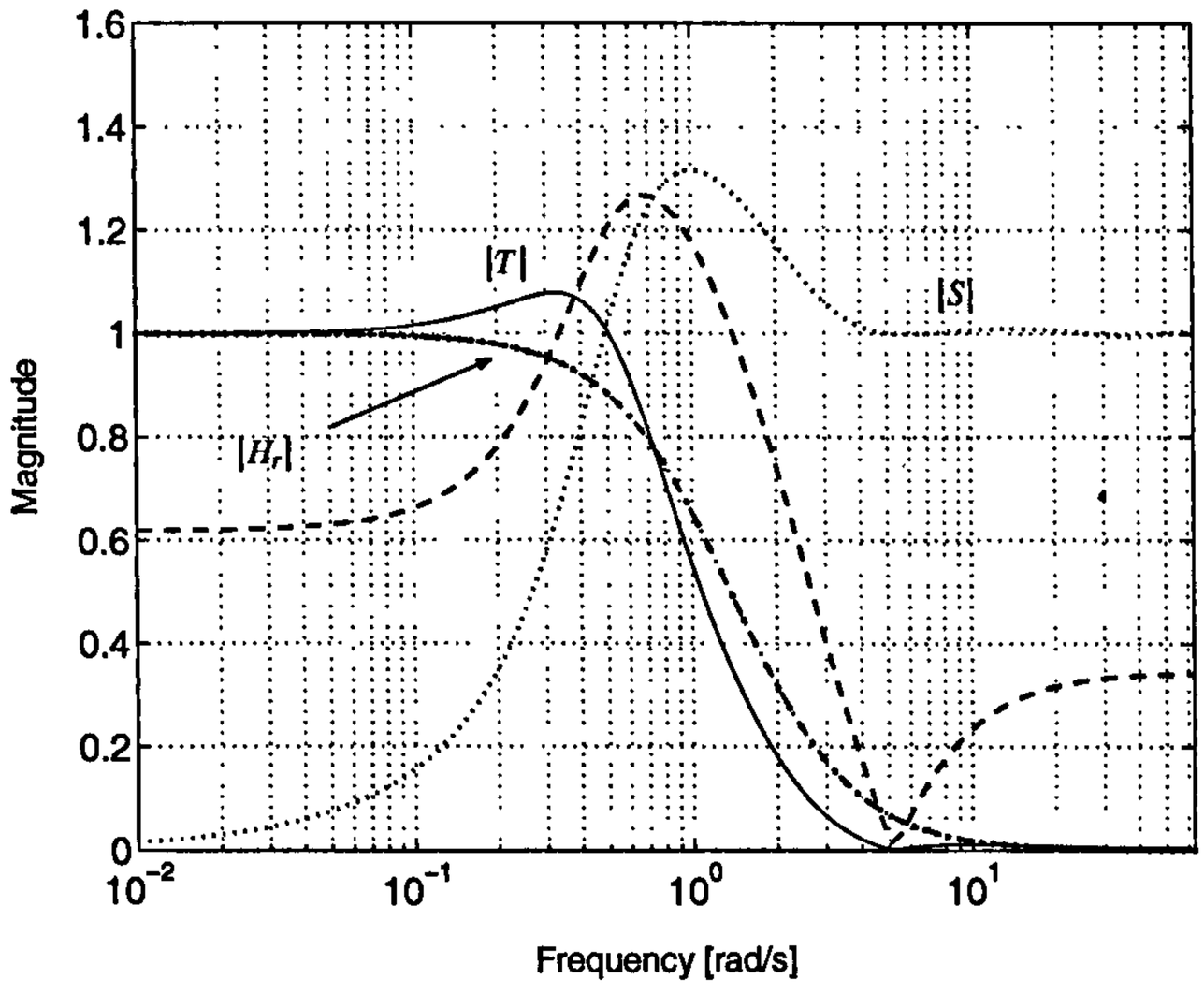

Figure 6.3: Frequency responses of the output sensitivity function S (dotted), complementary output sensitivity function T (solid) and reference model H_r (dash-dotted) for the cadence controller. The frequency response of the transfer function from an output disturbance to the control signal is plotted as a dashed line (normalised by the factor 7).

Results of Test CT

Results of Test CT are presented in Figure 6.4. The upper graph shows the cadence, both measured (solid line) and reference (dashed line). The lower part of the figure shows the control signal u. During this test the reference signal for cadence is changed in steps between 40 and 60 rpm.

Results of Test DR

A closed-loop disturbance rejection test is shown in Figure 6.5. Here, the desired speed is constant at 50 rpm. The nominal resistance (used for system identification) is applied during the periods indicated by the grey solid bars. Increased resistance is added to the trikes drive wheel during the period indicated by the dashed black bar in the graph whereas a reduced resistance was present during the period indicated by the solid black bar. Despite these load changes, the cadence is maintained close to its desired, constant value.

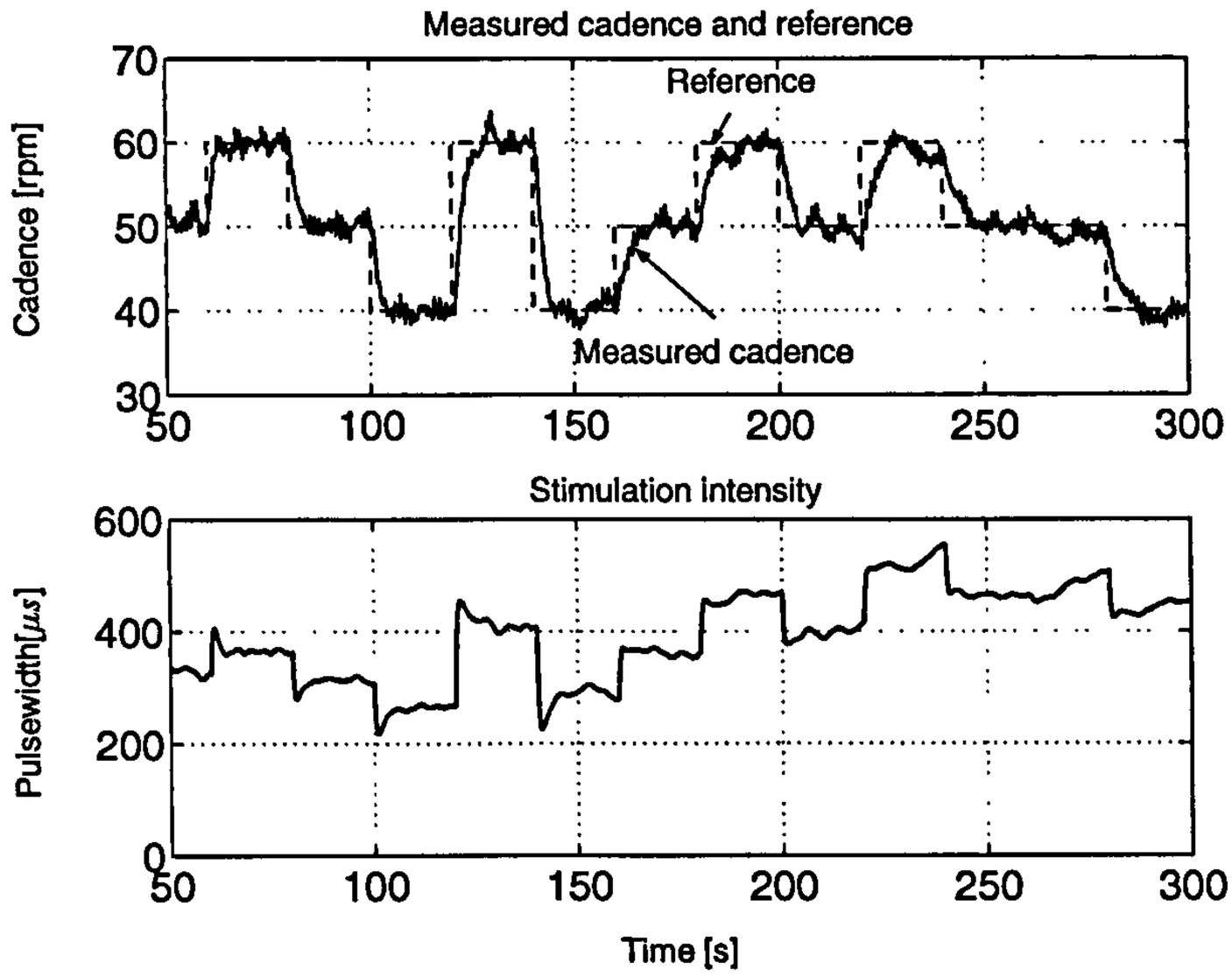

Figure 6.4: Closed-loop tracking test for the cadence control during isotonic cycling.

6.3.5 Discussion and Conclusions

It was found that a linear transfer function was sufficient for good approximation of the relationship between stimulation intensity and cadence. It can be seen that the model captures the dominant dynamic response of the cadence. For the purposes of control design, it is not necessary for the model to capture the high-frequency gravitational effects of the legs acting on the pedals since it is not desirable for the controller to try to counteract these effects. Instead, the design has to ensure that the high-frequency ripple in the cadence does not excite the control signal in the case of a closed-loop bandwidth close to these frequencies.

The disturbance test shows that the controller is able to reject disturbances sufficiently fast. Cadence can be well controlled in the range of 40 to 60 rpm. This allows to select an optimal operation condition for the cyclist. Both controller tests show a gradual increase in stimulation intensity due to the fatigue of the electrically stimulated muscles that is successfully compensated by the controller.

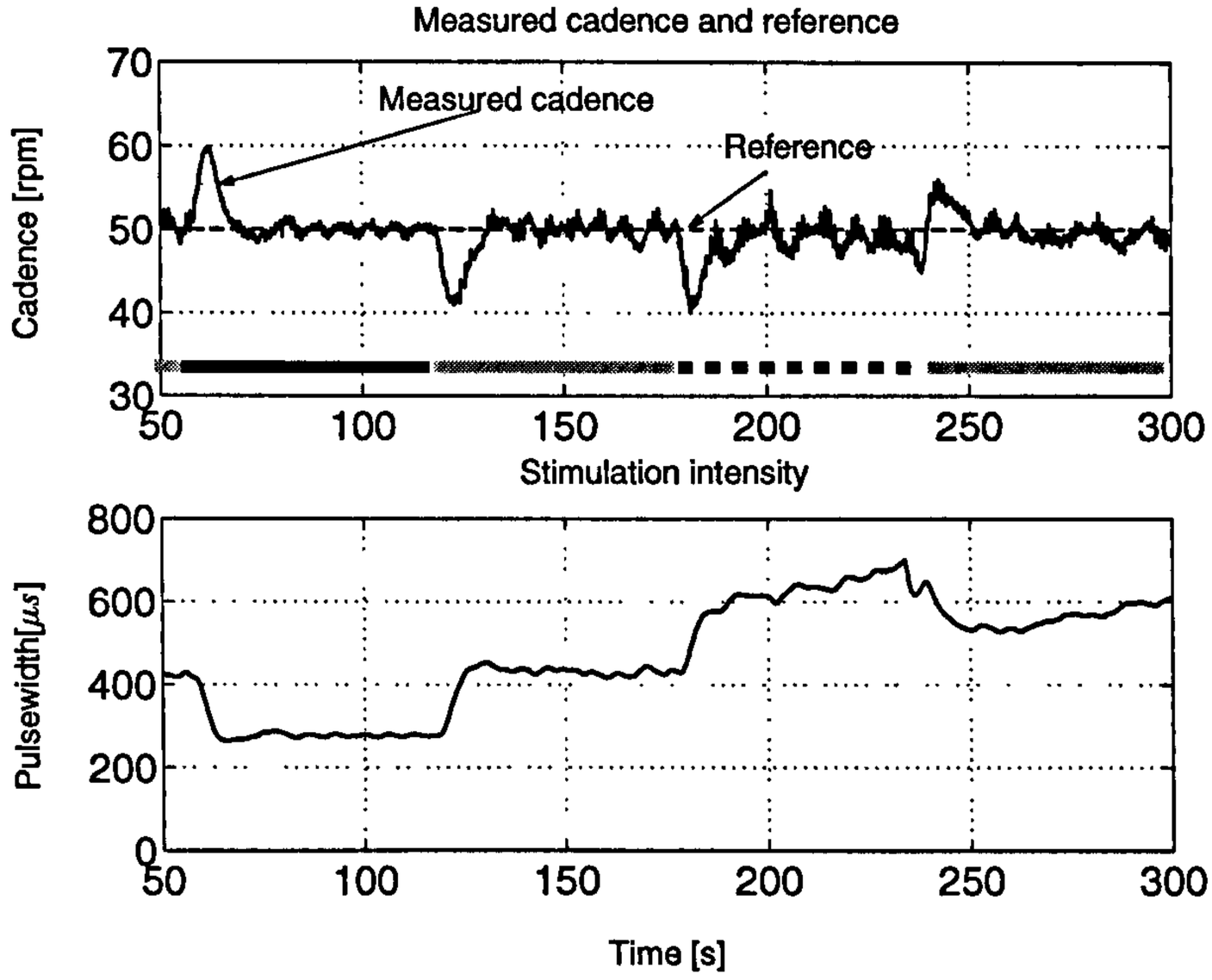

Figure 6.5: Closed-loop disturbance rejection test for the cadence control during isotonic cycling. (grey bar - period of nominal resistance, black bar - period of reduced resistance, dashed black bar - period of increased resistance).

Thus, the feasibility of this new methodology for the design of automatic speed controllers for FES cycling has been shown in preliminary experiments with paraplegic subjects. The approach is simple and can be applied rapidly to each cyclist at the start of an exercise session. This brings the advantage that the controller is tuned to each individual to ensure that the best feedback control performance is achieved. Further work is needed to quantify the variability of muscle dynamics between subjects and the day to day variations. Issues of robustness in the controller design have to be investigated. The significant differences in the identified models (see Table 6.2) for the two subjects indicate that robust control can only be achieved at the cost of reducing the general controller performance. Differences in the models are clearly reflected in DC gain and rise time.

6.4 Isokinetic Training: Self-Tuning Moment Control via FES

Control of the active crank moment produced by the muscles for isokinetic cycling ergometers is treated in this section. It is assumed that the cadence is well controlled by the motor, and that the frequency ranges of cadence control and torque control are well separated. Typically, the cadence control loop has a significantly larger bandwidth than the torque control loop. As a result, the two design problems can be separated.

6.4.1 Methods

As already mentioned several times, the work rate $W(t)$ is defined as the product of cadence ω and active drive torque m_A produced by the muscles at the crank:

$$W(t) = \omega(t) \cdot m_A(t). \tag{6.2}$$

For a given reference work rate $W_r(t)$ and a constant cadence $\omega(t) = \omega_r$, it is straightforward to calculate the reference for the active crank torque by

$$m_{A_r}(t) = W_r(t)/\omega_r. \tag{6.3}$$

Due to the limited bandwidth of the electrically stimulated muscles and the crude stimulation pattern it is not practicable to aim at realising $m_{A_r}(t)$ exactly by feedback controlled electrical stimulation. A more sensible aim is to control the average active crank torque over one crank cycle. This leads to the time-discrete controlled variable $y(k)$ defined by

$$y(k) \;=\; 1/T_s^\omega \int_{t=(k-1)T_s^\omega}^{kT_s^\omega} m_A(t)\,\mathrm{d}\,t, \quad k \in \mathbb{Z}. \tag{6.4}$$

where $T_s^\omega = 1/\omega_r$ is the sampling time and k is the sample index (crank cycle index). The reference r for this variable may be obtained by sampling $m_{A_r}(t)$:

$$r(k) \;=\; m_{A_r}(t = kT_s^\omega). \tag{6.5}$$

The sampling of the reference and the calculation of the average active drive torque are performed at a specified crank angle which is the same for every crank cycle. In this work, the zero crank angle is used.

The control signal $u(k)$ is the stimulation intensity which is modulated by the pulsewidth (same pulsewidth for all stimulated muscles). Over one crank cycle, the pulsewidth is kept constant. The pulsewidth signal is limited to the interval $[\underline{u}, \overline{u}]$. The lower bound $\underline{u}$ represents the minimal pulsewidth required to produce a measurable active crank torque. Physiologically, $\underline{u}$ is the stimulation threshold for releasing action potentials in the stimulated lower motor neurons. The upper bound $\overline{u}$ is either technically caused by the stimulator device or is the pulsewidth at which the maximal number of motor units is recruited and no force increase can be achieved by an increase in the stimulation intensity.

Model of Stimulation Intensity – Active Drive Torque Dynamics

A change of the pulsewidth at the sample instant $t = k/\omega_r$ has a direct impact on the next crank cycle. For the non-saturated pulsewidth, a simple linear model where the torque is proportional to the stimulation intensity can be postulated for the system behaviour:

$$y(k) = bq^{-1}(u(k) - \underline{u}) + x(k) = bq^{-1}u(k) - b\underline{u} + x(k). \tag{6.6}$$

Here, b is the system gain, $x(k)$ is white measurement noise, and q^{-1} is the delay operator. The system gain b is subject-specific and also depends on daily changing factors such as the electrode positions. The gain can be assumed to be slowy time-varying during a session of FES cycling. Muscle fatigue has an influence on the torque generation capability of the cyclist but evolves slowly compared to the system dynamics. The second model parameter $\underline{u}$ is time-invariant and can be experimentally identified. For this, the stimulation intensity is gradually increased and the lowest pulsewidth at which an active torque is produced by the stimulated muscles is recorded by the experimenter as bound $\underline{u}$.

Online Estimation of the System Gain

With the known lower bound $\underline{u}$, the system gain b can be estimated online by means of *Recursive Least Squares* (RLS) with forgetting factor [5]:

$$\hat{b}(k) = \hat{b}(k-1) + K(k)(y(k) - \hat{b}(k-1)(u(k-1) - \underline{u})) \tag{6.7}$$

$$K(k) = \frac{P(k-1)(u(k-1) - \underline{u})}{(\lambda + (u(k-1) - \underline{u})^2 P(k-1))} \tag{6.8}$$

$$P(k) = (1 - K(k)(u(k-1) - \underline{u})P(k-1)/\lambda. \tag{6.9}$$

In the equations above, $K(k)$ is the adaptation gain, $P(k)$ is variance of the estimation error, λ is the forgetting factor, and $\hat{b}(k)$ is the estimated gain. Tuning parameters of the RLS algorithm are the initial variance $P(0)$ of the estimation error, the initial estimate $\hat{b}(0)$ and the forgetting factor λ. The estimation of the system gain relies on input/output data (the pulsewidth u and the averaged active crank torque y) which are acquired online.

Self-Tuning Controller

On the basis of the online estimated system model, a two degree of freedom controller as introduced in Section 2.3 can be adapted at every sampling instant to the currently estimated plant model. The time-variant input transfer function of the model is given by

$$H_p(q^{-1}, k) = \frac{q^{-n_k}\mathsf{B}(q^{-1}, k)}{\mathsf{A}(q^{-1}, k)} u(k) = q^{-1}\hat{b}(k)u(k) \tag{6.10}$$

with $\mathsf{B}(q^{-1}, k) = \hat{b}(k) > 0$ and $\mathsf{A}(q^{-1}, k) = 1$. The controller is determined at every sampling instant by the procedure outlined in the Sections 2.3 and 2.5, using the pole-placement method. This gives the time-variant controller polynomials $\mathsf{R}(q^{-1}, k)$, $\mathsf{S}(q^{-1}, k)$ and $\mathsf{T}(q^{-1}, k)$ of the RST-controller.

Integral action is included in the controller, i.e. $\overline{\mathsf{R}}_d = 1 - q^{-1}$. This is required to compensate constant or slowly varying disturbances such as muscle fatigue. The offset term $-b\underline{u}$ of the model (6.6) represents in this sense a constant disturbance. Dependent on the chosen forgetting factor λ, both the controller integrator and the RLS algorithm can both react to a change in the system gain

caused by muscle fatigue. To avoid this dangerous competition, it is advisable to choose a small bandwidth for the parameter estimation loop, selecting a forgetting factor between ($0.98 \leq \lambda < 1$). To make sure that measurement noise does not generate large signals, $\overline{\mathsf{S}}_d = 1 + q^{-1}$ was assigned. No poles and zeros are cancelled by the controller. Taking this controller configuration, the degree estimate for the characteristic polynomial factor $\overline{\mathsf{A}}_{cl}$ by using Equation (2.39) is

$$\deg \overline{\mathsf{A}}_{cl} \leq 2. \tag{6.11}$$

Incomplete separation of command and disturbance response is selected in the controller design process, and two first order polynomials $\mathsf{A}_o(q^{-1})$ and $\mathsf{A}_r(q^{-1})$ are chosen, specified by the rise times $t_r^{\mathsf{A}_r}$ and $t_r^{\mathsf{A}_o}$. For this application rise times are usually specified in crank cycles. The characteristic polynomial of the windup observer is chosen as $\mathsf{A}_o(q^{-1}) = 1$ (dead beat observer).

6.4.2 Experimental Setup

The self-tuning controller for the active crank torque has been experimentally tested by one investigator (neurologically intact, male, age of 26, body weight of 90 kg) with the motorised ergometer (see Chapter 5). The stimulation parameters are the same as reported in Table 5.6 in Chapter 5. During the experiments, the customised cadence controller (see Section 5.7) for the DC motor has been applied with a reference cadence of 40 rpm. The active crank torque induced by FES is determined by the procedure outlined in Section 5.4.4.

6.4.3 Experimental Procedure

The experimental procedure for carrying out a power controlled isokinetic FES cycling test consists of the following steps.

1. Selection of a constant cadence, which is used in the following steps.

2. **Test P: Passive crank torque estimation.** The passive crank torque is experimentally determined for the selected cadence. In this test, the legs are passively moved solely by the electric motor for one minute while crank angles and motor torque have to be recorded. A functional relation between the passive crank torque (obtained from the motor torque) and the crank angle is extracted from the stored data.

3. **Test T: Threshold identification.** The motor controls the cadence. Stimulation intensity is increased in discrete steps manually by the experimenter until a muscularly produced torque above zero can be observed at the crank. The pulsewidth at which active crank torque rises above zero corresponds to the threshold $\underline{u}$. Optionally, the test can be continued, and the pulsewidth increased further to obtain an estimate for the maximal possible active crank moment, and, consequently, maximal possible work rate.

4. **Test WRT: Work Rate Tracking Test.** This is a test to evaluate the overall work rate control with the underlying self-tuning moment controller. A work rate profile (step changes) is specified together with the two tuning parameters $t_r^{A_r}$ and $t_r^{A_o}$ for the self-tuning controller. Larger rise times give slower tracking but reduce the sensitivity of the closed-loop system with respect to measurement noise. Controller parameters may be changed online if required (e.g. to reduce noise sensitivity). The reference for the active drive torque is calculated online from the work rate profile and the specified cadence.

It is assumed that a working cadence controller is already available. Notice, that Test T and Test WRT could be run as one test. As soon as $\underline{u}$ is known, the work rate control can start.

6.4.4 Experimental Results

Figure 6.6 shows the result for Test T. The upper graph shows the applied pulsewidth which is increased in steps. In the middle graph the measured active crank torque is plotted. The lower subplot represents the static relationship between pulsewidth and active crank torque. The circles indicate the end of each constant stimulation phase. Moment and pulsewidth at these points have been used to calculated the static relationship between pulsewidth and active crank torque. A threshold value of $\underline{u} = 100\,\mu$s has been obtained from Test T.

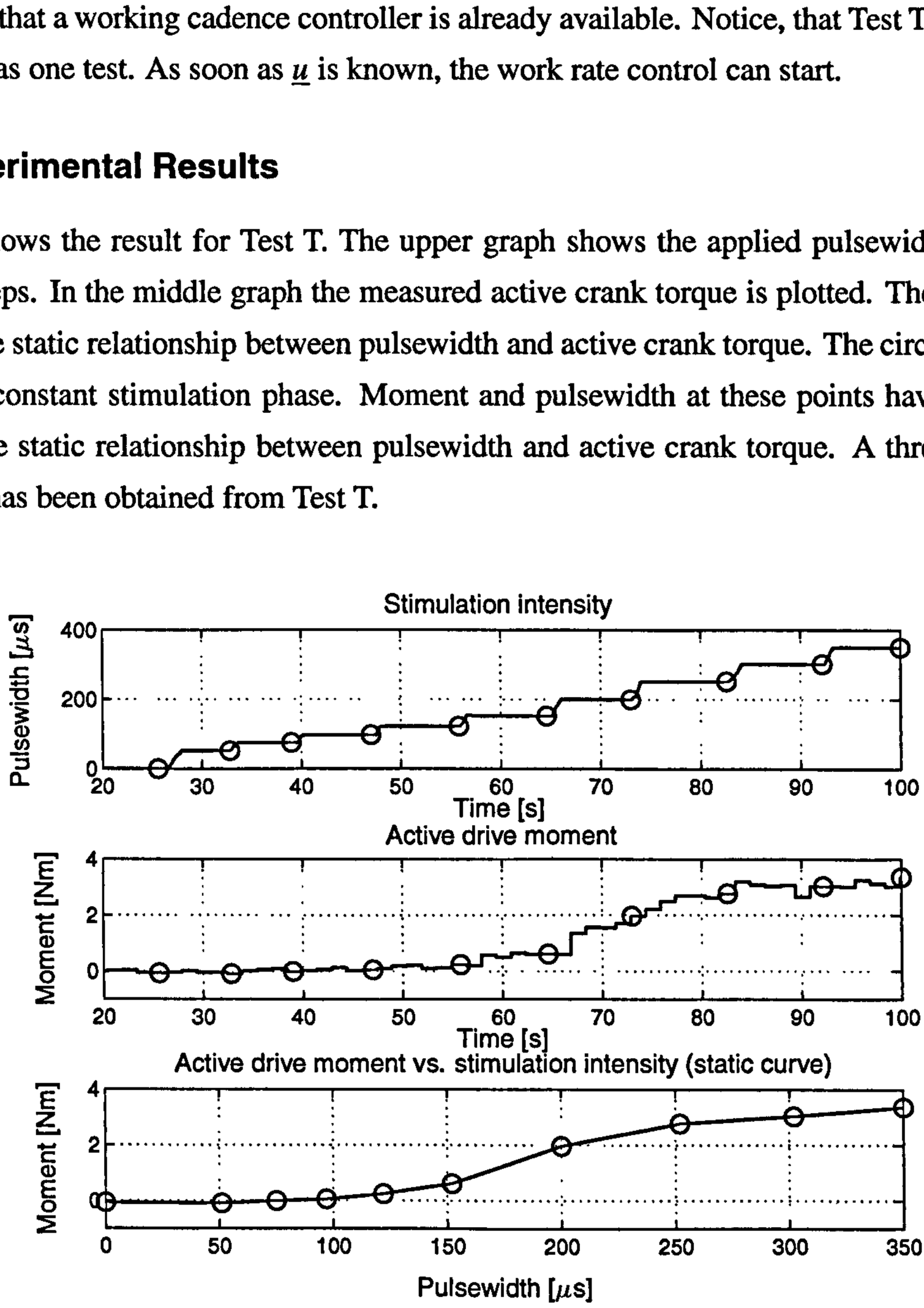

Figure 6.6: Results of Test T. Stimulation intensity is manually increased step by step and the resulting active drive torque (averages over one crank cycle) is measured. The end of each phase with constant stimulation intensity is indicated by a circle. The static moment at these time instants has been used to construct the static curve shown in the bottom graph.

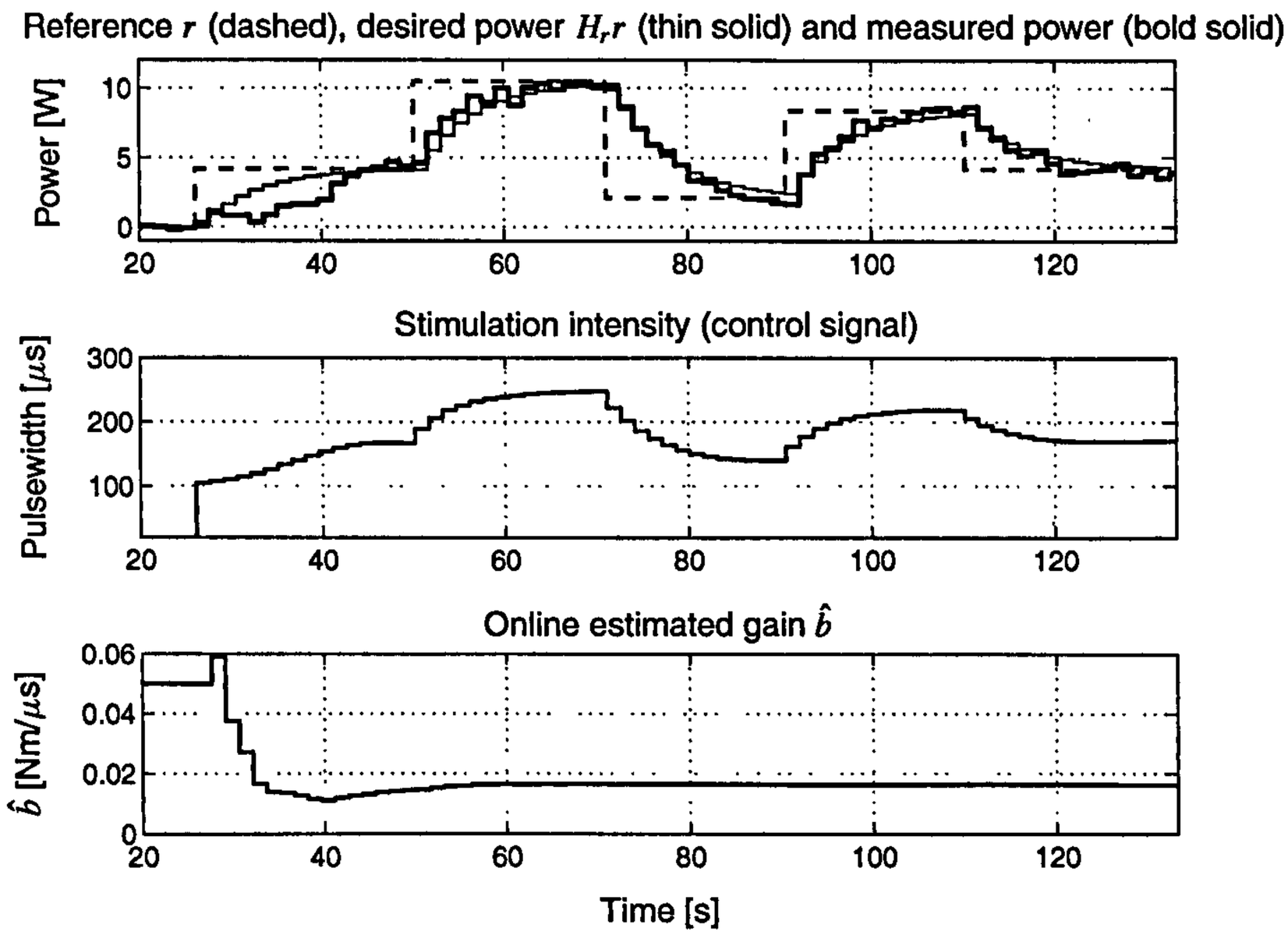

Figure 6.7: Power control test (Test WRT) for isokinetic training. Notice that the controlled power is the average over one cycle.

The results of the work rate control test are shown in Figure 6.7. The reference work rate (dashed) is plotted together with the measured power output (bold solid line). The work rate reference is changed in steps between 0 and 10.2 W. The desired power output is obtained by filtering the reference trough the reference model H_r. The resulting signal is shown as a thin solid line in the upper graph. The corresponding stimulation intensity (pulsewidth) is plotted in the middle part of Figure 6.7. The stimulation pulsewidth is seen to be smooth throughout.
In the lower graph of the figure, the estimated plant gain $\hat{b}(k)$ is shown ($\lambda = 0.95$). The estimate converges within 50 s. After convergence, the tracking performance meets the specification closely. The specified rise times $t_r^{A_r}$ and $t_r^{A_o}$ are 6 and 4 crank cycles respectively.

6.4.5 Discussion and Conclusions

The feasibility of a self-tuning moment controller in isokinetic FES cycling could be demonstrated. The approach allows, in conjunction with the cadence control presented in Section 5.7, an accurate control of work rate. There is no lower bound for the realisable work rate as in isotonic cycling. It was found that the simple model (6.6) is sufficient for the controller design. The assumption of linearity is justified for a large range of pulsewidth values. This can be clearly seen in the static pulsewidth–active drive torque curve plotted in the lower part of Figure 6.6.
The parameter estimation works also under static conditions since only one parameter has to be identified. No probing control signals or disturbances have to be introduced to successfully estimate the

system gain. The online controller calculation is always possible as long as the plant gain does not become zero. Parameter estimation and online controller adaptation are computationally inexpensive and can therefore be directly implemented in the stimulation device.
In summary, self-tuning control ensures that the a good feedback control performance for a subject is automatically achieved. The work rate control approach for isokinetic training significantly extends both the range and the exercise-test sensitivity for FES cycling. The methodology needs to be tested with paraplegic subjects in future.

6.5 Summary and Conclusions

Accurate work rate control in FES cycling could be achieved by the application of newly developed feedback control methods. For the isotonic case, the smallest achievable work rate by the cyclist is technically determined by the crank torque required to passively turn the legs at the smallest adjustable cycling resistance (unbraked system). For many SCI subjects, the magnitude of this work rate will be a substantial fraction of their maximal exercise capacity. In contrast to this, work rate control in isokinetic cycling devices extends the lower range of realisable work rates towards 0W. Furthermore, self-tuning control of the active drive moment for isokinetic cycling ergometers yields a subject specific controller without the need of a labour-intensive off-line system identification as required for the cadence control in the isotonic case.

7 Conclusions and Recommendations for Future Work

Different aspects of FES lower-limb cycling in paraplegia have been studied in this thesis. The feasibility of mobile FES cycling has been demonstrated in a one year pilot study with paraplegic subjects. Two of the subjects who participated in the study could cycle over distances of up to 3 km without motor assistance. This has been achieved with a low intensity training regime where cycling exercises have been carried out once a week only. However the small action radius of FES cycling and the observed low power output (<20 W) limit the recreational use. A clear conclusion of this work is that motor assistance is required in order to support locomotion by FES cycling. The motor can compensate for external disturbances (including slope, wind resistance and loss of muscle power), and it can greatly increase the overall power output, thereby significantly extending the range of operation. The development of control strategies for mobile motor assisted FES cycling must be an essential part of future work.

It was found that inexpensive FES cycling systems can be realised by the adaptation of commercially available recumbent tricycles or by the use of motorised ergometers. The systems fulfil the needs of paraplegic users and offer different training modes. Muscular action induced by FES can be performed against a constant resistive load (isotonic) or at a constant cadence (isokinetic). During the isokinetic mode, a motor assists or resists the cycling in order to maintain a constant cadence. It has been successfully demonstrated that repetitive control theory can be used to obtain low variations in the motor controlled cadence during isokinetic FES cycling. The isokinetic training mode allows a larger proportion of SCI persons to undertake FES cycling, i.e. those unable to generate and maintain sufficient muscle force to pedal independently, or in those with low tolerance to FES due to residual sensation.

Accurate work rate control can be achieved by the application of the feedback control methodologies which have been developed and presented in this thesis. In the isokinetic cycling mode, the full range of power output starting from 0 W is realisable. It is therefore recommended to use this cycling mode for exercise testing. The proposed adaptive control of the work-rate in the form of a self-tuning controller guarantees that the a good feedback control performance for a subject is automatically achieved.

Future studies on FES cycling should aim to optimise the performance and efficiency of this method.

The use of variable frequency trains represents one of the most promising approaches to increase power output, especially in the fatigued state of FES activated musculature. Implementation of such pulse trains is greatly simplified by the newly developed stimulation devices presented in this thesis. The stimulator in conjunction with the described motorised FES ergometer can be directly used for studies on variable frequency trains in FES cycling. The system is suitable for research because of its accuracy and the provided signals (crank angle, torque and cadence). With the help of the developed feedback control methods, well defined testing conditions can be realised.

Besides this use in research, the developed systems and methods should be integrated into a clinical environment and made available for home use.

Bibliography

[1] T. Angeli, M. Gföhler, T. Eberharter, P. Lugner, and H. Kern. Simulation and measurement on the optimised pedaling path by functional electrostimulation. In *Proc. of the European Medical and Biological Engineering Conference (EMBEC'99)*, pages 240–241, Vienna, Austria, November 1999.

[2] T. Angeli, M. Gföhler, T. Eberharter, and L. Rinder. Tricycle for paraplegics using functional electrostimulation. In *Proc. of the European Medical and Biological Engineering Conference (EMBEC'99)*, pages 326–327, Vienna, Austria, November 1999.

[3] Spinal Injuries Association. Annual report 2003-04. http://www.spinal.co.uk/PDF/siaAnReport04.pdf, Milton Keynes, UK, 2004.

[4] K.J. Åström and B. Wittenmark. *Computer-Controlled Systems: Theory and Design*. Prentice-Hall, Inc., Upper Saddle River, N.J., 3rd edition, 1997.

[5] K.J. Åström and B. Wittenmark. *Adaptive Control*. Addison-Wesley, 2nd edition, 1995.

[6] M. Bergström and E. Hultman. Energy cost and muscle fatigue during intermittent electrical stimulation electrical stimulation of human skeletal muscle. *J. Appl. Physiol.*, 65(4):1500–1505, 1988.

[7] R. Berkelmans, M. Arns, and J. Duysens. The development of a hybrid outdoor FES bike. In *Proc. of the 8th Annual Conference of the International Functional Electrical Stimulation Society (IFESS 2003)*, Maroochydore, Australia, July 2003.

[8] I. Bromley. *Tetraplegia and Paraplegia*. Churchill Livingstone, Edinburgh, UK, 5th edition, 1998.

[9] Carmen Brück. Pedal Power. Tomorrow's World, BBC TV program, November 1998.

[10] R.E. Burke, P. Radomin, and F.E. Zajac. Catch property in single mammalian motor units. *Science*, 168:122–124, 1970.

[11] H.-Y. Chen, N.-Y. Yu, K. Chen, K.-H. Tsai, L. Fu, S.-C. Chen, M.-H. Huang, and J.-J. J. Chen. Development of FES-cycling system with network capability for multi-center clinical studies. *Journal of Medical and Biological Engineering*, 21(2):85–92, 2001.

[12] J.-J.J. Chen, C.-T. Shih, D.-G. Huang, N.-Y. Yu, M.-S. Ju, and T.-C. Huseh. Development of FES-cycling system with closed-loop control. *Chinese J. Med. Bio. Eng.*, 14(3):195–208, 1994.

[13] J.-J.J. Chen, N.-Y. Yu, D.-G. Huang, B.-T. Ann, and G.-C. Chang. Applying fuzzy logic to control cycling movement induced by functional electrical stimulation. *IEEE Trans. Rehab. Eng.*, 5(2):158–169, June 1997.

[14] K. Chen, S.-C. Chen, K.-H. Tsai, J.-J.J. Chen, N.-Y. Yu, and M.-H. Huang. An improved design of home cycling system via functional electrical stimulation for paraplegics. *International Journal of Industrial Ergonomics*, 34:223–235, 2004.

[15] J.J. Daly, E. Byron, L.M. Mendell, W.Z. Rymer, A. Stefanocska, J. Wolpaw, and C. Kantor. Therapeutic neural effects of electrical stimulation. *IEEE Trans. Rehab. Eng.*, 4(4):218–230, 1996.

[16] R. Davoodi, B.J. Andrews, G.D. Wheeler, and R. Lederer. Development of an indoor rowing machine with manual FES controller for total body exercise in paraplegia. *IEEE Trans. Neural Syst. Rehabil. Eng.*, 10(3):197–203, 2002.

[17] M.J. De Vivo, R.D. Rutt, K.J. Black, B.K. Go, and S.L. Stover. Trends in spinal cord injury demographics and treatment outcomes between 1973 and 1986. *Arch. Phys. Med. Rehabil.*, 73 (5), 1992.

[18] K.F. Eichhorn, W. Schubert, and E. David. Maintenance, training and functional use of denervated muscles. *J. Biomed. Eng.*, 6:205–211, July 1984.

[19] P.C. Eser, N. de N. Donaldson, H. Knecht, and E. Stussi. Influence of different stimulation frequencies on power output and fatigue during FES-cycling in recently injured SCI people. *IEEE Trans. Neural Syst. Rehabil. Eng.*, 11(3):236–240, 2003.

[20] P.D Faghri, R.M. Glaser, and S.F. Figoni. Functional electrical stimulation leg cycle ergometer exercise: Training effects on cardiorespiratory responses of spinal cord injured subjects at rest and during submaximal exercise. *Arch. Phys. Med. Rehabil.*, 73:1085–1093, 1992.

[21] S. Ferrante, A. Pedrocchi, G.M. Foglia, M. Ianno, and G. Ferrigno. Cycling closed-loop FES: Customized cycle ergometer and first experiments at NITlab. In I. Swain and P. Taylor, editors, *Proc. of the 9th Annual Conference of the International Functional Electrical Stimulation Society (IFESS 2004)*. Bournemouth, UK, Sep. 2004.

[22] S. Ferrante, B. Saunders, L. Duffell, A. Pedrocchi, K. Hunt, T. Perkins, and N. Donaldson. Quantitative evaluation of stimulation patterns for FES cycling. In *Proc. of the 10th Annual Conference of the International Functional Electrical Stimulation Society (IFESS 2005)*, Montreal, Canada, July 2005. IFESS.

[23] C. Ferrario, B. Stone, K.J. Hunt, S.A. Ward, A.N. Mclean, and M.H. Fraser. Oxygen cost of different stimulation patterns for FES cycling. In I. Swain and P. Taylor, editors, *Proc. of the 9th Annual Conference of the International Functional Electrical Stimulation Society (IFESS 2004)*, Bournemouth, UK, Sep. 2004.

[24] S.F. Figoni, M.M. Rodgers, and R.M. Glaser. Effects of electrical stimulation of shank musculature during ES-leg cycle ergometry. *Med. Sci. Sports Exerc.*, 26:77, 1994.

[25] C. Fornusek and G.M. Davis. Maximizing muscle force via low-cadence functional electrical stimulation cycling. *J. Rehabil. Med.*, 36:1–7, 2004.

[26] C. Fornusek, G.M. Davis, P.J. Sinclair, and B. Milthorpe. Development of an isokinetic functional electrical stimulation cycle ergometer. *Neuromodulation*, 7(1):56–64, 2004.

[27] B.A. Francis and W.M. Wonham. The internal model principle of control theory. *Automatica*, 12:457–465, 1976.

[28] T. Fuhr, J. Quintern, and G. Schmidt. Stair ascending and descending with the cooperative neuroprothesis WALK! *Neuromodulation*, 6(1):57–67, 2003.

[29] M. Gföhler and P. Lugner. Cycling by means of functional electrical stimulation. *IEEE Trans. Rehab. Eng.*, 8(2):233–243, June 2000.

[30] M. Gföhler, M. Loicht, and P. Lugner. Exercise tricycle for paraplegics. *Med. & Bio. Eng. & Comp.*, 36(1):118–121, January 1998.

[31] M. Gföhler, T. Angeli, T. Eberharter, P. Lugner, W. Mayr, and C. Hofer. Test bed with force-measuring crank for static and dynamic investigations on cycling by the means of functional electrical stimulation. *IEEE Trans. Neural Syst. Rehabil. Eng.*, 9(2):169–179, June 2001.

[32] M. Gföhler and P. Lugner. Dynamic simulation of FES-cycling: Influence of individual parameters. *IEEE Trans. Neural Syst. Rehabil. Eng.*, 12(4):398–405, 2004.

[33] R.M. Glaser, J.A. Bruner, S.D. Feinberg, and S.R. Collins. Locomotion via paralyzed leg muscles, feasibility study for a leg propelled vehicle. *J. Rehab. Res. & Dev.*, 20:53–61, 1983.

[34] R.M. Glaser, S.F. Figoni, and S.P. Hooker. Efficiency of FNS leg cycle ergometry. In *Proc. of the IEEE Engineering in Medicine and Biology Society 11th Annual Internationational Conference*, pages 961–963, 1989.

[35] R.M. Glaser, W.P. Couch, T.W.J. Janssen, J.W. Almeyda, D.D. Pringle, S.R. Collins, and T. Mathews. A development system to enhance FES leg cycle ergometer technology. *RESNA*, (7-12):279–281, June 1996.

[36] P.H. Gorman and J.T. Mortimer. The effect of stimulus parameters on the recruitment characteristics of direct nerve stimulation. *IEEE Trans. Biom. Eng.*, 30:301–308, 1983.

[37] M.S. Grewal and A.P. Andrews. *Kalman Filtering*. Wiley-Interscience, 2001.

[38] E. Henneman. Recruitment of motoneurones: the size principle. In J. E. Desmedt, editor, *Motor Unit Types, Recruitment and Plasticity in Health and Disease. Progress in Clinical Neurophysiology*, pages 26–90. Karger, Basel, 9 edition, 1981.

[39] D.M. Hettinga, B.J. Andrews, G.D. Wheeler, J.Y. Jeon, J. Verellen, J.J. Laskin, L.M. Olenik, R. Lederer, R. Burnham, and R.D. Steadward. FES-rowing for persons with spinal cord injury. In I. Swain and P. Taylor, editors, *Proc. of the 9th Annual Conference of the International Functional Electrical Stimulation Society (IFESS 2004)*. Bournemouth, UK, Sep. 2004.

[40] M.C. Hogan, E. Ingham, and S.S. Kurdak. Contraction duration affects metabolic energy cost and fatigue in skeletal muscle. *Am. J. Physiol.*, 274(3):E397–403, 1998.

[41] K.J. Hunt. *Stochastic Optimal Control Theory with Application in Self-tuning Control*, volume 117 of *Lecture Notes in Control and Information Sciences*. Springer-Verlag, Berlin, 1989.

[42] K.J. Hunt and M. Sebek. Implied polynomial matrix equations in multivariable stochastic optimal control. *Automatica*, 27:395–398, 1997.

[43] K.J. Hunt, M. Rothe, T. Schauer, A. Ronchi, and N.-O. Negård. Automatic speed control in FES cycling. In *Proc. of the 6th Annual Conference of the International Functional Electrical Stimulation Society (IFESS 2001)*, pages 300–302, Cleveland (Ohio), USA, June 2001.

[44] K.J. Hunt, T. Schauer, N.-O. Negård, M.H. Fraser, and W. Stewart. A pilot study of lower-limb FES cycling in paraplegia. In *Proc. of the 7th Annual Conference of the International Functional Electrical Stimulation Society (IFESS 2002)*, pages 350–352, Ljubljana, Slovenia, June 2002.

[45] K.J. Hunt, B. Stone, N.-O. Negård, T. Schauer, and H.M. Fraser. FES-cycling with electric motor assist. In *Presented at the FESnet 2002 Conference*, pages 7–9, Glasgow, Scotland, September 2002.

[46] K.J. Hunt, B. Stone, N.-O. Negård, T. Schauer, M.H. Fraser, A.J. Cathcart, C. Ferrario, S. Grant, and S.A. Ward. Control strategies for integration of electrical motor assist and functional electrical stimulation in paraplegic cycling: Utility for exercise testing and mobile cycling. *IEEE Trans. Neural Syst. Rehabil. Eng.*, 12(1):89–101, 2004.

[47] E.S. Idsø, T.A. Johansen, and K.J. Hunt. Finding the metabolically optimal stimulation pattern for FES-cycling. In I. Swain and P. Taylor, editors, *Proc. of the 9th Annual Conference*

of the International Functional Electrical Stimulation Society (IFESS 2004), pages 239–241, Bournemouth, UK, Sep. 2004.

[48] R.P. Jaime. *On the control of paraplegic standing using functional electrical stimulation.* PhD thesis, University of Glasgow, 2002.

[49] G.C. Jang, J.J. Chen, C.T. Shih, and T.C. Huseh. Design of FES-cycling system and its stimulation patterns. *Chinese J. Med. Biologic. Eng.*, 13(4):305–316, December 1993.

[50] T.W.J. Janssen, R.M. Glaser, and D.B. Shuster. Clinical efficacy of electrical stimulation exercise training: effects on health, fitness, and function. *Topics in Spinal Cord Injury Rehabilitation*, 3(3):33–49, 1998.

[51] T.W.J. Janssen, M. Bakker, A. Wyngaert, K. Gerrits, and A. de Haan. Effects of stimulation pattern on electrical stimulation-induced leg cycling performance. *J. Rehabil. Res. Dev.*, 41 (6A):787–796, 2004.

[52] Jarvis J.C. Power production and working capacity of rabbit tibialis anterior muscle after chronic electrical stimulation at 10 Hz. *J. Physiol.*, 470:157–169, 1993.

[53] T.H. Kakebeeke, H.E. Lechner, and P.A. Knapp. The effect of passive cycling movements on spasticity after spinal cord injury: preliminary results. *Spinal Cord*, 43:483–488, 2005.

[54] H. Kern, M. Frey, J. Holle, W. Mayr, G. Schwanda, H. Stohr, and H. Thomas. Functional electrostimulation of paraplegic patients - 1 year's practical application. results in patients and experiences. *Z.-Orthop.*, 123:1–12, 1985.

[55] K.K. Chew and M. Tomizuka. Digital control of repetitive errors in disk drive systems. *IEEE Control Systems Magazine*, 10(1):16–20, 1990.

[56] A. Kralj and T. Bajd. *Functional Electrical Stimulation: Standing and Walking after Spinal Cord Injury.* CRC Press, Boca Raton, FL, 1989.

[57] V. Kucera. *Discrete Linear Control: The Polynomial Equation Approach.* Wiley, Chichester, U.K., 1979.

[58] L. Ljung. *System Identification.* Prentice Hall, New-Jersey, 2nd edition, 1999.

[59] T. Matsunaga, Y. Shimada, and K. Sato. Muscle fatigue from intermittent stimulation with low and high frequency electrical pulses. *Arch. Phys. Med. Rehabil.*, 80(1):48–53, 1999.

[60] D.L. Mutton, A.M.E. Scremin, T.J. Barstow, M.D. Scott, C.F. Kunkel, and T.G. Cagle. Physiologic responses during functional electrical stimulation leg cycling and hybrid exercise in spinal cord injured subjects. *Arch. Phys. Med. Rehabil.*, 78:712–718, 1997.

[61] O. Nelles. *Nonlinear System Identification: From Classical Approaches to Neural Networks and Fuzzy Models*. Springer-Verlag, 2000.

[62] W. Peng. Design study of a recument tricycle for paraplegic lower-limb cycling. Technical report, University of Glasgow, Scotland, 2001.

[63] T.A. Perkins, N. Donaldson, R. Fitzwater, G. Phillips, and D. E. Wood. Leg powered paraplegic cycling system using surface functional electrical stimulation. In *Proc. 7th Int. Workshop on FES*, Vienna, Austria, 2001.

[64] T.A. Perkins, N. de N. Donaldson, N.A.C. Hatcher, I.D. Swain, and D.E. Wood. Control of leg powered paraplegic cycling using stimulation of the lumbosacral anterior spinal nerve roots. *IEEE Trans. Neural Syst. Rehabil. Eng.*, 10(3):158–164, 2002.

[65] J.S. Petrofsky. New algorithm to control a cycle ergometer using electrical stimulation. *Med. & Bio. Eng. & Comp.*, 41(1):18–27, 2003.

[66] J.S. Petrofsky and M. Laymon. The effect of previous weight training and concurrent weight training on endurance for functional electrical stimulation cycle ergometry. *Eur. J. Appl. Physiol.*, 91(4):392–398, 2004.

[67] J.S. Petrofsky and J. Smith. Three-wheel cycle ergometer for use by men and women with paralysis. *Med. & Bio. Eng. & Comp.*, 30(3):364–369, May 1992.

[68] J.S. Petrofsky and R. Stacy. The effect of training on endurance and the cardiovascular responses of individuals with paraplegia during dynamic exercise induced by functional electrical stimulation. *Eur. J. Appl. Physiol.*, 64(2):487–492, 1992.

[69] J.S. Petrofsky, H. Heaten, and C.A. Phillips. Outdoor bicycle for exercise in paraplegics and quadriplegics. *Journal of Biomedical Engineering*, 5(4):292–296, Oct. 1983.

[70] J.S. Petrofsky, C.A. Phillips, H.H. Heaton, and R.M. Glaser. Bicycle ergometer for paralyzed muscle. *J. Clin. Eng.*, 9:13–19, 1984.

[71] G. F. Phillips, J. R. Adler, and S. J. G. Taylor. A portable programmable stimulator for surface FES. In *Proc. of Llubljana FES Conference*, pages 166–168, Ljubljana, Slovenia, 1993.

[72] D.J. Pons, C.L. Vaughan, and G.G. Jaros. Cycling device powered by the electrically stimulated muscles of paraplegics. *Med. & Bio. Eng. & Comp.*, (27):1–7, 1989.

[73] F. Previdi, T. Schauer, S.M. Savaresi, and K.J. Hunt. Data-driven control design for neuroprotheses: A virtual reference feedback tuning (VRFT) approach. *IEEE Transactions on Control System Technology*, 12(1):176–182, 2004.

[74] J. Rasmussen, S.T. Christensen, M. Gföhler, M. Damsgaard, and T. Angeli. Design optimization of a pedaling mechanism for paraplegics. *Structural and Multidisciplinary Optimization*, 26(1-2):132–138, January 2004.

[75] J. Raymond, K. Schoneveld, C.H. Van Kemenade, and G.M. Davis. Onset of electrical stimulation leg cycling in individuals with paraplegia. *Med. Sci. Sports Exerc.*, 34(10):1557–1562, 2002.

[76] R. Riener and T. Fuhr. Patient-driven control of FES-supported standing up: A simulation study. *IEEE Trans. Rehab. Eng.*, 6(2):113–124, June 1998.

[77] R. Riener, M. Ferrarin, E.E. Pavan, and C.A. Frigo. Patient-driven control of FES-supported standing up and sitting down: Experimental results. *IEEE Trans. Rehab. Eng.*, 8(4):523–529, Dec. 2000.

[78] M. Rothe. Engineering development and control design of a system for paraplegic tricycling. Master's thesis, University of Glasgow, Scotland, February 2001.

[79] D.N. Rushton. Functional electrical stimulation. *Physiol. Meas.*, 18:241–275, 1997.

[80] S. Binder-MacLeod and T. Kesar. Catchlike property of skeletal muscle: Recent findings and clinical implications. *Muscle Nerve*, 31(6):681–693, 2005.

[81] T. Schauer and K. Hunt. Linear modelling and controller design for the single limb movement of paraplegics using FES. In E. Carson and E. Salzsieder, editors, *Modelling and Control Biomedical Systems 2000 (Including Biological Systems): A Proceedings Volume from the 4th IFAC Symposium*, pages 7–12, Karlsburg/Greifswald, Germany, March-April 2000.

[82] T. Schauer, R. Salbert, N.-O. Negård, K. Hunt, and J. Raisch. Power control of electrical stimulation induced cycle ergometry (in German). *at - Automatisierungstechnik*, 53(12):607–614.

[83] T. Schauer, K.J. Hunt, A. Ronchi, M.H. Fraser, and W. Stewart. Robust control of knee-joint motion. In *Proc. of the 6th Annual Conference of the International Functional Electrical Stimulation Society (IFESS 2001)*, pages 232–234, Cleveland (Ohio), USA, June 2001.

[84] T. Schauer, K.J. Hunt, N.-O. Negård, M.H. Fraser, and W. Stewart. Cadence control for recumbent cycling of paraplegics (in German). *at - Automatisierungstechnik*, 50(6):271–278, June 2002.

[85] T. Schauer, N.-O. Negård, F. Previdi, K. J. Hunt, M.H. Fraser, E. Ferchland, and J. Raisch. Online identification and nonlinear control of the electrically stimulated quadriceps muscle. *Control Engineering Practice*, 13(9):1207–1219, 2005.

[86] L.M. Schutte, M.M. Rodgers, F.E. Zajac, and R.M. Glaser. Improving the efficacy of electrical stimulation-induced leg cycle ergometry: An analysis based on a dynamic musculoskeletal model. *IEEE Trans. Rehab. Eng.*, 1(2):109–125, 1993.

[87] P.J. Sinclair, G.M. Davis, R.M. Smith, B.S. Cheam, and J.R. Sutton. Pedal forces produced during neuromuscular electrical stimulation cycling in paraplegics. *Clin. Biomech.*, 11(1):51–57, 1996.

[88] R. B. Stein, P. H. Peckham, and D. P. Popovic. *Neural Protheses: Replacing Motor Function After Disease or Disability*. Oxford University Press, Oxford, 1992. ISBN 0-19-507216-2.

[89] R.B. Stein, S.L. Chong, K.B. James, and G.J. Bell. Evaluation of a leg-propelled wheelchair: physiological energy costs of voluntary activity and electrical stimulation. *Arch. Phys. Med. Rehab.*, 82:1198–1202, 2001.

[90] J. Szecsi, M. Fiegel, P. Krause, and J. Quintern. Individual adaptation of functional electrical stimulation of paraplegics in different cycling tasks. *Technology and Health Care*, 12(2):89–93, 2004.

[91] J. Szecsi, S. Krafczyk, J. Quintern, M. Fiegel, A. Straube, and T. Brandt. Paraplegic cycling using functional electrical stimulation. Experimental and model-based study of power output (in German). *Nervenarzt*, 75:1209–1216, 2004.

[92] T. Takahashi, M. Takazawa, Y. Nishiyama, E. Nakano, and Y. Handa. FES cycling chair for the lower limbs disabled people with electric motor power assist. In I. Swain and P. Taylor, editors, *Proc. of the 9th Annual Conference of the International Functional Electrical Stimulation Society (IFESS 2004)*. Bournemouth, UK, Sep. 2004.

[93] D. Theisen, C. Fornusek J. Raymond, and G.M. Davis. External power output changes during prolonged cycling with electrical stimulation. *J. Rehabil. Med.*, 34(4):171–175, 2002.

[94] M. Tomizuka, T.-C. Tsao, and K.-K. Chew. Analysis and synthesis of discrete-time repetitive controllers. *Journal of Dynamic Systems, Measurement and Control*, 111:353–358, 1989.

[95] R.D. Trumbower and P.D. Faghri. Improving pedal power during semireclined leg cycling. *IEEE Engineering in Medicine and Biology Magazine*, 23(2):62–71, 2004.

[96] R.D. Trumbower and P.D. Faghri. Relationship between isometric pedal force generation and stimulation intensity of individual leg muscles involved in FES-induced leg cycling. In *Proc. of the 10th Annual Conference of the International Functional Electrical Stimulation Society (IFESS 2005)*, Montreal, Canada, July 2005. IFESS.

[97] A.J. Van Soest, M. Gfoehler, and L.J.R. Casius. Consequences of ankle joint fixation on FES cycling power output: A simulation study. *Medicine & Science in Sports & Exercise*, 37(5): 797–806, 2005.

[98] K.C. Wang, S.C. Chen, L.W. Chang, J.S. Lai, and T.S. Kuo. EMG activity of human cycling at different constant velocities and load levels - A preliminary study for an FES ergometer system.

[99] I.M.S Wilkinson. *Essential Neurology.* Blackwell Publishing, 3rd edition, 1999.

[100] D.A. Winter. *Biomechanics and Motor Control of Human Movement.* Wiley, 3rd edition, 2004.